# La Dynamique Moléculaire dans les Globules Rouges

Andreas Stadler

Université Joseph Fourier – Grenoble 1
Ecole Doctorale de Physique

# THESE

**Andreas STADLER**

Pour obtenir le titre de
**Docteur en Sciences**
de l'Université Joseph Fourier – Grenoble 1

Spécialité : Biophysique

---

# Molecular Dynamics in Red Blood Cells

# La Dynamique Moléculaire dans les Globules Rouges

---

Composition du jury:

| | |
|---|---|
| Prof. Dr. Alessandro Paciaroni | Rapporteur |
| PD. Dr. Wolfgang Doster | Rapporteur |
| Prof. Dr. Judith Peters | Président |
| Prof. Dr. Gerhard Artmann | Examinateur |
| Dr. Moeava Tehei | Examinateur |
| Dr. Frank Gabel | Examinateur |
| Prof. Dr. Georg Büldt | Directeur de thèse |
| Dr. Giuseppe Zaccai | Directeur de thèse |
| Prof. Dr. Fritz Parak | Invité |

Thèse préparée à l'Institut Laue-Langevin, Grenoble,
et au Forschungszentrum Jülich

*Dedicated to*

*Estela Suarez Garcia,*

*Helga and Max Stadler*

# *Acknowledgements*

The thesis would not have been possible without the help of a number of people.
First of all, I would like to thank my supervisors Dr. Giuseppe Zaccai and Prof. Dr. Georg Büldt for their friendly guidance, continuous support and their openness for discussion throughout my thesis. I always had the opportunity to explore my own ideas some of which gave very interesting results.

I want to thank the members of the jury: Alessandro Paciaroni and Wolfgang Doster for kindly having accepted to be referee, Judith Peters for being president, Moeava Tehei, Frank Gabel, Gerhard Artmann, Fritz Parak for being part of the jury and Georg Büldt and Giuseppe Zaccai for being directors of my thesis.

Special thanks go to Moeava Tehei, Elisa Fabiani, Marion Jasnin, Frank Gabel and Martin Weik for inspiring discussions, the good atmosphere in the group and the nice moments spent together at workshops and conferences. In particular, I want to thank Moeava who helped me a lot during my first neutron scattering experiments and who was always open for discussion.

I also want to thank Gerhard Artmann, Ilya Digel, Kay Zerlin, Peter Kayser and Dariusz Porst for their help with sample preparation and organisation. I always spent a nice time in the lab in Jülich and the pool party is simply unforgettable. I also want to thank Birgit Gehrmann for all the help and support in many administrative issues.

I want to thank Jan Peter Embs, Fanni Juranyi, Tobias Unruh, Franz Demmel, Judith Peters and Francesca Natali who helped me as local contacts during the neutron experiments.

I want to thank Katy Wood, Alexander Grünwald, Beate Brüning, Tinka Spehr, Lola Ruiz Martin, Navid Qureshi, Audrey Schollier, Estelle Mossou, Clara Gonzalez Jimenez, Marc Laver and Amy Dee for all the nice moments spent together at ILL and in Grenoble.

Ich möchte mich besonders bei meiner Familie bedanken. Meinen Eltern Helga und Max für ihre Unterstützung und große Hilfe in allen Dingen, bei Gabi und Rainald und bei Korbinian und Carolina für die gemeinsam verbrachte Zeit.

Besonderer Dank gilt meiner Freundin Estela für ihre Gedult, ihre Unterstützung und ihre Liebe während all dieser Zeit.

# *Table of Contents*

# *1. Introduction Générale*

Cette thèse a été effectuée à l'Institut Laue-Langevin, Grenoble, et au Centre de Recherche Jülich, Allemagne, sous la direction du Dr. Joseph Zaccai et du Prof. Dr. Georg Büldt. Le sujet de la thèse concerne l'étude de la dynamique de l'hémoglobine et de l'eau *in-vivo* dans les globules rouges comparée à la dynamique de l'hémoglobine isolée en fonction de l'hydratation, mesurée par diffusion incohérente quasiélastique et élastique de neutrons. Le manuscrit est basé sur trois articles scientifiques. Deux sont déjà publiés, respectivement dans *Biophysical Journal* et *Journal of the American Chemical Society*, le troisième a été soumis pour publication à *Biophysical Journal* en janvier 2009.

Tous les organismes vivants sont formés par des cellules. Une thématique de recherche importante vise à comprendre les processus moléculaires qui ont lieu dans les cellules. Le but de la biophysique moléculaire est de comprendre la fonction, la structure, la dynamique et l'interaction avec le solvant des systèmes biomoléculaires comme les protéines, l'ADN, ou les membranes au niveau atomique. Les protéines sont des macromolécules qui sont produites dans les cellules et qui sont responsables d'une grande partie des fonctions dans l'organisme. Le génome humain contient l'information pour des dizaines de milliers de protéines différentes. Chacune a sa ou ses fonctions spécifiques. Quelques protéines fonctionnent comme des enzymes et catalysent des réactions chimiques. D'autres forment le tissu et des structures comme les muscles, la peau ou le cytosquelette. Des protéines spécialisées transforment l'énergie solaire en énergie chimique via la photosynthèse. D'autres encore transportent et stockent des substances de façon vivement régulée, comme c'est le cas de l'hémoglobine avec l'oxygène. Les protéines font souvent partie de grands assemblages avec d'autres protéines, l'ADN, l'ARN, des sucres, ou des lipides. La connaissance de la structure au niveau atomique est nécessaire pour comprendre comment les protéines peuvent réaliser toutes leurs fonctions. Néanmoins, les protéines ne sont pas des objets statiques mais leur structure est animée par des fluctuations permanentes. Elles sont des objets mous et

déformables. La dynamique et les fluctuations ont une importance fondamentale pour la fonction biologique.

La technique de diffusion incohérente des neutrons est très bien adaptée pour étudier la dynamique des biomolécules dans la gamme de temps de la picoseconde à la nanoseconde et la gamme de longueur de l'Ångstrom. La section efficace de diffusion incohérente de l'hydrogène est d'un ordre de grandeur plus élevé que celles des autres éléments qui constituent normalement la matière biologique, ainsi que celle du deutérium. Les atomes d'hydrogène sont distribués quasi-uniformément dans les protéines. Pratiquement, un atome sur deux dans une protéine est un atome d'hydrogène. En conséquence, la diffusion incohérente de neutrons mesure la dynamique moyenne des protéines. La technique de diffusion quasiélastique de neutrons est particulièrement bien adaptée pour mesurer la dynamique de l'eau dans la gamme de temps correspondant aux mouvements rapides de l'eau volumique à ceux plus lents de l'eau interfaciale. Le système biologique choisi pour cette thèse est l'hémoglobine dans les globules rouges. L'hémoglobine est le constituant macromoléculaire principal des globules rouges. La protéine transporte, avec une régulation extrêmement fine, l'oxygène des poumons aux tissus. Les globules rouges sont des cellules plutôt simples, comme ils ne possèdent pas de noyau ou d'organelles et ils ne sont pas capables de synthétiser des protéines. Des expériences d'aspiration de globules rouges humains individuels utilisant des micropipettes ont montré qu'il existe une transition de passage à la température physiologique (Artmann et al. 1998). Des expériences de viscosimétrie avec des solutions d'hémoglobine très concentrées ont montré qu'il y a une transition colloïdale d'un gel à un état fluidique également à la température physiologique (Kelemen et al. 2001). Des expériences de dichroïsme circulaire et de diffusion dynamique de la lumière ont été effectuées sur l'hémoglobine de différentes espèces à températures physiologiques différentes. Elles ont montré que la température de transition est corrélée directement à la température physiologique (Digel et al. 2006 ; Zerlin et al. 2007). Le but de la thèse était d'étudier par diffusion des neutrons s'il y a une transition dans le comportement dynamique de l'hémoglobine ou du solvant autour de la température du corps. Une série d'expériences de diffusion de neutrons ont été faites sur des globules rouges entiers et comparées à des expériences sur des poudres d'hémoglobine hydratées et sur l'hémoglobine en solution concentrée.

Suite à l'introduction générale, le deuxième chapitre de la thèse présente une introduction à l'hémoglobine et aux globules rouges. Les expériences sur la transition de l'hémoglobine à la température physiologique sont résumées dans ce chapitre.

Le troisième chapitre décrit la diffusion des neutrons appliquée à l'étude de la dynamique des biomolécules. La dynamique des protéines en générale et les propriétés de la dynamique de l'eau dans les systèmes biologiques sont présentées. Les propriétés du neutron et les méthodes de production et de détection des neutrons sont données. Des éléments de la théorie de diffusion de neutrons qui sont nécessaires pour la compréhension de la thèse sont résumés. Les méthodes de la diffusion élastique et quasiélastique de neutrons et les instruments sont décrits. Finalement, les concepts de déplacement carré moyen et constante de force obtenus par diffusion élastique de neutrons sont expliqués et les modèles utilisés pour interpréter les expériences quasiélastiques sont résumés.

Le quatrième chapitre est basé sur un article publié dans *Biophysical Journal*. Il présente une étude sur la dynamique de l'hémoglobine dans les globules rouges mesurée par diffusion quasiélastique de neutrons.
Hemoglobin Dynamics in Red Blood Cells: Correlation to Body Temperature (2008) Stadler A. M., I. Digel, G. M. Artmann, J. P. Embs, G. Zaccai, and G. Büldt. *Biophysical Journal* 95: 5449–5461
Dans l'étude, la dynamique interne de l'hémoglobine et la diffusion macromoléculaire globale ont été mesurées. L'expérience a montré qu'il y a une transition dans la géométrie des mouvements internes à 36.9°C. À des températures plus élevées que la température du corps, la dynamique des chaînes latérales des acides amimés occupent des volumes plus grands que prévu par l'effet normal de la température. La diffusion macromoléculaire globale a été interprétée avec des concepts théoriques pour des particules colloïdales.

Le cinquième chapitre présente un article basé sur la dynamique de l'hémoglobine en fonction de l'hydratation. L'article a été soumis au *Biophysical Journal*.
From Powder to Solution: Hydration Dependence of Human Hemoglobin Dynamics Correlated to Body Temperature. Stadler A. M., I. Digel, J. P. Embs, T. Unruh, M. Tehei, G. Zaccai, G. Büldt, and G. M. Artmann.
L'influence de l'hydratation sur la dynamique de l'hémoglobine a été mesurée par diffusion élastique et quasiélastique de neutrons. Les temps de résidence entre les sauts locaux, de

l'ordre de quelques picosecondes, sont réduits en solution concentrée et augmentés en poudre d'hémoglobine hydratée. La transition dans la géométrie des mouvements internes à la température du corps a été trouvée dans la solution concentrée mais non dans la poudre hydratée. Ceci indique que les mouvements rapides impliqués dans la transition sont activés seulement à partir d'un certain niveau d'hydratation. Un résultat annexe est que les poudres hydratées ne pourraient pas montrer tous les aspects dynamiques dans l'ordre de quelques picosecondes, qui pourraient être nécessaires pour la fonction biologique.

Le sixième chapitre est basé sur un article scientifique publié dans *Journal of the American Chemical Society* qui décrit des expériences sur la dynamique de l'eau cellulaire dans les globules rouges.

Cytoplasmic Water and Hydration Layer Dynamics in Red Blood Cells (2008) Andreas M. Stadler, Jan P. Embs, Ilya Digel, Gerhard M. Artmann, Tobias Unruh, Georg Büldt, and Giuseppe Zaccai. *Journal of the American Chemical Society* 130 (50): 16852–16853

La dynamique de l'eau dans les globules rouges a été mesurée par diffusion quasiélastique de neutrons. Des spectromètres de neutrons à résolution en temps de 40, 13 et 7 picosecondes ont été combinés pour couvrir l'échelle de temps des mouvements de l'eau volumique et de l'eau interfaciale. Une fraction d'eau cellulaire d'environ 90% est caractérisée par un coefficient de diffusion translationnel similaire à l'eau volumique. Une partie de l'eau cellulaire (~10%) montre par contre une dynamique significativement ralentie. Le ralentissement a été attribué à l'interaction avec la surface de l'hémoglobine. La fraction de l'eau ralentie correspond à environ la moitié des molécules d'eau dans la première couche d'hydratation.

Le septième chapitre présente un résumé du travail, les conclusions et les perspectives.

# 1. General Introduction

The present PhD thesis was carried out at the Institut Laue-Langevin, Grenoble, and at the Research Centre Jülich, Germany, under the joint supervision of Dr. Giuseppe Zaccai and Prof. Dr. Georg Büldt. The subject concerns incoherent quasielastic and elastic neutron scattering experiments on the dynamics of hemoglobin and water in whole red blood cells *in-vivo,* and as a comparison, hemoglobin dynamics in response to hydration. The document is based on three scientific articles. Two of them are published in *Biophysical Journal* and *Journal of the American Chemical Society,* respectively. The third one has been submitted for publication to *Biophysical Journal,* in January 2009.

All living organisms consist of cells. One subject of research lies in a detailed understanding of the molecular processes that occur in cells. Molecular biophysics focuses on the investigation of biological systems at the atomic level, such as for example proteins, membranes, DNA and their interactions with the surrounding solvent. Proteins are responsible for a large variety of different functions. The human genome contains the information for several tens of thousands of different proteins. Each one has got one or more specific functions. Some proteins work as enzymes and catalyse chemical reactions. Others form tissues and structures such as muscles, skin or the cytoskeleton. Specialised proteins convert solar energy via photosynthesis into chemical energy, or transport and store substances in a sophisticated way, as it is the case for hemoglobin that carries oxygen. Proteins are often part of complex macromolecular assemblies that consist of other proteins, DNA, RNA, sugar or lipid molecules. The knowledge of its structure at the atomic level is necessary to understand how a protein can fulfil its specific task. However, proteins are not static structures but they are soft and deformable. The dynamics and fluctuations of proteins are of fundamental importance for biological function.

Incoherent neutron scattering is a particular well suited technique to study biomolecular dynamics in the picosecond to nanosecond time and Ångstrom length scale. The incoherent scattering cross section of hydrogen is one order of magnitude larger than all other elements that usually occur in biological matter, and deuterium. Hydrogen atoms are uniformly distributed in proteins and constitute nearly every second atom. Neutron scattering therefore probes average protein dynamics. The technique of quasielastic incoherent neutron scattering is especially useful for the study of the dynamics of water in the time scales of fast motions of bulk water to slower dynamics of interfacial water. The biological system that was studied in the thesis is hemoglobin in red blood cells. Hemoglobin is the main macromolecular constituent of red blood cells. The protein transports oxygen from the lungs to the tissues in a highly coordinated and regulated way. Red blood cells are simple cells as they do not contain a nucleus or organelles, and are not able to synthesize proteins. Micropipette experiments on single red blood cells identified a passage transition at body temperature (Artmann et al. 1998). Viscosity measurements of hemoglobin solutions at high concentration showed that there equally occurs a colloidal gel to fluid transition of hemoglobin solutions at body temperature (Kelemen et al. 2001). Circular dichroism and dynamic light scattering experiments further revealed that the temperature transition of hemoglobin is directly correlated to the body temperature of different species (Digel et al. 2006; Zerlin et al. 2007). The aim of the thesis was to study if a transition in the dynamics of hemoglobin or solvent occurs at body temperature. This was achieved in a series of incoherent neutron scattering experiments on whole red blood cells that were compared to results of hydrated hemoglobin powder, and concentrated hemoglobin solution samples.

Following the general introduction, the second chapter of the thesis gives an introduction to hemoglobin and red blood cells. Recent experiments on the temperature transition of hemoglobin at body temperature are summarized.

The third chapter deals with neutron scattering applied to the study of biomolecular dynamics. Protein dynamics and the dynamic properties of water in biological systems are presented. The general properties of the neutron and methods of neutron production and detection are described. The elements of neutron scattering theory that are necessary for the further understanding of the thesis are summarized. The methods of elastic and quasielastic incoherent neutron scattering are presented and the commonly used instruments are described. Finally, the concepts of mean square displacements and force constants that are obtained from

elastic incoherent neutron scattering are explained and typical models that are used for quasielastic neutron scattering are summarized.

The fourth chapter is based on a published article in *Biophysical Journal* about hemoglobin dynamics in red blood cells measured with quasielastic incoherent neutron scattering:
Hemoglobin Dynamics in Red Blood Cells: Correlation to Body Temperature (2008) Stadler A. M., I. Digel, G. M. Artmann, J. P. Embs, G. Zaccai, and G. Büldt. *Biophysical Journal* 95: 5449–5461
Internal protein dynamics and global macromolecular diffusion were separated. The experiments revealed a change in the geometry of internal protein dynamics above 36.9°C. Above this temperature amino acid side-chain dynamics occupy larger volumes than expected from normal temperature dependence. Global macromolecular diffusion was interpreted favourable with theoretical concepts for short-time self-diffusion of non-charged hard sphere colloids.

The fifth chapter presents an article about hemoglobin dynamics as response to hydration. The article has been submitted to *Biophysical Journal*.
From Powder to Solution: Hydration Dependence of Human Hemoglobin Dynamics Correlated to Body Temperature. Stadler A. M., I. Digel, J. P. Embs, T. Unruh, M. Tehei, G. Zaccai, G. Büldt, and G. M. Artmann.
The influence of hydration on hemoglobin dynamics was studied with elastic and quasielastic incoherent neutron scattering. The residence times of localized jumps in the order of a few picoseconds were found to be significantly reduced in concentrated solution compared to fully hydrated powder. The body temperature transition in protein dynamics was found in the concentrated solution sample but was absent in the fully hydrated powder, indicating that picosecond protein dynamics responsible for the transition is activated only at a sufficient level of hydration. A collateral result from the study is that fully hydrated protein powder samples do not accurately describe all aspects of protein picosecond dynamics that might be necessary for biological function.

The sixth chapter deals with the dynamic properties of cellular water in red blood cells in the form of a scientific article that was published in *Journal of the American Chemical Society*.

Cytoplasmic Water and Hydration Layer Dynamics in Red Blood Cells (2008) Andreas M. Stadler, Jan P. Embs, Ilya Digel, Gerhard M. Artmann, Tobias Unruh, Georg Büldt, and Giuseppe Zaccai. *Journal of the American Chemical Society* 130 (50): 16852–16853
The dynamics of water in human red blood cells was measured with quasielastic incoherent neutron scattering. Neutron spectrometers with time resolutions of 40, 13, and 7 ps were combined to cover time scales of bulk water dynamics to reduced mobility interfacial water motions. A major fraction of around 90% of cell water is characterized by a translational diffusion coefficient similar to bulk water. A minor fraction of around 10% of cellular water exhibits reduced dynamics. The slow water fraction was attributed to dynamically bound water on the surface of hemoglobin, which accounts for approximately half of the hydration layer.

The seventh chapter gives a summary of the performed work and presents an outlook on future perspectives.

# *2. Hemoglobin and Red Blood Cells*

## 2.1 Biological Background

The main natural environment of proteins is within the cell, and protein function necessarily is adapted to these conditions. In bacteria and eukaryotic cells macromolecular interactions are likely to be influenced by the high cellular protein concentration (Hall and Minton 2003; Minton 2001; Zimmerman and Minton 1993). This effect, called 'crowding', results from high volume occupancy and steric hindrance of the protein molecules between each other. The free distance between macromolecules in the cell is in the order of a few Ångstroms (Krueger and Nossal 1988) and intercellular water is in close vicinity to the protein surfaces. There is much interest and discussion about similarities and differences in structure and dynamics of cytoplasmic and bulk water (Ball 2008). Little is still known on how protein dynamics is influenced by the crowded cytoplasmic environment and the special properties of cellular water.

The main protein constituent of red blood cells is hemoglobin (92% of dry weight) (see **Figure 1**). Its biological function is to carry oxygen from the lungs to the tissues. The X-ray structure of hemoglobin is shown in **Figure 2**. The protein is a tetramer with a molecular weight of around 64 kDa. It consists of two α-chains and two β-chains, each having 141 and 146 amino acid residues, respectively. The α-chains contain seven and the β-chains eight helices (Perutz 1987). Each chain carries one heme group, in a pocket, to which oxygen and several other small molecules can bind reversibly. The concentration of hemoglobin in the red blood cells is around 330 mg/ml (Krueger and Nossal 1988).

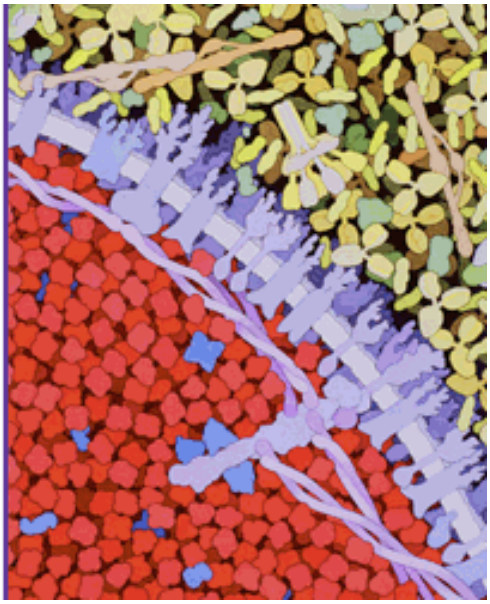

**Figure 1:** Illustration of a red blood cell in the lower half of the picture with surrounding blood serum proteins in the upper half. The red blood cell is densely filled with hemoglobin, drawn in red. The cell wall with membrane proteins is coloured purple. (Goodsell 2000).

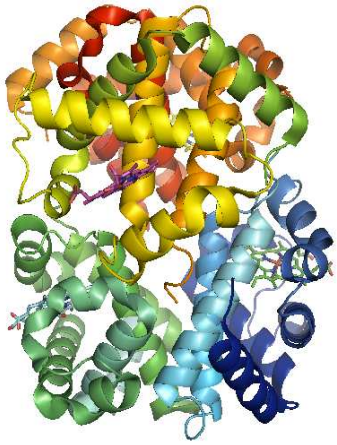

**Figure 2:** Hemoglobin is a tetrameric protein. It consists of two α- and two β-chains. Every chain carries one heme molecule in a pocket to which oxygen binds reversible. (PDB code 1G09)

## 2.2 Body Temperature Transition of Hemoglobin

Hemoglobin at high concentration shows a variety of interesting effects. Micropipette experiments with aspirated single human red blood cells revealed a sudden change in the behaviour of the cells from blockage of the pipette below $T_{Pipette}$=36.4 ± 0.4 °C to easy passage above. The transition temperature $T_{Pipette}$ of cell passage was surprisingly very close to human body temperature. During the micropipette experiment water is pressed out of the red blood cell and the hemoglobin concentration rises to values of more than 500 mg/ml (Kelemen et al. 2001).

Viscosity measurements were performed on human hemoglobin solutions between 330 mg/ml and 500 mg/ml to study the flow properties at such concentrations (Artmann et al. 1998). The experiments found a sharp drop in viscosity in Arrhenius plots, at concentrations higher than 450 mg/ml at body temperature. The drop was absent at the physiological concentration of 330 mg/ml. The results were interpreted as a colloidal phase transition in highly concentrated hemoglobin solution from a gel-like to a fluid state at body temperature (Artmann et al. 1998; Kelemen et al. 2001). In the fluid-like state, above body temperature, hemoglobin exhibits pronounced aggregation, whereas at lower temperatures hemoglobin aggregation is suppressed (Artmann et al. 1998).

Further studies with circular dichroism investigated changes of the protein secondary structure around the transition temperature. A partial loss of alpha-helical content was found at a temperature $T_{CD}$=37.2 ± 0.6 °C for human hemoglobin (Artmann et al. 2004). The loss of hemoglobin alpha-helical structure at a specific temperature $T_{CD}$ was also observed for hemoglobin molecules of a large variety of different species (Digel et al. 2006; Zerlin et al. 2007). Amazingly, the transition temperatures $T_{CD}$ were directly correlated to the body temperature of the animals ranging from 34 °C, for the duck-billed platypus, to 42 °C for a bird, the spotted nutcracker. It was excluded that the partial loss of protein structure at $T_{CD}$ results from irreversible protein denaturation which occurs at distinctly higher temperatures. Independently of these experiments, two-dimensional infrared correlation spectroscopy suggested a structural perturbation stage of bovine hemoglobin between 30 °C and 44 °C (Yan et al. 2004). The observed perturbations were assigned to hydrogen-bonded extended chains that connect the helices. It was concluded that the passage transition of red blood cells is caused by hemoglobin molecules and that the observed small structural changes of

hemoglobin at $T_{CD}$ might be the cause for the drop of viscosity at $T_{Pipette}$ (Kelemen et al. 2001). It has been speculated that partial unfolding of the α-helical structure at body temperature goes in hand with an increase in surface hydrophobicity that promotes protein aggregation (Digel et al. 2006), which causes a drop in colloidal osmotic pressure (Artmann et al. 2008).

## 2.3 References

Artmann GM, Burns L, Canaves JM, Temiz-Artmann A, Schmid-Schonbein GW, Chien S, Maggakis-Kelemen C (2004) Circular dichroism spectra of human hemoglobin reveal a reversible structural transition at body temperature. Eur. Biophys. J. 33:490-6

Artmann GM, Kelemen C, Porst D, Büldt G, Chien S (1998) Temperature transitions of protein properties in human red blood cells. Biophys. J. 75:3179-83

Artmann GM, Zerlin KF, Digel I (2008) Hemoglobin Senses Body Temperature. In: Artmann GM, Chien S (eds) Bioengineering in Cell and Tissue Research, vol IV. Springer Verlag, Berlin, Heidelberg, pp 415-447

Ball P (2008) Water as an Active Constitutent in Cell Biology. Chem. Rev. 108:74-108

Digel I, Maggakis-Kelemen C, Zerlin KF, Linder P, Kasischke N, Kayser P, Porst D, Temiz Artmann A, Artmann GM (2006) Body temperature-related structural transitions of monotremal and human hemoglobin. Biophys. J. 91:3014-21

Goodsell DS (2000) http://mgl.scripps.edu/people/goodsell/illustration/public

Hall D, Minton AP (2003) Macromolecular crowding: qualitative and semiquantitive successes, quantitative challenges. Biochim. Biophys. Acta 1649:127-139

Kelemen C, Chien S, Artmann GM (2001) Temperature transition of human hemoglobin at body temperature: effects of calcium. Biophys. J. 80:2622-30

Krueger S, Nossal R (1988) SANS studies of interacting hemoglobin in intact erythrocytes. Biophys. J. 53:97-105

Minton AP (2001) The Influence of Macromolecular Crowding and Macromolecular Confinement on Biochemical Reactions in Physiological Media. J. Biol. Chem. 276:10577-10580

Perutz MF, G. Fermi, B. Luisi (1987) Stereochemistry of Cooperative Mechanisms in Hemoglobin. Acc. Chem. Res. 20:309-321

Yan YB, Wang Q, He HW, Zhou HM (2004) Protein thermal aggregation involves distinct regions: sequential events in the heat-induced unfolding and aggregation of hemoglobin. Biophys. J. 86:1682-90

Zerlin KF, Kasischke N, Digel I, Maggakis-Kelemen C, Temiz Artmann A, Porst D, Kayser P, Linder P, Artmann GM (2007) Structural transition temperature of hemoglobins correlates with species' body temperature. Eur. Biophys. J. 37:1-10

Zimmerman SB, Minton AP (1993) Macromolecular Crowding: Biochemical, Biophysical and Physiological Consequences. Ann. Rev. Biophys. Biomol. Struct. 22:27-65

# 3. Neutron Spectroscopy to Study Biomolecular Dynamics

The chapter starts with a presentation of protein and water dynamics in general. Physical concepts and equations that are necessary for the understanding of the theory of incoherent neutron scattering are schematized. Inelastic and elastic scattering processes and incoherent and coherent neutron scattering are presented. The application of elastic and quasielastic incoherent neutron scattering to measure biomolecular dynamics is explained at the end of the chapter.

## 3.1 Protein and Water Dynamics

First studies on protein dynamics used sperm whale myoglobin as a model system. It was the first protein of which the structure could be solved by X-ray crystallography (Kendrew et al. 1960). The protein serves as a scaffold for the iron containing heme-group that is responsible for oxygen binding and transport. The crystal structure showed clearly that there are no permanent channels in the protein structure through which the oxygen molecule could migrate from the surrounding solvent to its binding place deep in the protein. Only fluctuations of the protein structure can allow the rapid opening and closing of channels in the protein structure for the purpose of oxygen binding indicating that knowledge of both protein structure and dynamics is necessary for a complete understanding of protein function.

Ligand rebinding in myoglobin was measured with optical absorption in the range of $10^{-6}$ to $10^{3}$ seconds after photo flash dissociation (Austin et al. 1975). In total, up to four different rebinding processes were found that depend differently on temperature. Between around 180 K to 280 K all four processes could be found; below around 180 K only the first rebinding process occurs. The rebinding processes were identified with four different activation energy barriers that the ligand has to pass before rebinding. It was concluded that the first energy barrier corresponds to direct rebinding of the ligand to the iron atom. Nonexponential rebinding rates were found for the first process below 180 K. The results

imply that the first energy barrier is in fact a distribution of activation energies. The authors explained this by the assumption that myoglobin does not exist in only one fixed structure but it possesses many slightly different conformational states. Below 180 K each protein is frozen and trapped in one of the conformational states. Above 180 K the protein can interchange between the different conformations. The differences between many different structural conformations need to be rather small as they could not be seen with X-ray crystallography (Frauenfelder et al. 1979). These experiments led to the picture of conformational substates of proteins (Frauenfelder et al. 1988). In the native state a protein does not exist in a single static structure. Instead it fluctuates between a large ensemble of slightly different conformational structures. The free enthalpy of all substates is the same (or very close) and the different conformations are separated by activation energy barriers. The sampling of the conformational substates leads to the entropic stabilisation of proteins.

Motions in biological macromolecules and proteins occur over a very broad range of time scales: from fast vibrations and electron transfer processes in the order of some femtoseconds, to protein folding events in the order of some seconds. The amplitudes of motion lie between around 0.1 Å for fast atomic vibrations up to several 10 Å for collective motions. A short overview of time and length scales of motions in biological macromolecules is given in **Table 1**.

**Table 1:** Typical time and length scales of internal motion in proteins modified after (McCammon and Harvey 1987)

| **Motion** | **Spatial extend [nm]** | **Amplitude [nm]** | **Log10 characteristic time [s]** |
|---|---|---|---|
| Relative vibration of bonded atoms | 0.2 to 0.5 | 0.001 to 0.01 | -14 to -13 |
| Elastic vibration of globular region | 1 to 2 | 0.005 to 0.05 | -12 to -11 |
| Rotation of sidechains at surface | 0.5 to 1 | 0.5 to 1 | -11 to -10 |
| Torsional libration of buried groups | 0.5 to 1 | 0.05 | -11 to -9 |
| Relative motion of different globular regions (hinge bending) | 1 to 2 | 0.1 to 0.5 | -11 to -7 |
| Rotation of medium-sized sidechains in interior | 0.5 | 0.5 | -4 to 0 |
| Allosteric transitions | 0.5 to 4 | 0.1 to 0.5 | -5 to 0 |
| Local denaturation | 0.5 to 1 | 0.5 to 1 | -5 to +1 |

First experiments on protein dynamics came from Mößbauer spectroscopy studies of myoglobin. The technique specifically probes the dynamics of the iron atom in the heme group with very high resolution. Motions in the time scale up to 140 ns are detected. The results showed that the mean square displacements of the iron atom increase linearly with temperature up to around 180 K. Above 180 K the mean square displacements increase with a steeper gradient. This was interpreted in terms of supplemental anharmonic motions that contribute to the dynamics above 180 K (Parak et al. 1982). The results obtained with Mößbauer spectroscopy were interpreted with a model of an overdamped Brownian oscillator (Knapp et al. 1982). Below the dynamical transition temperature of 180 K proteins are trapped in conformational substates and perform harmonic oscillations. Above 180 K the proteins switch by thermal activation to a more flexible state, in which internal quasi-diffusive motions are possible.

The nature of the hydration shell of myoglobin was investigated with infrared spectroscopy and calorimetry (Demmel et al. 1997; Doster et al. 1986). At low temperature the hydration water turns into an amorphous, disordered state with strongly reduced dynamics. The experiments revealed a glass-like transition of the hydration water at around 200 K which is close to the dynamical transition temperature of myoglobin. The authors emphasized the importance of the glass-like transition of the solvent near 200 K for the dynamical transition of myoglobin. They concluded that the cooperativity of the hydrogen bonding network provides the intimate coupling between solvent and protein dynamics (Doster et al. 1986). The important role of the solvent on the dynamical transition was further demonstrated in a Mößbauer experiment that investigated myoglobin dynamics in a sucrose- water solvent (Lichtenegger et al. 1999). The dynamic transition of myoglobin was shifted to 240 K due to the higher viscosity of the solvent.

Incoherent neutron scattering is dominated by hydrogen atom motions as their incoherent scattering cross section is one order of magnitude bigger than that of all other elements which usually occur in biological matter, and deuterium (Sears 1992). The technique probes average protein dynamics because hydrogen atoms are uniformly distributed in the natural abundance protein. The time and length scales of molecular motions that are accessible are determined by the energy resolution and the scattering vector range of the spectrometer, respectively. On the ps-Å time-length scale, hydrogen atoms that are covalently bound to amino acid side-chains reflect the dynamical behaviour of the bigger chemical units (Reat et al. 1998; Smith 1991; Wood et al. 2008).

The dynamical transition at about 180 K was revealed to exist for the motion of all hydrogen atoms in myoglobin by energy resolved incoherent neutron scattering (Doster et al. 1989). The dynamical transition was also found by neutron scattering in a membrane protein (Ferrand et al. 1993). Below 180 K the dynamics of myoglobin are similar to a harmonic solid. At 180 K additional non-vibrational motions set on that were attributed to jumps of the hydrogen atoms between two states (Doster et al. 1989). The jump motion was described with a double well model for two states separated with a temperature independent distance $d$ and a free energy difference. The amplitude of the jump distance was found to be $d$=1.5 Å which was interpreted being due to dihedral angle fluctuations (Doster et al. 1989). A fast β-process and a slower α-process were identified in the inelastic spectra of myoglobin (Cusack and

Doster 1990; Doster et al. 1989, 1990). The fast β-process was attributed to localised jumps with correlation times of ~0.5ps, the slower α-process was brought into connection with the α-process that occurs in liquids and polymers (Doster et al. 1989). The onset of the α-process occurs at 240 K and was attributed to collective excitations that are induced by the melting of glassy water in the hydration shell (Demmel et al. 1997; Doster et al. 1986; Doster et al. 1989). Model independent mean square displacements were obtained in the Gaussian approximation that included the contributions of the α-, the β-process and vibrational motions (Doster et al. 1989). In that way, the amplitudes of the α-process were obtained as a function of temperature. The slow α-process is absent in dehydrated powders. Recently, the β-process was attributed to localised jumps of amino acid side-chains (Doster 2008). The shape of the inelastic spectra of the α- and β-process could be described quantitatively with predictions of mode coupling theory (Doster et al. 1990). It was concluded that a cage effect of nearest neighbours is responsible for the spectral features. However, the difference between protein dynamics and glass physics was pointed out, as the structure of a protein imposes restrictions to the possible movements in the long time limit, amino acid side chains are attached to the protein backbone for example (Doster et al. 1990). In analogy to the glass transition, the onset of the slower α-process at 240 K was defined as the dynamical transition temperature and the α-process was identified as the elementary step of diffusion. The onset at 180 K due to fast jumps between states of different energy is a precursor of the slower α-process (Doster 2008).

Depending on the energy resolution and scattering vector range of the neutron spectrometer, a third inflection in the thermal displacements, which is hydration-independent, was observed at a temperature between 100 and 150 K. It has been attributed to methyl group rotations (Cornicchi et al. 2006; Doster and Settles 2005; Roh et al. 2006; Roh et al. 2005). These local jumps contribute to the sampling of a large number of conformational substates that are responsible for the entropic stabilization of proteins (Fraunfelder et al. 1991).

A model for protein dynamics related to the Doster et al. (1989) double well used in this work was proposed by Bicout and Zaccai (Bicout and Zaccai 2001). Protein dynamics is interpreted with a picture of a quasi-harmonic average potential well for the complex macromolecular force field (Bicout and Zaccai 2001; Zaccai 2000). The model assumes that protein dynamics can be described by two states: local fluctuations around the equilibrium positions with small amplitude and larger amplitude fluctuations in a cage formed by neighboring molecules. The two states are separated by a free energy difference and the transition from the low amplitude

state to the large amplitude state is activated by temperature. The dynamical transition is defined as the deviation of the mean square displacements from low temperature linear behaviour. In the model this occurs when a small fraction (10%) of the total population of particles in the small amplitude state changes into the large amplitude state.

Following the Bicout and Zaccai model, protein flexibility was defined as the amplitude of atomic motions $\sqrt{\langle u^2 \rangle}$ which corresponds to the width of the quasi-harmonic average potential well. Protein thermal stability would correspond to the depth of the well (Tehei et al. 2001; Tehei and Zaccai 2007). A mean effective force constant $<k'>$ can be obtained from the dependence of the $<u^2>$ as function of temperature. This mean effective force constant, called resilience, describes the shape of the well (Zaccai 2000). Many conformational substates exist within the average well and are sampled by localized jump-diffusion (Fraunfelder et al. 1991). The geometry and activation energy of localized jumps can be determined by QENS. From elastic incoherent neutron scattering (EINS) mean square displacements $<u^2>$ of the thermal cloud of atomic motions can be determined. Quasielastic neutron scattering (QENS) on the other hand, enables to distinguish between vibrational and diffusive components (Bee 1988). This technique allows the quantification of internal diffusion coefficients, residence times and the determination of the average geometry of motions.

Both protein function and dynamics are closely linked to sufficient hydration. Enzymes are non-functional in the dry state and catalytic function is only possible above a sufficient threshold hydration level of around 0.2g $H_2O$/ g protein (Rupley and Careri 1991). In a membrane protein, anharmonic processes are only activated above a hydration level of around 0.35g $H_2O$/ g protein (Ferrand et al. 1993). Recent work in literature points out that it is the onset of translational diffusion of the solvent molecules that enables the protein dynamical transition (Tarek and Tobias 2002; Tournier et al. 2003; Wood et al. 2007). The dynamical properties of water that is in close contact to protein surfaces are therefore of high importance for the understanding of protein function.

The cytoplasmic environment in cells is very crowded and protein concentrations range up to ~400 mg/ml (Ellis and Minton 2003). Distances between macromolecules are in the order of ~1nm, which corresponds to only a few layers of water. A large fraction of water molecules is therefore in close contact to protein surfaces. The translational diffusion coefficient of hydration water on the surface of C-phycocyanin was found to be 3 times reduced (Bellissent-

Funel et al. 1996; Dellerue and Bellissent-Funel 2000) compared to that of bulk water (Teixeira et al. 1985). The dynamics of water in contact with hydrophilic and hydrophobic peptides at high concentration was found to be reduced compared to bulk water (Russo et al. 2005). Molecular dynamics simulations showed that mostly water molecules in protein surface cavities exhibit strongly reduced dynamics (Makarov et al. 2000). Water in cells was therefore assumed to show different dynamics than bulk water. Recent work on water dynamics in cells proved the contrary: Jasnin et al. measured the dynamics of cellular water in *Escherichia coli* with neutron scattering (Jasnin et al. 2008). The authors reported that the average translational and rotational diffusion coefficients of cell water show similar behaviour to bulk water. The residence times of cell water were twice as long which was attributed to the longer times spent in the hydration shell. Persson and Halle measured water dynamics in *E. coli* with NMR spectroscopy (Persson and Halle 2008). They concluded that around 85% of cell water has similar dynamics to bulk water, and around 15% of cell water interacts with the surface of biomolecules, being slowed down by a factor of around 15 ± 3 compared to bulk water.

The halophilic cell is a special case. The cell accumulates large amounts of KCl in the molar level in its cytoplasm and halophilic proteins are only stable at such high salt concentrations. Solvent interactions of halophilic proteins are particularly strong and halophilic proteins bind both water and salt ions in their hydration shell (Madern et al. 2000). A previous experiment on water dynamics in the halophilic organism *Haloarcula marismortui* revealed a major cellular water fraction of around 76% with 250 times slower dynamics than bulk water (Tehei et al. 2007). The slow water fraction at 300 K showed characteristic signs for confined motions in a restricted volume. That study also revealed that cell water dynamics in *E. coli* is not governed by such a slow water fraction (Tehei et al. 2007). Tehei et al. therefore suggested that an ordering effect of water molecules, KCl and halophilic proteins is responsible for the large slow water fraction in *H. marismortui* (Tehei et al. 2007).

Fast bulk-like dynamics of water are in the order of some picoseconds, whereas interfacial water motions are slowed down and are in the order of some ten picoseconds. Quasielastic neutron scattering is a well suited technique for the study of the microscopic nature of water dynamics.

## 3.2 Properties, Production and Detection of Neutrons

The neutron is a nuclear particle that decays into a proton, an electron and an electron antineutrino with a half-life of 887.6±3 s (Mampe et al. 1989) (ß decay mediated via the weak interaction). The energy of 0.77 MeV that is produced during the decay is shared between the proton, the electron and the antineutrino.

$$n \rightarrow p^{+} + e^{-} + \overline{\upsilon}_{e} + 0.77 Mev$$

Neutrons can be described as waves with the wave vector $\vec{k}$ defined by

$$\left|\vec{k}\right| = \frac{2\pi}{\lambda}, \qquad \textbf{( 3.1 )}$$

where $\lambda$ is the wave length of the neutron.

The momentum $\vec{p}$ of the neutron is given by

$$\vec{\mathrm{p}} = \mathrm{m_n}\vec{\mathrm{v}} = \hbar\vec{\mathrm{k}}, \qquad \textbf{( 3.2 )}$$

with the mass of the neutron $m_n$ and its velocity $\vec{\mathrm{v}}$. The kinetic energy of the neutron is

$$\mathrm{E_{kin}} = \frac{\hbar^2 \mathrm{k}^2}{2\mathrm{m_n}}. \qquad \textbf{( 3.3 )}$$

Several properties of the neutron are summarized in **Table 2**.

**Table 2:** Properties of the neutron

| | |
|---|---|
| Mass | $m_n$=1.675·10$^{-27}$ kg |
| Charge | 0 |
| Spin | 1/2 |
| Magnetic Moment | $\mu_n$=-0.966·10$^{-26}$ J T$^{-1}$ |

Although ~50% of all matter consists of neutrons, it is difficult to extract bound neutrons from the atomic nuclei. Free neutrons need to be produced by nuclear reactions. A high flux is mandatory for scientific investigations using neutron beams. Research neutron sources either use nuclear fission or spallation for the production of high flux neutron beams. Both nuclear fission and spallation are schematically presented in **Figure 1**. Examples for reactor neutron sources are the High Flux Reactor at the Institut Laue-Langevin (Grenoble, France) and the Research Reactor Heinz Maier-Leibnitz at the Technical University Munich (Garching, Germany). Neutron spallation sources are the ISIS pulsed spallation source at the Rutherford Appleton Laboratory (Didcot, United Kingdom) and the continuous spallation source SINQ at Paul Scherrer Institut (Villigen, Switzerland).

The produced neutrons have energies in the range of some MeV. This energy is too high for neutron scattering experiments. In reactor sources, the neutron energy has also to be reduced in order to maintain the chain reaction. Therefore, the kinetic energy of the neutrons needs to be changed by thermal equilibration with moderator elements that are kept at different temperatures. In the moderators the neutrons exchange their kinetic energy with the moderator atoms through collisions. At thermal equilibrium the velocities of the neutrons follow a Maxwell distribution determined by the temperature of the moderator. So called thermal neutrons are produced with moderators at ambient temperature, while cold neutrons are obtained from mainly liquid hydrogen or deuterium moderators at ~25 K.

A thermal neutron produced by a moderator at T=293 K has got in average a kinetic energy of E=25 meV, a wavelength of $\lambda$=1.8 Å and a velocity of 2200 m/s.

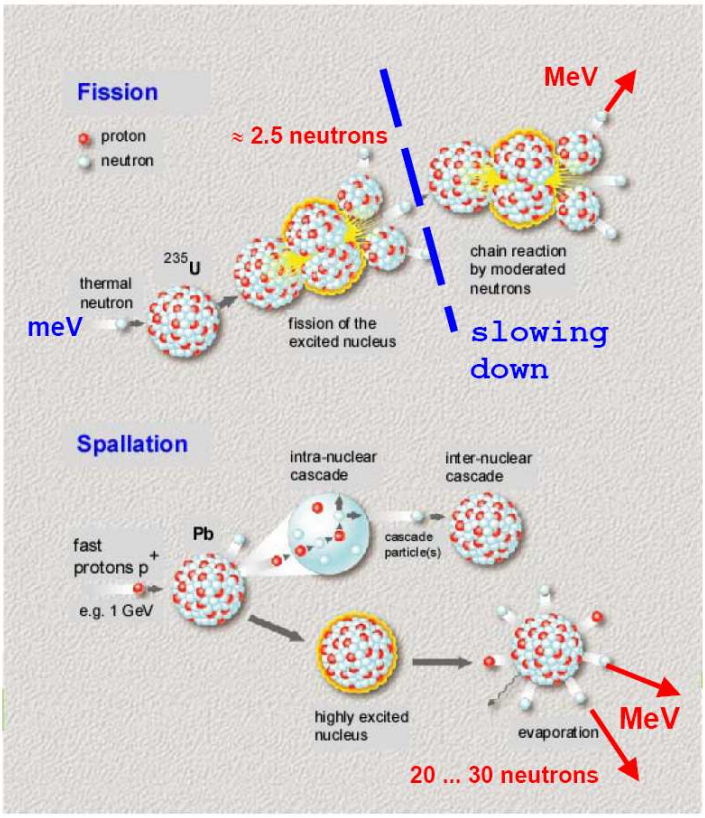


**Figure 1:** Schematic presentation of the nuclear fission and spallation process (Richter 2003). Neutrons are produced in reactors through the fission of Uranium$^{235}$. The excited Uranium decays into a series of fission products, including in average ~2.5 neutrons with energies in the order of some MeV. These high energy neutrons need to be moderated such that they can maintain the nuclear chain reaction. In spallation sources, protons are accelerated to high energies and brought to collision with heavy metal targets. The excited target nuclei evaporate in average ~20-30 neutrons with energies in the order of some MeV.

Neutrons are detected indirectly via nuclear reactions that produce charged particles. The charged particles can then be detected by appropriate detectors such as for example proportionality counters or photo multipliers.

Proportionality counters are filled with a gas that contains $^{3}$He. The helium isotope absorbs neutrons efficiently. The products of the nuclear reaction are charged protons or tritons with energies in the order of one MeV and $e^{-}$. Scintillation counters are enriched with $^{6}$Li and ZnS. Neutron absorption leads to fluorescence radiation that can be detected with photo multipliers.

## 3.3 Scattering Processes and Observational Limits

We now consider the scattering of a neutron by a sample. Let $\vec{k}$ and $\vec{k}'$ be the wave vectors of the incident and scattered neutron, respectively. A scheme of the scattering process is given in **Figure 2**.

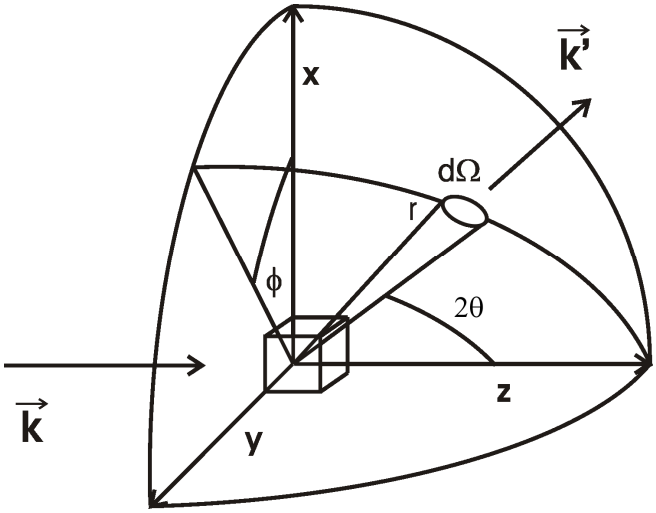


**Figure 2:** Scheme of the scattering process of neutrons with a sample. An incident neutron enters from the left and is scattered into the solid angle $d\Omega$. The incident neutron has got the wave vector $\vec{k}$, the scattered neutron the wave vector $\vec{k}'$. The direction of $\vec{k}'$ is determined by the scattering angle $2\theta$ and the azimuthal angle $\phi$. The sample is indicated as a box at the centre of the coordinate system and the wave vector of the incident neutron beam is parallel to the *z*-axis.

The difference in kinetic energy *E* between the incident and scattered neutron is

$$E = \frac{\hbar^2}{2m_n}\left(k^2 - k'^2\right), \qquad \textbf{( 3.4 )}$$

*E* is also called energy transfer. Positive values of *E* correspond to the situation when the neutron deposits energy in the sample. In the case of negative values of *E*, the neutron gains energy from the sample.

If $E$=0 than the process is called *elastic scattering*. If there occurs exchange of energy between the neutron and the sample with $E \neq 0$, then the event is called *inelastic scattering*.

The difference in momentum between the incident and scattered neutron is

$$\hbar\vec{q} = \hbar\vec{k} - \hbar\vec{k}', \qquad \textbf{( 3.5 )}$$

with the so called scattering vector $\vec{q}$. Sometimes, in analogy with crystallography, the scattering vector is defined as $\vec{q} = \vec{k}' - \vec{k}$.

In the case of elastic scattering $k = k'$ and the scattering vector $q$ can be written as

$$q = |\vec{q}| = 4\pi \frac{\sin(\theta)}{\lambda}, \qquad \textbf{( 3.6 )}$$

with the scattering angle $2\theta$ as defined in **Figure 2**.

For inelastic scattering processes it is $k \neq k'$ and **equation ( 3.6 )** is not valid anymore. The connection $\hbar\vec{q} = \hbar\vec{k} - \hbar\vec{k}'$ can be written as

$$\mathrm{q}^2 = \mathrm{k}'^2 + \mathrm{k}^2 - 2\mathrm{k}'\mathrm{k}\cos(2\theta). \qquad \textbf{( 3.7 )}$$

With the energy transfer $E$ it is

$$k'^2 = k^2 - \frac{2m_n E}{\hbar^2}. \qquad \textbf{( 3.8 )}$$

This can be written finally as

$$q^2 = 2k^2 - \frac{2m_n E}{\hbar^2} - 2k\cos(2\theta)\sqrt{k^2 - \frac{2m_n E}{\hbar^2}}, \qquad \textbf{( 3.9 )}$$

which describes the fundamental kinematic connection for neutrons between scattering vector *q*, energy transfer *E* and scattering angle $2\theta$. This relation gives the limiting boundaries of the accessible *q*-*E* space for any neutron spectrometer. The connection between *q*, *E* and $2\theta$ according to **equation ( 3.9 )** is plotted exemplarily in **Figure 3** for neutrons with the incident energy $E_{kin}$=3.14 meV. It is important to notice that the scattering vector *q* changes as a function of *E* at a fixed scattering angle $2\theta$.

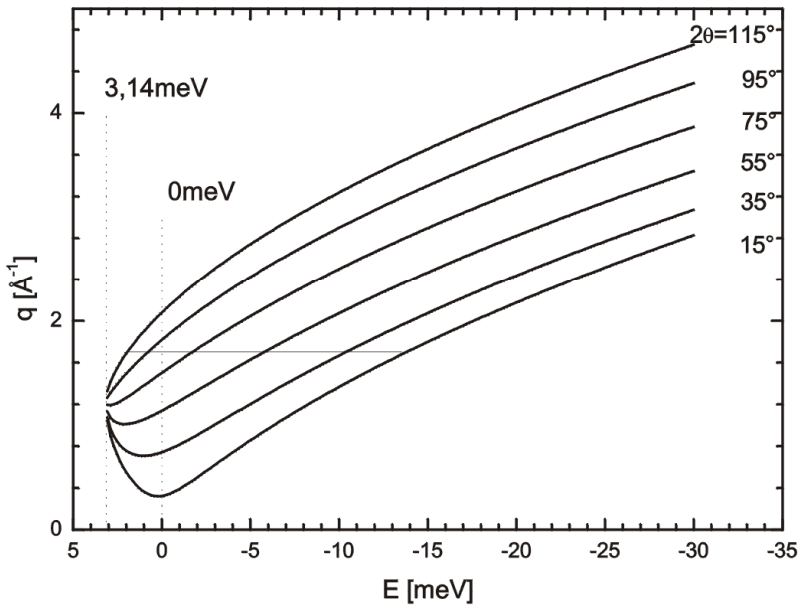


**Figure 3:** The connection between scattering vector *q*, energy transfer *E* and scattering angle $2\theta$. In this plot the kinetic energy of the incident neutron is $E_{kin}$=3.14 meV, which corresponds to a neutron wave length of $\lambda$=5.1Å. The maximum energy transfer E is determined by the kinetic energy of the neutron that it can deposit in the sample; it is indicated by the vertical dotted line at E=3.14 meV. The energy transfer in the case of elastic scattering is E=0, which is shown by the vertical dotted line at E=0. The solid horizontal line indicates the scattering vector q=1.7Å$^{-1}$, as shown in **Figure 4**.

If the incident neutrons have a fixed kinetic energy and neutron scattering shall be measured at constant scattering vector *q* as a function of energy transfer *E*, then the scattering angle value of the detector position has to be varied according to **equation ( 3.9 )** (see **Figure 3**).

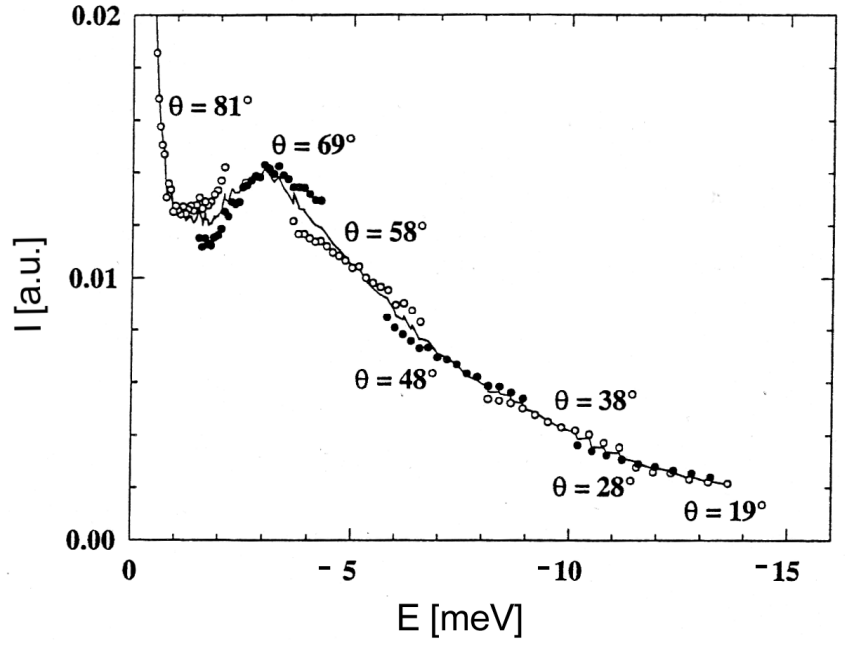


**Figure 4:** Different scattering angles need to be connected to cover a broad energy transfer range at constant scattering vector q=1.7Å$^{-1}$. It is schematically illustrated how experimental data measured at different detector positions are joined together (Settles 1996). At energy transfer values close to E=0 it is not necessary to merge different detector positions.

## 3.4 Elements of Neutron Scattering Theory

A neutron scattering experiment with angular and energy resolution measures the double differential scattering cross section $\frac{\mathrm{d}^2\sigma}{\mathrm{d}\Omega\mathrm{d}E}$, which is the number of neutrons that are scattered per second into the solid angle $d\Omega$ in the direction of the scattering vector $\vec{k}'$ with an energy in the interval between $E$ and $E+dE$, normalised by the incident neutron flux $\Phi$.

The incident neutron wave can be written as a plane wave with

$$\psi(\vec{r}) = e^{i\vec{k}\vec{r}} \qquad \textbf{( 3.10 )}$$

The scattered neutron wave $\psi'(\vec{r})$ can be written at sufficient large distance as a sum of the transmitted wave and a spherical wave multiplied with the scattering amplitude $f(\Omega)$

$$\psi'(\vec{r}) = e^{i\vec{k}\vec{r}} + \frac{e^{i\vec{k}'\vec{r}}}{r} f(\Omega). \qquad \textbf{( 3.11 )}$$

The neutron interacts with the sample via nuclear and magnetic forces. The nuclear interaction depends on the element, the isotope and the orientation of the spin of the neutron and the spin of the nucleus of the sample.

The magnetic interaction is neglected in the following and only the nuclear interaction is further considered. The wave length of thermal neutrons is in the order of some $10^{-10}$ m, the diameter of the nucleus of an atom is around $10^{-15}$ m which is much smaller than the neutron wave length. The phenomenological assumption of a point like interaction potential (Fermi pseudo potential) has been proven to be very successful in the theory of neutron scattering. However, this assumption is only valid to describe scattering of cold and thermal neutrons and fails completely for high energy neutrons.

The Fermi pseudo potential has the form

$$V(\vec{r}) = \frac{2\pi\hbar^2}{m_n} \cdot b \cdot \delta\left(\vec{r} - \vec{R}\right), \qquad \textbf{( 3.12 )}$$

with the scattering length *b* that is a complex number. The real part of *b* describes the scattering strength, the imaginary part of *b* the absorption.

The further evaluations of the double differential scattering cross section take into account the Fermi pseudo potential and the so called Born approximation that is a first order approximation of the scattering process. Only single scattering is considered. The double differential scattering cross section finally can be written as

$$\frac{\mathrm{d}^2\sigma}{\mathrm{d}\Omega\mathrm{d}E} = \frac{1}{2\pi\hbar}\frac{\mathrm{k}'}{\mathrm{k}}\sum_{\mathrm{j},\mathrm{j}'}\int_{-\infty}^{+\infty} < \mathrm{b}_{\mathrm{j}}\mathrm{b}_{\mathrm{j}'}\exp\left[\mathrm{i}\vec{\mathrm{q}}\vec{\mathrm{r}}_{\mathrm{j}}(0)\right]\exp\left[-\mathrm{i}\vec{\mathrm{q}}\vec{\mathrm{r}}_{\mathrm{j}'}(\mathrm{t})\right] > \mathrm{e}^{-\mathrm{i}\omega\mathrm{t}}\mathrm{dt}\,. \qquad \textbf{( 3.13 )}$$

The indices *j* and *j'* account for the atoms in the sample. The scattering length $b_j$ depends on the element, the isotope and the orientation of the spins. The position of the atom j at time t=0 is $\vec{r}_j(0)$; its position is $\vec{r}_j(t)$ at time t.

The sum in **equation ( 3.13 )** can be split into two parts,

$$\frac{d^2\sigma}{d\Omega dE} = \frac{1}{2\pi\hbar}\frac{k'}{k}b_{coh}{}^2\sum_{j,j'}\int_{-\infty}^{+\infty} < \exp\left[i\vec{q}\vec{r}_j(0)\right]\exp\left[-i\vec{q}\vec{r}_{j'}(t)\right] > e^{-i\omega t}dt + \qquad \textbf{( 3.14 )}$$

$$\frac{1}{2\pi\hbar}\frac{k'}{k}b_{inc}{}^2\sum_{j}\int_{-\infty}^{+\infty} < \exp\left[i\vec{q}\vec{r}_j(0)\right]\exp\left[-i\vec{q}\vec{r}_j(t)\right] > e^{-i\omega t}dt \,,$$

with the so called *coherent* scattering length $b_{coh}$

$$\mathrm{b}_{\mathrm{coh}}{}^2 = \langle \mathrm{b} \rangle^2, \qquad \textbf{( 3.15 )}$$

and the so called *incoherent* scattering length $\mathrm{b}_{inc}$

$$\mathrm{b_{inc}}^2 = \left\langle \mathrm{b}^2 \right\rangle - \left\langle \mathrm{b} \right\rangle^2 . \qquad \textbf{( 3.16 )}$$

The coherent scattering length is the average scattering length of the element. The incoherent scattering length is the standard deviation from the average.

The first term in **equation ( 3.13 )** is called *coherent scattering*, while the second term is the *incoherent scattering*. The double sum in the first term of **equation ( 3.14 )** contains cross terms of the different atoms *j* and *j'*; the second term only contains the self term and runs over the different atom as a single sum of *j*. The double differential scattering cross section can be written shortly as

$$\frac{d^2\sigma}{d\Omega dE} = \frac{d^2\sigma}{d\Omega dE}_{coh} + \frac{d^2\sigma}{d\Omega dE}_{inc} . \qquad \textbf{( 3.17 )}$$

Coherently scattered neutrons from different nuclei can interfere with each other. These interferences contain both information of structure and collective excitations of the sample. An ideal system would give purely coherent scattering if all atoms in the sample of the same element have the average scattering length of the element <*b*> and do not deviate from the average. Deviation from the average occurs, for example, with variation in the spin state of the nuclei.

Incoherent scattering contains information about the dynamics of the individual atoms. It can be interpreted as a superposition of neutron waves that were scattered from the same nucleus at different times. The time range is determined by the energy resolution of the instrument. The physical reason for the existence of incoherent scattering is the random distribution of scattering nuclei that have a deviation from the average scattering length <*b*>.

Scattering cross sections $\sigma_{inc}$, $\sigma_{coh}$ and scattering lengths $b_{inc}$, $b_{coh}$ are connected by the relations:

$$\sigma_{inc} = 4\pi {b_{inc}}^2 , \qquad \textbf{( 3.18 )}$$

$$\sigma_{coh} = 4\pi b_{coh}^{\ 2}. \qquad \textbf{( 3.19 )}$$

The incoherent scattering cross section of hydrogen is the largest of all elements that usually occur in biological matter (see **Table 3**). The reason for this behaviour is that the scattering length for different spin orientations between the neutron and the proton spin differs rather strongly. Incoherent scattering of natural abundance proteins is dominated by hydrogen atoms. The incoherent scattering cross section of hydrogen is around 40 times larger than that of deuterium. Therefore, hydrogen/ deuterium labelling is made possible. Scattering of natural abundance proteins in $D_2O$ solvent is dominated by the protein signal, whereas scattering of deuterated proteins hydrated with $H_2O$ allows to focus on the signal of the solvent. The unit of the scattering cross section is the barn with 1 barn = $10^{-24}$ $cm^2$.

**Table 3:** Coherent and incoherent scattering cross sections for elements occurring in biological systems (Sears 1992).

| **Element** | **$\sigma_{coh}$ [barn]** | **$\sigma_{inc}$ [barn]** |
|---|---|---|
| H | 1.7568 | 80.26 |
| D | 5.592 | 2.05 |
| C | 5.551 | 0.001 |
| N | 11.01 | 0.5 |
| O | 4.232 | 0.0008 |
| P | 3.307 | 0.005 |
| S | 1.0186 | 0.007 |
| Fe | 11.22 | 0.4 |

## 3.5 Connecting Theory with Experiments

The Van Hove pair correlation function describes the microscopic structure and dynamics of the sample (Van Hove 1954). Van Hove showed mathematically in his article how the theoretical pair correlation function can be related to measurable neutron scattering quantities. The work paved the ground for all the models on microscopic motion that came afterwards. The pair correlation function is defined as

$$G(\vec{r},t) = \frac{1}{N}\sum_{j,j'}^{N}\left\langle \delta\left[\vec{r} + \vec{r}_j(0) - \vec{r}_{j'}(t)\right]\right\rangle . \qquad \textbf{( 3.20 )}$$

The pair correlation function contains the probability to find a scattering particle at time *t* at the position $\vec{r}(t)$, when it was at time *t*=0 at the position $\vec{r}(0)$. *N* is the number of atoms.

The self term of the pair correlation function is

$$\mathrm{G_s}(\vec{\mathrm{r}},\mathrm{t}) = \frac{1}{\mathrm{N}}\sum_{\mathrm{j}}^{\mathrm{N}}\left\langle \delta\left[\vec{\mathrm{r}} + \vec{\mathrm{r}}_{\mathrm{j}}(0) - \vec{\mathrm{r}}_{\mathrm{j}}(\mathrm{t})\right]\right\rangle . \qquad \textbf{( 3.21 )}$$

The intermediate scattering function

$$I(\vec{q},t) = I_{coh}(\vec{q},t) + I_{inc}(\vec{q},t) \qquad \textbf{( 3.22 )}$$

is obtained by a space Fourier transformation of the Van Hove pair correlation function. The incoherent part of the intermediary scattering function $I_{inc}(\vec{q},t)$ is related with the self-term $\mathrm{G_s}(\vec{\mathrm{r}},\mathrm{t})$. The coherent part $I_{coh}(\vec{q},t)$ is connected with the pair correlation function $\mathrm{G}(\vec{\mathrm{r}},\mathrm{t})$:

$$\mathrm{I_{coh}}(\vec{\mathrm{q}},\mathrm{t}) = \int \mathrm{G}(\vec{\mathrm{r}},\mathrm{t})\mathrm{e}^{-\mathrm{i}\vec{\mathrm{q}}\vec{\mathrm{r}}}\,\mathrm{d}\vec{\mathrm{r}} = \frac{1}{\mathrm{N}}\sum_{\mathrm{j,j'}}\left\langle \exp\left[\mathrm{i}\vec{\mathrm{q}}\vec{\mathrm{r}}_{\mathrm{j}}(0)\right]\exp\left[-\mathrm{i}\vec{\mathrm{q}}\vec{\mathrm{r}}_{\mathrm{j'}}(\mathrm{t})\right]\right\rangle \qquad \textbf{( 3.23 )}$$

$$I_{inc}(\vec{q},t) = \int G_s(\vec{r},t)e^{-i\vec{q}\vec{r}}d\vec{r} = \frac{1}{N}\sum_j \left\langle \exp\left[i\vec{q}\vec{r}_j(0)\right]\exp\left[-i\vec{q}\vec{r}_j(t)\right]\right\rangle . \quad \textbf{( 3.24 )}$$

The intermediary scattering functions can be calculated nowadays from molecular dynamics simulations. Measured neutron data can be compared to these simulations and molecular events that are responsible for the measured processes can be eventually identified.

The scattering function $S(\vec{q},\omega)$ in energy space is obtained by a time Fourier transformation of the intermediate scattering function

$$S(\vec{q},\omega) = \frac{1}{2\pi}\int I(\vec{q},t)e^{-i\omega t}dt . \quad \textbf{( 3.25 )}$$

The scattering function $S(\vec{q},\omega)$ can also be divided into a coherent part and an incoherent part

$$S(\vec{q},\omega) = S_{coh}(\vec{q},\omega) + S_{inc}(\vec{q},\omega) . \quad \textbf{( 3.26 )}$$

The experimentally accessible double differential scattering cross section is connected to the scattering function with

$$\frac{d^2\sigma}{d\Omega dE} = N\frac{\sigma_{coh}}{4\pi}\frac{k'}{k}S(q,\omega)_{coh} + N\frac{\sigma_{inc}}{4\pi}\frac{k'}{k}S(q,\omega)_{inc} . \quad \textbf{( 3.27 )}$$

Measured incoherent neutron scattering data in the form of $\frac{d^2\sigma}{d\Omega dE}_{inc}$ can be corrected with computer programs for the term $\frac{k'}{k}$ and the scattering function $S(q,\omega)_{inc}$ is containing information about the dynamics of the sample.

## 3.6. Elastic and Quasielastic Incoherent Neutron Scattering

Energy resolved incoherent neutron scattering allows the study of molecular motions in the order of picoseconds to nanoseconds. The observable time range is determined by the energy resolution of the spectrometer. The detectable length scale of the motion is in the range of some Ångstrom and is given by the scattering vector range of the instrument. Energy and time ranges of molecular motions that can be detected by neutron spectroscopy are given and compared to other experimental techniques in **Figure 5**. Incoherent neutron scattering data of biomolecules or water informs about the dynamics of hydrogen atoms as their scattering cross section is much larger than all other elements that usually occur in biological matter. Hydrogen atoms are uniformly distributed in proteins and around every second atom of a protein is a hydrogen atom. Therefore, average protein dynamics can be detected with incoherent neutron scattering experiments.

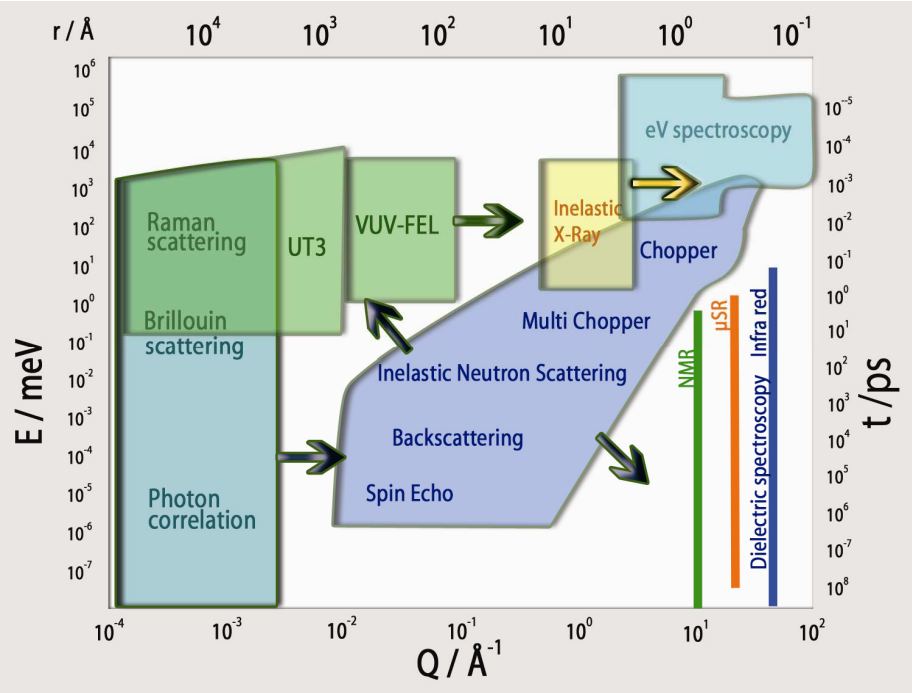


**Figure 5:** The covered energy and time range that can be covered with inelastic neutron scattering is compared with other various experimental methods. Chopper, multi chopper, backscattering and spin echo neutron spectrometers are different instrumental techniques that allow increasing energy resolution (http://neutron.neutron-eu.net/n_nmi3 2008).

A typical incoherent neutron scattering spectrum is shown in **Figure 6** when molecular long range diffusion is absent. The graph shows elastic, quasielastic and inelastic neutron scattering features.

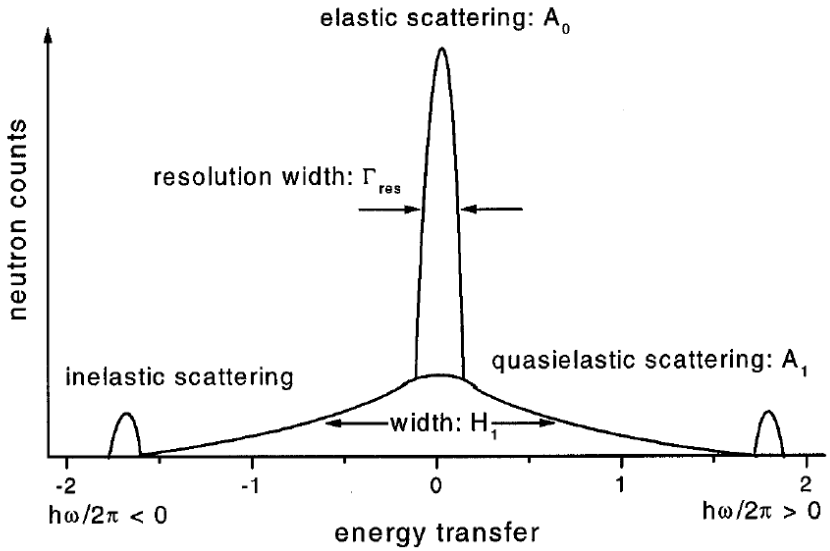


**Figure 6:** Typical incoherent neutron scattering data at a fixed scattering vector. Elastic, quasielastic and inelastic parts of the spectrum are indicated. Elastic neutron scattering refers to the detected intensity $A_0$ at the energy transfer $E=0$. The elastic peak is always broadened by the finite energy resolution $\Gamma_{res}$ of the instrument. Quasielastic intensity is caused by diffusive motion and is responsible for the broad wings of the spectrum with the width $H_1$. Inelastic scattering is caused by molecular excitations and vibrations and causes features in the spectrum at large energy transfer values (Fitter and Lechner 1998).

Elastic incoherent neutron scattering (EINS) refers to neutrons that do not exchange energy with the sample and are detected at zero energy transfer $E=0$. The elastic peak with intensity $A_0$ is always broadened by the finite energy resolution $\Gamma_{res}$ of the instrument. The intensities of the elastic peak as a function of the scattering vector contain information about the amplitude and geometry of molecular motion.

Quasielastic neutron scattering (QENS) is visible as broad wings centred at zero energy transfer around the elastic peak. Molecular diffusive and rotational motions give rise to the quasielastic broadening. Simple diffusion is described by a single exponential in time space. The Fourier transformation of an exponential is a Lorentzian function in energy space. The quasielastic signal is mathematically described by a sum of Lorentzian functions with

characteristic intensities and half-widths at half-maximum (HWHM) $\Gamma$. Microscopic model are employed to analyse the HWHM. Within the framework of the models diffusion coefficients *D*, residence times $\tau$ and correlation times $\tau_c = 1/\Gamma$ can be determined. The measured energy transfer range of QENS spectra depends strongly on both the energy resolution and the instrumental properties of the neutron spectrometer. Approximately, on a time-of-flight instrument with an energy resolution of ~100μeV the energy transfer range used for QENS is in between around -1.5meV and +1.5meV.

Molecular excitations cause inelastic neutron scattering at high values of the energy transfer |*E*|. The typical measured energy transfer range of inelastic neutron scattering is in between ~1 and 200meV.

In this work we focus only on elastic and quasielastic neutron scattering.

The theoretical scattering function for elastic and quasielastic neutron scattering can be written as (Bee 1988)

$$S_{theo}(q,\omega) = e^{-<x^2>q^2} \cdot \left[ A_0(q) \cdot \delta(\omega) + \sum_n A_n(q) \cdot L_n(\omega) \right] \qquad \textbf{( 3.28 )}$$

The delta function $\delta(\omega)$ needs to be taken into account if there are motions in confinement, or if the dynamics are much slower than the resolution of the instrument. The factor $A_0(q)$ is called *Elastic Incoherent Structure Factor* (EISF) and contains information about the amplitude and geometry of motions. The quasielastic component is described by a sum of Lorentzians $L_n(\omega)$ with the Quasielastic Incoherent Structure Factors $A_n(q)$. Faster vibrational motions are contained in the Debye-Waller factor $e^{-<x^2>q^2}$, with $<x^2>$ the mean square displacement of fast vibrational motions.

In the presence of long range translational diffusion the theoretical scattering function needs to be extended. It is commonly assumed in literature that long-range translational diffusion and internal motions are independent of each other, as it facilitates data analysis. This might not necessarily be the case for all systems and is then only an approximation. The presence of

long range translational diffusion then leads to a convolution of **equation ( 3.28 )** with the scattering function for long-range translational diffusion $S_{TD}(q,\omega)$

$$S_{theo}(q,\omega) = e^{-<x^2>q^2} \cdot \left[ A_0(q) \cdot S_{TD}(q,\omega) + \left( \sum_n A_n(q) \cdot L_n(\omega) \right) \otimes S_{TD}(q,\omega) \right]. \qquad \textbf{( 3.29 )}$$

When there is a fraction *p* of hydrogen atoms that appear immobile within the resolution of the spectrometer, the EISF can be written as

$$A_0(q) = p + (1-p) \cdot A_0'(q), \qquad \textbf{( 3.30 )}$$

with $A_0'(q)$ the EISF for the dynamics of the hydrogen atoms that appear mobile.

The measured QENS data are then fitted with the theoretical scattering function $S_{theo}(q,\omega)$ that is convoluted with the instrumental energy resolution $S_{res}(q,\omega)$ as

$$S_{meas}(q,\omega) = [S_{theo}(q,\omega) + B] \otimes S_{res}(q,\omega), \qquad \textbf{( 3.31 )}$$

where *B* is a linear function that accounts for background contribution.

## 3.7 Instruments Used for Incoherent Neutron Spectroscopy

All neutron spectrometers need to measure the intensity of scattered neutrons by the sample as a function of energy transfer *E* and scattering vector *q*. Two experimental techniques, *time-of-flight spectroscopy* and *backscattering spectroscopy*, were used in this work to measure elastic and quasielastic incoherent neutron scattering. Three axis neutron spectrometers are widely used in condensed matter physics for the study of collective excitations in single crystals. The highest energy resolution is reached with neutron spin echo spectrometers and slow relaxation times up to 200 ns can be detected with current instruments. A neutron spin echo spectrometer at the American spallation source SNS is in construction which is planned to detect relaxation times up to 1 µs.

At reactor sources a monochromatic neutron beam needs to be extracted by the primary spectrometer from the polychromatic neutron beam coming from the reactor. In the case of crystal time-of-flight and backscattering spectrometers this is achieved with a single crystal using Bragg reflections. After the single crystal the monochromatic beam is then cut into neutron pulses with a rotating chopper. Multi chopper time-of-flight instruments use a set of counter rotating chopper discs to prepare a monochromatic and pulsed neutron beam. The prepared monochromatic neutron beam has a certain energy bandwidth given by $\Delta E$. At spallation sources the time structure of the incident neutron beam allows the use of a polychromatic beam for measurements. The neutrons then interact with the sample contained in the sample holder, located inside of a cryostat for temperature control.

Time-of-flight instruments contain a large neutron detector bank of up to 400 detectors that are placed at a certain distance, radially around the sample. The large number of detectors allows a simultaneous measurement of scattered neutrons over a large solid angle. Time-of-flight spectrometers are therefore efficient for a rapid mapping of a large scattering vector range. A pulsed beam of neutrons arrives at the sample. Neutron scattering in the detector bank is then measured as a function of time. Neutrons that gain energy from the sample will be faster and arrive first at the detectors. Elastically scattered neutrons without energy exchange arrive afterwards and neutrons that deposit part of their kinetic energy in the sample arrive latest. The time resolution of these instruments is determined by the energy bandwidth $\Delta E$ of the prepared neutron beam. Typically, crystal time-of-flight instruments operate at energy resolutions between around 50 to 200 µeV (FWHM). Multi-Chopper time-of-flight spectrometers can be set to a nearly continuous energy resolution between around 5 µeV and 5 meV (FWHM).

Backscattering spectrometers reach a high energy resolution by the principle of Bragg reflection. If a neutron beam is reflected by a crystal in a geometry close to 90° the reflected beam has a very small energy dispersion. Neutrons are scattered by the sample in the direction of analyzer plates. The analyzer plates reflect and focus the neutrons under nearly backscattering conditions into neutron detectors. In this way typical energy resolutions between 0.9 and 8 µeV are reached at reactor sources. Due to the small energy bandwidth, neutron backscattering has always lower counting statistics than time-of-flight spectroscopy. To compensate at least partially this effect neutron analyser plates need to cover large solid angles at the expense of scattering vector resolution. At spallation sources, the so called

*inverse backscattering spectrometers* are used. This class of instruments utilizes a polychromatic neutron beam and the time structure given by the spallation source. Higher counting rates are possible at the expense of energy resolution.

**Table 4:** Time-of-flight and backscattering spectrometers at the institutes ILL, ISIS, PSI and FRM-II used in this work. Given is the incident wavelength, the instrumental energy resolution, the corresponding time resolution and the covered scattering vector range.

| **Instrument** | **λ [Å]** | **ΔE [μeV]** | **Δt [ps]** | **q [Å$^{-1}$]** |
|---|---|---|---|---|
| IN13, ILL | 2.23 | 8 | ~100 | 0.2-5.0 |
| IRIS, ISIS | ~5 | 17 | ~40 | 0.3-1.8 |
| FOCUS, PSI | 6 | 50 | ~13 | 0.4-1.6 |
| TOFTOF, FRM-II | 5.1 | 100 | ~7 | 0.4-2.0 |

The characteristic properties of neutron spectrometers that were used in this work are given in **Table 4**.

In an incoherent neutron experiment the sample inside the aluminium sample holder and the empty sample holder need to be measured. To obtain only the scattered intensities of the sample, the empty sample holder has to be correctly subtracted. The neutron detectors are calibrated by a reference scatterer. In the case of hydrated powder samples this can be done with the sample itself at low temperature where molecular motions are strongly reduced (usually between 10 to 20 K). If the sample contains larger amounts of water which can form ice at low temperatures or if the sample is sensitive to freezing then vanadium is used as a reference. The coherent scattering cross section of vanadium is around 300 times smaller than the incoherent scattering cross section (Sears 1992). Quasielastic line broadening is absent and the inelastic signal due to phonon excitations is small compared to the elastic signal. The Debye-Waller factor of vanadium is large; therefore vanadium gives a purely incoherent and isotropic signal that can be used for neutron detector calibration.

## 3.8 Mean Square Displacements and Force Constants obtained from Elastic Incoherent Neutron Scattering

Model independent mean square displacements $<u^2>$ can be determined from the measured intensities at zero energy transfer.

The intermediary incoherent scattering function $I(\vec{q},t)_{inc}$ of a system consisting of *N* atoms is

$$I(\vec{q},t)_{inc} = \frac{1}{N}\sum_i \left\langle \exp\left(i\vec{q}\left[\vec{r}_i(0) - \vec{r}_i(t)\right]\right)\right\rangle . \qquad \textbf{( 3.32 )}$$

This expression can be simplified in the Gaussian approximation. The approximation assumes that the distribution of the atoms around their average position follows a Gaussian function. However, as *q* approaches zero, the approximation is valid for any motion localised in the length-time window of the spectrometer. Knapp simplified $I(\vec{q},t)_{inc}$ under this assumption as (Knapp et al. 1982)

$$I(\vec{q},t)_{inc} \approx \frac{1}{N}\sum_i \exp\left(-\frac{1}{6}\cdot q^2 \langle\left[\vec{r}_i(0) - \vec{r}_i(t)\right]^2\rangle\right). \qquad \textbf{( 3.33 )}$$

The mean square displacements $\left\langle u_i^2 \right\rangle$ of atom *i* are introduced as

$$\left\langle u_i^2 \right\rangle = \langle\left[\vec{r}_i(0) - \vec{r}_i(t)\right]^2\rangle . \qquad \textbf{( 3.34 )}$$

They correspond to the full amplitude of motion (Smith 1991) and can be compared to values obtained from molecular dynamic simulations.

In the long time limit with $t \to \infty$ the elastic incoherent scattering function $S(q,0)_{inc}$ reads

$$S(q,0)_{inc} = \frac{1}{N}\sum_i \exp\left(-\frac{1}{6}\cdot q^2 \left\langle u_i^{\,2}\right\rangle\right) \qquad \textbf{( 3.35 )}$$

and the average mean square displacement can be obtained from the slope of the logarithm of the scattered intensities versus $q^2$ according to

$$\left\langle u^2 \right\rangle = \frac{-6 \cdot \Delta \ln S(q,0)}{\Delta q^2} . \qquad \textbf{( 3.36 )}$$

This approach is formally similar to the Guinier approximation in small angle scattering experiments (Guinier and Fournet 1955). The approximation is strictly valid for $q^2 \to 0$ but holds up to $\left\langle u^2 \right\rangle \cdot q^2 \sim 2$ (Réat et al. 1997).

A neutron scattering instrument always has a finite energy resolution $\Delta E$ and a corresponding time resolution of $\Delta t = \frac{\hbar}{\Delta E}$; a certain scattering vector range is covered by the instrument. Only motions that are in the accessible length scale given by the scattering vector range and the time resolution of the instrument can be detected. Therefore, mean square displacements $<u^2>$ depend on the kind of neutron spectrometer used.

Mean square displacements are often measured as a function of temperature in so called elastic scans on backscattering instruments with high energy resolution. The measured intensities at zero energy transfer are rather large, thus elastic scans rapidly allow a determination of the molecular dynamics as a function of temperature. As an example, **Figure 7** shows the measured mean square displacements of purple membrane in the dry and hydrated state.

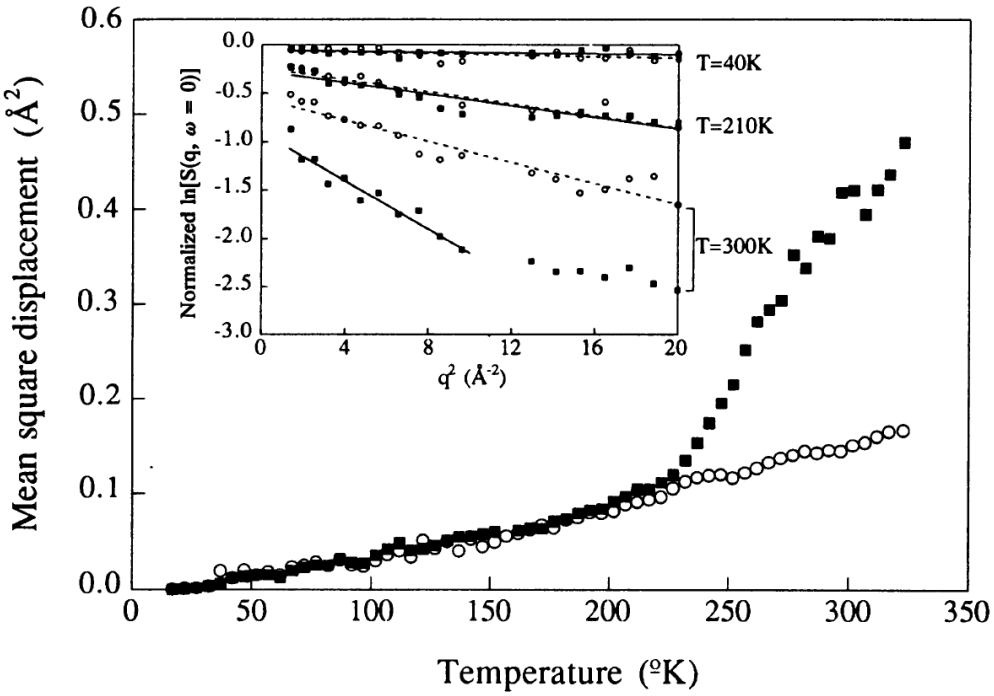


**Figure 7:** Hydrogen mean square displacements $<u^2>$ of purple membrane in dry (○) and hydrated state (■) in the length and time scale given by the instrumental scattering vector range (see inset) and energy resolution. Water content in hydrated state was 0.55 $D_2O$/ g dry membrane (Ferrand et al. 1993). Data was measured on the backscattering instrument IN13 at ILL and was analysed within the Gaussian approximation according to **equation ( 3.35 )**. The inset shows measured intensities as a function of $q^2$ at different temperatures.

A mean effective force constant $<k'>$ can be obtained from the dependence of the $<u^2>$ as function of temperature (Zaccai 2000). The force constant is defined as

$$< k >= \frac{0.00276}{d < u^2 > / dT}, \qquad \textbf{( 3.37 )}$$

the values are chosen in such a way that $<k>$ is in N/m when $<u^2>$ is in Å$^2$ and $T$ in Kelvin.

# 3.9 Models for Quasielastic Neutron Scattering

Quasielastic incoherent neutron scattering allows a precise determination of molecular dynamics. The geometry of motions can be extracted from the EISF. The half-widths at half-maximum (HWHM) of the quasielastic components contain information about diffusion coefficients and residence times. The dependence of the HWHM as a function of the scattering vector contains information on the nature of diffusive dynamics. Microscopic models are needed to interpret QENS data. In the following the common models that were used in this work are presented.

## *3.9.1 Long Range Translational Diffusion*

The scattering function for continuous translational diffusion can be written as a simple Lorentzian with (Bee 1988)

$$S_{TD}(q,\omega) = \frac{1}{\pi} \cdot \frac{Dq^2}{\omega^2 + \left(Dq^2\right)^2} \qquad \textbf{( 3.38 )}$$

$S_{TD}(q,\omega)$ was already introduced in equation **( 3.29 )**.

The HWHM intercept zero for $q^2 \to 0$ and have the typical form of $\Gamma(q) = Dq^2$ with the translational diffusion coefficient *D*.

Singwi and Sjölander (Singwi and Sjölander 1960) developed a model for translational jump-diffusion of liquid water. In this model a molecule performs oscillatory motion around its equilibrium position for a time $\tau_0$. After that it diffuses for a time $\tau_1$ by continuous diffusion. This process is then repeated. The scattering function can be evaluated in two limiting cases: when the time of continuous diffusion is much longer than the time of oscillatory motion $\tau_1 >> \tau_0$, the scattering function is identical to that of continuous translational diffusion given in **equation ( 3.38 )**. The second case is when the time of oscillatory motion is much longer than the time of continuous diffusion $\tau_1 << \tau_0$. Then the scattering function can be described by a single Lorentzian with the HWHM $\Gamma(q)$ and the Debye-Waller factor *exp(-2W)* as

$$\Gamma(q) = \frac{1}{\tau_0}\left[1 - \frac{\exp(-2W)}{1 + Dq^2\tau_0}\right]. \qquad \textbf{( 3.39 )}$$

When the amplitude of molecular vibrations are small compared to the diffusive steps fulfilling the condition $2W << Dq^2\tau_0$, then the HWHM can be simplified to

$$\Gamma(q) = \frac{Dq^2}{1 + Dq^2\tau_0}. \qquad \textbf{( 3.40 )}$$

Characteristic properties of the HWHM are to intersect zero for $q^2 \to 0$ and to follow $\Gamma(q) = Dq^2$ for very small $q^2$-values. At large $q^2$-values they tend to the asymptotic value of $\Gamma_\infty = 1/\tau_0$.

Teixeira measured the dynamics of water with QENS (Teixeira et al. 1985). Rotational and translational diffusive motions of the water molecules could be separated. The translational component could be described to high accuracy with the jump-diffusion model of Singwi and Sjölander. The measured HWHM in **Figure 8** nicely show the $\Gamma(q) = Dq^2$ law at small scattering vectors and the plateau $\Gamma_\infty = 1/\tau_0$ at large $q^2$ especially for low temperatures.

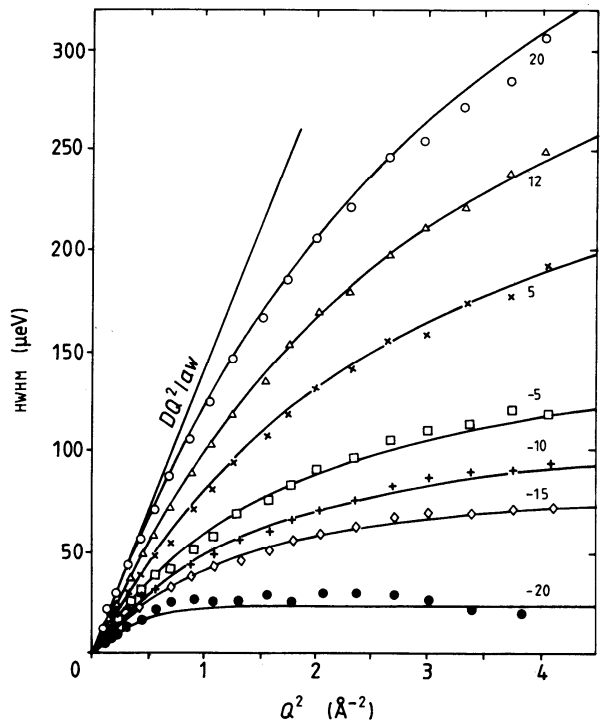


**Figure 8:** Half-widths at half-maximum (HWHM) of translational diffusion of liquid water as a function of $q^2$ at different temperatures (Teixeira et al. 1985). Solid lines are fits with the model of jump diffusion. At low $q^2$-value the $\Gamma(q) = Dq^2$ law is indicated, at high scattering values $q^2$ the plateau $\Gamma_\infty = 1/\tau_0$ is reached, being especially visible at low temperatures.

### *3.9.2 Rotational Diffusion*

The formalism of Sears (Sears 1966) is often used to describe molecular rotational diffusion. The scattering function of the model is a sum of one delta function and several Lorentzians

$$S(q,\omega) = A_0(q)\cdot\delta(\omega) + \sum_{l=1}^{\infty} A_l \cdot \frac{1}{\pi}\frac{\Gamma_{rot,l}}{\omega^2 + \Gamma_{rot,l}^{\ 2}}. \qquad \textbf{( 3.41 )}$$

The prefactors are given by $A_l = (2l+1)\cdot j_l^{\,2}(qr)$, $j_l$ are the first order spherical Bessel functios of $l^{\text{th}}$ kind. The HWHM are $\Gamma_{rot,l} = l\cdot(l+1)\cdot D_{rot}$ with the rotational diffusion coefficient $D_{rot}$.

The characteristic feature of rotational diffusion is that the HWHM of the quasielastic intensities are independent of the scattering vector and have constant line-width $\Gamma_{rot}$. The correlation time of rotational motion can be obtained as $\tau_{cor} = 1/\Gamma_{rot}$.

For the description of rotational diffusion of liquid water often only the first two Lorentzians are taken into account with prefactors $A_n(q)$ taken from the Sears model (Teixeira et al. 1985). In a simplified approach QENS data of water can also be approximated by only one Lorentzian for the rotational diffusion (Tehei et al. 2007).

### *3.9.3 Diffusion within Confined Space*

A model for continuous diffusion in a sphere with impermeable boundaries was developed by Volino and Dianoux (Volino and Dianoux 1980). It is rather useful in the investigation of protein dynamics with QENS as it gives analytical expressions for the measured EISF.

The scattering function of this model reads as

$$S(q,\omega) = A_0^0(q)\cdot\delta(\omega) + \sum_{(l,n)\neq(0,0)}(2l+1)\cdot A_n^l(q)\cdot\frac{1}{\pi}\frac{\lambda_l^n D}{\omega^2 + \left(\lambda_l^n D\right)^2} \qquad \textbf{( 3.42 )}$$

The $\lambda_l^n$ are eigenvalues of a differential equation defined in the article by Volino and Dianoux. In their work (Volino and Dianoux 1980) the first 99 values of $\lambda_l^n$ were calculated numerically. The values of $A_n^l(q)$ can then be calculated from $\lambda_l^n$.

It is important to note that the EISF has got an analytical solution with

$$A_0^0(q) = \left[\frac{3j_1(qr)}{qr}\right]^2, \qquad \textbf{( 3.43 )}$$

where $j_1$ is the first order spherical Bessel function of first kind and $r$ is the sphere radius. The value of $r$ can be deduced easily from measured EISF.

The HWHM of the quasielastic intensities of the Volino-Dianoux model are plotted in **Figure 9**. Its characteristic features are that at high scattering vector values the model converges towards the $Dq^2$ behaviour of continuous diffusion. At small q-values the HWHM converge to a plateau $\Gamma_0$ for $q < \frac{\pi}{r}$. The value of $\Gamma_0$ is related to the diffusion coefficient *D* with

$$\Gamma_0 = \frac{4.33 \cdot D}{r^2}. \qquad \textbf{( 3.44 )}$$

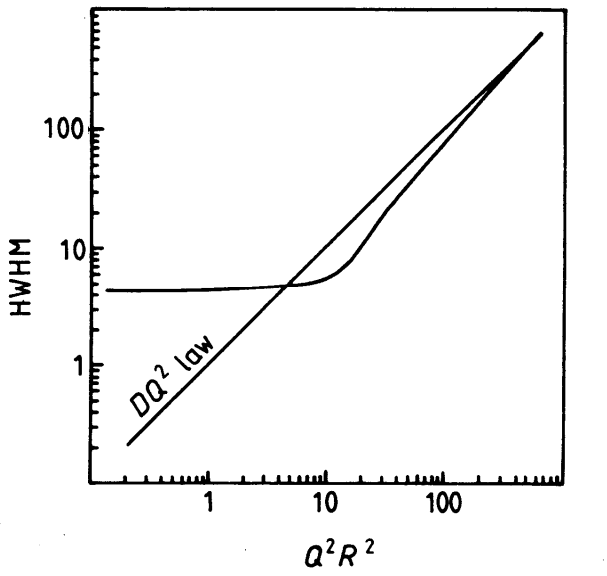


**Figure 9:** Half-widths at half-maximum of the Volino-Dianoux model for continuous diffusion in a sphere (Volino and Dianoux 1980). At small $q^2$ values the HWHM reach a plateau.

Hall and Ross developed a model for random jump diffusion in restricted geometry (Hall and Ross 1981). The Hall and Ross model exhibits both the characteristics of jump diffusion and diffusion within a restricted volume, see **Figure 10**. The model is commonly applied in QENS of protein dynamics to describe the dynamics of hydrogen atoms that are attached to amino-acid side chains. Amino-acid side chains perform restricted jump-diffusion in a cage formed by the neighbouring side-chains. The picture was taken from (Bee 1988).

At small scattering vector values the Hall and Ross model shows the behaviour of diffusion in a sphere. The HWHM converge to a plateau at high scattering vector values as the elementary jumps are not infinitely small but have a finite size. This behaviour can be described with the jump-diffusion model of Singwi and Sjölander.

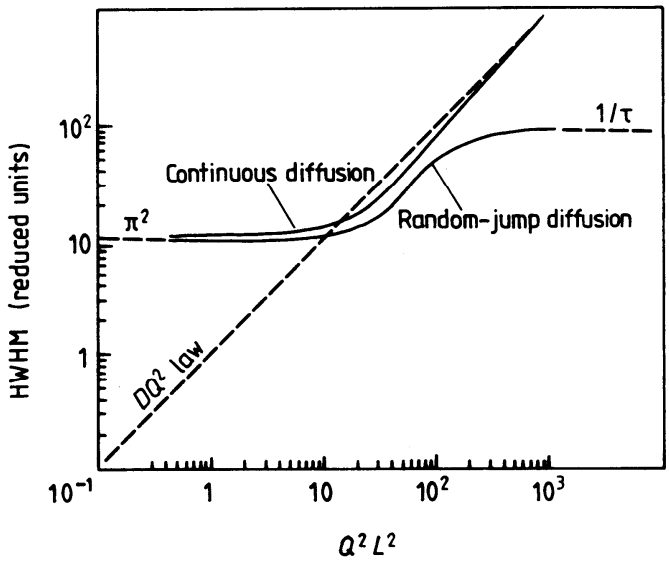


**Figure 10:** Half-widths at half-maximum for jump-diffusion in restricted geometry described by the model of Hall and Ross (Hall and Ross 1981). At small scattering vector values the HWHM follow the model for diffusion in a sphere. At large scattering vector values the HWHM approach a plateau and can be approximated by a jump-diffusion model. The picture was taken from (Bee 1988).

## 3.10 References

Austin RH, Beeson KW, Eisenstein L, Frauenfelder H, Gunsalus IC (1975) Dynamics of ligand binding to myoglobin. Biochemistry 14:5355-73

Bee M (1988) Quasielastic neutron scattering. Principles and Applications in Solid State Chemistry, Biology and Materials Science. Adam Hilger, Bristol and Philadelphia

Bellissent-Funel MC, Zanotti JM, Chen SH (1996) Slow dynamics of water molecules on the surface of a globular protein. Faraday Discuss. 103:281-294

Bicout DJ, Zaccai G (2001) Protein Flexibilty from the Dynamical Transition: A Force Constant Analysis. Biophys. J. 80:1115-1123

Cornicchi E, Marconi M, Onori G, Paciaroni A (2006) Controlling the protein dynamical transition with sugar-based bioprotectant matrices: a neutron scattering study. Biophys J 91:289-97

Cusack S, Doster W (1990) Temperature dependence of the low frequency dynamics of myoglobin. Measurement of the vibrational frequency distribution by inelastic neutron scattering. Biophys J 58:243-51

Dellerue S, Bellissent-Funel MC (2000) Relaxational dynamics of water molecules at protein surface. Chem. Phys. 258:315-325

Demmel F, Doster W, Petry W, Schulte A (1997) Vibrational frequency shifts as a probe of hydrogen bonds: thermal expansion and glass transition of myoglobin in mixed solvents. Eur Biophys J 26:327-35

Doster W (2008) The dynamical transition of proteins, concepts and misconceptions. Eur Biophys J 37:591-602

Doster W, Bachleitner A, Dunau R, Hiebl M, Lüscher E (1986) Thermal properties of water in myoglobin crystals and solutions at subzero temperatures. Biophys J 50:213-219

Doster W, Cusack S, Petry W (1989) Dynamical transition of myoglobin revealed by inelastic neutron scattering. Nature 337:754-6

Doster W, Cusack S, Petry W (1990) Dynamic instability of liquidlike motions in a globular protein observed by inelastic neutron scattering. Phys Rev Lett 65:1080-1083

Doster W, Settles M (2005) Protein-water displacement distributions. Biochim. Biophys. Acta 1749:173-186

Ellis RJ, Minton AP (2003) Join the crowd. Nature 425:27-28

Ferrand M, Dianoux AJ, Petry W, Zaccai G (1993) Thermal Motions and Function of Bacteriorhodopsin in Purple Membranes - Effects of Temperature and Hydration Studied by Neutron-Scattering. Proc. Natl. Acad. Sci. U.S.A. 90:9668-9672

Fitter J, Lechner RE (1998) Incoherent neutron scattering (INS), http://www.fz-juelich.de/inb/inb-2/datapool/page/17/method.pdf

Frauenfelder H, Parak F, Young RD (1988) Conformational substates in proteins. Annu Rev Biophys Biophys Chem 17:451-79

Frauenfelder H, Petsko GA, Tsernoglou D (1979) Temperature-dependent X-ray diffraction as a probe of protein structural dynamics. Nature 280:558-63

Fraunfelder H, Sligar SG, Wolynes PG (1991) The energy landscapes and motions of proteins. Science 254:1598-1603

Guinier A, Fournet G (1955) Small Angle Scattering of X-Rays. Wiley, New York

Hall PL, Ross DK (1981) Incoherent neutron scattering functions for random jump diffusion in bounded and infinite media. Mol. Phys. 42:673-682

http://neutron.neutron-eu.net/n_nmi3 (2008) NMI3 - Integrated Infrastructure Initiative for Neutron Scattering and Muon Spectroscopy

Jasnin M, Moulin M, Haertlein M, Zaccai G, Tehei M (2008) Down to atomic-scale intracellular water dynamics. EMBO reports 9:543-547

Kendrew JC, Dickerson RE, Strandberg BE, Hart RG, Davies DR, Phillips DC, Shore VC (1960) Structure of myoglobin: A three-dimensional Fourier synthesis at 2 A. resolution. Nature 185:422-7

Knapp EW, Fischer SF, Parak F (1982) The influence of protein dynamics on Mössbauer spectra. J. Chem. Phys. 78:4701-4711

Lichtenegger H, Doster W, Kleinert T, Birk A, Sepiol B, Vogl G (1999) Heme-solvent coupling: a Mossbauer study of myoglobin in sucrose. Biophys J 76:414-22

Madern D, Ebel C, Zaccai G (2000) Halophilic adaptation of enzymes. Extremophiles 4:91-8

Makarov VA, Andrews BK, Smith PE, Pettitt BM (2000) Residence Times of Water Molecules in the Hydration Sites of Myoglobin. Biophys. J. 79:2966-2974

Mampe W, Ageron P, Bates C, Pendlebury JM, Steyerl A (1989) Neutron lifetime measured with stored ultracold neutrons. Phys. Rev. Lett. 63:593-596

McCammon JA, Harvey SC (1987) Dynamics of Proteins and Nuclear Acids

Cambridge University Press, Cambridge, UK

Parak F, Knapp EW, Kucheida D (1982) Protein dynamics. Mossbauer spectroscopy on deoxymyoglobin crystals. J Mol Biol 161:177-94

Persson E, Halle B (2008) Cell water dynamics on multiple time scales. Proc. Natl. Acad. Scie. U.S.A. 105:6266-6271

Reat V, Patzelt H, Ferrand M, Pfister C, Oesterhelt D, Zaccai G (1998) Dynamics of different functional parts of bacteriorhodopsin: H-2H labeling and neutron scattering. Proc. Natl. Acad. Sci. U.S.A. 95:4970-5

Réat V, Zaccai G, Ferrand M, Pfister C (1997) Functional dynamics in purple membranes Biological Macromolecular Dynamics. Adenine Press, New York, pp 117-122

Richter D (2003) Properties of the Neutron - Elementary Scattering Processes, vol Matter and Materials, Volume 15. Forschungszentrum Jülich

Roh JH, Curtis JE, Azzam S, Novikov VN, Peral I, Chowdhuri Z, Gregory RB, Sokolov AP (2006) Influence of hydration on the dynamics of lysozyme. Biophys J 91:2573-88

Roh JH, Novikov VN, Gregory RB, Curtis JE, Chowdhuri Z, Sokolov AP (2005) Onsets of anharmonicity in protein dynamics. Phys. Rev. Lett. 95:038101

Rupley JA, Careri G (1991) Protein hydration and function. Adv. Protein Chem. 41:37-172

Russo D, Murarka RK, Copley JRD, Head-Gordon T (2005) Molecular View of Water Dynamics near Model Peptides. J. Phys. Chem. B 109:12966-12975

Sears VF (1966) THEORY OF COLD NEUTRON SCATTERING BY HOMONUCLEAR DIATOMIC LIQUIDS: II. HINDERED ROTATION. Can. J. Phys. 44:1299-1311

Sears VF (1992) Neutron scattering lengths and cross sections. Neutron News 3:26-37

Settles M (1996) Die Zeitabhängigkeit und die Geometry der intramolekularen Dynamik globulärer Proteine bis 100ps aus Neutronenstreudaten Physik Department E13, vol Dissertation. Technische Universität München, Garching

Singwi KS, Sjölander A (1960) Diffusive Motions in Water and Cold Neutron Scattering. Phys. Rev. 119:863-871

Smith JC (1991) Protein Dynamics - Comparison of Simulations with Inelastic Neutron-Scattering Experiments. Q. Rev. Biophys. 24:227-291

Tarek M, Tobias DJ (2002) Role of Protein-Water Hydrogen Bond Dynamics in the Protein Dynamical Transition. Phys. Rev. Lett. 88:138101

Tehei M, Franzetti B, Wood K, Gabel F, Fabiani E, Jasnin M, Zamponi M, Oesterhelt D, Zaccai G, Ginzburg M, Ginzburg BZ (2007) Neutron scattering reveals extremely slow cell water in a Dead Sea organism. Proc. Natl. Acad. Sci. U.S.A. 104:766-71

Tehei M, Madern D, Pfister C, Zaccai G (2001) Fast dynamics of halophilic malate dehydrogenase and BSA measured by neutron scattering under various solvent conditions influencing protein stability. Proc Natl Acad Sci U S A 98:14356-61

Tehei M, Zaccai G (2007) Adaptation to high temperatures through macromolecular dynamics by neutron scattering. Febs J 274:4034-43

Teixeira J, Bellissentfunel MC, Chen SH, Dianoux AJ (1985) Experimental-Determination of the Nature of Diffusive Motions of Water-Molecules at Low-Temperatures. Phys. Rev. A 31:1913-1917

Tournier AL, Xu J, Smith JC (2003) Translational Hydration Water Dynamics Drives the Protein Glass Transition. Biophys. J. 85:1871-1875

Van Hove L (1954) Correlations in Space and Time and Born Approximation Scattering in Systems of Interacting Particles. Phys. Rev. 95:249-262

Volino F, Dianoux AJ (1980) Neutron Incoherent-Scattering Law for Diffusion in a Potential of Spherical-Symmetry - General Formalism and Application to Diffusion inside a Sphere. Mol. Phys. 41:271-279

Wood K, Grudinin S, Kessler B, Weik M, Johnson M, Kneller GR, Oesterhelt D, Zaccai G (2008) Dynamical Heterogeneity of Specific Amino Acids in Bacteriorhodopsin. J. Mol. Biol. 380:581-591

Wood K, Plazanet M, Gabel F, Kessler B, Oesterhelt D, Tobias DJ, Zaccai G, Weik M (2007) Coupling of protein and hydration-water dynamics in biological membranes. Proc. Natl. Acad. Sci. U.S.A. 104:18049-54

Zaccai G (2000) How soft is a protein? A protein dynamics force constant measured by neutron scattering. Science. 288:1604-1607

# 4. Hemoglobin Dynamics in Red Blood Cells: Correlation to Body Temperature

The technique of incoherent quasielastic neutron scattering was used to measure hemoglobin dynamics in human red blood cells in the picosecond time and Ångstrom length scale. The experiment allowed the separation between macromolecular centre of mass diffusion and internal protein dynamics. Internal protein dynamics showed a more pronounced increase in protein flexibility above body temperature than expected from normal temperature dependence. The temperature behaviour was interpreted with partial unfolding of hemoglobin at body temperature. The measured half-widths at small scattering vector values for global hemoglobin diffusion showed typical signs for dynamics in confinement. This was interpreted that neighbouring hemoglobin molecules form a cage structure in which the central protein is trapped on the picosecond time scale. The rather large errors of the measured line-widths at large scattering values did not allow an unambiguous decision if global hemoglobin diffusion is characterised by translational or jump diffusion. The obtained diffusion coefficients for global translational centre of mass diffusion were favourable compared to results of hydrodynamic theory that were originally developed for colloidal particles.

The following chapter is based on an article published in *Biophysical Journal*. For the purpose of continuity, the article is presented in the general layout of the manuscript.

*Biophysical Journal*, December 2008, 95: 5449–5461

# Hemoglobin Dynamics in Red Blood Cells: Correlation to Body Temperature

A. M. Stadler*[†], I. Digel[‡], G. M. Artmann[‡], J. P. Embs[§¶], G. Zaccai*, and G. Büldt[†]

*Institut Laue-Langevin, Grenoble, France; [†]Research Centre Juelich, Juelich, Germany;

[‡]Department of Cellular Engineering, Aachen University of Applied Sciences, Juelich, Germany;

[§]Laboratory for Neutron Scattering ETH Zurich & Paul Scherrer Institut, Villigen-PSI, Switzerland;

[¶]Saarland University, Physical Chemistry, Saarbrücken, Germany

corresponding author: zaccai@ill.fr

**Keywords:** neutron scattering - in vivo dynamics – hemoglobin - structural transition temperature - internal molecular motions - self-diffusion

## 4.1 Abstract

A transition in hemoglobin behavior close to body temperature has been discovered recently by micropipette aspiration experiments on single red blood cells (RBC) and circular dichroism spectroscopy on hemoglobin solutions. The transition temperature was directly correlated to the body temperature of a variety of species. In an exploration of the molecular basis of the transition, we present neutron scattering measurements on the temperature dependence of hemoglobin dynamics in whole human RBC, *in vivo*. The data revealed a change in the geometry of internal protein motions at 36.9 °C, at human body temperature. Above that temperature, amino acid side-chain motions occupy bigger volumes than expected from normal temperature dependence, indicating partial unfolding of the protein. Global protein diffusion in RBC was also measured and compared favorably with theoretical predictions for short-time self-diffusion of non-charged hard-sphere colloids. The results demonstrated that changes in molecular dynamics in the picosecond time range and Ångstrom length scale might well be connected to a macroscopic effect on whole red blood cells occurring at body temperature.

## 4.2 Introduction

The function of biological macromolecules depends not only on their structure but also on their dynamics. Many functional properties of proteins cannot be completely understood from the average protein structure as determined from X-ray crystallography or NMR. Reaction rates for example are closely related to protein dynamics (Austin et al. 1975). Protein dynamics covers a very large range of timescales, from fast electronic rearrangements in the femtosecond scale to slow protein folding events in the order of seconds to minutes (Creighton 1992). Motions in the pico- and nanosecond time scale are believed to act as a lubricant for much slower protein dynamics in the millisecond time range (Brooks III C.L. 1988)

Below a dynamical transition temperature between 180 and 240K, atomic motions are predominantly harmonic (Frauenfelder et al. 1988; Fraunfelder et al. 1991). In this state, the

atoms vibrate around their structural equilibrium positions. Above the dynamical transition temperature at sufficient hydration, the mean-square displacements increase significantly because of the contribution of internal anharmonic, diffusive motions. These diffusive motions may contribute to the sampling of different so-called conformational substates on a complex energy landscape (Frauenfelder et al. 1988; Fraunfelder et al. 1991). The forces that maintain biological molecular structure and allow atomic motions are 'weak' because they are similar to thermal energy at physiological temperatures (Brooks III C.L. 1988). The amplitudes of atomic motions are a measure of the internal macromolecular flexibility because they correspond to the width of the potential well in which atoms move (Zaccai 2000). In this picture, equilibrium protein stabilization would correspond to the depth of the well (Tehei et al. 2001). The dependence of mean square displacements on temperature has been interpreted in terms of an effective force constant that was called resilience (Zaccai 2000), which is related to the shape of the well. Protein thermal stability was supposed to be inversely correlated to protein flexibility (Tang and Dill 1998; Tsai et al. 2001), although this point is still largely debated (Fitter et al. 2001; Tehei et al. 2001). The dynamics of lysozyme has been studied with quasielastic neutron scattering during the unfolding process (De Francesco et al. 2004), and it was concluded that compared to the folded state, the unfolded state is characterized by significantly larger amplitudes of diffusive motion of amino acid side-chains. Protein unfolding was therefore related to a loss of macromolecular resilience.

There is considerable evidence that protein dynamics is strongly influenced by the local environment and the level of hydration (Lehnert et al. 1998; Paciaroni et al. 2002; Perez et al. 1999; Tsai et al. 2001). Solvent molecules can act either as plasticizer or stabilizer by allowing or preventing the protein groups to jump between conformational substates (Gregory 1995). Water, which is the natural solvent of biomolecules, is a well known plasticizer. Pacciaroni et al. (Paciaroni et al. 2002) could show that internal lysozyme dynamics gets activated when the environment is altered from pure glycerol, which is a stabilizer, towards a plasticizer by increasing the level of hydration.

The main natural environment of proteins is within the cell, and protein function necessarily is adapted to these conditions. In bacteria and eukaryotic cells macromolecular interactions are likely to be influenced by the high cellular protein concentration (Hall and Minton 2003; Minton 2001; Zimmerman and Minton 1993). This effect, called 'crowding', results from high volume occupancy and steric hindrance of the protein molecules between each other. The free distance between macromolecules in the cell is in the order of some Ångstroms (Krueger and Nossal 1988) and intercellular water is in close vicinity to the protein surfaces. There is much interest and discussion about similarities and differences in structure and dynamics of cytoplasmic and bulk water (Ball 2008). Little is still known on how protein dynamics is influenced by the crowded cytoplasmic environment and the special properties of cellular water. Doster and Longeville (Doster and Longeville 2007) have measured the global diffusion of hemoglobin in red blood cells with neutron spin-echo spectroscopy. They found a reduced diffusion coefficient of hemoglobin compared to dilute solution and attributed the reduction to direct interactions between protein molecules and to hydrodynamic interactions with the solvent. The authors deduced that hydrodynamic effects dominate macromolecular transport at high protein concentration. In recent work, Jasnin et al. have investigated macromolecular and water dynamics in *Escherichia coli* bacteria with quasielastic neutron scattering in a wide range of time scales (Jasnin et al. 2008; Jasnin et al. 2008). An appreciable increase of internal molecular flexibility as compared to fully hydrated protein powders was revealed. The authors concluded that intracellular complexity influences protein dynamics which is necessary for biological activity. The study of global and internal protein diffusive motions is of importance for a fundamental understanding of macromolecular transport and functional protein internal flexibility in cells.

The fast trajectories in the pico- and nanosecond time scale can be directly accessed by molecular dynamics simulations (McCammon 1987) and incoherent neutron scattering (Doster et al. 1989). Incoherent neutron scattering has the advantage that the proteins under study are not limited to a maximum molecular weight, samples do not have to be crystalline or even monodisperse. Neutrons penetrate deeply in the sample without causing radiation damage which makes them an ideal tool to probe radiation sensitive biological matter. The incoherent scattering cross section of hydrogen atoms is one magnitude larger than all other elements which occur in biological material. As hydrogen atoms are uniformly distributed in proteins, neutron scattering probes

average protein dynamics. Incoherent neutron scattering experiments have been performed on hydrated protein powders (Doster et al. 1989; Reat et al. 1998; Zanotti et al. 1999), protein solutions (Longeville et al. 2003; Perez et al. 1999; Russo et al. 2002) and even *in-vivo* on whole cells (Doster and Longeville 2007; Jasnin et al. 2008; Tehei et al. 2004).

Hemoglobin is the main protein constituent of red blood cells (92% of dry weight). Its biological function is to carry oxygen from the lungs to the tissues. The discovery of the structure of hemoglobin by Max Perutz is one of the major breakthroughs in the history of molecular biology (Perutz et al. 1960). The protein is a tetramer with a molecular weight of around 64 kDa. It consists of two α-chains and two β-chains, each having 141 and 146 amino acid residues, respectively. The α-chains contain seven and the β-chains eight helices (Perutz 1987). Every chain carries one heme group in a pocket to which oxygen and several other small molecules can bind reversible. The concentration of hemoglobin in the red blood cells is around 330 mg/ml (Krueger and Nossal 1988) which corresponds to a volume fraction of 0.25. Recently it has become clear that hemoglobin at higher concentration shows a variety of interesting effects. Micropipette experiments with aspirated single human red blood cells showed a sudden passage phenomenon of the cells which is very close to human body temperature. A drop in viscosity of concentrated hemoglobin solutions at temperatures higher than the transition temperature was found and it was hypothesized that protein aggregation is the cause for the cellular passage effect and the drop in viscosity (Artmann et al. 1998). Additionally it was found that hemoglobin shows a pronounced loss of its α-helical content at body temperature. Amazingly, the transition temperatures were directly correlated to the body temperature of a big variety of species (Digel et al. 2006; Zerlin et al. 2007). It was speculated that this reflects partial unfolding of the helical structure and goes in hand with an increase in surface hydrophobicity which promotes protein aggregation (Digel et al. 2006).

In the following we present an incoherent quasielastic neutron scattering study on the temperature dependence of hemoglobin dynamics in whole red blood cells. The experiment was performed at temperatures between 16.9 °C and 45.9 °C. Global and internal protein motions could be separated. A change in the amplitudes of protein side-chain diffusion was found close to human body temperature which was attributed to partial unfolding of hemoglobin.

# 4.3 Materials and Methods

## *4.3.1 Sample preparation*

For neutron scattering experiments, samples of human venous blood from healthy adults were drawn with tubes containing heparin to prevent blood coagulation. The blood samples were suspended in HEPES buffer solution at pH=7.4 and 290 mOsm (137 mM NaCl, 4 mM KCl, 1.8 mM $CaCl_2$, 0.8 mM $Na_2HPO_4$, 0.2 mM $NaH_2PO_4$, 0.7 mM $MgSO_4$, 8.4 mM HEPES, 4 mM NaOH). The cells were washed twice and collected by centrifugation at 560 rcf for 10 min. The supernatant was removed together with the 'buffy coat' on top of the cells. The washed cells and the successively used buffer solutions were then gassed with CO to increase the stability of hemoglobin. The cells were resuspended in TRIS buffer (20 mM TRIS, 145 mM NaCl) at pH=5.5 and treated with neuraminidase (from *Clostridium perfringens* Type VI, purchased from Sigma-Aldrich) to remove the glycocalyx matrix as described elsewhere (Elgsaeter and Branton 1974). Afterwards the cells were washed in $H_2O$ HEPES buffer. To reduce the neutron scattering contribution of the buffer, the cells were washed with $D_2O$ HEPES buffer (pD=7.4, 290 mOsm), incubated for around 30 min and centrifuged at 560 rcf. The washing steps were repeated until the level of $H_2O$ was estimated to be below 0.1 vol% assuming that the $H_2O$-$D_2O$ exchange through the cell membrane reaches a constant value in this time. No cell lysis was detected during the preparation and the shape of the cells was checked with optical microscopy at the end. After a final centrifugation step the cell pellet was sealed in a flat aluminum sample holder of 0.2 mm thickness for the neutron scattering experiment. The scattering from the aluminum screws was blocked using a cadmium mask. It was checked by weighting that there occurred no loss of sample material during the experiment.

Hemoglobin samples for dynamic light scattering experiments were prepared from around 75 µl of human red blood cells which were taken from the finger tip with a heparinized glass capillary. We tried to perform the light scattering measurements in conditions that resemble the saline environment in the red blood cell. Although the extracellular concentration of sodium is around 145 mM, the intercellular concentration is between 5 and 15 mM only. Inversely, the intracellular

concentration of potassium is around 140 mM and the extracellular concentration is around 5mM (Alberts B. 2002). Therefore, we used potassium chloride instead of sodium chloride for the light scattering experiments. The cell sample was washed as described above with buffer solution (0.1M KCl, 61.3 mM $K_2HPO4$, 5.33 mM $KH_2PO4$, pH 7.4, 290-300 mOsm). The cells were then hemolyzed in 200 µl distilled $H_2O$ and diluted with 800 µl buffer. The solution was centrifuged twice at 20000 rcf to remove cytoskeleton and membrane parts. Oxy-hemoglobin solutions of 4.0 mg/ml, 1.2 mg/ml and 0.3 mg/ml were prepared and filtered twice using 0.25 µm nitrocellulose filters into dust-free glass scintillation vials used for dynamic light scattering experiments. The hemoglobin concentration was determined spectrophotometrically using extinction coefficients of 13.8 at 541 nm and 128 at 405 nm for oxy-hemoglobin (Antonini and Brunori 1970).

### *4.3.2 Neutron scattering experiments*

The experiment was performed on the cold time-of-flight spectrometer FOCUS at the neutron spallation source SINQ (Paul Scherrer Institut, Villigen, Switzerland). A detailed description of the instrument can be found in (Janssen et al. 1997). The incident wavelength was set to 6 Å. The q-dependent elastic energy resolution ranges from 41 µeV (full-width at half-maximum) at q=0.5 $Å^{-1}$ to 61 µeV at q=1.6 $Å^{-1}$, as determined from a vanadium measurement. During the experiment we could largely profit from the high neutron flux delivered by the liquid metal target of the MEGAPIE project (Bauer et al. 2001). Samples were measured in the temperature range of 16.9°C to 45.9°C in which no hemolysis occurs. All samples, including the 1 mm thick vanadium slab and empty sample holder, were oriented at 135° with respect to the incident neutron beam direction. The measured time-of-flight spectra were corrected for empty cell scattering, normalized to vanadium, transformed into energy transfer and scattering vector space and binned into 12 groups with 0.5 $Å^{-1} \leq q \leq 1.6$ $Å^{-1}$. The spectra were corrected with a detailed balance factor. Data treatment was done using the DAVE package (http://www.ncnr.nist.gov/dave). Multiple scattering was neglected as the transmission of all samples was between 0.9 and 0.95.

### *4.3.3 Data analysis*

An exhaustive description of quasielastic neutron scattering can be found in Bée (Bee 1988). The application to protein dynamics has been reviewed in Gabel et al. (Gabel et al. 2002) and Smith (Smith 1991). In concentrated protein solutions both internal and global diffusive motions of the proteins contribute to the measured signal. In the case that internal and global motions are uncorrelated, the theoretical incoherent quasielastic scattering function can be written as (Bee 1988)

$$S_{theo}(q,\omega) = e^{-\langle x^2 \rangle q^2} \cdot S_G(q,\omega) \otimes S_I(q,\omega), \qquad (4.1)$$

where the scattering function $S_G(q,\omega)$ corresponds to global protein motions, the scattering function $S_I(q,\omega)$ to internal motions and $\langle x^2 \rangle$ stands for the mean square vibrational displacements. The scattering function for internal motions can be separated into an elastic and a Lorentzian part

$$S_I(q,\omega) = A_0(q) \cdot \delta(\omega) + (1 - A_0(q)) \cdot \frac{1}{\pi} \cdot \frac{\Gamma_I(q)}{\omega^2 + \Gamma_I(q)^2}, \qquad (4.2)$$

with $A_0(q)$ the elastic incoherent structure factor (EISF) that contains information about the geometry of internal motions. Global protein motions are a combination of translational and rotational diffusion. A recent work by Perez et al. (Perez et al. 1999) showed that the global scattering function for proteins in solution can be approximated by a single Lorentzian

$$S_G(q,\omega) = \frac{1}{\pi} \cdot \frac{\Gamma_G(q)}{\omega^2 + \Gamma_G(q)^2}, \qquad (4.3)$$

with the apparent diffusion coefficient $\Gamma_G = D_{app} \cdot q^2$. This study found that in the case of the small protein lysozyme the value of $D_{app}$ is 1.27 times higher than free Brownian diffusion due to the contribution of rotational motion. We followed the calculations given in (Perez et al. 1999) for the bigger protein hemoglobin and found that the apparent diffusion coefficient is also 1.27

times higher than an assumed free translational diffusion coefficient of $D_0$=8.61*10$^{-7}$cm$^2$/s with a radius of R=31Å and a rotational diffusion coefficient given by $D_{rot} = \frac{3D_0}{4R^2}$.

The theoretical scattering function then reads

$$S_{theo}(q,\omega) = e^{-\langle x^2 \rangle q^2} \cdot \left[ \frac{A_0(q)}{\pi} \cdot \frac{\Gamma_G(q)}{\omega^2 + \Gamma_G(q)^2} + \frac{1 - A_0(q)}{\pi} \cdot \frac{\Gamma_G(q) + \Gamma_I(q)}{\omega^2 + [\Gamma_G(q) + \Gamma_I(q)]^2} \right] + B_0 \qquad (4.4)$$

where $B_0$ is an inelastic background due to vibrational modes of lowest energy (phonons) (Bee 1988).

The measured data were fitted with the PAN routine of the DAVE software package (http://www.ncnr.nist.gov/dave) using the following relation

$$S_{meas} = S_{theo}(q,\omega) \otimes S_{res}(q,\omega), \qquad (4.5)$$

in which $S_{res}(q,\omega)$ is the instrumental resolution determined by vanadium. The fits were performed over the energy transfer range from -0.75 meV to +0.75 meV.

In the following, we outline the essential steps of the calculation of the global scattering function for proteins in solution: The scattering function of free translational diffusion takes the form of

$$S_{trans}(q,\omega) = \frac{1}{\pi} \cdot \frac{\Gamma_{trans}(q)}{\omega^2 + \Gamma_{trans}(q)^2}, \qquad (4.6)$$

with the diffusion coefficient $D_0 = \Gamma_{trans} \cdot q^2$ (Bee 1988). Rotational diffusion on the surface of a sphere is described by the formalism developed by Sears (Sears 1966). We assume that the protein has spherical shape of radius R and that hydrogen atoms are homogeneously distributed within this sphere. The Sears model then needs to be integrated over the protein volume to

correctly account for the distribution of hydrogen atoms (Perez et al. 1999). The scattering function for rotational protein diffusion then is (Perez et al. 1999)

$$S_{rot}(q,\omega) = B_0(q)\cdot\delta(\omega) + \sum_{l=1}^{\infty} B_l(q)\cdot\frac{1}{\pi}\cdot\frac{\Gamma_l}{\omega^2+{\Gamma_l}^2}, \qquad (4.7)$$

with $\Gamma_l = l(l+1)\cdot D_{rot}$ and the rotational diffusion coefficient $D_{rot}$ as defined above. The integrals in the terms $B_0(q)$ and $B_l(q)$ are an extension to the Sears model to describe the distribution of hydrogen atoms within the protein,

$$B_0(q) = \int_{r=0}^{R} 4\pi r^2\cdot {j_0}^2(qr)\,dr\,,\ B_{l\geq 1}(q) = \int_{r=0}^{R} 4\pi r^2\cdot(2l+1)\cdot {j_l}^2(qr)\,dr\,. \qquad (4.8)$$

The terms $j_l$ are the $l^{th}$-order spherical Bessel function of the first kind. Rotational and translational diffusion are assumed to be uncorrelated. Therefore, the global scattering function $S_G(q,\omega)$ is then the convolution of both terms and reads

$$S_G(q,\omega) = \frac{1}{\pi}\cdot\sum_{l=0}^{\infty} B_l(q)\cdot\frac{\Gamma_{trans}(q)+\Gamma_l(q)}{\omega^2+[\Gamma_{trans}(q)+\Gamma_l(q)]^2}\,. \qquad (4.9)$$

The terms $B_l(q)$ were integrated numerically using the mathematical software Maple (Waterloo Maple Inc.) for *q*-values in the range of 0.5 Å$^{-1}$ to 2.0 Å$^{-1}$. The Lorentzians in Eq. ( 4.9 ) were summed over the experimentally covered energy range. Depending on the radius of the protein and the *q*-value, different numbers of terms are needed to reach convergence in the infinite sum of Eq. ( 4.9 ). At the scattering vector $q$=2.0 Å$^{-1}$, 39 terms were necessary to be included for the small protein lysozyme with a radius of $R$=19 Å (Perez et al. 1999). For the bigger protein hemoglobin with a radius of $R$=31 Å, 70 terms at $q$=2.0 Å$^{-1}$ had to be included. The obtained global scattering function $S_G(q,\omega)$ could be perfectly approximated by a single Lorentzian as stated in Eq. ( 4.3 ) (data not shown). The apparent diffusion coefficient $D_{app}$ was calculated from

the half-widths by $\Gamma_G = D_{app} \cdot q^2$ and compared to the assumed free translational diffusion coefficient $D_0$, which gave the relation of $D_{app} / D_0 = 1.27$.

Although predominant incoherent scattering is due to nonexchangeable hydrogen atoms of the protein, scattering from $D_2O$ solvent contributes partially to the signal. The incoherent scattering cross section of human carbonmonoxy hemoglobin was estimated from the amino acid sequence taken from pdb file 2DN3 (Park et al. 2006) assuming that 13% of the protons exchange with deuterons (Elantri et al. 1990). The fraction of $D_2O$ in the sample was determined by drying and weighting of an aliquot. These theoretical estimations give a $D_2O$ solvent incoherent scattering cross section of around 9% of the total incoherent scattering cross section. Even so, it still could be that $D_2O$ dynamics contribute strongly to the measured signal as the characteristic relaxation times of $D_2O$ are mostly in the picosecond time range, whereas protein dynamics might be slower and appear more dominant at slower timescales only, which could be out of the accessible time-space window of the neutron spectrometer. The coherent structure factor of $D_2O$ begins to increase above 0.8 $Å^{-1}$ and reaches a maximum at around 2 $Å^{-1}$ (Bosio et al. 1989), thus a stronger contribution of $D_2O$ to the measured signal is expected at higher q-values.

To estimate the incoherent and coherent contribution of $D_2O$ to the measured signal, we compared the measured elastic intensity of equal amounts of $D_2O$ buffer and red blood cell sample (data not shown). The elastic intensity of $D_2O$ is around 6% at low q-values and reaches around 10% above 1.3 $Å^{-1}$ of the elastic intensity of the red blood cell sample. When corrected for the fraction of $D_2O$ in the red blood cell sample, we obtain $D_2O$ contributions of 4.5% at low scattering vectors and 7.5% above 1.3 $Å^{-1}$. This demonstrates that protein dynamics gives a strong signal compared to $D_2O$ buffer at the energy resolution of 50 µeV.

### *4.3.4 Dynamic light scattering measurement*

Dynamic light scattering was measured with a DAWN-EOS instrument equipped with a quasielastic light scattering module (Wyatt Technology, Santa Barbara, CA) in a temperature range of 16.9 °C to 45.9 °C. Temperature variations never exceeded ± 0.2°C. The ASTRA 5 software package from the manufacturer was used for data acquisition and calculation of the diffusion coefficients. The instrument was used in batch mode and around 5 ml of sample was measured in glass scintillation cells.

## 4.4 Results

### *4.4.1 Neutron Scattering*

Typical quasielastic neutron spectra at 16.9 °C, 31.9 °C and 45.9 °C at q=1.6 $Å^{-1}$ together with the results from the fits using equation ( 4.5 ) are shown in **Figure 1**. The narrow Lorentzian corresponds to global protein motions and the broad Lorentzian to internal protein dynamics.

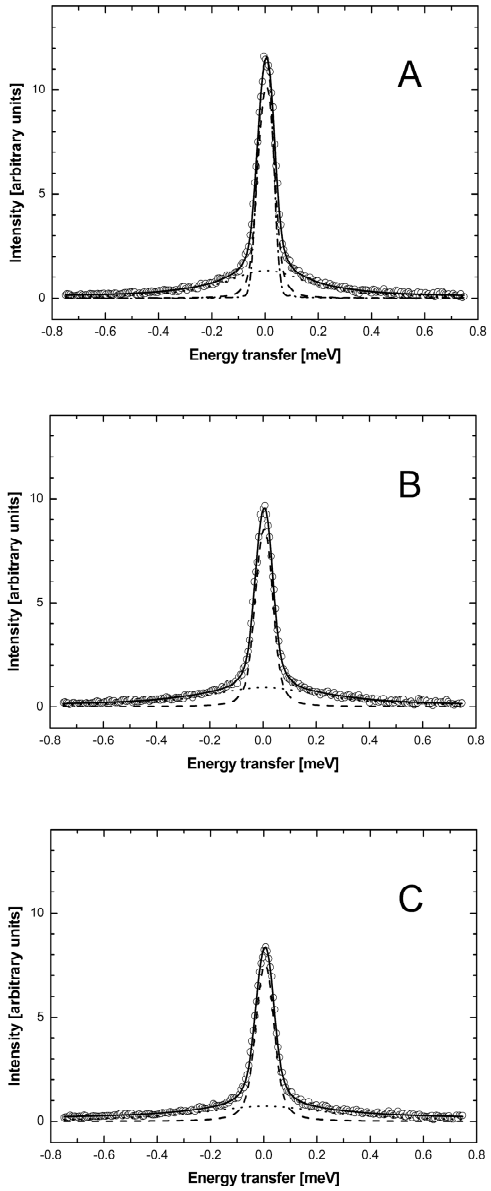


**Figure 1:** Quasielastic neutron scattering spectra of hemoglobin in human red blood cells at the different temperatures (A) 16.9 °C, (B) 31.9 °C and (C) 45.9 °C at the scattering vector q=1.6 $Å^{-1}$. The circles show measured data and the solid line presents the fit over the energy transfer range from -0.75 meV to +0.75 meV. The components correspond to the narrow Lorentzian (dashed line) and the broad Lorentzian (dotted line). The instrumental energy resolution determined by vanadium is indicated in (A), (dashed-dotted line).

### *4.4.2 Global Motions*

The line-widths $\Gamma_G(q)$ of the narrow Lorentzian at the temperatures 16.9 °C and 45.9 °C as a function of $q^2$ are shown in **Figure 2 A**. $\Gamma_G(q)$ does not intercept $q^2=0$ as it would be expected for free translational diffusion. Above around 1.0 $Å^{-2}$ the $\Gamma_G$-values increase with $q^2$, below this $q^2$-value the half-widths $\Gamma_G(q)$ converge to a plateau $\Gamma_0$ at $q^2=0$. This is interpreted as resulting from global hemoglobin diffusion within a restricted volume formed by the neighboring protein molecules. All protein hydrogen atoms are involved in the global motions, the plateau in the line-widths at small $q^2$ therefore represents center of mass diffusion. The model of Volino and Dianoux was developed for free diffusion in a restricted spherical volume of radius $r$ (Volino and Dianoux 1980). It is characterized by a plateau of the half-widths $\Gamma_0$ until $q < \frac{\pi}{r}$ and for $q > \frac{\pi}{r}$ by a limiting behavior of the half-widths at large $q^2$ with $\Gamma(q) = D_{app} \cdot q^2$, where $D_{app}$ is the apparent translational diffusion coefficient. In a preliminary, simplified and speculative approach we use the model of free diffusion to describe the measured data. Especially at the lowest temperature, deviations from linear behavior are visible. The linear fits appear more justified at higher temperatures. An alternative interpretation with a jump-diffusion model is presented further below.

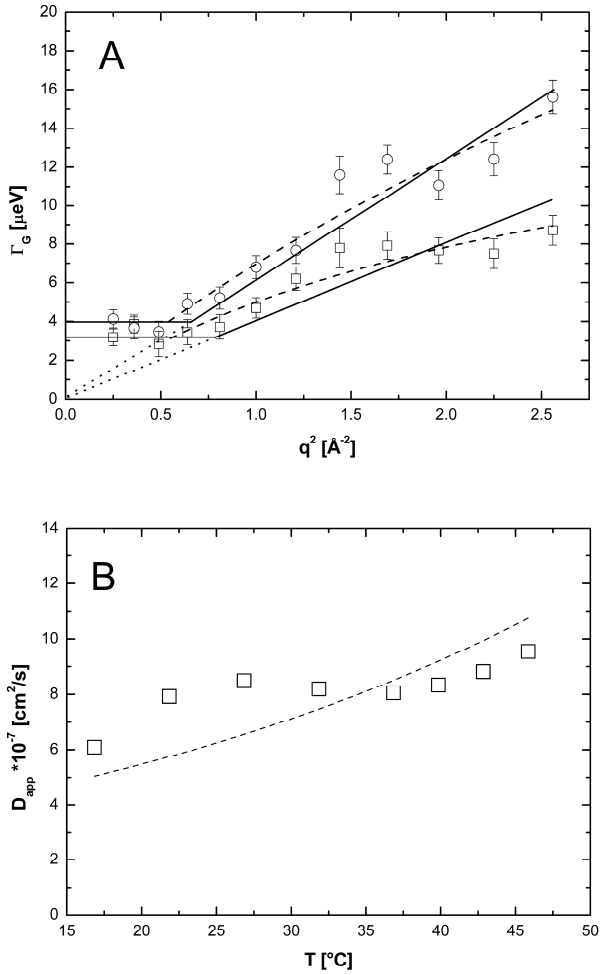


**Figure 2:** (A) Half-widths at half-maximum $\Gamma_G$ of the narrow Lorentzian as a function of $q^2$ at T=16.9 °C (squares) and 45.9 °C (circles). The line-widths reach a plateau at small $q^2$ which is interpreted as global diffusion within confined space. The solid lines are linear fits in the $q^2$-range of 1.0 Å$^{-2}$ to 2.56 Å$^{-2}$ which are extended to intersect the constant plateaus at smaller $q^2$-values. The linear fits pass through zero which is indicated by the dotted lines. The dashed lines are fits according to a jump-diffusion model in the $q^2$-range of 0.49 Å$^{-2}$ to 2.56 Å$^{-2}$. (B) Temperature behavior of the apparent translational diffusion coefficients of hemoglobin in red blood cells, the error bars are within the symbols. The dashed line indicates expected normal thermal behavior according to the Stokes-Einstein equation with $D_{app}(T) = k_B T / 6\pi\eta(T) R_h$ where $\eta(T)$ is the viscosity of pure $D_2O$ and $R_h$=31.3 Å the hydrodynamic radius of hemoglobin.

The apparent translational diffusion coefficients $D_{app}$ were calculated according to $\Gamma_G(q) = D_{app} \cdot q^2$ in the $q^2$-range of 1.0 Å$^{-2}$ to 2.56 Å$^{-2}$. The obtained values of $D_{app}$ as a function of temperature are presented in **Figure 2 B**. Following the model of Volino and Dianoux (Volino and Dianoux 1980) and the corrected translational diffusion coefficient $D_{trans}$=$D_{app}$/1.27, the radius $r$ of the spherical volume can be estimated by $r^2 = 4.33 \cdot D_{trans} / \Gamma_0$. The obtained radii lie between $r$=2.1±0.2 Å at 16.9 °C and $r$=2.3 ± 0.2 Å at 45.9 °C which are constant within the errors.

Normal temperature behavior of the diffusion coefficient follows the Stokes-Einstein equation $D_{app}(T) = \frac{k_B T}{6\pi\eta(T)R_h}$, with the solvent viscosities $\eta(T)$ and the hydrodynamic radius of the protein $R_h$. The Stokes-Einstein equation was fitted to the diffusion coefficients $D_{app}$ by taking literature values of the viscosities $\eta(T)$ of pure $D_2O$ (Cho C.H. 1999) and the hydrodynamic radius $R_h$ as a free parameter, see Figure 2 B. We obtain a value of $R_h$=31.3 Å which is nearly identical to the published hydrodynamic radius of human hemoglobin of 31.7 Å (Digel et al. 2006).

To check the validity of the Volino and Dianoux model, and the approach of assumed free diffusion at large $q^2$, we examined the behavior of the plateau $\Gamma_0$ at small $q$. The sphere radius $r$ is then given by the upper limit $q = \frac{\pi}{r}$ at which the plateau $\Gamma_0$ ends. This yields radii between $r$=3.4 Å at 16.9 °C and 4.0 Å at 45.9 °C, which are in average 1.7 times bigger than the values from the approach of free diffusion at large $q^2$. Diffusion coefficients $D_{local}$ were estimated according to $D_{local} = \frac{r^2 \cdot \Gamma_0}{4.33}$ (Volino and Dianoux 1980). We get values ranging between 13.7*10$^{-7}$ cm$^2$/s at 16.9 °C and 22.0*10$^{-7}$ cm$^2$/s at 45.9 °C. The reasons for the discrepancy are considered in the 'Discussion' section.

At larger $q^2$-values, the half-widths present some deviation from linear behavior. There might be signs for saturation at 16.9 °C and 45.9 °C, which is less visible at high temperatures. In the Volino and Dianoux model for restricted free diffusion, the elementary steps of motion are assumed to be infinitely small and therefore the half-widths show linear behavior at large $q^2$-values. In the case of elementary steps of motion with a finite size, these steps become observable at high $q^2$. A plateau at high $q^2$-values is then a sign for a possible jump-diffusion mechanism. The line-widths were approximated with a jump-diffusion model $\Gamma_G = \frac{D_{jump} q^2}{1 + D_{jump} q^2 \tau}$, with the diffusion coefficient $D_{jump}$ and the mean residence time $\tau$ (Bee 1988). The fits are presented in Figure 2 A. The residence time on one site between jumps is $\tau = 1/\Gamma_\infty$, where $\Gamma_\infty$ is obtained from the asymptotic behavior at high q while Γ approaches a constant value. The Γ-value at high $q$ is still increasing over the $q$-range examined, and has not yet reached a constant value. Therefore, the constant value was estimated using the presented equation of the jump-diffusion model and extrapolated to higher $q$. The behavior of the residence times $\tau$ can be approximated by an Arrhenius relation with $\tau = \tau_0 \exp\left(E_a / k_B T\right)$ in the investigated temperature range. The residence times $\tau$ are presented in an Arrhenius plot in **Figure 3**. We obtained for the activation energy a value of $E_a$=6.6 ± 1.8 kcal/mol. All values $D_{jump}$ are constant within the errors and have the average value of 12.6 ± 0.2 * $10^{-7}$ $cm^2/s$.

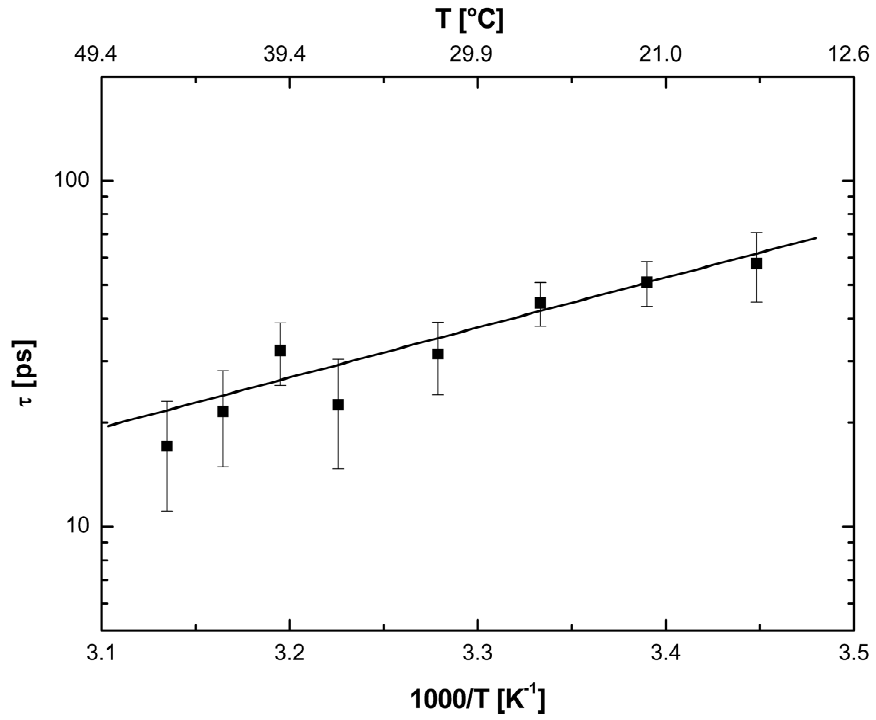


**Figure 3:** Arrhenius plot of the residence time τ of the jump diffusion model for global hemoglobin motion.

The measured line-widths at large $q^2$ can be approximated both with a jump-diffusion model and the Volino-Dianoux model for free diffusion in confined space. However, the errors are too big to decide clearly which model is appropriate. A jump-diffusion mechanism seems to be more favorable at low temperatures than at high temperatures. How far a whole globular protein with a molecular weight of 64kDa can perform jump-diffusive motion is still not understood. The diffusion coefficient is mostly determined by the behavior of the line-widths at small $q^2$. The diffusion coefficients were estimated from the half-widths at small $q$ within the Volino-Dianoux model and with an approach of free confined diffusion at large $q^2$. The level of the resolution ranges between 20 µeV at q=0.5 $Å^{-1}$ and 30 µeV at q=1.6 $Å^{-1}$ (HWHM). All measured line-widths are at the lower limit of energy resolution. If limited energy resolution should play a role, then this would influence the low temperature data stronger as the line-widths are generally smaller than at high temperature. At this point, we cannot decide clearly if the plateau at high $q^2$-values is an artifact or a real feature. The obtained diffusion coefficients for free diffusion should be

considered rather as average values, as the plateau at high $q^2$ influences the data. The validity of these average diffusion coefficients is checked by the comparison to expected normal temperature behavior.

### *4.4.3 Internal Motions*

Conclusions about protein internal motions can be drawn from the amplitudes $A_0(q)$ and the half-widths $\Gamma_I(q)$ of the broad Lorentzian. Information about the average geometry of internal protein motion and the fraction of hydrogen atoms participating in this motion is contained in the Elastic Incoherent Structure Factor (EISF) which appears in front of the delta-function in Eq. (4.2). In the case of a protein solution the delta-function for internal protein motion is convoluted with the Lorentzian for global protein motion (Perez et al. 1999; Russo et al. 2002). We used a pseudo-EISF which appears as the prefactor $A_0$ of the narrow Lorentzian in Eq. (4.4). The values of $A_0$ were fitted using a model for 'diffusion in a sphere' proposed by Volino and Dianoux (Volino and Dianoux 1980) with

$$A_0(q) = p + (1-p)\cdot\left[\frac{3j_1(qa)}{qa}\right]^2, \qquad (4.10)$$

where $j_1$ is the first-order spherical Bessel function of the first kind and a is the sphere radius. The populations of hydrogen atoms which appear as immobile and mobile are represented by the fractions $p$ and $(1-p)$, respectively.

Molecular dynamics simulations showed that the polydispersity of protein internal motions and geometries are best represented by a free discrete distribution of sphere radii (Dellerue et al. 2001). As the measured experimental results cover only a limited q-region of $A_0(q)$, a fit with a completely free discrete distribution of sphere radii was not feasible. A simplified model assuming a Gaussian distribution $f(a)$ of the sphere radii with $f(a) = \frac{2}{\sigma\sqrt{2\pi}}\exp\left(-a^2/2\sigma^2\right)$ and the standard deviation σ as free parameter (Perez et al. 1999) gave good results. The mean value

of the sphere radius is then given by $\hat{a} = \sigma\sqrt{\frac{2}{\pi}}$. The fits to the EISF together with the Gaussian distributions are shown in **Figure 4 A** and B. Due to the used model of a Gaussian distribution of spheres the EISF decays slowly with *q* and reaches the constant value of the immobile hydrogen fraction only at very high *q*-values. The inset in **Figure 4 A** illustrates this behavior of the EISF. With increasing temperature the Gaussian distributions change from narrow to broad above 36.9 °C. The mean radii $\hat{a}$ as a function of temperature are given in **Figure 5 A**. The values between 16.9 °C and 31.9 °C increase slightly linear with temperature, whereas there appears a kink at 36.9 °C with a much steeper increase at higher temperatures. The fraction of immobile hydrogen atoms are shown in **Figure 5 B**. They are roughly constant within the errors between 16.9 °C and 39.9 °C and have an average value of 0.35±0.01. The value at 42.9 °C and 45.9 °C are slightly above the average.

In a recent study on the dynamics of apo-calmodulin, Gibrat et al. used a lognormal distribution to describe the polydispersity of protein motions and to fit the measured EISF (Gibrat et al. 2008). The lognormal distribution is defined by $f(a) = \frac{1}{a\sigma\sqrt{2\pi}} \cdot \exp\left[-\frac{(\ln(a)-\mu)^2}{2\sigma^2}\right]$ where $\mu$ and $\sigma$ are the mean and the standard deviation of the variable's natural logarithm. A lognormal distribution is appropriate if the variable is the product, whereas a Gaussian distribution is valid if the variable is the sum of a large number of independent, identically distributed variables.

It was shown that the radius of the sphere of diffusion of a hydrogen atom along an aliphatic chain fixed at one end increases linearly with distance from the fixed end (Carpentier et al. 1989). It was argued by Gibrat et al. that the motions of the hydrogen atoms that are bound to a carbon atom of the aliphatic chain are then the 'product' of the motions of the previous hydrogen atoms in the chain (Gibrat et al. 2008). In this sense, it was concluded that a lognormal distribution would be more appropriate than a Gaussian distribution (Gibrat et al. 2008) to describe the polydispersity of hydrogen motion in the amino acid side-chains of a protein.

In fact, we found that both a Gaussian and a lognormal distribution for the Volino and Dianoux model could fit the measured EISF equally well. The obtained average sphere radii of the lognormal and the Gaussian distribution were identical within the errors and showed similar temperature behavior, but the standard deviations of the lognormal distributions were much

bigger than those of the Gaussian distributions. Therefore, we use the results of the fits with the Gaussian distributions in the following. Fits to the EISF using a single sphere radius gave only poor results.

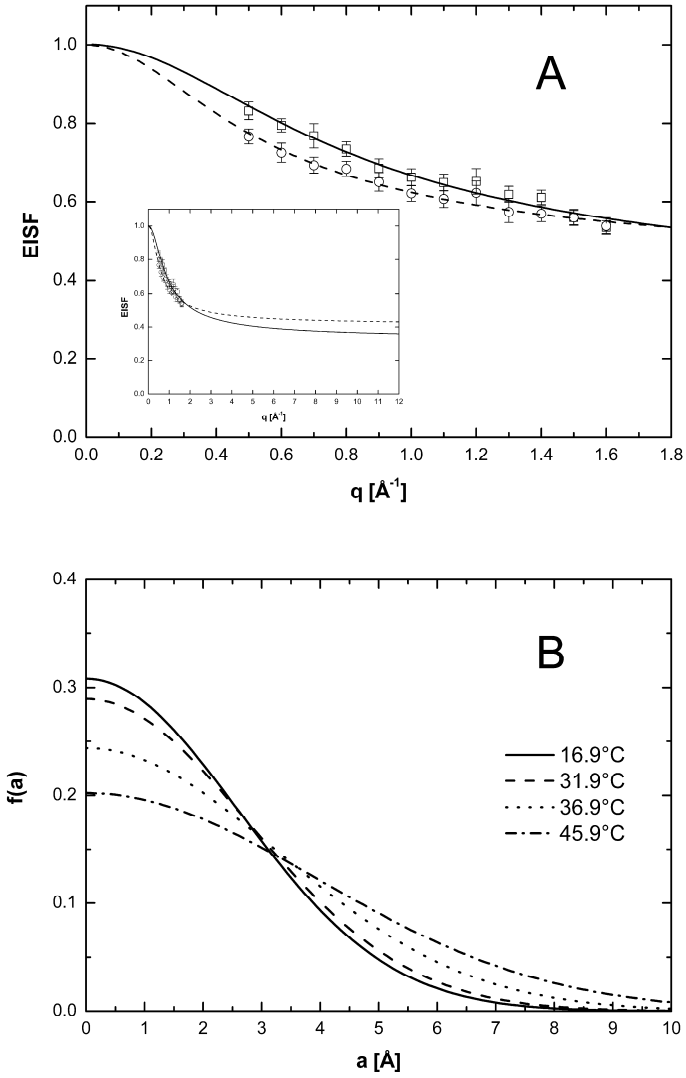


**Figure 4:** (A) Variation of the EISF as a function of q at the temperatures 16.9 °C (squares) and 45.9 °C (circles).The solid and dashed lines are fits with a model for diffusion in a sphere with a Gaussian distribution of radii. The inset shows the slow decay of the model which reaches the limiting value of the immobile hydrogen fraction only at high q-values. (B) Gaussian distribution of the sphere radius f(a) at different temperatures.

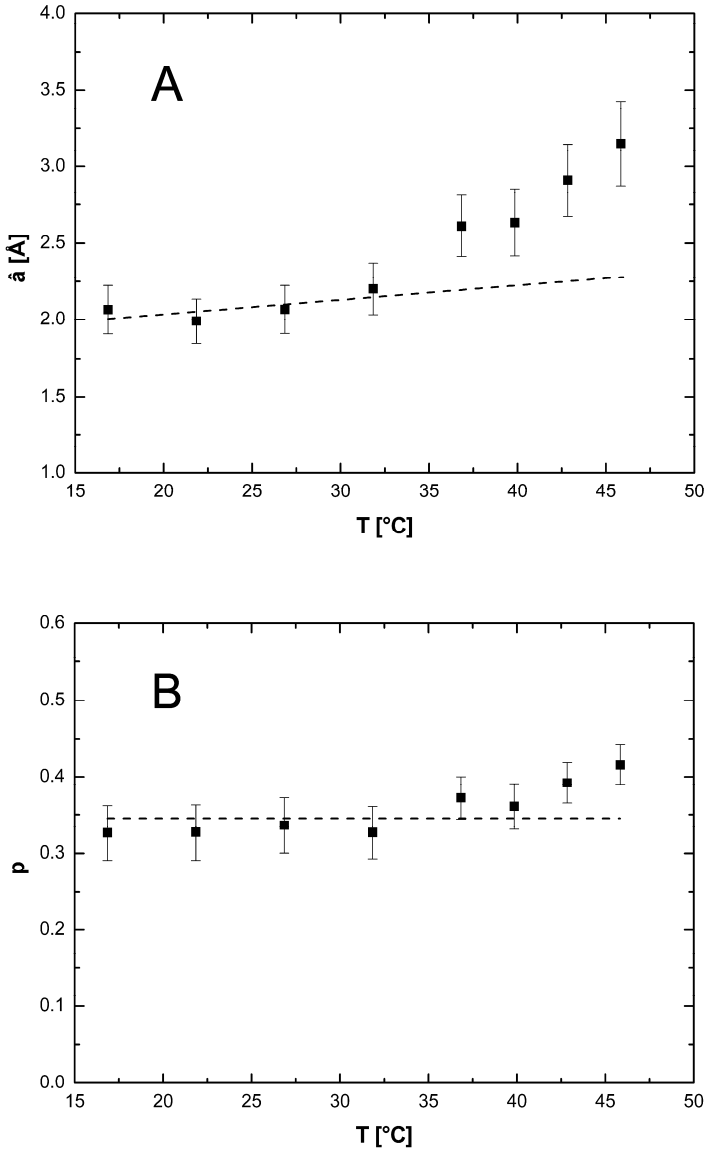


**Figure 5:** (A) Mean value â of the Gaussian distribution as a function of temperature. The dashed line is a linear fit to the values between 16.9 °C and 31.9 °C and serves as a guide for the eye. (B) Fraction of hydrogen atoms which appear immobile within the instrumental energy resolution. The average value between 16.9 °C and 39.9 °C is indicated by the dashed line.

The half-widths $\Gamma_I(q)$ of the broad Lorentzian are shown in **Figure 6**. The half-widths tend to a constant value of around 100 µeV for $q^2 \to 0$. At higher $q^2$-values, the line-widths follow the behavior of a jump-diffusion model (Bee 1988). A plateau $\Gamma_\infty$ at highest $q^2$-values is approached which ranges approximately between 170 µeV at 16.9 °C and 240 µeV at 45.9 °C. $\Gamma_\infty$ corresponds to a correlation time of $\tau = 1/\Gamma_\infty$, which is roughly between 3.9 ps at 16.9 °C and 2.7 ps at 45.9 °C. However, the determination of $\Gamma_I$ is inaccurate and doesn't allow a more precise analysis.

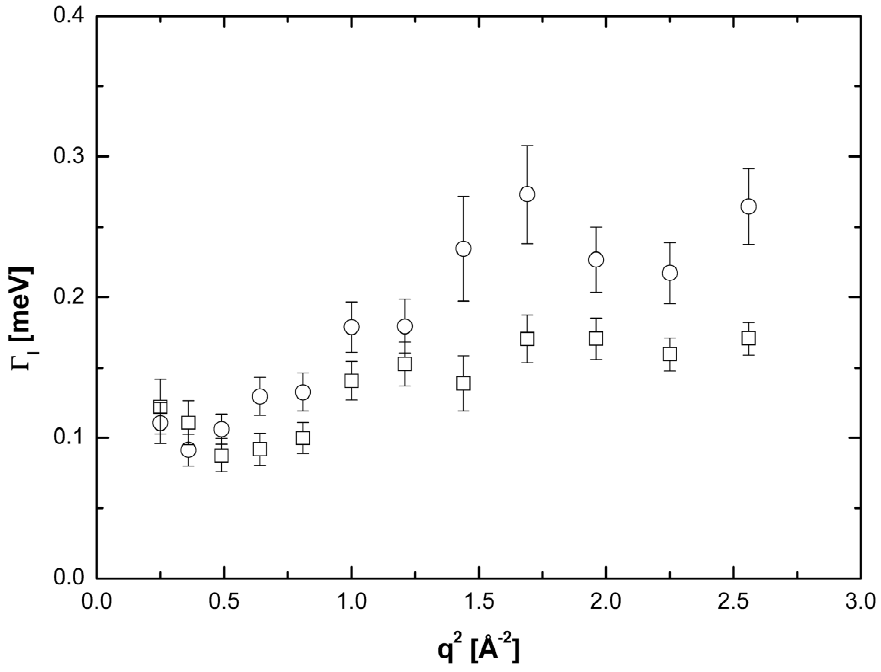


**Figure 6:** Half-widths at half-maximum $\Gamma_I$ of the broad Lorentzian as a function of $q^2$ at T=16.9 °C (squares) and 45.9 °C (circles).

### *4.4.4 Dynamic light scattering*

The diffusion coefficients of hemoglobin in $H_2O$ buffer at the concentrations 0.3 mg/ml, 1.2 mg/ml and 4.0 mg/ml were measured with dynamic light scattering in the temperature range of 16.9 °C to 45.9 °C. The diffusion coefficients at infinite dilution were obtained by linearly extrapolating the measured values to zero concentration. The measurements in $D_2O$ buffer showed pronounced hemoglobin aggregation. Therefore the values in $H_2O$ buffer were corrected for pure $D_2O$ and $H_2O$ viscosities (Cho C.H. 1999) to estimate the diffusion coefficients of hemoglobin in $D_2O$ buffer.

## 4.5 Discussion

### *4.5.1 Global Motions*

Hemoglobin molecules are densely packed in the cytoplasm with intermolecular distances in the order of some Ångstrom (Krueger and Nossal 1988). Well studied model systems for such a highly crowded protein solution are suspensions of colloidal particles (Hunter 2001). Colloidal particles are small enough that their motions are governed by thermal energy and big enough that the solvent molecules participate to the interactions only in an averaged way. The diffusion of these colloidal particles at infinite dilution $D_0$ is described by the Stokes-Einstein relation. At higher concentration the interactions between individual colloidal particles become important. In this case, direct Van-der-Waals and electrostatic forces determine particle diffusion, but hydrodynamic interactions mediated by the solvent play an important role (Dhont 1996). These hydrodynamic interactions describe how a colloidal particle moves in the flow-field which is determined by its neighboring particles. If a colloidal particle has collided and interacted directly with other particles, the diffusion coefficient approaches a constant value which is now termed long-time self-diffusion coefficient $D_S^L$. The time that a particle needs to cross a typical

interparticle distance d is referred to as structural relaxation time $\tau_D$. At timescales shorter than this structural relaxation time, the particle moves in an approximately constant configuration of the surrounding particles. This stage is governed by hydrodynamic interactions and the displacements of the colloidal particle are characterized by the so-called short-time self-diffusion coefficient $D_S^S$. The relaxation time is then given by $\tau_D \approx \frac{d^2}{6D_S^S}$. Beenakker and Mazur (Beenakker and Mazur 1984) first evaluated the coefficient $D_S^S$ over a large range of volume fractions. Due to configurational relaxation at long time scales, the long-time self-diffusion coefficient $D_S^L$ is always slower than the short-time self-diffusion coefficient $D_S^S$.

The values of $D_S^S$ and $D_S^L$ as a function of the volume fraction φ for non-charged hard-sphere particles were calculated by Tokoyama and Oppenheim (Tokuyama and Oppenheim 1994) taking into account both short and long range hydrodynamic interactions. Their theory predicts experimental data of uncharged colloids at intermediate and high volume fraction quite well. The volume fraction of hemoglobin in red blood cells is φ=0.25 (Krueger and Nossal 1988) and their calculations yield values of $D_S^S = 0.56 \cdot D_0$ and $D_S^L = 0.28 \cdot D_0$ with the diffusion coefficient at infinite dilution $D_0$.

Doster and Longeville measured the long-time self-diffusion coefficient of hemoglobin in red blood cells with neutron spin-echo spectroscopy (Doster and Longeville 2007) and applied for the first time in neutron spectroscopy the above mentioned concepts of hydrodynamic theory to interpret their data. They found a slightly reduced long-time self-diffusion coefficient of hemoglobin as compared to the predicted theoretical value. This reduction was explained due to the influence from the protein hydration shell which was supposed to stick to the surface of the protein and to move in a joint way.

In our work, we used the behavior of the line-widths $\Gamma_G(q)$ of the narrow Lorentzian to gain information about the short-time self-diffusion coefficient, the interparticle distance d and the residence time of hemoglobin diffusion in red blood cells. Neutron scattering results show the dependency of the length scale. The form of the half-widths is in agreement with a model for confined diffusion within a restricted spherical volume (Volino and Dianoux 1980). At small $q^2$-

values, longer real space length scales get visible and the effects of the boundaries dominate; the line-widths tend to a constant value $\Gamma_0$ instead of a zero intercept and a $Dq^2$ behavior for $q^2 \rightarrow 0$. At large $q^2$-values, the dynamic behavior at small real space length scales dominates. In the case of free diffusion, the elementary steps of motions are supposed to be infinitely small and the half-widths follow a limiting behavior of $\Gamma(q) = D \cdot q^2$ at large $q^2$. If the elementary steps of motions have a finite size, then the half-widths tend to an asymptotic value $\tau = 1/\Gamma_\infty$ (Bee 1988).

In our study, we calculated apparent average diffusion coefficients for assumed free diffusion from the behavior of the half-widths at large $q^2$ according to $\Gamma(q) = D_{app} \cdot q^2$. The temperature behavior of these apparent diffusion coefficients is well approximated with the Stokes-Einstein equation and a hydrodynamic radius of $R_h$=31.3 Å that is nearly identical to the published hydrodynamic radius of human hemoglobin of 31.7 Å (Digel et al. 2006). The sphere radius *r* of global confined motion was estimated from the value of constant $\Gamma_0$ at small $q^2$ and the diffusion coefficients according to the model of Dianoux and Volino with $r^2 = 4.33 \cdot D_{trans} / \Gamma_0$. If the assumptions are valid, then the sphere radius r should equally be given by the value of $q = \pi / r$ at which the plateau $\Gamma_0$ ends. These sphere radii are in average 1.7 times larger than those radii which were calculated using the diffusion coefficients of free diffusion and the value of $\Gamma_0$.

Dellerue et al. performed molecular dynamics simulations of a globular protein. They were able to analyze amino acid side-chain and backbone dynamics separately with a model for diffusion within a sphere with a distribution of radii (Dellerue et al. 2001). The authors calculated scattering functions from the simulations that were compared to neutron scattering results. They demonstrated that only in an ideal case for diffusion in a single-sphere with radius *r*, the plateau $\Gamma_0$ ends promptly at $q = \pi / r$. In the case of a distribution of sphere radii, the plateau exhibits a more gradual change and the plateau ends at an apparent smaller value *q'* than in the single sphere case. Consequently, if a sphere size is determined from the position of *q'*, the obtained apparent sphere radius is bigger than the real average value of the sphere radii distribution (Dellerue et al.

2001). For the side-chains and the backbone, the apparent sphere radii were between 1.7 and 1.8 times bigger than the average value of the distribution.

In our study, we found a factor of 1.7 between the sphere radii obtained with the two methods, which agrees nicely with the work of Dellerue et al. In this sense, the validity of our approach is confirmed. Obviously, this also demonstrates that confined global diffusion of hemoglobin in the red blood cells is best described by a distribution of sphere radii. In fact, recent small angle neutron scattering work points to the existence of a higher concentration of hemoglobin close to the internal membrane surface than in average in the cell (Garvey et al. 2004). Necessarily, the factor between apparent and average sphere radius will depend on the precise nature of the sphere distribution. In the following we limit our discussion to the sphere radii which were obtained from the value of constant $\Gamma_0$ at small $q^2$ and the average diffusion coefficients obtained from linear approximation at higher $q^2$-values.

We estimated a temperature independent radius $r$=2.2±0.2 Å of confined global hemoglobin diffusion. This has to be understood as the radius of the sphere in which the center of mass of the protein moves. This is in agreement with high resolution neutron-backscattering measurements of protein dynamics in whole *Escherichia coli* bacteria which found an average jump-length of 2.2±0.3 Å at 10.9 °C and an average jump-length of 1.9±0.2 Å at 29.9 °C of the protein population (Jasnin et al. 2008). Another neutron-backscattering study with concentrated myoglobin solution at φ=0.26 found a protein jump-diffusion length of 1.4 Å (Busch 2007). In this experiment the pH was not controlled which might have influenced the packing density of the protein, leading to a slightly reduced value.

From our measurements we conclude that the hemoglobin molecules diffuse in a cage of 2.2 Å radius before they interact directly with the neighbor proteins. The diffusion coefficient $D_0$ at infinite dilution in $D_2O$ buffer was obtained from dynamic light scattering experiments. The theoretical prediction yields $D_S^S = 0.56 \cdot D_0 = 2.85 \cdot 10^{-7} cm^2/s$ at 16.9 °C and $D_S^S = 5.83 \cdot 10^{-7} cm^2/s$ at 45.9 °C (Tokuyama and Oppenheim 1994). From these values we obtain structural relaxation times ranging from 280 ps to 140 ps. Even if the real short-time self-

diffusion coefficient might deviate from the theoretical predictions, the calculations show that the structural relaxation time is in the order of several hundred picoseconds.

We deduced the global apparent diffusion coefficient from the line-widths of the narrow Lorentz function. The correlation times of these line-widths range from 47 ps at 1.0 $Å^{-2}$ to 150 ps at 2.56 $Å^{-2}$. This is smaller than the structural relaxation time and therefore the experimentally measured apparent diffusion coefficients reflect short-time self-diffusion behavior of hemoglobin.

The measured apparent global diffusion coefficients are bigger than the true translational diffusion coefficients as they contain the contribution of rotational motion (Perez et al. 1999). Calculations for free diffusion of hemoglobin at infinite dilution give a correction factor of 1.27 between the apparent and true translational diffusion coefficients, similar to myoglobin and lysozyme solutions (Perez et al. 1999). However, the translational diffusion coefficient of hemoglobin in red blood cells is strongly reduced as compared to free diffusion (Doster and Longeville 2007). This is due to the high concentration of hemoglobin and resulting crowding effects, the correction factor can therefore serve only as an estimate.

The apparent global diffusion coefficients of hemoglobin were divided by 1.27 to obtain the translational diffusion coefficients $D_{trans}$. The diffusion coefficients at infinite dilution were scaled by a factor 0.56 (Tokuyama and Oppenheim 1994) to yield the theoretical predictions for short-time self-diffusion. The calculated quantities as a function of temperature are compared in **Figure 7**. The lines in the graph represent expected normal thermal behavior. In the investigated temperature range this is nearly linear in temperature. The translational diffusion coefficients in the red blood cells are around 1.5 times bigger than the predicted short-time self-diffusion values. An explanation could be that the concepts for non-charged hard-sphere colloids are not fully applicable to the much smaller protein molecules. It remains to be studied, if the solvent can be treated equivalently as a continuum both for large colloid particles and for the smaller protein molecules.

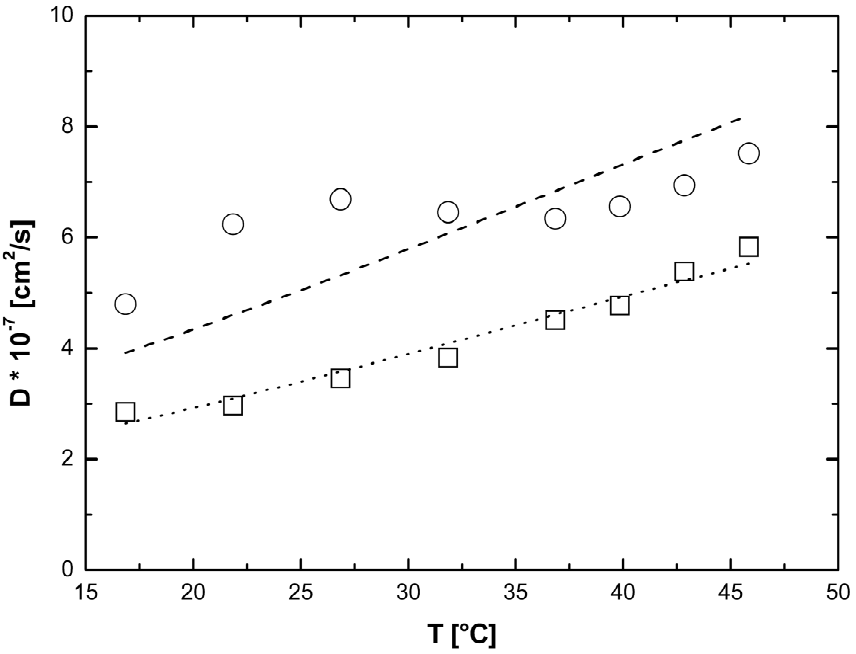


**Figure 7:** The apparent global diffusion coefficients of hemoglobin were divided by 1.27 to obtain the translational diffusion coefficients $D_{trans}$ (circles). The diffusion coefficients at infinite dilution were scaled by a factor 0.56 to yield the theoretical predictions for short-time self-diffusion $D_S^S$ (squares). The dashed and dotted lines show expected thermal behavior of the diffusion coefficients.

Hemoglobin carries only small total charge at the used pH values (Krueger and Nossal 1988) but it has got a distribution of positive and negatively charged residues on the protein surface. The interactions between proteins in concentrated solution are not expected to be described only by hard-sphere interactions. Recent investigations using small angle scattering and molecular dynamics simulations have shown the importance of both attractive and repulsive interactions between proteins in concentrated solution (Cardinaux et al. 2007; Stradner et al. 2006; Stradner et al. 2007; Stradner et al. 2004). How these repulsive and attractive protein-protein interactions influence hemoglobin self-diffusion in red blood cells requires further studies. Doster and Longeville argue that the hydration shell moves with the protein and needs to be included into the

volume fraction to correctly describe hemoglobin diffusion in red blood cells measured with neutron spin-echo spectroscopy (Doster and Longeville 2007). In this way they obtain effective volume fractions between 0.32 and 0.36. Taking into account these effective volume fractions, the discrepancy between our measured translational diffusion coefficients and the predicted short-time self-diffusion coefficients would then be even bigger. This interesting fact could be investigated further in detail by using neutron spectrometers with higher energy resolution to observe the change-over between hemoglobin short-time to long-time self-diffusion.

As discussed above, the line-widths might show signs of saturation at high $q^2$-values. We calculated the residence times between jumps from the analysis with a jump-diffusion model. Busch et al. (Busch 2007) found a residence time of 80ps at 20 °C in concentrated myoglobin solution and Jasnin et al. (Jasnin et al. 2008) obtained a residence time of 590ps at 30 °C in whole bacteria with high resolution neutron backscattering. In our work we obtained residence times of 51ps at 21.9 °C and 31ps at 31.9 °C. This is close to the values of concentrated myoglobin solution but differs strongly of the results of whole bacteria. We obtained an activation energy of $E_a$=6.6 ± 1.8 kcal/mol from the residence times. The residence time of jump-diffusion of pure water cannot be described in a general way by an Arrhenius law over a broad temperature range (Teixeira et al. 1985). We applied an Arrhenius law to literature values for the purpose of comparison for a restricted temperature range (Teixeira et al. 1985). In this way, the activation energy of pure water residence times in the range between 5 °C to 20 °C was found to be 6.7 ± 0.5 kcal/mol. This is very close to our obtained activation energy of hemoglobin residence times and could point out that hydrogen bond fluctuations are involved in hemoglobin global diffusion. The measured line-widths at large $q^2$ can be approximated both with a jump-diffusion model and assumed free diffusion in confined space. However, the errors are too big to decide clearly which model is appropriate. A jump-diffusion model might be more favorable to describe the measured data. How far a whole globular protein with a molecular weight of 64kDa can perform jump-diffusive motion is still not understood.

Global protein diffusion was estimated from the broadening of the narrow Lorentzian. The experimentally measured line-widths reach down to 3 µeV which correspond to correlation times

of 200ps. Usually any motions which result in line-widths smaller than the Gaussian resolution function – in our case 25 µeV in average (HWHM) – are considered to produce elastic scattering. It was shown by Perez et al. (Perez et al. 1999) and verified by Russo et al. (Russo et al. 2002) that in the case of protein solution this is not the case. Global protein diffusion results in detectable line-widths that are even smaller than the instrumental resolution itself. However, it should be noted that a Lorentzian has a significantly wider tailing than the Gaussian resolution function, which facilitates detection of small line-widths.

### *4.5.2 Internal Motions*

Internal protein dynamics covers a very broad distribution of time-scales ranging from motions in the pico- to nanosecond scale up to motions in the millisecond range. Fast internal motions in the picosecond time range are contained within the measured broad Lorentzian, whereas slow motions which cannot be resolved by the instrument contribute to the elastic part in the internal scattering function. The extracted quantities yield therefore only phenomenological information about average internal dynamics. Nevertheless, the obtained information is valid to study changes of the average internal dynamics as a function of temperature. We gained information about the geometries from the analysis of the EISF.

Micropipette experiments with aspirated single human red blood cells revealed a sudden change in the behavior of the cells from blockage of the pipette below $T_{Pipette}$=36.4 ± 0.4 °C to easy passage above. The transition temperature $T_{Pipette}$ of cell passage was surprisingly very close to human body temperature. The effect was interpreted as pronounced reduction in the viscosity of concentrated hemoglobin solution at $T_{Pipette}$ (Artmann et al. 1998). Further studies with circular dichroism (CD) investigated changes of the protein secondary structure around the transition temperature. A partial loss of alpha-helical content was found at a temperature $T_{CD}$=37.2 ± 0.6 °C (Artmann et al. 2004). The loss of hemoglobin alpha-helical structure at a specific temperature $T_{CD}$ was also observed for hemoglobin molecules of a big variety of different species (Digel et al. 2006; Zerlin et al. 2007). Amazingly, the transition temperatures $T_{CD}$ were directly correlated to the body temperature of the animals ranging from 34 °C for the duck-billed platypus to 42 °C for a bird, the spotted nutcracker. It was excluded that the partial loss of protein structure at $T_{CD}$

results from irreversible protein denaturation which occurs at distinctly higher temperatures. Independent of these experiments two-dimensional infrared correlation spectroscopy suggested a structural perturbation stage of bovine hemoglobin between 30 °C and 44 °C (Yan et al. 2004). The observed perturbations were assigned to hydrogen-bonded extended chains that connect the helices. It was concluded that the passage transition of red blood cells is caused by hemoglobin molecules and that the observed small structural changes of hemoglobin at $T_{CD}$ might be the cause for the drop of viscosity at $T_{Pipette}$ (Kelemen et al. 2001).

In our work we could determine the mean radius â of the distribution of spheres in which the mobile protein protons – in the used model mostly hydrogen atoms in side-chains – diffuse. The mean radii increase linearly between 16.9 °C and 31.9 °C due to higher thermal amplitudes. At 36.9 °C and higher temperatures the mean radii deviate from the low temperature linear behavior and increase with a significantly steeper slope. This pronounced increase in average sphere size is interpreted as partial unfolding of hemoglobin which begins at human body temperature.

In the partially unfolded state the side-chains can move in a larger space than in the more compact low temperature state. At 45.9 °C the accessible volume is around three times bigger than at 31.9 °C. The fraction of immobile protons p remains roughly constant within the errors; only the temperatures at 42.9 °C and 45.9 °C are slightly above the average. Hydrogen atoms which move so slowly that they contribute to the immobile fraction p are mainly located in the protein interior and in the protein backbone, amino acids towards the exterior and on the surface of the protein contribute mostly to the mobile fraction (Dellerue et al. 2001).

It was proposed that aggregation of hemoglobin in red blood cells occurs above body temperature and that an increase in surface hydrophobicity could be the reason for it (Digel et al. 2006). At first sight the aggregation effect at 36.9°C seems to be in contradiction with the observed larger volume of side-chain diffusion above this temperature. The observed change in side-chain mobility might reflect structural rearrangements that cause the increase in surface hydrophobicity. In this way the observed dynamical and structural changes in the picosecond time range and Ångstrom length scale could influence protein-protein interactions in the crowded cell environment. The cooperated effects of the protein interactions would then cause the measured

passage effect of whole red blood cells seen with micropipette experiments. This might be an intriguing example how atomic effects influence macroscopic properties of whole red blood cells.

The onset of protein aggregation might be as well the cause for the small increase in the fraction of immobile hydrogen atoms at 42.9 °C and 45.9 °C. Although the majority of external protein side-chains can access a larger space at these temperatures, a small side-chain fraction might get slowed down due to strong protein-protein interactions. The hydrogen atoms of these slowed down side-chains could then contribute to the fraction of immobile protons. Removing the protons from the average would also lead to a larger sphere radius in the Volino-Dianoux model.

As the immobile fraction p changes only slightly while the mean radii increase strongly above 36.9 °C, we conclude that the observed changes in the mobility occur mostly in amino acid side-chains on the surface of hemoglobin. If hydrogen atoms in the protein interior were involved during partial unfolding, then we would expect more pronounced changes in the fraction p of immobile protons. Large changes in the immobile fraction p go in hand with protein unfolding and denaturation (Fitter 2001; Gibrat et al. 2008; Russo et al. 2002) when internal side-chains and backbone hydrogen atoms become more mobile. In this case the immobile fraction approaches zero in the unfolded state. Our results confirm that the internal structure of hemoglobin unfolds only partially and does not denature completely in the investigated temperature range.

It is not yet understood if the observed effects of hemoglobin around body temperature are related to hemoglobin function in the human body. The temperature close to the core of the human body is some degrees Celsius higher then in the extremities. If and how hemoglobin function and the properties of red blood cells are influenced by this temperature difference is still an open question.

## 4.6 Conclusion

We have used incoherent quasielastic neutron scattering to measure the dynamics of hemoglobin in whole human red blood cells around body temperature. In our approach we could separate global protein diffusion from internal hemoglobin motions. We complemented our neutron experiments with dynamic light scattering measurements to obtain the diffusion coefficient of hemoglobin at infinite dilution. Theoretical predictions for concentrated suspensions of non-charged hard-sphere colloids were used to compare the global diffusion coefficients of hemoglobin in red blood cells with hemoglobin diffusion coefficients at infinite dilution. The values of the hemoglobin diffusion coefficients in the cells are in the same order as it is expected for short-time self-diffusion. The hemoglobin molecules are trapped in cages formed by neighboring proteins. The cage radius is in agreement with results of neutron backscattering studies on the average protein population in *Escherichia coli* cells and on concentrated myoglobin solutions (Busch et al. 2007; Jasnin et al. 2008). Internal protein motion was analyzed with a model for diffusion in a sphere with a distribution of radii. At temperatures higher than 36.9 °C amino acid side-chain motions occupy larger volumes than expected from normal temperature dependence. These results indicate partial unfolding of hemoglobin around human body temperature which is in agreement with circular dichroism experiments (Artmann et al. 2004; Digel et al. 2006; Zerlin et al. 2007). It was deduced that these changes are caused mostly by amino acid side-chains towards the exterior and on the surface of the proteins. Micropipette experiments with single red blood cells found a passage phenomenon from complete blockage of the pipette below body temperature to sudden passage at higher temperatures. It was suggested that intracellular hemoglobin aggregation at temperatures above human body temperature is responsible for the passage effect (Artmann et al. 1998). The observed changes in the geometry of amino acid side-chain motion at body temperature could reflect an increase in surface hydrophobicity which might cause an increase in protein-protein attraction and cause protein aggregation. Further studies on hemoglobin interactions in red blood cells would help to shed light on this issue. It is still unknown if the changes in the behavior of hemoglobin at body temperature are necessary for hemoglobin function in the human body. Protein dynamics and

structural changes in the picosecond time range and Ångstrom length scale might be connected to a macroscopic effect of whole red blood cells.

## 4.7 Acknowledgements

We thank Prof. Aysegül Temiz Artmann and Dipl. Ing. Dariusz Porst for taking blood and help during the sample preparation. This work is based on experiments performed at the Swiss spallation neutron source SINQ, Paul Scherrer Institute, Villigen, Switzerland. This research project has been supported by the European Commission under the 6th Framework Programme through the Key Action: Strengthening the European Research Area, Research Infrastructures. Contract n°: RII3-CT-2003-505925.

## 4.8 References

Alberts B. AJ, J. Lewis, M. Raff, K. Roberts, P. Walter (2002) Molecular biology of the cell, 4th edn. Garland Science, New York

Antonini E, Brunori M (1970) Hemoglobin. Ann. Rev. Biochem. 39:977-1042

Artmann GM, Burns L, Canaves JM, Temiz-Artmann A, Schmid-Schonbein GW, Chien S, Maggakis-Kelemen C (2004) Circular dichroism spectra of human hemoglobin reveal a reversible structural transition at body temperature. Eur. Biophys. J. 33:490-6

Artmann GM, Kelemen C, Porst D, Büldt G, Chien S (1998) Temperature transitions of protein properties in human red blood cells. Biophys. J. 75:3179-83

Austin RH, Beeson KW, Eisenstein L, Frauenfelder H, Gunsalus IC (1975) Dynamics of ligand binding to myoglobin. Biochem. 14:5355-73

Ball P (2008) Water as an Active Constitutent in Cell Biology. Chem. Rev. 108:74-108

Bauer GS, Salvatores M, Heusener G (2001) MEGAPIE, a 1 MW pilot experiment for a liquid metal spallation target. J. Nuc. Mat. 296:17-33

Bee M (1988) Quasielastic neutron scattering. Principles and Applications in Solid State Chemistry, Biology and Materials Science. Adam Hilger, Bristol and Philadelphia

Beenakker CWJ, Mazur P (1984) Diffusion of Spheres in a Concentrated Suspension .2. Physica A 126:349-370

Bosio L, Teixeira J, Bellissent-Funel MC (1989) Enhanced density fluctuations in water analyzed by neutron scattering. Phys Rev A 39:6612-6613

Brooks III C.L. MK, and B.M. Pettitt (1988) Proteins: A Theoretical Perspective of Dynamics, Structure, and Thermodynamics, vol 71. John Wiley & Sons, New York, USA

Busch S (2007) Microscopic Protein Diffusion at High Concentration. In: P.E. Sokol HK, D. Baxter, R. Pynn, D. Bossev, M. Leuschner (ed) QENS2006. Materials Research Society, Bloomington, Indiana, USA, pp 107-114

Busch S, Doster W, Longeville S, Garcia Sakai V, Unruh T (2007) Microscopic protein diffusion at high concentration. In: Sokol PE, Kaiser H, Baxter D, Pynn R, Bossev D, Leuschner M (eds) QENS2006. Materials Research Society, Bloomington, IN, pp 107-114

Cardinaux F, Stradner A, Schurtenberger P, Sciortino F, Zaccarelli E (2007) Modeling equilibrium clusters in lysozyme solutions. Europhys. Lett. 77:1-5

Carpentier L, Bee M, Giroud-Godquin AM, Maldivi P, Marchon JC (1989) Alkyl chain motions in columnar mesophases - A quasielastic neutron scattering study of dicopper tetrapalminat. Mol Phys 68:1367-1378

Cho C.H. JU, S. Singh, and G. Wilse Robinson (1999) Thermal Offset Viscosities of Liquid H2O, D2O, and T2O. J. Phys. Chem. B 103:1991-1994

Creighton TE (1992) Proteins: Structures and Molecular Properties, 2nd edn. W.H. Freeman & Co Ltd, New York

De Francesco A, Marconi M, Cinelli S, Onori G, Paciaroni A (2004) Picosecond Internal Dynamics of Lysozyme as Affected by Thermal Unfolding in Nonaqueous Environment. Biophys. J. 86:480-487

Dellerue S, Petrescu AJ, Smith JC, Bellissent-Funel MC (2001) Radially softening diffusive motions in a globular protein. Biophys. J. 81:1666-76

Dhont JKG (1996) An Introduction to Dynamics of Colloids. Elsevier, Amsterdam

Digel I, Maggakis-Kelemen C, Zerlin KF, Linder P, Kasischke N, Kayser P, Porst D, Temiz Artmann A, Artmann GM (2006) Body temperature-related structural transitions of monotremal and human hemoglobin. Biophys. J. 91:3014-21

Doster W, Cusack S, Petry W (1989) Dynamical transition of myoglobin revealed by inelastic neutron scattering. Nature 337:754-6

Doster W, Longeville S (2007) Microscopic diffusion and hydrodynamic interactions of hemoglobin in red blood cells. Biophys. J. 93:1360-8

Elantri S, Sire O, Alpert B (1990) Relationship between Protein Solvent Proton-Exchange and Progressive Conformation and Fluctuation Changes in Hemoglobin. Eur. J. Biochem 191:163-168

Elgsaeter A, Branton D (1974) Intramembrane particle aggregation in erythrocyte ghosts. I. The effects of protein removal. J. Cell. Biol. 63:1018-36

Fitter J (2001) Dynamical properties of a-amylase in the folded and unfolded state: the role of thermal equilibirum fluctuations for conformational entropy and protein stabilisation. Physica B 301:1-7

Fitter J, Herrmann R, Dencher NA, Blume A, Hauss T (2001) Activity and stability of a thermostable alpha-amylase compared to its mesophilic homologue: mechanisms of thermal adaptation. Biochemistry 40:10723-31

Frauenfelder H, Parak F, Young RD (1988) Conformational Substates in Proteins. Ann. Rev. of Biophys. Biophys. Chem. 17:451-479

Fraunfelder H, Sligar SG, Wolynes PG (1991) The energy landscapes and motions of proteins. Science 254:1598-1603

Gabel F, Bicout D, Lehnert U, Tehei M, Weik M, Zaccai G (2002) Protein dynamics studied by neutron scattering. Q. Rev. Biophys. 35:327-67

Garvey CJ, Knott RB, Drabarek E, Kuchel PW (2004) Shear-induced alignment of self-associated hemoglobin in human erythrocytes: small angle neutron scattering studies. Eur Biophys J 2004:589-595

Gibrat G, Assairi L, Blouquit Y, Craescu CT, Bellissent-Funel MC (2008) Biophysical study of thermal denaturation of apo-calmodulin: II-Dynamics of native and unfolded states. Biophys. J. doi:10.1529/biophysj:107.120147

Gregory RB (1995) Protein-Solvent Interactions. Marcel Dekker, New York

Hall D, Minton AP (2003) Macromolecular crowding: qualitative and semiquantitive successes, quantitative challenges. Biochim. Biophys. Acta 1649:127-139

http://www.ncnr.nist.gov/dave

Hunter RJ (2001) Foundations of Colloid Science, 2nd edn. Oxford University Press, Oxford

Janssen S, Mesot J, Holitzner L, Furrer A, Hempelmann R (1997) FOCUS: A hybrid TOF-spectrometer at SINQ. Physica B 234:1174-1176

Jasnin M, Moulin M, Haertlein M, Zaccai G, Tehei M (2008) Down to atomic-scale intracellular water dynamics. EMBO reports 9:543-547

Jasnin M, Moulin M, Haertlein M, Zaccai G, Tehei M (2008) In vivo measurement of internal and global macromolecular motions in E. coli. Biophys. J. 95:857-864

Kelemen C, Chien S, Artmann GM (2001) Temperature transition of human hemoglobin at body temperature: effects of calcium. Biophys. J. 80:2622-30

Krueger S, Nossal R (1988) SANS studies of interacting hemoglobin in intact erythrocytes. Biophys. J. 53:97-105

Lehnert U, Reat V, Weik M, Zaccai G, Pfister C (1998) Thermal motions in bacteriorhodopsin at different hydration levels studied by neutron scattering: correlation with kinetics and light-induced conformational changes. Biophys. J. 75:1945-52

Longeville S, Doster W, Kali G (2003) Myoglobin in crowded solutions: structure and diffusion. Chem. Phys. 292:413-424

McCammon JA, and S.C. Harvey (1987) Dynamics of Proteins and Nucleic Acids. Cambridge University Press, Cambridge UK

Minton AP (2001) The Influence of Macromolecular Crowding and Macromolecular Confinement on Biochemical Reactions in Physiological Media. J. Biol. Chem. 276:10577-10580

Paciaroni A, Cinelli S, Onori G (2002) Effect of the Environment on the Protein Dynamical Transition: A Neutron Scattering Study. Biophys. J. 83:1157-1164

Park SY, Yokoyama T, Shibayama N, Shiro Y, Tame JRH (2006) 1.25 angstrom resolution crystal structures of human haemoglobin in the oxy, deoxy and carbonmonoxy forms. J. Mol. Biol. 360:690-701

Perez J, Zanotti JM, Durand D (1999) Evolution of the internal dynamics of two globular proteins from dry powder to solution. Biophys. J. 77:454-69

Perutz MF, G. Fermi, B. Luisi (1987) Stereochemistry of Cooperative Mechanisms in Hemoglobin. Accounts of Chemical Research 20:309-321

Perutz MF, Rossmann MG, Cullis AF, Muirhead H, Will G, North ACT (1960) Structure of Haemoglobin: A Three-Dimensional Fourier Synthesis at 5.5-Å Resolution, Obtained by X-Ray Analysis. Nature 185:416-422

Reat V, Patzelt H, Ferrand M, Pfister C, Oesterhelt D, Zaccai G (1998) Dynamics of different functional parts of bacteriorhodopsin: H-2H labeling and neutron scattering. Proc. Natl. Acad. Sci. U.S.A. 95:4970-5

Russo D, Perez J, Zanotti JM, Desmadril M, Durand D (2002) Dynamic transition associated with the thermal denaturation of a small beta protein. Biophys. J. 83:2792-2800

Sears VF (1966) Theory of Cold Neutron Scattering by Homonuclear Diatomic Liquids .2. Hindered Rotation. Canadian Journal of Physics 44:1299-&

Smith JC (1991) Protein Dynamics - Comparison of Simulations with Inelastic Neutron-Scattering Experiments. Q. Rev. Biophys. 24:227-291

Stradner A, Cardinaux F, Schurtenberger P (2006) A small-angle scattering study on equilibrium clusters in lysozyme solutions. J. Phys. Chem. B 110:21222-21231

Stradner A, Foffi G, Dorsaz N, Thurston G, Schurtenberger P (2007) New insight into cataract formation: Enhanced stability through mutual attraction. Phys. Rev. Let. 99:1-4

Stradner A, Sedgwick H, Cardinaux F, Poon WC, Egelhaaf SU, Schurtenberger P (2004) Equilibrium cluster formation in concentrated protein solutions and colloids. Nature 432:492-5

Tang KES, Dill K (1998) Native protein fluctuations: the conformational-motion temperature and the inverse correlation of protein flexibility with protein stability. J. Biomol. Struct. Dyn. 16:397-411

Tehei M, Franzetti B, Madern D, Ginzburg M, Ginzburg BZ, Giudici-Orticoni MT, Bruschi M, Zaccai G (2004) Adaptation to extreme environments: macromolecular dynamics in bacteria compared in vivo by neutron scattering. Embo Reports 5:66-70

Tehei M, Madern D, Pfister C, Zaccai G (2001) Fast dynamics of halophilic malate dehydrogenase and BSA measured by neutron scattering under various solvent conditions influencing protein stability. Proc. Nat. Acad. Sci. U.S.A. 98:14356-61

Teixeira J, Bellissentfunel MC, Chen SH, Dianoux AJ (1985) Experimental-Determination of the Nature of Diffusive Motions of Water-Molecules at Low-Temperatures. Phys. Rev. A 31:1913-1917

Tokuyama M, Oppenheim I (1994) Dynamics of Hard-Sphere Suspensions. Phys. Rev. E 50:R16-R19

Tsai AM, Udovic TJ, Neumann DA (2001) The inverse relationship between protein dynamics and thermal stability. Biophys. J. 81:2339-2343

Volino F, Dianoux AJ (1980) Neutron Incoherent-Scattering Law for Diffusion in a Potential of Spherical-Symmetry - General Formalism and Application to Diffusion inside a Sphere. Mol. Phys. 41:271-279

Yan YB, Wang Q, He HW, Zhou HM (2004) Protein thermal aggregation involves distinct regions: sequential events in the heat-induced unfolding and aggregation of hemoglobin. Biophys. J. 86:1682-90

Zaccai G (2000) How soft is a protein? A protein dynamics force constant measured by neutron scattering. Science. 288:1604-1607

Zanotti JM, Bellissent-Funel MC, Parello J (1999) Hydration-coupled dynamics in proteins studied by neutron scattering and NMR: The case of the typical EF-hand calcium-binding parvalbumin. Biophys. J. 76:2390-2411

Zerlin KF, Kasischke N, Digel I, Maggakis-Kelemen C, Temiz Artmann A, Porst D, Kayser P, Linder P, Artmann GM (2007) Structural transition temperature of hemoglobins correlates with species' body temperature. Eur. Biophys. J. 37:1-10

Zimmerman SB, Minton AP (1993) Macromolecular Crowding: Biochemical, Biophysical and Physiological Consequences. Ann. Rev. Biophys. Biomol. Struct. 22:27-65

# *5. From Powder to Solution: Hydration Dependence of Human Hemoglobin Dynamics Correlated to Body Temperature*

Hemoglobin dynamics in concentrated solution and hydrated powder was measured with elastic and quasielastic incoherent neutron scattering. Global protein diffusion is absent in hydrated powder and strongly reduced in the solution sample at high concentration. Hemoglobin centre of mass diffusion did not contribute to the measured signal on the time scale of the used instruments. The experiments allowed the determination of internal protein dynamics with high accuracy. Hemoglobin dynamics in concentrated solution showed a larger flexibility above body temperature than expected from normal temperature dependence in agreement with the body temperature transition of hemoglobin that has been interpreted as partial unfolding. The results on hemoglobin dynamics in concentrated solution confirm the body temperature transition of hemoglobin dynamics in whole red blood cells described in chapter four of the thesis. Interestingly, the body temperature transition of hemoglobin dynamics was absent in the hydrated powder sample. The hydration level was sufficient to allow the well known dynamical transition at around 240 K. Therefore, protein specific motions are present at physiological temperatures in the hydrated powder sample. However, the rates of internal protein motion were suppressed in the hydrated powder sample compared to concentrated hemoglobin solution.

Hydrated protein powder samples have been considered as good model systems for studies on protein dynamics, and it was with such a sample, for example, that the dynamical transition at about 200K was discovered. In the comparison of powder, solution and cell samples, we concluded that fully hydrated protein powder samples might not accurately describe all protein picosecond dynamics aspects that are necessary for biological function.

The following chapter is based on an article submitted to *Biophysical Journal*.

Submitted to *Biophysical Journal*

# *From Powder to Solution: Hydration Dependence of Human Hemoglobin Dynamics Correlated to Body Temperature*

A. M. Stadler*[,#,1], I. Digel[§], J. P. Embs[||,**], T. Unruh[##], M. Tehei[§§, ||||], G. Zaccai*[2], G. Büldt[#], and G. M. Artmann[§]

* Institut Laue-Langevin, 38042 Grenoble, France;
# Research Centre Juelich, 52425 Jülich, Germany;
§ Institute of Bioengineering, Aachen University of Applied Science, 52428 Jülich, Germany;
|| Laboratory for Neutron Scattering ETH Zurich & Paul Scherrer Institut, 5232 Villigen-PSI, Switzerland;
** Saarland University, Physical Chemistry, 66123 Saarbrücken, Germany;
## Technische Universität München, Forschungsneutronenquelle Heinz Maier-Leibnitz (FRM II), 85747 Garching, Germany;
§§ School of Chemistry, University of Wollongong, 2522 Wollongong, Australia
|||| Australian Institute of Nuclear Science and Engineering (AINSE), Menai, Australia

corresponding author: zaccai@ill.fr

**Keywords:** neutron scattering – quasielastic - protein dynamics – hemoglobin – body temperature – hydration dependence

## 5.1 Abstract

A transition in hemoglobin (Hb), involving partial unfolding and aggregation, has been shown previously by various biophysical methods. The correlation between the transition temperature and body temperature for Hb from different species, suggested that it might be significant for biological function. In order to focus on such biologically relevant human Hb dynamics, we studied the protein internal picosecond motions as a response to hydration, by elastic and quasielastic neutron scattering. Rates of fast diffusive motions were found to be significantly enhanced with increasing hydration from fully hydrated powder to concentrated Hb solution. In concentrated protein solution, the data revealed that amino acid side-chains can explore larger volumes above body temperature than expected from normal temperature dependence. The body temperature transition in protein dynamics was absent in fully hydrated powder, indicating that picosecond protein dynamics responsible for the transition is activated only at a sufficient level of hydration. A collateral result from the study is that fully hydrated protein powder samples do not accurately describe all aspects of protein picosecond dynamics that might be necessary for biological function.

## 5.2 Introduction

Hemoglobin (Hb) in red blood cells and at high concentration in solution shows a variety of interesting effects (Artmann et al. 2008). Micropipette experiments with aspirated single human red blood cells found a sudden passage phenomenon of the cells at a transition temperature $T_{Pipette}$=36.4 ± 0.4°C close to human body temperature (36.6°C or 309.8 K) (Artmann et al. 1998). The diameter of the micropipette (~1.5 µm ) was small compared to the entire cells (~7 µm). Part of the cellular membrane is aspirated into the tight pipette tip and forms a tongue. The major fraction of the cell forms a sphere filled with Hb outside of the pipette. At temperatures lower than body temperature the cell cannot pass into the pipette completely and blocks the tip. Above body temperature, the trailing sphere can be compressed easily and all cells pass into the pipette with no apparent resistance (Artmann et al. 1998). Under normal conditions the concentration of Hb in red blood cells is ~330 mg/ml (Krueger and Nossal 1988). During the aspiration process below body temperature intracellular water is pressed out of the red blood cell, and it was estimated that Hb concentration reaches values of more than ~500 mg/ml (Artmann et al. 1998). Viscosity measurements were performed on Hb solutions between 330 mg/ml and 500 mg/ml to study the flow properties at such concentrations (Artmann et al. 1998). The experiments found a sharp drop in viscosity in Arrhenius plots at concentrations higher than 450 mg/ml at body temperature. The drop was absent at the physiological concentration of 330 mg/ml. The results were interpreted as a colloidal phase transition in highly concentrated Hb solution from a gel-like to a fluid state at body temperature (Artmann et al. 1998; Kelemen et al. 2001).

It has been further investigated, if the transition temperature of Hb is correlated to changes of the protein structure; the thermal stability of Hb secondary structure was investigated with circular dichroism spectroscopy (CD) (Artmann et al. 2004). The study showed a pronounced loss of α-helical content at $T_{CD}$=37.2 ± 0.6 °C, which is again close to human body temperature. Interestingly, further CD experiments established that thermal stability of Hb secondary structure of different animals is directly correlated to the corresponding body temperature of the species. The results ranged from $T_{CD}$=34.0±0.5°C for the duck-billed platypus (body temperature 33.0±1.0°C) to $T_{CD}$=42.0±1.0°C for a bird, the spotted nutcracker (body temperature 42.2±0.5°C°C) (Digel et al. 2006; Zerlin et al. 2007). It has been speculated that the mechanism behind Hb temperature behavior might be partial unfolding of

the α-helical structure at body temperature, which goes in hand with an increase in surface hydrophobicity that promotes protein aggregation (Digel et al. 2006).

Energy resolved incoherent neutron scattering is a powerful technique for the study of dynamics of biological macromolecules and its dependence on environmental conditions. Protein dynamics has been studied with neutron scattering in hydrated powders (Doster et al. 1989; Ferrand et al. 1993) and as a response to environmental conditions, in particular to the level of hydration (Cornicchi et al. 2006; Paciaroni et al. 2002; Paciaroni et al. 2006). In the past years, neutron scattering has been applied to study protein dynamics in whole cells *in-vivo* (Doster and Longeville 2007; Jasnin et al. 2008; Stadler et al. 2008; Tehei et al. 2004), in solution (Perez et al. 1999; Russo et al. 2002; Tehei et al. 2006), as well as recently in time-resolved experiments after photo-excitation (Combet et al. 2008; Pieper et al. 2008). Incoherent neutron scattering is dominated by hydrogen atom motions as their incoherent scattering cross section is one order of magnitude bigger than that of all other elements which usually occur in biological matter, and deuterium (Sears 1992). The technique probes average protein dynamics because hydrogen atoms are uniformly distributed in the natural abundance protein. The time and length scales of molecular motions that are accessible are determined by the energy resolution and the scattering vector range of the instrument, respectively. In general, the method covers the picosecond to nanosecond time range and angstrom length scale. At this time-length scale, hydrogen atoms that are covalently bound to amino acid side-chains reflect the dynamical behavior of these bigger chemical units (Reat et al. 1998; Smith 1991; Wood et al. 2008a). Below a so-called dynamical transition temperature of around 180-240K protein dynamics is predominantly harmonic. Harmonic motions correspond to vibrations of atoms around their structural equilibrium positions. Above the dynamical transition, and at sufficient hydration, additional anharmonic motions are activated (Doster et al. 1989; Ferrand et al. 1993; Lehnert et al. 1998). Depending on the energy resolution and scattering vector range of the neutron spectrometer, a second inflection in the thermal displacements, which is hydration-independent, was observed at a temperature between 100 and 150 K, and has been attributed to methyl group rotations (Cornicchi et al. 2006; Roh et al. 2006; Roh et al. 2005; Wood et al. 2007). These local jumps contribute to the sampling of a large number of conformational substates that are responsible for the entropic stabilization of proteins (Fraunfelder et al. 1991). From elastic incoherent neutron scattering (EINS) mean square displacements $<u^2>$ of the thermal cloud of atomic motions can be determined. The measured $<u^2>$ include both vibrational and diffusive motions (Reat et al. 1998). Quasielastic

neutron scattering (QENS) on the other hand, enables to distinguish between vibrational and diffusive components (Bee 1988). The technique allows the quantification of internal diffusion coefficients, residence times and the determination of the average geometry of motions.

Protein dynamics has been interpreted with a picture of a quasi-harmonic average potential well for the complex macromolecular force field (Bicout and Zaccai 2001; Zaccai 2000). In this sense, protein flexibility was defined as the amplitude of atomic motions $\sqrt{\langle u^2 \rangle}$ which corresponds to the width of the potential well. Protein thermal stability would correspond to the depth of the well (Tehei et al. 2001; Tehei and Zaccai 2007). A mean effective force constant $<k'>$ can be obtained from the dependence of the $<u^2>$ as function of temperature. This mean effective force constant, called resilience, describes the shape of the well (Zaccai 2000). Many conformational substates exist within the average well and are sampled by localized jump-diffusion (Fraunfelder et al. 1991). The geometry and activation energy of localized jumps can be determined by QENS.

Recently, we measured protein dynamics of Hb in human red blood cells *in vivo* with QENS (Stadler et al. 2008). At temperatures higher than human body temperature, amino acid side-chains dynamics showed a change in the geometry of motion towards larger volumes than expected from normal temperature dependence. This change under physiological hydration conditions was interpreted as a result of partial unfolding of Hb at body temperature. The partially unfolded state above body temperature was found to be less rigid than Hb below body temperature. Our goal in the present study was to investigate in detail with neutron scattering from powder to solution, how the different motions of human Hb depend on hydration. A change in the geometry of amino acid side-chain dynamics was identified close to human body temperature in concentrated Hb solution. Fully hydrated Hb powder showed the well known dynamical transition at around 180-240 K, but the change in the geometry of protein motions at body temperature was not found.

# 5.3 Material and Methods

## *5.3.1 Sample preparation*

Human Hb was purchased from Sigma (Sigma-Aldrich, St. Louis, MO, USA). To remove the exchangeable hydrogen atoms, around 1g protein was dissolved in 10 ml $D_2O$ and lyophilized afterwards. For the preparation of the hydrated powder sample, $D_2O$ exchanged Hb powder was dried over silica gel until no further loss of weight was observed. The dried powder was then rehydrated in $D_2O$ atmosphere to a level of 0.4 g $D_2O$/ 1 g protein. That level is not sufficient to cover the protein surface with a complete monolayer (Ball 2008), but this amount of non-freezing water permits the onset of anharmonic motions above the dynamical transition temperature of around 180-240 K (Rupley and Careri 1991). In this article we consider this as one full hydration layer. For the preparation of the Hb solution sample, $D_2O$ buffer (0.1M KCl, 61.3 mM $K_2HPO_4$, 5.33 mM $KH_2PO_4$, pD 7.4) was added to the $D_2O$ exchanged protein powder to a level of 1.1 g $D_2O$/ 1 g. The obtained concentration (570 mg/ml) corresponds to roughly three hydration layers. The concentration of potassium buffer was chosen to resemble saline conditions in whole cells (Alberts B. 2002), but it shall be noted that the choice of saline buffer can have an influence on protein dynamics (Gabel et al. 2004). The samples were rapidly sealed in flat aluminum sample holders for the experiments. It was checked by weighting that there occurred no loss of sample material during the experiment. The scattering cross section of Hb in the concentrated solution was estimated to be >96% and in hydrated powder to be >98.5%. Therefore, we neglected the contribution of the $D_2O$ solvent to the measured data.

## *5.3.2 Neutron scattering experiments*

The experiments were performed on the cold neutron multi-disk-chopper time-of-flight spectrometer TOFTOF (Unruh et al. 2007) at the research reactor FRM-II (TU München, Garching, Germany), on the cold neutron time-of-flight spectrometer FOCUS (Janssen et al. 1997), at the neutron spallation source SINQ (PSI, Villigen, Switzerland) and on the thermal neutron backscattering spectrometer IN13 (Natali et al. 2008) at the ILL high flux research reactor (ILL, Grenoble, France).

On TOFTOF, the incident wavelength was set to 5.1 Å and a chopper frequency of 12,000 rpm was chosen which corresponds to a scattering vector independent instrument resolution of approximately 100 µeV (full-width at half-maximum, FWHM). Hb in solution was measured on TOFTOF between 280 K and 325 K. On FOCUS, the incident wavelength was set to 6 Å, which corresponds to only a moderately scattering vector dependent elastic energy resolution between 41 µeV (FWHM) at $q$=0.4 Å$^{-1}$ and 61 µeV (FWHM) at $q$=1.6 Å$^{-1}$. Hydrated Hb powder was measured on FOCUS between 285 K and 322 K. The backscattering spectrometer IN13 is characterized by an energy resolution of 8 µeV (FWHM) and an incident wavelength of 2.23 Å. Hydrated Hb powder was measured between 20 K and 320 K on IN13. All samples, including the vanadium slab and empty sample holder, were oriented at 135° with respect to the incident neutron beam direction.

The measured spectra were corrected for energy dependent detector efficiency, empty cell scattering, normalized to vanadium, transformed into energy transfer and scattering vector space, and corrected with a detailed balance factor. Data on IN13 were normalized to the recorded intensities at 20 K instead of vanadium. On IN13 elastic neutron scattering was measured between 0.2 Å$^{-1}$ ≤ q ≤ 5.0 Å$^{-1}$. TOFTOF data were binned into 16 groups with 0.5 Å$^{-1}$ ≤ $q$ ≤ 2.0 Å$^{-1}$, FOCUS data were binned in 13 groups with 0.4 Å$^{-1}$ ≤ q ≤ 1.6 Å$^{-1}$. QENS data reduction and analysis was done using the programs FRIDA for TOFTOF (Wuttke 2006) and DAVE (2008) for FOCUS data. IN13 data were reduced with ILL standard programs. Multiple scattering was neglected as the transmission of all samples was higher than 0.9.

The resolution function of the instruments was determined with vanadium measurements for TOFTOF and FOCUS. The instrumental energy resolutions of $\Delta E$= 8, 50 and 100 µeV correspond to observable time scales in the order of $\Delta t$~ 80, 13 and 7 ps, respectively, using the relation $\Delta t = \hbar / \Delta E$.

### *5.3.3 Quasielastic Neutron Scattering Analysis*

An exhaustive description of quasielastic neutron scattering can be found in Bée (Bee 1988). The application to protein dynamics has been reviewed by Gabel et al. (Gabel et al. 2002) and Smith (Smith 1991). QENS spectra in this study were well described with a theoretical scattering function $S_{theo}(q,\omega)$ that contains a delta-function for the fraction of hydrogen atoms that appear localized within the time-space window of the instrument and one Lorentzian $L(\omega,q)$ for the quasielastic signal,

$$S_{theo}(q,\omega) = A_0(q) \times \delta(\omega) + (1 - A_0(q)) \times L(q,\omega). \qquad (5.1)$$

The elastic incoherent structure factor $A_0(q)$ (EISF) contains information about the geometry of motions. Mean square displacements of fast vibrational motions $\langle u^2 \rangle_{vib}$ (defined as the full amplitude of the motion (Smith 1991)) were taken into account by a Debye-Waller factor $\exp\left(-\langle u^2 \rangle_{vib} q^2 / 6\right)$ and were deduced from the scattering vector dependence of the summed intensities (Tehei et al. 2006). The quasielastic component is a Lorentzian $L(q,\omega) = \frac{1}{\pi} \cdot \frac{\Gamma(q)}{\omega^2 + \Gamma(q)^2}$, with half-widths at half-maximum $\Gamma(q)$.

The scattering function $S(q,\omega)$ plus background was convoluted with the instrumental resolution function $S_{res}(q,\omega)$ and fitted to the measured data according to

$$S_{meas} = \left[\exp\left(-\langle u^2 \rangle_{vib} q^2 / 6\right) \times S_{theo}(q,\omega) + B_0\right] \otimes S_{res}(q,\omega). \qquad (5.2)$$

The fits were performed over the energy transfer range from -1.5 meV to +1.5 meV for TOFTOF data and over the energy transfer range from -0.75 meV to +0.75 meV for FOCUS data.

Depending on the instrumental energy resolution and the used scattering vector range both internal protein dynamics and global translational diffusion of the macromolecules contribute to the measured signal in protein solution (Doster and Longeville 2007; Gaspar et al. 2008; Perez et al. 1999; Russo et al. 2002; Stadler et al. 2008). Due to the high protein concentration of our solution sample, global protein diffusion is strongly suppressed and cannot be resolved with the energy resolution of 100 µeV of the spectrometer TOFTOF (Tehei et al. 2006). In hydrated protein powders global macromolecular diffusion is absent. Therefore, it was possible to perform the experiment on FOCUS with a higher energy resolution of 50 µeV.

### *5.3.4 Elastic Neutron Scattering Analysis*

Elastic incoherent neutron scattering on IN13 was interpreted in terms of the Gaussian approximation. Mean square displacements $<u^2>$ were obtained from the scattering vector dependence of the elastic intensity *I(q)* according to $\langle u^2 \rangle = \frac{-6 \cdot \Delta(\ln I(q))}{\Delta q^2}$, where we use the definition of $<u^2>$ given by Smith that accounts for the full amplitude of motion (Smith 1991). This approach is formally similar to the Guinier approximation in small angle scattering experiments (Guinier and Fournet 1955). The analogy to small angle scattering has been discussed in (Gabel 2005; Réat et al. 1997). The obtained $<u^2>$ describe the spatial extend of the atomic thermal motions and include both vibrational and diffusive dynamics. The approximation is strictly valid for $q^2 \to 0$ but holds up to $\langle u^2 \rangle \cdot q^2 \sim 2$ (Réat et al. 1997). The calculations were performed in the smallest accessible $q^2$-range of IN13 data between 0.04 $Å^{-2} \leq q^2 \leq 2.02$ $Å^{-2}$ in which the Gaussian approximation is valid. Mean force constants $<k>$ that describe the protein resilience were obtained from the slope of $<u^2>$ versus temperature T according to $\langle k \rangle = 0.00276 / \left( d\langle u^2 \rangle / dT \right)$. Effective force constants $<k'>$ that include anharmonic dynamics of proteins were calculated according to $\langle k' \rangle = 0.00276 / \left( d\langle u^2 \rangle / dT \right)$ in a quasi-harmonic approximation (Zaccai 2000). The units are chosen so that $<k>$ is in N/m when $<u^2>$ is in Å2 and *T* is in K.

# 5.4 Results

## *5.4.1 Quasielastic Neutron Scattering*

Typical quasielastic neutron scattering spectra of hydrated Hb powder at 285 K measured on the spectrometer FOCUS and of Hb solution at 290 K measured on the instrument TOFTOF are shown in **Figure 1**. The measured data could be described with an elastic peak for the hydrogen fraction which appears localized in the time-length scale given by the energy resolution and scattering vector range of the instrument, and one Lorentzian for diffusive internal protein dynamics.

Conclusions about protein internal motions can be drawn from the $q$ dependences of the intensities and half-widths $\Gamma(q)$ of the elastic peaks and the Lorentzians, respectively. Information about the geometry of the motions is contained in the EISF $A_0(q)$, and about their correlation times in $\Gamma(q)$.

Hydrogen atoms that are covalently bound to amino acid side-chains reflect the dynamical behaviour of the bigger chemical units (Reat et al. 1998; Wood et al. 2008a). The ‘diffusion in a sphere’ model proposed by Volino and Dianoux (Volino and Dianoux 1980) accounts well for the motions of amino acid side-chains which perform diffusive jumps in a spherical volume restricted by neighboring amino acid side-chains. The radius can then be deduced from

$$A_0(q) = p + (1-p)\cdot\left[\frac{3j_1(qa)}{qa}\right]^2, \qquad (5.3)$$

where $j_1(qa)$ is the first-order spherical Bessel function of the first kind, $a$ is the sphere radius, and $A_0(q)$ is the EISF (Volino and Dianoux 1980). The populations of hydrogen atoms which appear as immobile and mobile within the instrumental energy resolution are represented by the fractions p and (1-p), respectively (Bellissent-Funel et al. 1992).

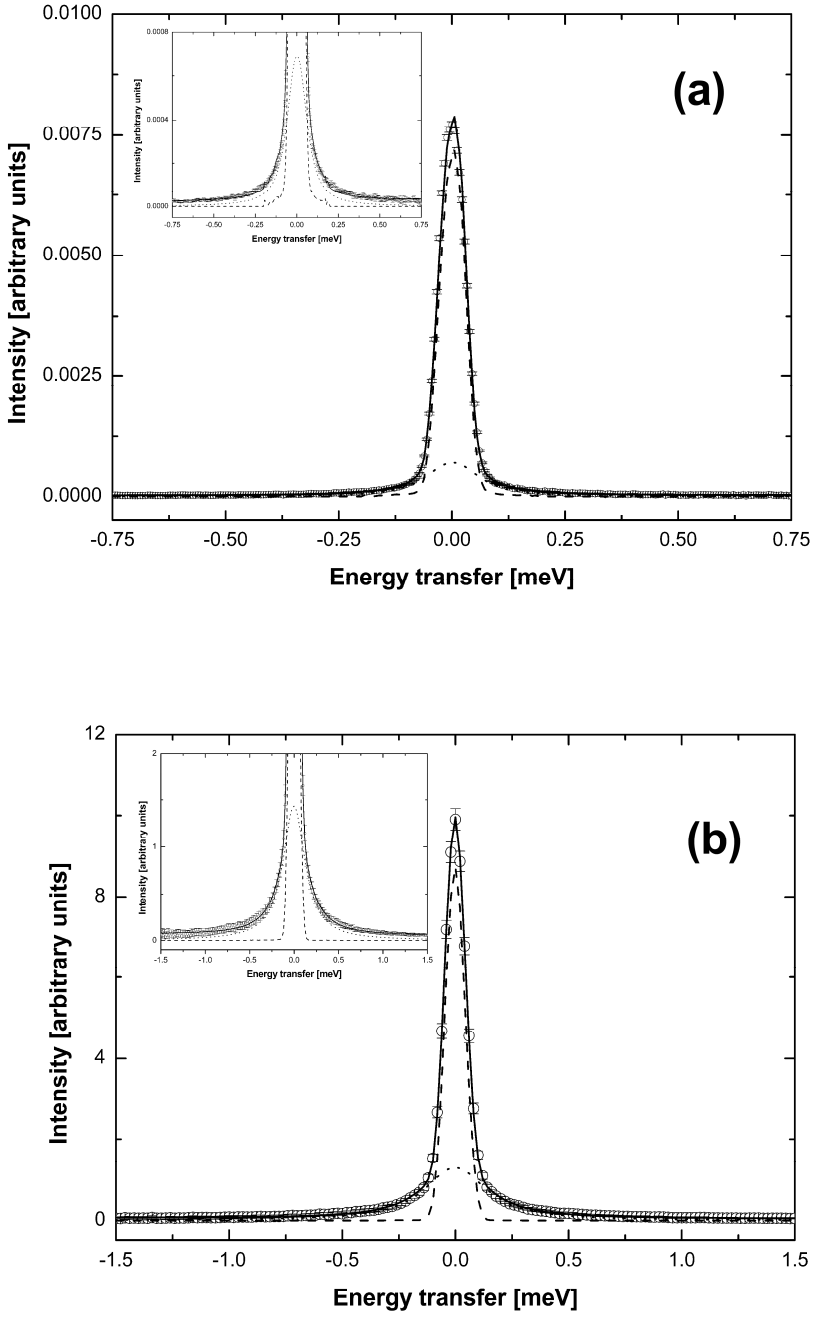


**Figure 1:** Quasielastic neutron spectra of (a) hydrated hemoglobin powder measured on FOCUS at the temperature 285 K at the scattering vector q=1.6 $Å^{-1}$, and (b) hemoglobin in solution measured on TOFTOF at the temperature 290 K at the scattering vector q=1.8 $Å^{-1}$. The circles show measured data and the solid line presents the fit (eq. 5.2). The components correspond to the elastic fraction (dashed line) and the Lorentzian (dotted line). The insets in (a) and (b) show magnifications of the spectra.

A Gaussian distribution *f(a)* of sphere radii *a* was used to describe measured EISF data of proteins to a high degree of accuracy (Russo et al. 2002). The Gaussian distribution is defined as $f(a) = \frac{2}{\sigma\sqrt{2\pi}} \exp\left(-a^2 / 2\sigma^2\right)$, with the standard deviation σ as free parameter. The mean value of the sphere radius is then given by $\hat{a} = \sigma\sqrt{\frac{2}{\pi}}$ .We recently measured Hb dynamics in whole red blood cells *in vivo* (Stadler et al. 2008*)* and interpreted the obtained EISF with the model for 'diffusion in a sphere' including a Gaussian distribution of sphere radii. For the purpose of continuity and comparison with the previous study, we used this model to interpret the EISF of the present work. Fits of the EISF were done over the scattering vector range of $q$=0.6-1.8 Å$^{-1}$ for TOFTOF and of $q$=0.5-1.6 Å$^{-1}$ for FOCUS. The EISF of Hb powder at the temperatures 285 K and 322 K and Hb solution at the temperatures of 290 K and 325 K are shown together with the fits of the model for diffusion in a sphere with a Gaussian distribution of radii in **Figure 2 a)** and **b)**. The mean sphere radius $\hat{a}$ of the Gaussian distribution as a function of temperature is given in **Figure 3** for Hb powder and Hb solution. The mean radii of the hydrated powder sample remain constant in the investigated temperature range and have the average value of $\hat{a}$=2.06 ± 0.02 Å. The mean values $\hat{a}$ of the Hb solution sample show different behavior. Within the errors, they increase linearly with temperature between the values $\hat{a}$=2.27 ± 0.06 Å at 280 K and $\hat{a}$=2.58 ± 0.09 Å at 310 K. There is an inflection point at 310 K above which the mean sphere radii increase linearly with a significantly steeper slope up to 3.44 ± 0.09 Å at 325 K. The values of the immobile fraction were found to be constant with temperature for the concentrated Hb solution sample with $p$=0.38 and to decrease linearly with increasing temperature for the Hb powder sample with $p$=0.67 at 285 K and $p$=0.53 at 322 K.

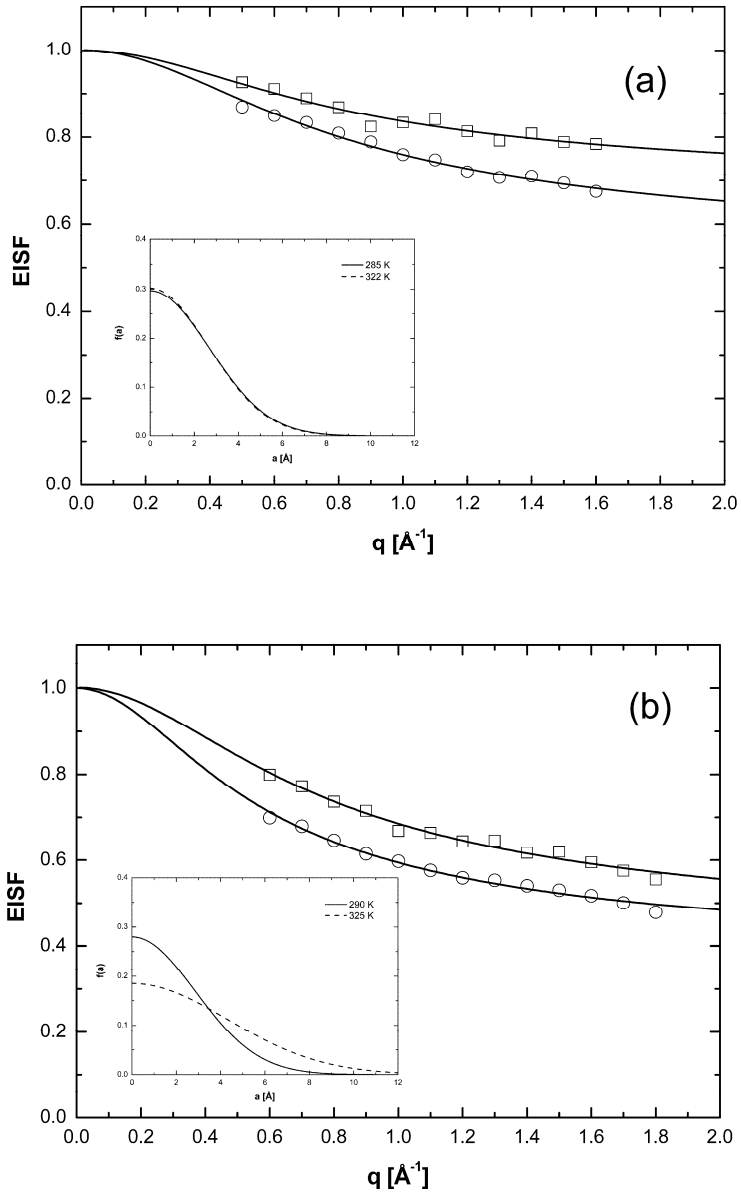


**Figure 2 (a)** EISF of hydrated hemoglobin powder at the temperatures 285 K (squares) and 322 K (circles) measured on FOCUS, **(b)** EISF of hemoglobin solution at the temperatures 290 K (squares) and 325 K (circles) measured on TOFTOF. The error bars are within the symbols. The solid lines present the fit (eq. 5.3) with a Gaussian distribution *f(a)* of radii. The insets in **(a)** and **(b)** show the distributions *f(a)* at the indicated temperatures for hemoglobin powder and solution, respectively.

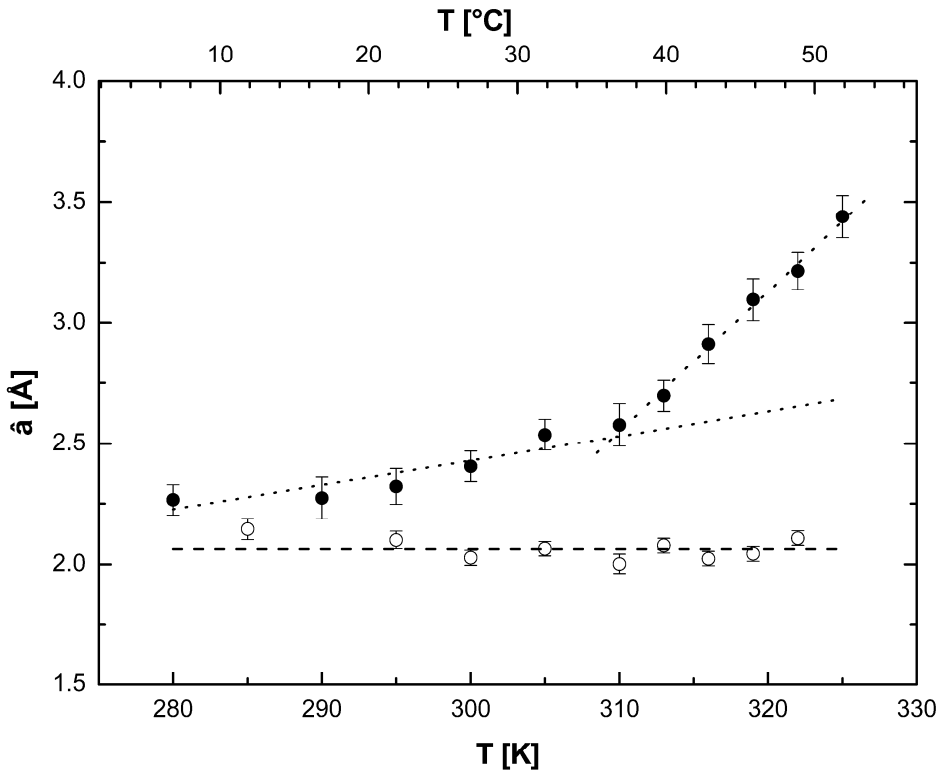


**Figure 3:** Mean value â of the Gaussian distribution as a function of temperature of hemoglobin in solution (filled circles) and hydrated hemoglobin powder (empty circles). The dashed and dotted lines are linear fits and serve as a guide for the eye.

The half-widths at half-maximum $\Gamma$ of the Lorentzian are shown in **Figure 4** as a function of the squared scattering vector $q^2$ at 285 K and 322 K for hydrated powder and at 290 K and 322 K for Hb solution. The measured half widths $\Gamma$ of the Hb solution sample show clear signs for restricted jump-diffusion (Hall and Ross 1981). The half widths $\Gamma$ approach a constant value $\Gamma_0$ at small $q^2$ at 290 K. Small $q^2$-values correspond to larger real space distances and the effects of boundaries on the dynamics of amino acid side-chains become visible. At the highest measured temperature of 322 K the plateau due to confinement would be visible only at very small $q^2$ values and is outside of the instrumental accessible scattering vector range as it was also found in protein solution (Bu et al. 2000). The limiting behavior of $\Gamma$ at small $q^2$-values is approximately described by the Volino-Dianoux model for diffusion in confined geometry (Volino and Dianoux 1980). The model assumes diffusion that is restricted to a sphere of radius $a$. It predicts constant half widths $\Gamma_0$ at $q$ values smaller then $q < \pi/a$ (Volino and Dianoux 1980). In the case of a distribution of sphere radii, the plateau ends at a smaller value $q'$ than in the single sphere case as shown with molecular dynamics simulations (Dellerue et al. 2001). We extracted the scattering vector positions from the article of Dellerue et al. (Dellerue et al. 2001) and concluded that the value $q'$ is approximately 1.7 times smaller for amino acid side-chain dynamics than predicted by the Volino-Dianoux model for a single sphere of radius $\hat{a}$ that is the average value of the sphere distribution (Dellerue et al. 2001). In our work, at the temperature of 290 K the obtained mean sphere radius is $\hat{a}$=2.27 Å and at 322 K the mean radius is $\hat{a}$=3.22 Å. The constant value $\Gamma_0$ should therefore end at $q^2 = \left(\pi/1.7 \cdot \hat{a}\right)^2 = 0.7 Å^{-2}$ at the temperature 290 K and at $q^2$=0.3 Å$^{-2}$ at the temperature 322 K. The $q$ resolution of the experiment is not very precise but the constant value of $\Gamma_0$ at 290 K ends between $q^2$=0.64 Å$^{-2}$ and 0.81 Å$^{-2}$ which agrees well with the derived value from the model. The constant value at 322 K would therefore be visible only below $q^2$=0.3 Å$^{-2}$ which cannot be measured with the instrument. Additionally, this supports our assumption of a distribution of sphere radii to describe the measured EISF.

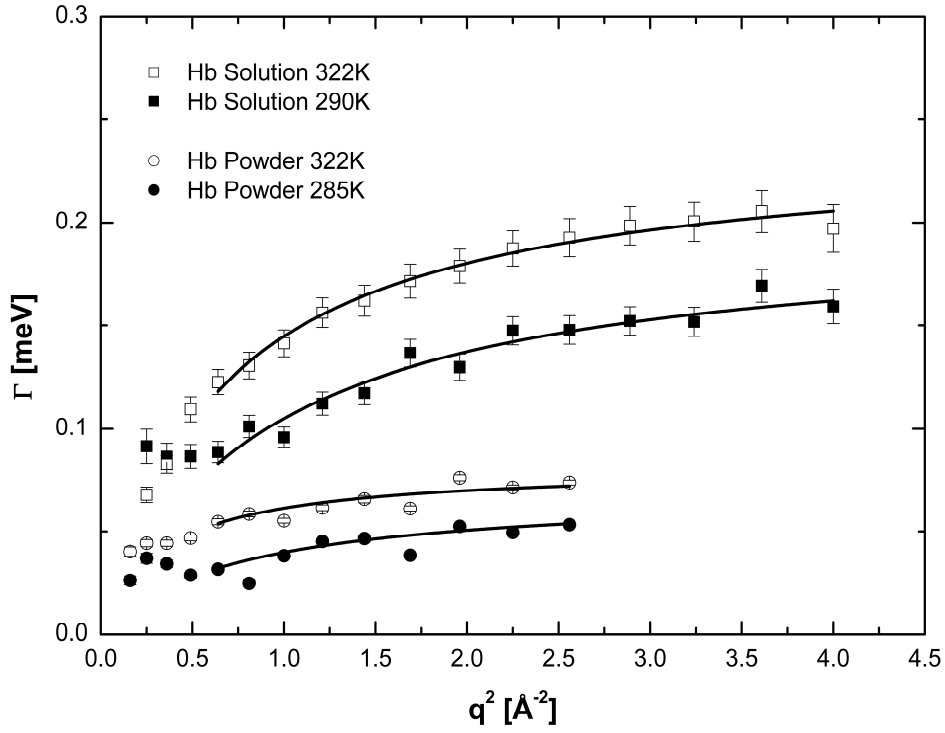


**Figure 4:** Half-widths at half-maximum $\Gamma$ of the Lorentzian as a function of scattering vector at different temperatures of hemoglobin in solution and as hydrated powder. The solid lines are fits according to a jump-diffusion model in the $q^2$-range from 0.64 Å$^{-2}$ to 4.0 Å$^{-2}$ and from 0.64 Å$^{-2}$ to 2.56 Å$^{-2}$.

At large scattering vector values of the Hb solution sample, the elementary nature of the diffusive jumps of the amino acid side-chains becomes evident. As these jumps are not infinitely small but occur over a finite length, the half-widths $\Gamma$ approach asymptotically a plateau $\Gamma_\infty$ at large $q^2$. The behavior of the half-widths can be described by a model of jump-diffusion according to $\Gamma = \frac{Dq^2}{1+Dq^2\tau}$, with the residence time before a jump $\tau$ and the jump-diffusion coefficient $D$ (Bee 1988). Fits were done with the jump-diffusion model in the $q^2$-range between 0.64 Å$^{-2}$ and 4.0 Å$^{-2}$. The values of the residence time $\tau$ as a function of temperature are presented in **Figure 5**. The obtained residence times follow the Arrhenius law $\tau(T) = \tau_0 \times e^{\frac{E_a}{k_B T}}$, and we extracted an activation energy of $E_a$=1.45 ± 0.18 kcal/mol.

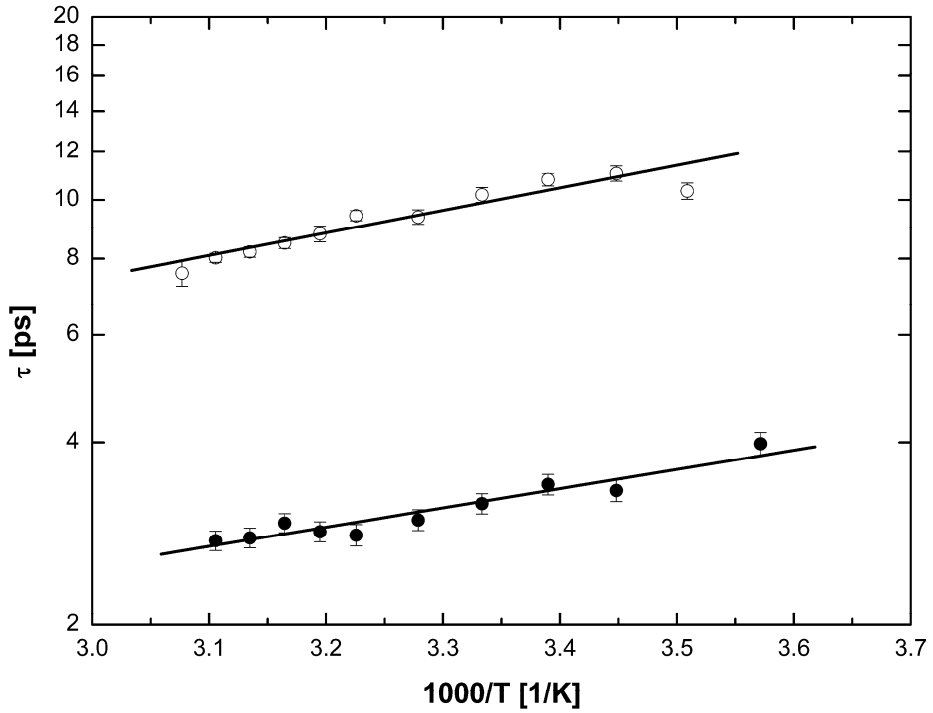


**Figure 5:** Residence time $\tau$ of hemoglobin in solution (filled circles) and hydrated hemoglobin powder (empty circles). The straight lines indicate fits according to the Arrhenius law. Activation energies of $E_a$=1.45 ± 0.18 kcal/mol for hemoglobin in solution, and $E_a$=1.70 ± 0.12 kcal/mol for hydrated hemoglobin powder were obtained.

The line-widths $\Gamma$ of the Hb powder sample increase with $q^2$, which is a sign for diffusive motions. Similar behavior was already observed in hydrated lysozyme and myoglobin powders (Perez et al. 1999). The line-widths do not intercept zero at the smallest $q^2$-values, which is characteristic for diffusion in a confined space (Bee 1988). For the purpose of comparison with the Hb solution, the half-widths of the Hb powder were also approximated with the jump-diffusion model as described above in the $q^2$-range of 0.64-2.56 Å$^{-2}$. The plateau $\Gamma_\infty$ of the half-widths was obtained by extrapolation of the model to higher $q^2$-values. In this way, we calculated residence times which are shown in **Figure 5**. The residence times follow the Arrhenius law and we obtain an activation energy of $E_a$=1.70 ± 0.12 kcal/mol.

The half widths of the Hb solution are at all $q^2$-values and all temperatures larger than those of Hb powder. As correlation times and line widths are inversely correlated, the larger half widths of the Hb solution compared to the hydrated powder indicate that the rates of side-chain diffusion get enhanced with increasing hydration.

### *5.4.2 Elastic Neutron Scattering*

Mean square displacements $\langle u^2 \rangle$ of hydrated Hb powder measured on IN13 were calculated from the data in the $q^2$-range up to $q^2$=2.02 Å$^{-2}$ and are given in **Figure 6**. The $\langle u^2 \rangle$ include both vibrational and diffusive motions of protein dynamics and show the well known dynamical transition at around 240 K (Doster et al. 1989; Ferrand et al. 1993; Parak et al. 1982). Values of the force constants of $\langle k \rangle = 1.18 \pm 0.29$ N/m for the low temperature range below 240 K and $\langle k' \rangle = 0.17 \pm 0.01$ N/m for the high temperature range above 240 K were obtained. QENS experiments allow the separation of vibrational and diffusive dynamics. Mean square displacements of fast vibrational motions $\langle u^2 \rangle_{vib}$ of the Hb powder sample measured with QENS on FOCUS are presented in **Figure 6**. The $\langle u^2 \rangle_{vib}$ agree with good accuracy with expected values obtained from linear extrapolation of the low temperature vibrational values $\langle u^2 \rangle$ measured on IN13.

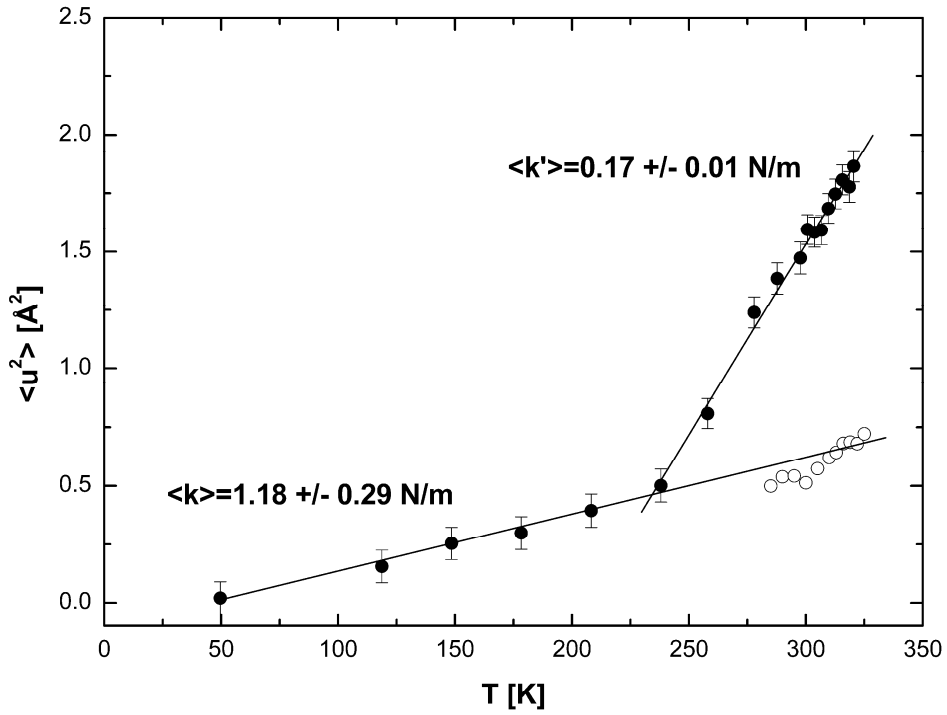


**Figure 6**. Mean square displacements $\langle u^2 \rangle$ of hydrated hemoglobin powder measured on IN13 (filled circles) and mean square displacements of fast vibrational motions $\langle u^2 \rangle_{vib}$ (using eq. 5.1 and 5.2) measured on FOCUS (empty circles). The error bars of $\langle u^2 \rangle_{vib}$ are within the symbols. The straight lines are linear fits to $\langle u^2 \rangle$ measured on IN13 below and above the dynamical transition temperature. The energy resolution of IN13 is 8μeV.

## 5.5 Discussion

It has previously been reported in the literature that protein flexibility is linked to protein structure: A neutron scattering study found that β-sheet proteins are less flexible than α-helical proteins. Proteins which consist of both α- and β-structure elements are more flexible than pure α-helical proteins and unstructured proteins were found to be the most flexible ones (Gaspar et al. 2008). Additionally, it has been shown that the unfolded state of lysozyme is more flexible and less resilient than the folded state (De Francesco et al. 2004). Consistently with these results, neutron scattering measurements of whole bacteria *in vivo* revealed that average protein flexibility is increased and macromolecular resilience is reduced in heat denatured bacteria cells as compared to native cells (Tehei et al. 2004). Furthermore, protein flexibility, resilience and internal diffusion rates have been found to be closely linked to the degree of hydration. Neutron scattering combined with hydrogen/ deuterium labeling of specific amino acids allowed the determination of average protein dynamics and active core fluctuations of bacteriorhodopsin as a function of hydration. Increasing the level of hydration from dry powder to a complete hydration layer coverage of bacteriorhodopsin permitted the onset of anharmonic motions above the dynamical transition temperature of around 180-240 K at a certain threshold hydration; a further increase of hydration led to a decrease of protein resilience (Lehnert et al. 1998; Paciaroni et al. 2002; Paciaroni et al. 2006; Wood et al. 2008b). Neutron scattering measurements of dry and hydrated protein powders, as well as of protein solution showed that the rates and amplitudes of amino acid side-chains diffusion on the protein surface are enhanced with higher hydration (Marconi et al. 2008; Perez et al. 1999). A study on lysozyme pointed out that internal protein dynamics get more activated when the environment changes from being a stabilizer to a plasticizer with increasing hydration (Paciaroni et al. 2002; Paciaroni et al. 2006). Paciaroni et al. (Paciaroni et al. 2002) concluded that protein internal dynamics seems to be ruled on the whole by the dynamical features of the environment. Further work on protein dynamics under physiological conditions in *E. coli* showed that hydrated powders do not accurately represent the dynamical behavior of macromolecules in whole cells. The higher amount of water in cells, as compared to fully hydrated protein powders, increases internal molecular flexibility and diffusive motion rates in the picosecond time-range (Jasnin et al. 2008).

We verified with EINS that the well know dynamical transition at around 240 K occurs at the chosen hydration of the Hb powder sample. At low temperatures only solid-like vibrational

motions are detected; at temperatures above the dynamical transition temperature $T_c$ protein specific quasi-diffusive motions are activated and contribute to the measured $\langle u^2 \rangle$ (Parak et al. 1982). From QENS experiments vibrational and diffusive motions can be separated. As expected, the obtained vibrational motions $\langle u^2 \rangle_{vib}$ are in good agreement with linear extrapolation of low temperature $\langle u^2 \rangle$ obtained from the EINS measurement. This supports the concept of quasi-diffusive motions in proteins being activated at $T_c$ that cause the pronounced increase of $\langle u^2 \rangle$ at temperatures above $T_c$ (Fraunfelder et al. 1991; Parak et al. 1982).

Our experiments revealed that increasing hydration of Hb has a strong influence on the rates of diffusive motions. The residence times of amino acid side-chain jump-diffusion in Hb solution lie between $\tau$=4.0 ± 0.2 ps at 280 K and 2.8 ± 0.1 ps at 322 K, whereas we obtain significantly higher residence times between $\tau$=10.3 ± 0.3 ps at 285 K and $\tau$=7.6 ± 0.4 ps at 325 K for hydrated Hb powder. The obtained activation energy $E_a$ of the residence times raises from 1.45 ± 0.18 kcal/mol for Hb solution to 1.70 ± 0.12 kcal/mol for hydrated Hb powder. We conclude that an increase of hydration from a single layer to nearly three layers enhances the rates of diffusive motions. The supplementary amount of water decreases the activation energy barriers between diffusive jumps and thus facilitates protein dynamics, as shown with QENS.

Protein folding and stability around body temperature is important for medical engineering and of high relevance for medicine and biology in general. Artmann et al. (Artmann et al. 1998) reported a transition temperature of human Hb at body temperature that was interpreted as Hb partial unfolding and acts as a precursor for protein aggregation. Further evidence for perturbations of Hb secondary structure at a specific transition temperature came from CD experiments (Digel et al. 2006; Zerlin et al. 2007). These studies of Digel et al. and Zerlin et al. established the fact that the transition temperature of Hb from a big variety of different animals is directly linked to the species' body temperature. Sequence alignments of Hb of different species were performed to identify an eventual region for the structural perturbation (Zerlin et al. 2007). Hb tertiary structure is highly conserved in general. However, but it was found that the amino acid sequences of the first two helices of the α- and β-subunits of Hb were of low similarity (~40-50% similarity), whereas the other parts have significantly higher similarity (~70-80% similarity), and especially the inner parts of the protein that are in close contact to the heme groups are highly conserved (up to 100% similarity). The parts of low

sequence similarity are located at external parts of the subunit and are solvent exposed. It was suggested that these solvent-exposed amino acid residues might be responsible for the onset of Hb partial unfolding and protein aggregation (Zerlin et al. 2007). In this work, we were able to investigate the geometry of amino acid-side chain diffusion of Hb as a function of temperature and hydration. QENS measurements allow an accurate analysis of protein diffusive motions (Bee 1988). A study of Engler et al. (Engler et al. 2003) classified hydrogen atoms in myoglobin in three dynamic groups: methyl group, long side-chain, and backbone hydrogen atoms. The authors concluded that above the dynamical transition at around 180-240 K mean square displacements measured by incoherent neutron scattering are dominated by the side chains, whereas the main chain stays rather rigid on a time scale faster than 100 ps (Engler et al. 2003). Therefore, in this study, we used the model of 'diffusion in a sphere' (Volino and Dianoux 1980) that is best suited to describe amino acid side-chain diffusion. Amino acid side-chain dynamics within proteins were found to be characterized by a distribution of flexibility. Side-chains in the protein interior are more rigid, whereas they possess a higher degree of flexibility towards the outside of the protein (Dellerue et al. 2001). The term flexibility corresponds in this sense to the restricted volume in which the amino acid side-chains can move. A recent neutron scattering study on bacteriorhodopsin using hydrogen/ deuterium labeling concluded that a mixture of local environment and residue type defines amino acid side-chain dynamics; further it was pointed out that different amino acids of the same type have different dependencies on their environment (Wood et al. 2008a). Therefore, we used an extended version of the 'diffusion in a sphere' model, which takes into account of a distribution of sphere radii (Perez et al. 1999; Russo et al. 2002; Stadler et al. 2008). We do not claim that the model by Volino and Dianoux (Volino and Dianoux 1980) which implies motions in a sphere with impermeable surface is the most appropriate one to describe the atomic nature of protein dynamics. However, it is able to describe the measured EISF with high accuracy. As we are mostly interested in the temperature dependence of protein flexibility, it is a valid approach to use this model for the purpose of comparison. We observed a sudden change in the geometry of amino acid side-chains at human body temperature towards larger volumes in concentrated Hb solution. This change at body temperature was absent in hydrated protein powder.

In recent studies of Hb dynamics in red blood cells, the break at 310 K in the sphere radii was interpreted as partial unfolding of Hb at human body temperature (Stadler et al. 2008). The same interpretation is valid for the results of Hb in concentrated solution. In this sense, the partially unfolded state of Hb solution at temperatures above 310 K has got higher flexibility

than the low temperature state, as its distribution is shifted to larger volumes. The fact that partial unfolding and the consequent changes of dynamics do not occur in hydrated powder implies a crucial role of hydration in this process. It was previously suggested that solvent accessible amino acid side-chains might be responsible for Hb partial unfolding (Digel et al. 2006; Zerlin et al. 2007). The experimental facts presented in this work justify this view. Diffusive motion rates of side-chains are strongly suppressed in hydrated Hb powder as compared to Hb in concentrated solution. We concluded previously that protein dynamics and changes in the complex macromolecular force field might be responsible for structural rearrangements and pronounced protein aggregation above body temperature (Stadler et al. 2008). The molecular properties of Hb therefore could determine in this sense the macroscopic properties of whole red blood cells (Artmann et al. 1998). We identified a fast process in the order of some picoseconds that is responsible for the change in geometry of protein dynamics at body temperature. A sufficient level of hydration beyond one surface layer is crucial for the activation of this fast process.

## 5.6 Conclusion

We studied protein dynamics of human Hb with elastic and quasielastic incoherent neutron scattering from fully hydrated powder to highly concentrated solution. The change in the level of hydration strongly influences the rates and activation energies of diffusive motions in the order of some picoseconds. The geometry of amino acid side-chain diffusion was described by a distribution of sphere radii that takes into account the polydispersity of internal protein flexibility. Above 310 K and only in highly concentrated solution, amino acid side-chain motions occupy larger volumes than expected from normal temperature dependence. These results are in agreement with CD measurements and micropipette experiments that reported partial unfolding of Hb and a passage transition of single red blood cells at body temperature (Artmann et al. 1998; Artmann et al. 2008; Digel et al. 2006; Zerlin et al. 2007). The change in Hb properties at body temperature was suggested to be related to biological function (Artmann et al. 1998; Artmann et al. 2008; Stadler et al. 2008). Therefore, it was concluded that dynamical processes of Hb in the order of a few picoseconds could be relevant for the properties of whole cells. Fully hydrated powder samples might not accurately describe fast protein dynamics that are relevant for biological function.

## 5.7 Acknowledgments

This study is based on experiments performed at FRM-II, TU München, Garching, Germany, at SINQ, PSI, Villigen, Switzerland, and at ILL, Grenoble, France. The research project was supported by the European Commission under the 6th Framework Programme through the Key Action: Strengthening the European Research Area, Research Infrastructures. Contract n°: RII3-CT-2003-505925. We thank Prof. Dr. Judith Peters and Dr. Francesca Natali for assistance on the instrument IN13, Dr. Marion Jasnin for fruitful discussion and critical reading of the manuscript. M. Tehei acknowledges the ILL and the AINSE for financial support.

## 5.8 References

(2008) DAVE Data Analysis and Visualisation Environment, http://www.ncnr.nist.gov/dave, vol 2008

Alberts B. AJ, J. Lewis, M. Raff, K. Roberts, P. Walter (2002) Molecular biology of the cell, 4th edn. Garland Science, New York

Artmann GM, Burns L, Canaves JM, Temiz-Artmann A, Schmid-Schonbein GW, Chien S, Maggakis-Kelemen C (2004) Circular dichroism spectra of human hemoglobin reveal a reversible structural transition at body temperature. Eur. Biophys. J. 33:490-6

Artmann GM, Kelemen C, Porst D, Büldt G, Chien S (1998) Temperature transitions of protein properties in human red blood cells. Biophys. J. 75:3179-83

Artmann GM, Zerlin KF, Digel I (2008) Hemoglobin Senses Body Temperature. In: Artmann GM, Chien S (eds) Bioengineering in Cell and Tissue Research, vol IV. Springer Verlag, Berlin, Heidelberg, pp 415-447

Ball P (2008) Water as an Active Constituent in Cell Biology. Chem. Phys. 108:74-108

Bee M (1988) Quasielastic neutron scattering. Principles and Applications in Solid State Chemistry, Biology and Materials Science. Adam Hilger, Bristol and Philadelphia

Bellissent-Funel MC, Teixeira J, Bradley KF, Chen SH (1992) Dynamics of hydration water in protein. J. Phys. I France 2:995-1001

Bicout DJ, Zaccai G (2001) Protein Flexibilty from the Dynamical Transition: A Force Constant Analysis. Biophys. J. 80:1115-1123

Bu Z, Neumann DA, Lee SH, Brown CM, Engelmann DM, Han CC (2000) A view of dynamics changes in the molten globule-native folding step by quasielastic neutron scattering. J. Mol. Biol. 301:525-536

Combet S, Pieper J, Coneggo F, Ambroise JP, Bellissent-Funel MC, Zanotti JM (2008) Coupling of laser excitation and inelastic neutron scattering: attempt to probe the dynamics of light-induced C-phycocyanin dynamics Eur. Biophys. J. 37:693-700

Cornicchi E, Marconi M, Onori G, Paciaroni A (2006) Controlling the Protein Dynamical Transition with Sugar-Based Bioprotectant Matrices: A Neutron Scattering Study. Biophys. J. 91

De Francesco A, Marconi M, Cinelli S, Onori G, Paciaroni A (2004) Picosecond Internal Dynamics of Lysozyme as Affected by Thermal Unfolding in Nonaqueous Environment. Biophys. J. 86:480-487

Dellerue S, Petrescu AJ, Smith JC, Bellissent-Funel MC (2001) Radially softening diffusive motions in a globular protein. Biophys. J. 81:1666-76

Digel I, Maggakis-Kelemen C, Zerlin KF, Linder P, Kasischke N, Kayser P, Porst D, Temiz Artmann A, Artmann GM (2006) Body temperature-related structural transitions of monotremal and human hemoglobin. Biophys. J. 91:3014-21

Doster W, Cusack S, Petry W (1989) Dynamical transition of myoglobin revealed by inelastic neutron scattering. Nature 337:754-6

Doster W, Longeville S (2007) Microscopic diffusion and hydrodynamic interactions of hemoglobin in red blood cells. Biophys. J. 93:1360-8

Engler N, Ostermann A, Niimura N, Parak F (2003) Hydrogen atoms in proteins: Positions and dynamics. Proc. Nat. Acad. Sci. U.S.A. 100:10243-10248

Ferrand M, Dianoux AJ, Petry W, Zaccai G (1993) Thermal Motions and Function of Bacteriorhodopsin in Purple Membranes - Effects of Temperature and Hydration Studied by Neutron-Scattering. Proc. Natl. Acad. Sci. U.S.A. 90:9668-9672

Fraunfelder H, Sligar SG, Wolynes PG (1991) The energy landscapes and motions of proteins. Science 254:1598-1603

Gabel F (2005) Protein dynamics in solution and powder measured by incoherent elastic neutron scattering: the influence of Q-range and energy resolution. Eur. Biophys. J. 34:1-12

Gabel F, Bicout D, Lehnert U, Tehei M, Weik M, Zaccai G (2002) Protein dynamics studied by neutron scattering. Q. Rev. Biophys. 35:327-67

Gabel F, Weik M, Doctor BP, Saxena A, Fournier D, Brochier L, Renault F, Masson P, Silman I, Zaccai G (2004) The influence of solvent composition on global dynamics of human butyrylcholinesterase powders: a neutron-scattering study. Biophys J 86:3152-65

Gaspar AM, Appavou MS, Busch S, Unruh T, Doster W (2008) Dynamics of well-folded and natively disordered proteins in solution: a time-of-flight neutron scattering study. Eur. Biophys. J. 37:573-582

Guinier A, Fournet G (1955) Small Angle Scattering of X-Rays. Wiley, New York

Hall PL, Ross DK (1981) Incoherent neutron scattering functions for random jump diffusion in bounded and infinite media. Mol. Phys. 42:673-682

Janssen S, Mesot J, Holitzner L, Furrer A, Hempelmann R (1997) FOCUS: A hybrid TOF-spectrometer at SINQ. Physica B 234:1174-1176

Jasnin M, Moulin M, Haertlein M, Zaccai G, Tehei M (2008) In vivo measurement of internal and global macromolecular motions in E. coli. Biophys. J. 95:857-864

Kelemen C, Chien S, Artmann GM (2001) Temperature transition of human hemoglobin at body temperature: effects of calcium. Biophys. J. 80:2622-30

Krueger S, Nossal R (1988) SANS studies of interacting hemoglobin in intact erythrocytes. Biophys. J. 53:97-105

Lehnert U, Reat V, Weik M, Zaccai G, Pfister C (1998) Thermal motions in bacteriorhodopsin at different hydration levels studied by neutron scattering: correlation with kinetics and light-induced conformational changes. Biophys. J. 75:1945-52

Marconi M, Cornicchi E, Onori G, Paciaroni A (2008) Comparative study of protein dynamics in hydrated powders and in solution: A neutron scattering investigation. Chem. Phys. 345:224-229

Natali F, Peters J, Russo D, Barbieri S, Chiapponi C, Cupane A, Deriu A, Di Bari MT, Farhi E, Gerelli Y, Mariani P, Paciaroni A, Rivasseau C, Schirograve G, Sonvico F (2008) IN13 Backscattering Spectrometer at ILL: Looking for Motions in Biological Macromolecules and Organisms Neutron News 19:14-18

Paciaroni A, Cinelli S, Onori G (2002) Effect of the environment on the protein dynamical transition: a neutron scattering study. Biophys. J. 83:1157-1164

Paciaroni A, Cornicchi E, De Francesco A, Marconi M, Onori G (2006) Conditioning action of the environment on the protein dynamics studied through elastic neutron scattering. Eur. Biophys. J. 35:591-599

Parak F, Knapp EW, Kucheida D (1982) Protein dynamics. Mossbauer spectroscopy on deoxymyoglobin crystals. J Mol Biol 161:177-94

Perez J, Zanotti JM, Durand D (1999) Evolution of the internal dynamics of two globular proteins from dry powder to solution. Biophys. J. 77:454-69

Pieper J, Buchsteiner A, Dencher NA, Lechner RE, Hauss T (2008) Transient Protein Softening during the Working Cycle of a Molecular Machine. Phys. Rev. Let. 100:228103

Reat V, Patzelt H, Ferrand M, Pfister C, Oesterhelt D, Zaccai G (1998) Dynamics of different functional parts of bacteriorhodopsin: H-2H labeling and neutron scattering. Proc. Natl. Acad. Sci. U.S.A. 95:4970-5

Réat V, Zaccai G, Ferrand M, Pfister C (1997) Functional dynamics in purple membranes Biological Macromolecular Dynamics. Adenine Press, New York, pp 117-122

Roh JH, Curtis JE, Azzam S, Novikov VN, Peral I, Chowdhuri Z, Gregory RB, Sokolov AP (2006) Influence of hydration on the dynamics of lysozyme. Biophys J 91:2573-88

Roh JH, Novikov VN, Gregory RB, Curtis JE, Chowdhuri Z, Sokolov AP (2005) Onsets of anharmonicity in protein dynamics. Phys. Rev. Lett. 95:038101

Rupley JA, Careri G (1991) Protein Hydration and Function Adv. Prot. Chem. 41:37-172

Russo D, Perez J, Zanotti JM, Desmadril M, Durand D (2002) Dynamic transition associated with the thermal denaturation of a small beta protein. Biophys. J. 83:2792-2800

Sears VF (1992) Neutron scattering lengths and cross sections. Neutron News 3:26-37

Smith JC (1991) Protein Dynamics - Comparison of Simulations with Inelastic Neutron-Scattering Experiments. Q. Rev. Biophys. 24:227-291

Stadler AM, Digel I, Artmann GM, Embs JP, Zaccai G, Büldt G (2008) Hemoglobin Dynamics in Red Blood Cells: Correlation to Body Temperature. Biophys. J. 95:5449-5461

Tehei M, Franzetti B, Madern D, Ginzburg M, Ginzburg BZ, Giudici-Orticoni MT, Bruschi M, Zaccai G (2004) Adaptation to extreme environments: macromolecular dynamics in bacteria compared in vivo by neutron scattering. EMBO Reports 5:66-70

Tehei M, Madern D, Pfister C, Zaccai G (2001) Fast dynamics of halophilic malate dehydrogenase and BSA measured by neutron scattering under various solvent conditions influencing protein stability. Proc Natl Acad Sci U S A 98:14356-61

Tehei M, Smith JC, Monk C, Ollivier J, Oettl M, Kurkal V, Finney JL, Daniel RM (2006) Dynamics of immobilized and native Escherichia coli dihydrofolate reductase by quasielastic neutron scattering. Biophys. J. 90:1090-7

Tehei M, Zaccai G (2007) Adaptation to high temperatures through macromolecular dynamics by neutron scattering. Febs J 274:4034-43

Unruh T, Neuhaus J, Petry W (2007) The high-resolution time-of-flight spectrometer TOFTOF. Nuclear Instruments and Methods in Physics Research Section A: Accelerators, Spectrometers, Detectors and Associated Equipement 580:1414-1422

Volino F, Dianoux AJ (1980) Neutron Incoherent-Scattering Law for Diffusion in a Potential of Spherical-Symmetry - General Formalism and Application to Diffusion inside a Sphere. Mol. Phys. 41:271-279

Wood K, Grudinin S, Kessler B, Weik M, Johnson M, Kneller GR, Oesterhelt D, Zaccai G (2008a) Dynamical Heterogeneity of Specific Amino Acids in Bacteriorhodopsin. J. Mol. Biol. 380:581-591

Wood K, Lehnert U, Kessler B, Zaccai G, Oesterhelt D (2008b) Hydration dependence of active core fluctuations in bacteriorhodopsin. Biophys. J. 95:194-202

Wood K, Plazanet M, Gabel F, Kessler B, Oesterhelt D, Tobias DJ, Zaccai G, Weik M (2007) Coupling of protein and hydration-water dynamics in biological membranes. Proc. Natl. Acad. Sci. U.S.A. 104:18049-54

Wuttke J (2006) FRIDA (fast reliable inelastic data analysis) http://sourceforge.net/projects/frida

Zaccai G (2000) How soft is a protein? A protein dynamics force constant measured by neutron scattering. Science. 288:1604-1607

Zerlin KF, Kasischke N, Digel I, Maggakis-Kelemen C, Temiz Artmann A, Porst D, Kayser P, Linder P, Artmann GM (2007) Structural transition temperature of hemoglobins correlates with species' body temperature. Eur. Biophys. J. 37:1-10

# 6. Cytoplasmic Water and Hydration Layer Dynamics in Human Red Blood Cells

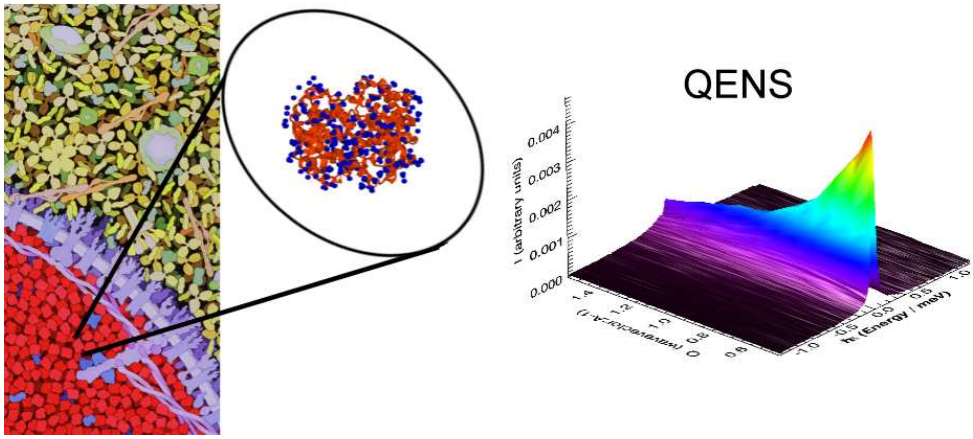


The dynamics of water in human red blood cells was measured with quasielastic incoherent neutron scattering in the temperature range between 290 K and 320 K. Neutron spectrometers with time resolutions of 40 ps, 13 ps and 7 ps were combined to cover time scales from that of bulk water dynamics to that of reduced mobility interfacial water motions. A major fraction of around 90% of cell water is characterized by a translational diffusion coefficient similar to bulk water. A minor fraction of around 10% of cellular water exhibits strongly reduced dynamics. This slow water fraction was attributed to dynamically bound water on the surface of hemoglobin which accounts for approximately half of the hydration layer.

The following chapter is based on a communication published in the *Journal of the American Chemical Society*. The length of the communication in edited form was limited to two pages. Therefore, details on sample preparation protocols, neutron scattering experiments, data analysis and surface area calculations are given in Supporting Information. For the purpose of continuity, the article is presented in the general layout of the manuscript.

*Journal of the American Chemical Society*, December 2008, 130 (50): 16852–16853

# *Cytoplasmic Water and Hydration Layer Dynamics in Human Red Blood Cells*

Andreas M. Stadler[†,‡], Jan P. Embs[§,¶], Ilya Digel[‖], Gerhard M. Artmann[‖], Tobias Unruh[††], Georg Büldt[‡], Giuseppe Zaccai*[,†]

ILL, 38042 Grenoble, France

Research Centre Jülich, 52425 Jülich, Germany;

LNS ETH Zurich & PSI, 5232 Villigen-PSI, Switzerland; Saarland University, 66123 Saarbrücken, Germany;

Aachen University of Applied Science, 52428 Jülich, Germany;

Technische Universität München, Forschungsneutronenquelle Heinz Maier-Leibnitz (FRM II), 85747 Garching, Germany

corresponding authour: zaccai@ill.fr

## 6.1 Introduction

Water is essential to life and a major scientific interest lies in a detailed understanding of how it interacts with biological macromolecules in cells. The cellular environment is extremely crowded with macromolecular concentrations up to 400 mg/ml (Ellis and Minton 2003). Distances between macromolecules are in the order of 1 nm, which corresponds to only few layers of water. Water that is in close contact with hydrophilic or hydrophobic protein surfaces (Russo et al. 2005) or which is trapped in surface cavities (Makarov et al. 2000) is shown to have significantly different behavior than bulk water. Recent studies point out that a major fraction of water in cells and bacteria shows bulk like dynamics (Jasnin et al. 2008; Persson and Halle 2008). We measured quasielastic incoherent neutron scattering (QENS) of $H_2O$ in red blood cells (RBC), *in vivo*. The data revealed two populations of water in RBC: a major fraction of ~90% which has translational properties similar to those of bulk water (time scale ~ps) and a minor fraction of ~10% which is interpreted as bound hydration water with significantly slower dynamics (time scale ~40 ps).

## 6.2 Material and Methods

QENS is a well-suited technique to study water dynamics in the ps-ns and Å time and length scale, respectively. Incoherent neutron scattering predominantly detects the motion of hydrogen nuclei, which have an incoherent scattering cross section which is more than 40 times larger than all other elements that occur in biological matter, and deuterium (Gabel et al. 2002). By subtracting experimental data of natural abundance RBC in $D_2O$ buffer from natural abundance RBC in $H_2O$ buffer, the cytoplasmic dynamics of $H_2O$ was separated from membrane and macromolecular dynamics. RBC consist mostly of $H_2O$ and hemoglobin at a concentration of ~330 mg/ml (Krueger and Nossal 1988). Samples of human venous blood were prepared in $H_2O$ and $D_2O$ HEPES buffer (see Supporting Information). Extracellular water content was found to be less than 10% of the total water content. We estimate that the incoherent cross section of the intracellular $H_2O$ is more than three times that of the macromolecules. In $D_2O$, the incoherent cross section of water is 8% that of the macromolecules. The difference is therefore dominated by the water signal, and we neglected changes in membrane and macromolecular dynamics due to isotope effects. Energy resolved neutron scattering was measured on the spectrometers IRIS at

ISIS, FOCUS at PSI and TOFTOF at FRM-II. A neutron spectrometer is characterized by its energy resolution and scattering vector ($q$) range, which determine the observable time and lengths scales of hydrogen motions. The energy resolution of the instruments IRIS, FOCUS and TOFTOF was 17 µeV, 50 µeV and 100 µeV, respectively, corresponding to longest observable times scales in the order of 40 ps, 13 ps and 7 ps. The theoretical scattering function of water dynamics is well described by a narrow and a broad Lorentzian for translational and rotational diffusion, and a delta function for the fraction of slow hydrogen motions that appear localized on the time scale corresponding to the energy resolution of the instrument (Bee 1988). The dependence of the half-widths at half-maximum (HWHM) of the narrow Lorentzian as a function of $q$ yields information about the atomic scale translational diffusion process (Bee 1988) (see 6.8 Supporting Information).

## 6.3 Results

The HWHM of cytoplasmic $H_2O$ measured on IRIS are shown with fits according to a jump-diffusion model in **Figure 1 a)**; in **Figure 1 b)** a measured spectrum on FOCUS together with the fitted components is given.

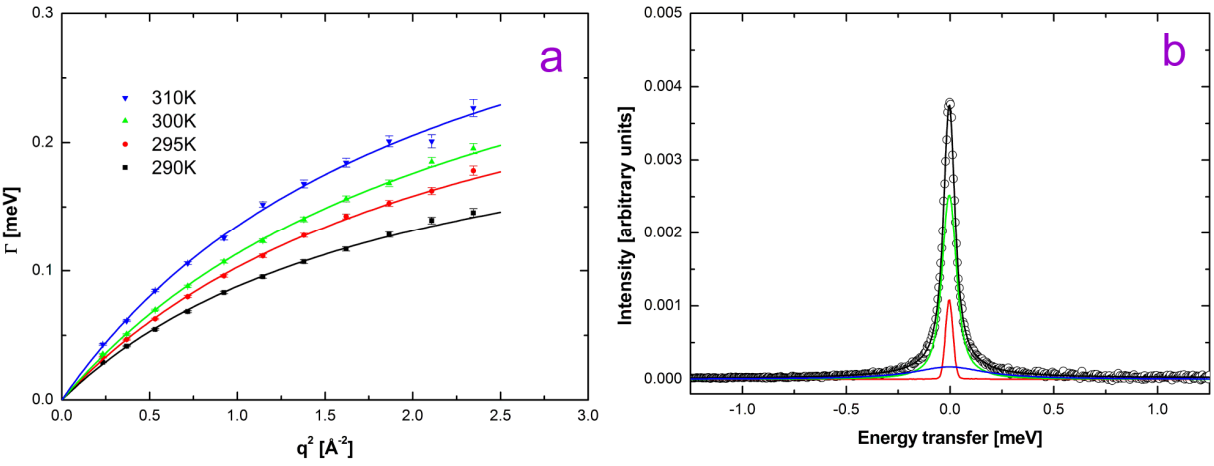


***Figure 1:*** a) Half-widths at half-maximum of the translational diffusion process of cytoplasmic $H_2O$ in RBC measured on IRIS at different temperatures. Solid lines represent fits according to a jump-diffusion model. b) QENS spectrum on FOCUS of cytoplasmic $H_2O$ in RBC at 290 K and q=0.55 $Å^{-1}$. Symbols show measured data, the black line presents the result of the fit. The components correspond to the immobile fraction (red line), the narrow Lorentzian (green line) and the broad Lorentzian (blue line).

**Figure 2 a)** reports the obtained translational diffusion coefficients *D* of $H_2O$ buffer and cytoplasmic $H_2O$ as a function of temperature measured with IRIS, FOCUS and TOFTOF. The data demonstrate that the translational diffusion coefficient of cellular water is nearly identical to $H_2O$ buffer on all spectrometers. The dashed line indicates normal temperature behavior of $H_2O$ buffer following an Arrhenius law and serves as reference. The measured diffusion coefficients of intracellular water with the instrument IRIS show perfect agreement with the reference; the results of TOFTOF and FOCUS deviate only slightly above and below, respectively. Residence times were found to be larger in intracellular than in bulk water (see 6.8 Supporting Information). The results indicate that translational diffusion of water in RBC behaves similarly to bulk water.

A QENS study on translational and rotational diffusion of water in *Escherichia coli* concluded that the main fraction of intracellular water shows similar dynamic behavior as bulk water with residence times twice as long (Jasnin et al. 2008). NMR work on rotational diffusion of cytoplasmic water found that approximately 85% of cell water in *Escherichia coli* has bulk-like dynamics (Persson and Halle 2008).

We could identify a significant fraction of immobile water in RBC that is absent in $H_2O$ buffer. The immobile water fraction was determined by the amplitude of the elastic peak divided by the integrated total intensity. Experimental data is presented in **Figure 2 b)** for the smallest accessible scattering vector of q~0.6 $Å^{-1}$ which reports on all movements up to around 10 Å real space distance. On this length scale confining effects of protein surface cavities or boundaries on water become observable. From the *q* dependence of the elastic intensity we estimated root mean square displacements $\langle u^2 \rangle^{1/2}$ of ~2.3 Å and ~2.1 Å for IRIS and FOCUS, respectively, which are smaller than the mean distance between water molecules (around 3 Å) and emphasize the localized nature of immobile water. Immobile water correlation times need to be longer than around 40 ps which is the time resolution of the high resolution spectrometer IRIS.

The obtained immobile water fraction of the RBC sample varies between 11% and 8% in the investigated temperature range. The uncertainty due to background subtraction was estimated to be below 2%. In contrast, the immobile fraction of $H_2O$ buffer is below 1% at all temperatures. The temperature dependence of the immobile fraction of $H_2O$ in RBC follows Arrhenius behavior with an activation energy of $E_a$=2.15 ± 0.10 kcal/mol.

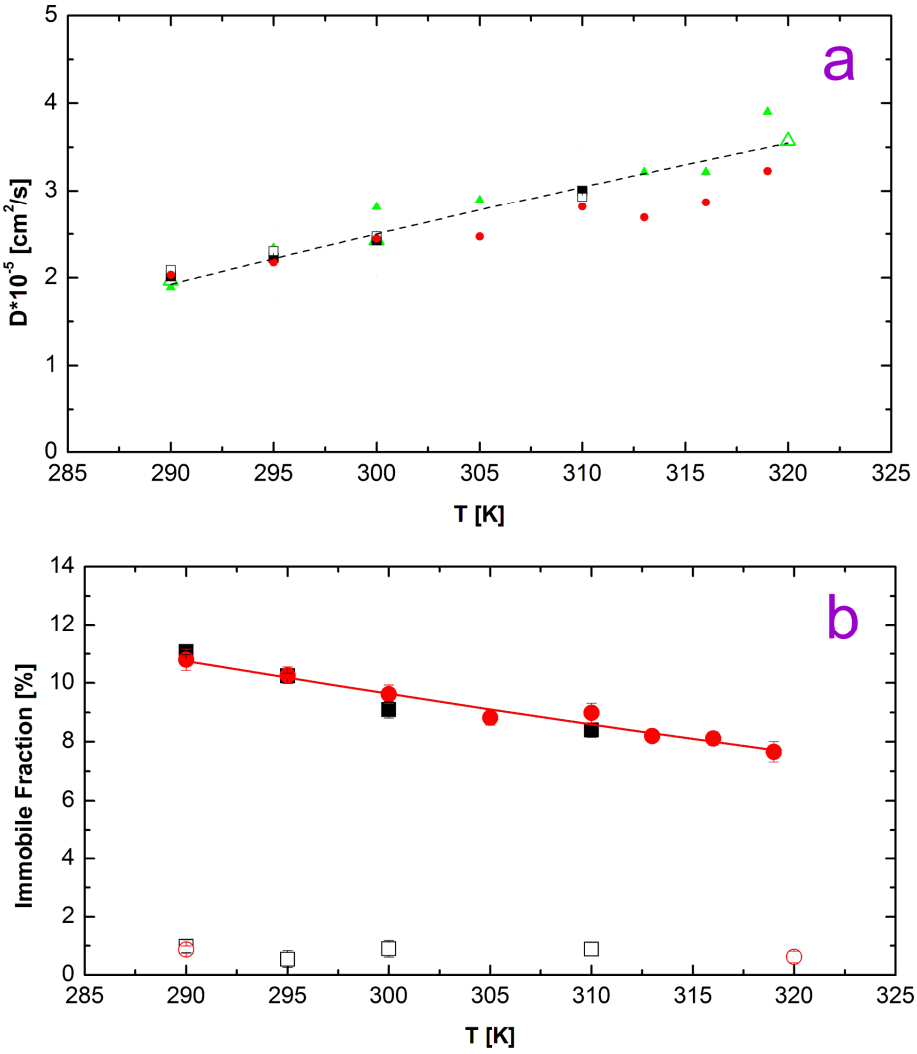


***Figure 2*: a)** Translational diffusion coefficient *D* of $H_2O$ in RBC measured on the instruments IRIS (filled black squares), FOCUS (filled red circles) and TOFTOF (filled green triangles); $H_2O$ buffer was measured on the instruments IRIS (empty black squares) and TOFTOF (empty green triangles). The dashed line indicates normal temperature behavior of $H_2O$ buffer. **b)** Percentage of immobile fraction of $H_2O$ in RBC measured on IRIS at q=0.61 $Å^{-1}$ (filled black squares) and FOCUS at q=0.55 $Å^{-1}$ (filled red circles) are compared to values of $H_2O$ buffer measured on IRIS (empty black squares) and FOCUS (empty red circles). The straight red line represents Arrhenius behavior.

## 6.4 Discussion

Hydrodynamic calculations of hemoglobin needed to include a bound water coverage of around 50% of the first hydration layer to predict quantitatively experimentally measured hydrodynamic parameters (Garcia de la Torre 2001). We estimated that approximately 2300 water molecules are in the first hydration layer of hemoglobin (see 6.8 Supporting Information). A study with High-Frequency Dielectric Spectroscopy (between 45 MHz-20 GHz) reported a value of 1030±70 dynamically bound $H_2O$ molecules on the surface of hemoglobin with highly restricted rotational dynamics (Wei et al. 1994) corresponding to a ~50% occupation of the first hydration layer. Site-directed tryptophan mutations combined with femtosecond spectroscopy identified two water populations in the protein hydration layer with fast (~1-8 ps) and slow (~20-200 ps) dynamics (Zhang et al. 2007). Assuming a cellular hemoglobin concentration of ~330 mg/ml, approximately 28% of all cellular water molecules are in direct contact with the surface of hemoglobin. Considering half of the first hydration layer to be bound, roughly 14% of cytoplasmic water would be bound in the protein hydration layer. This value is remarkably close to our results of the immobile water fraction. We therefore conclude that there exist two populations of water in RBC: a major fraction of ~90% which has translational properties similar to bulk water and a fraction of ~10% of immobile water which could be identified as dynamically bound water in the hydration layer of hemoglobin, *in vivo*. This bound hydration water should have important properties concerning protein stability and interactions in living cells.

## 6.5 Acknowledgment

We thank Franz Demmel for help with the experiment on IRIS, Aysegül Temiz Artmann and Dariusz Porst for help during sample preparation, Moeava Tehei and Marion Jasnin for fruitful discussions. This work is based on experiments performed at the neutron sources SINQ FRM II and ISIS. This research project has been supported by the European Commission under the 6$^{th}$ Framework Programme through the Key Action: Strengthening the European Research Area, Research Infrastructures. Contract n°: RII3-CT-2003-505925

# 6.6 Supporting Information

## *6.6.1 Sample preparation*

For neutron scattering experiments, samples of human venous blood from healthy adults were drawn with tubes containing heparin to prevent blood coagulation. The blood samples were suspended in HEPES buffer solution at pH=7.4 and 290 mOsm (137 mM NaCl, 4 mM KCl, 1.8 mM $CaCl_2$, 0.8 mM $Na_2HPO_4$, 0.2 mM $NaH_2PO_4$, 0.7 mM $MgSO_4$, 8.4 mM HEPES, 4 mM NaOH). The cells were washed twice and collected by centrifugation at 560 rcf for 10 min. The supernatant was removed together with the 'buffy coat' on top of the cells. The washed cells and the successively used buffer solutions were then gassed with CO to increase the stability of hemoglobin. The cells were resuspended in TRIS buffer (20 mM TRIS, 145 mM NaCl) at pH=5.5 and treated with neuraminidase (from *Clostridium perfringens* Type VI, purchased from Sigma-Aldrich) to remove the glycocalyx matrix as described elsewhere (Elgsaeter and Branton 1974). Afterwards the cells were washed in $H_2O$ HEPES buffer. To reduce the neutron scattering contribution of the buffer, a portion of the cells were washed with $D_2O$ HEPES buffer (pD=7.4, 290 mOsm), incubated for around 30 min and centrifuged at 560 relative centrifugal force. The washing steps were repeated until the level of $H_2O$ was estimated to be below 0.1 vol% assuming that the $H_2O$-$D_2O$ exchange through the cell membrane reaches a constant value in this time. No cell lysis was detected during the preparation and the shape of the cells was checked with optical microscopy at the end. After a final centrifugation step the cell pellet was sealed in a flat aluminum sample holder of 0.2 mm thickness for the neutron scattering experiment. The scattering from the aluminum screws was blocked using a cadmium mask. It was checked by weighing that there occurred no loss of sample material during the experiment.

The amount of water in the cell sample was determined by drying of an aliquot. Taking into account a cellular hemoglobin concentration of 330 mg/ml, we obtained an extracellular water content of less then 10%.

### *6.6.2 Neutron experiments*

High resolution neutron scattering was measured on the inverted time-of-flight backscattering spectrometer IRIS (Carlile and Adams 1992) at the ISIS neutron spallation source (Rutherford Appleton Laboratory, Didcot, United Kingdom). The energy resolution of the instrument was approximately 17 µeV. Neutron scattering with middle energy resolution was measured on the cold time-of-flight spectrometer FOCUS (Janssen et al. 1997) at the neutron spallation source SINQ (Paul Scherrer Institut, Villigen, Switzerland). The incident wavelength was set to 6 Å, yielding an average energy resolution of around 50 µeV. Low resolution neutron scattering was measured on the cold neutron time-of-flight spectrometer TOFTOF (Unruh et al. 2007) at the research reactor FRM-II (Research Reactor Heinz Maier-Leibnitz, Garching, Germany). The incident wavelength was set to 5.1 Å and the chopper speed to 12000 rpm which corresponds to an instrument resolution at the elastic line of approximately 100 µeV.

Samples were measured in the temperature range of 290 K to 320 K in which no hemolysis occurs. All samples, including the 1 mm thick vanadium slab and empty sample holder, were oriented at 135° with respect to the incident neutron beam direction. Measured data of the cell sample in $D_2O$ buffer was subtracted from data of the cell sample in $H_2O$ buffer to obtain the contribution of $H_2O$. Experimental data of RBC samples in $H_2O$ buffer and $D_2O$ buffer measured on the instrument FOCUS at 290 K are shown **in Figure 3**. The relatively big difference of both samples allowed a clear separation of the $H_2O$ contribution.

In the case of vanadium which gives purely incoherent and isotropic scattering and $H_2O$ HEPES buffer, the empty cell was subtracted instead. The measured time-of-flight spectra were normalized to vanadium, transformed into energy transfer and scattering vector space and corrected with a detailed balance factor. IRIS data was binned into 17 groups with $0.48\ Å^{-1} \leq q \leq 1.85\ Å^{-1}$, FOCUS data was binned in 12 groups with $0.5\ Å^{-1} \leq q \leq 1.6\ Å^{-1}$, TOFTOF data in 13 groups with $0.6\ Å^{-1} \leq q \leq 1.8\ Å^{-1}$. The instrumental energy resolution was measured with vanadium. Data treatment and analysis was done with the instrument specific program packages DAVE (2008a), IDA (Wuttke) and MODES (2008b). Multiple scattering was neglected as the transmission of all samples was higher than 0.9.

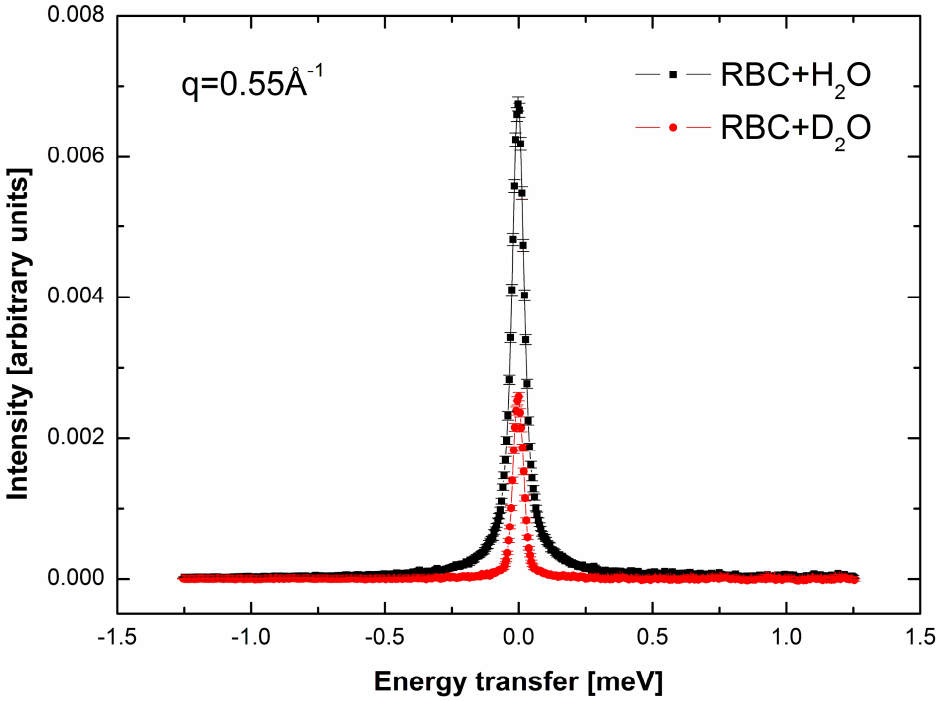


**Figure 3:** Experimental QENS data of RBC in $H_2O$ and $D_2O$ buffer measured on FOCUS at the temperature 290 K and at the scattering vector q=0.55 Å$^{-1}$. The larger intensities of the elastic and quasielastic part of RBC in $H_2O$ buffer as compared to RBC in $D_2O$ buffer result from $H_2O$ dynamics.

### *6.6.3 Data analysis*

The theoretical scattering function for translational and rotational diffusion of water can be approximated as (Bee 1988)

$$S_{theo}(q,\omega) = e^{-\langle x^2 \rangle \cdot q^2} \left\{ A_1(q) \cdot \frac{\Gamma_T(q)}{\omega^2 + \Gamma_T(q)^2} + A_2(q) \cdot \frac{\Gamma_T(q) + \Gamma_R(q)}{\omega^2 + [\Gamma_T(q) + \Gamma_R(q)]^2} \right\}, \qquad (6.1)$$

where $\langle x^2 \rangle$ stands for the mean square displacement of fast vibrational motion; the first Lorentzian in the curly brackets represents translational diffusion, the second Lorentzian

combines translational and rotational diffusion with the half-widths at half-maximum (HWHM) $\Gamma_T(q)$ and $\Gamma_R(q)$, respectively. The experimental measured scattering function $S_{\exp}(q,\omega)$ is obtained by convolution of $S_{theo}(q,\omega)$ with the instrumental energy resolution $S_{res}(q,\omega)$ according to

$$S_{\exp}(q,\omega) = \left[ e^{-\langle x^2 \rangle q^2} \cdot A_0(q) \cdot \delta(\omega) + S_{theo}(q,\omega) + B_0 \right] \otimes S_{res}(q,\omega), \qquad (6.2)$$

where $A_0(q)$ is the elastic incoherent structure factor of slow hydrogen dynamics that appear immobile within the instrumental energy resolution and $B_0$ is linear background.

All QENS data were fitted according to equations (6.1) and (6.2): IRIS data was described well with only one Lorentzian for translational diffusion. Fits were performed in the energy range of -0.5 meV to +0.5 meV. Rotational diffusion of water can be treated as flat background on IRIS in the investigated energy range. Focus data was described by two Lorentzians and the data was fitted in the energy range of -1.25 meV to +1.25 meV. TOFTOF data was fitted by two Lorentzians in the energy range of -1.5 meV to +1.5 meV.

The HWHM of translational diffusion $\Gamma_T(q)$ were best fitted with a jump-diffusion model given by (Bee 1988) $\Gamma_T(q) = \frac{Dq^2}{1 + Dq^2\tau_0}$, with the translational diffusion coefficient $D$ and the residence time between jumps $\tau_0$. HWHM $\Gamma_T(q)$ of $H_2O$ in RBC and $H_2O$ buffer measured on TOFTOF, FOCUS and IRIS are shown with fits according to a jump-diffusion model in **Figure 4**.

The residence times $\tau_0$ of water in RBC were up to 4 times larger than those of the reference buffer (**Table 1**), strongly depending on the instrument.

**Table 1:** Residence times $\tau_0$ of intracellular $H_2O$ in RBC, $\tau_0$ of buffer $H_2O$, and the ratio between both. All values are at the temperature 290 K.

| | **$\tau_0$ $H_2O$ in RBC** | **$\tau_0$ $H_2O$ buffer** | **($\tau_0$ $H_2O$ in RBC)/ ($\tau_0$ $H_2O$ buffer)** |
|---|---|---|---|
| IRIS (17µeV) | 2.53 ± 0.06 ps | 0.57 ± 0.03 ps | 4.4 |
| FOCUS (50µeV) | 1.12 ± 0.05 ps | 1.02 ± 0.09 ps | 1.1 |
| TOFTOF (100µeV) | 1.68 ± 0.03 ps | 0.68 ± 0.03 ps | 2.5 |

The obtained residence times of $H_2O$ buffer are smaller than the literature value of $\tau_0$=1.1 ps for pure water at 298 K (Bellissent-Funel et al. 1995).

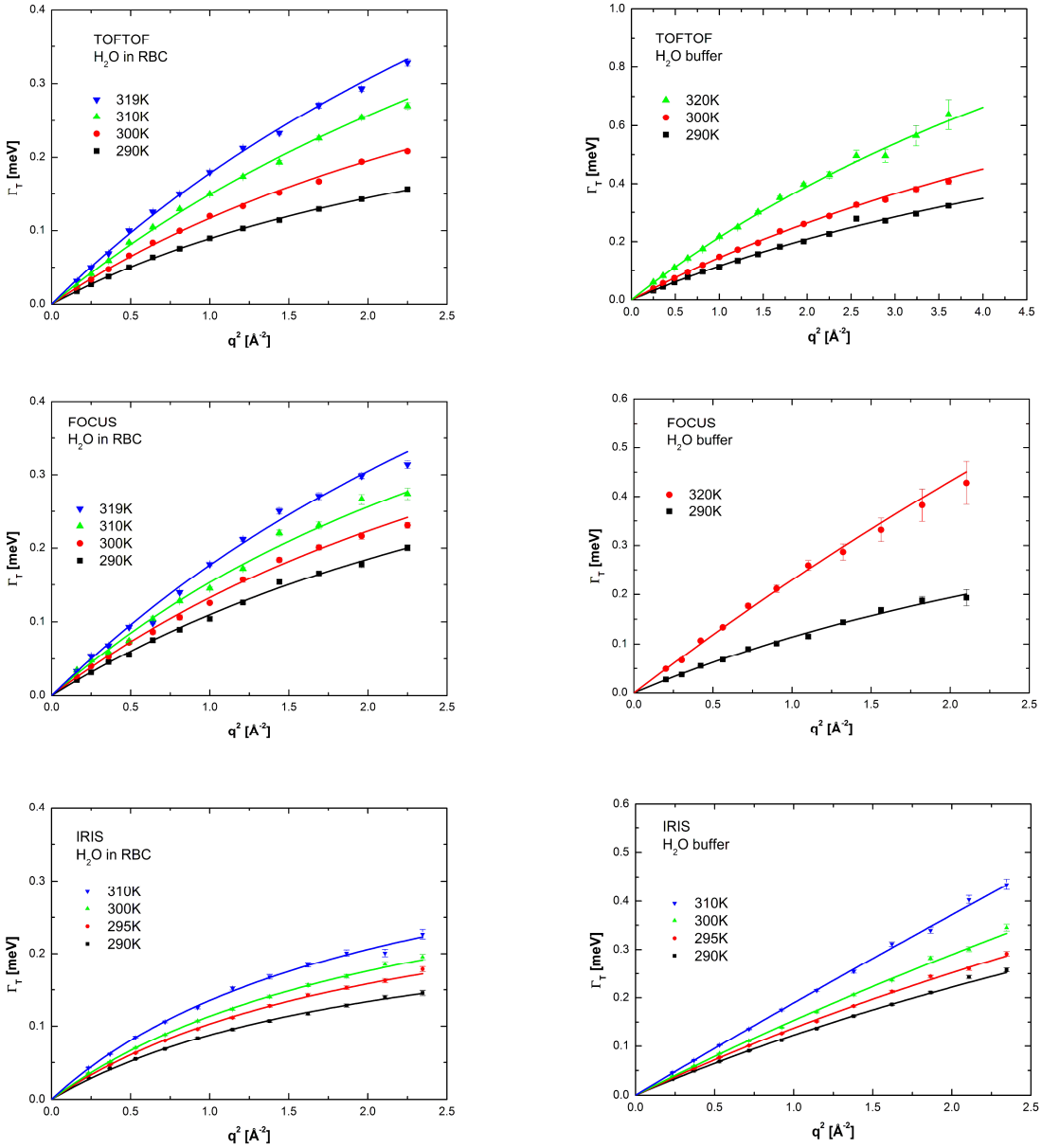


**Figure 4:** Half-widths at half-maximum $\Gamma_T$ of the translational diffusion process of $H_2O$ in RBC and of $H_2O$ buffer measured on TOFTOF, FOCUS and IRIS. Solid lines represent fits according to a jump-diffusion model.

The HWHM of rotational diffusion $\Gamma_R(q)$ measured on TOFTOF are shown in **Figure 5 a)**. The values of the half-widths are independent of the scattering vector, as expected for rotational diffusion. The rotational correlation times $\tau_{Cor,R} = \frac{1}{\Gamma_R}$ are given in **Figure 5 b)**, they are however smaller than the literature value of $\tau_{Cor,R}$ =3.3 ps at 298 K for pure water(Bellissent-Funel et al. 1995).

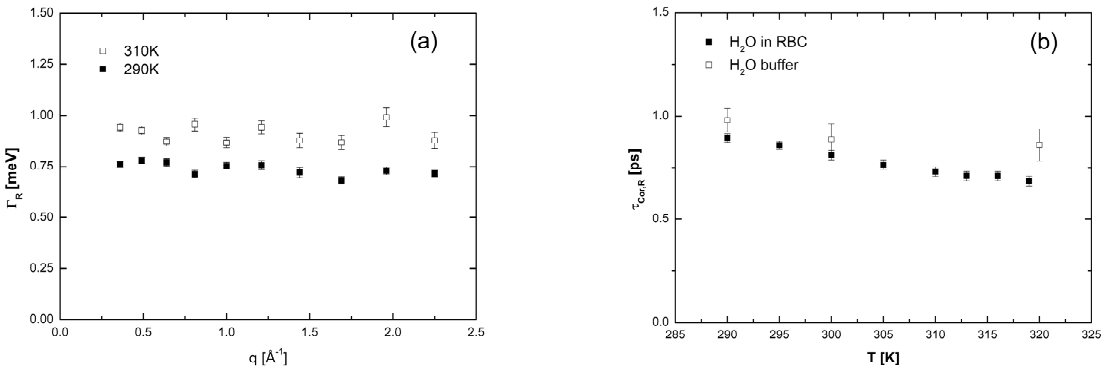


**Figure 5: a)** Half-widths at half-maximum $\Gamma_R$ of the rotational diffusion process of $H_2O$ in RBC measured on TOFTOF. **b)** Rotational correlation times $\tau_{Cor,R}$ of $H_2O$ in RBC and $H_2O$ buffer as determined with TOFTOF.

The immobile fraction of $H_2O$ in RBC at the scattering vector q was determined according to $p = \frac{A_0(q)}{\int S_{\exp}(\omega, q)\, d\omega}$ and the temperature dependence was described by an Arrhenius equation with the activation energy $E_a$ with $p(T) = p_0 \cdot \exp\left(\frac{E_a}{k_B T}\right)$.

Mean square displacements $\langle u^2 \rangle$ can be obtained from the scattering vector dependence of the elastic intensity $A_0(q)$ according to

$$\langle u^2 \rangle = \frac{-6 \cdot \Delta(\ln A_0(q))}{\Delta q^2}. \qquad (6.3)$$

This approach is formally similar to the Guinier approximation of small angle scattering(Guinier and Fournet 1955). The mean square displacements report on the average radius of atomic thermal motion, where we follow the definition of $\langle u^2 \rangle$ given by Smith (Smith 1991). Equation (6.3) is strictly valid for $q^2 \to 0$ but holds for $\langle u^2 \rangle \cdot q^2 \approx 2$. Mean square displacements were calculated from IRIS data in the range of $q^2$=0.37-1.14 Å$^{-2}$ and yielded a temperature independent value of $\langle u^2 \rangle$=5.4±0.7 Å$^2$. From FOCUS data, $\langle u^2 \rangle$ were calculated in a similar range of $q^2$=0.30-1.10 Å$^{-2}$ and we obtained a temperature independent value of $\langle u^2 \rangle$=4.5±0.5 Å$^2$.

### *6.6.4 Surface Area Calculations*

We calculated the Surface Accessible Surface Area (SASA) per human deoxy-hemoglobin from a neutron crystallographic structure (pdb file 2DXM) with the web based server GETAREA (Fraczkiewicz and Braun 1998) and obtained a value of 24,550 Å$^2$. Persson et Halle (Persson and Halle 2008) report a value of ~10.75 Å$^2$ that a water molecule occupies on the surface of a protein. Taking this value, we obtain that around 2,300 $H_2O$ molecules are in direct contact with the surface of one hemoglobin protein. We further assume that the volume of one RBC is around 100 µm$^3$ as given in Artmann et al. (Artmann et al. 1998) For the purpose of simplicity, we approximate the RBC by a sphere with equal volume. This yields a total surface area of the cytoplasmic and periplasmic cell side of $A_{RBC} = 208 \mu m^2$. Considering a cellular hemoglobin concentration of 330 mg/ml, we obtain a total SASA of intracellular hemoglobin of $A_{Hb} = 7.6 \cdot 10^4 \mu m^2$. The ratio $A_{Hb} / A_{RBC} \approx 400$ indicates that the amount of water in the hemoglobin hydration layer is two orders of magnitude larger than water in the membrane hydration layer. Extracellular matrix and glycocalix was removed during sample preparation, as it might be strongly interacting with water.

## 6.7 References

(2008a) DAVE Data Analysis and Visualisation Environment, vol 2008

(2008b) MODES a Graphic User Interface for Iris Data Analysis, vol 2008

Artmann GM, Kelemen C, Porst D, Büldt G, Chien S (1998) Temperature Transitions of Protein Properties in Human Red Blood Cells. Biophys. J. 75:3179-3183

Bee M (1988) Quasielastic neutron scattering. Principles and Applications in Solid State Chemistry, Biology and Materials Science. Adam Hilger, Bristol and Philadelphia

Bellissent-Funel MC, Chen SH, Zanotti JM (1995) Single-particle dynamics of water molecules in confined space. Phys. Rev. E 51:4558-4569

Carlile CJ, Adams MA (1992) The Design of the IRIS Inelastic Neutron Spectrometer and Improvements to its Analysers. Physica B 182:431-440

Elgsaeter A, Branton D (1974) Intramembrane particle aggregation in erythrocyte ghosts. I. The effects of protein removal. J. Cell. Biol. 63:1018-36

Ellis RJ, Minton AP (2003) Join the crowd. Nature 425:27-28

Fraczkiewicz R, Braun W (1998) Exact and Efficient Analytical Calculation of the Accessible Surface Areas and Their Gradients for Macromolecules. J. Comp. Chem. 19:319-333

Gabel F, Bicout D, Lehnert U, Tehei M, Weik M, Zaccai G (2002) Protein dynamics studied by neutron scattering. Q. Rev. Biophys. 35:327-67

Garcia de la Torre J (2001) Hydration from hydrodynamics. General considerations and applications of bead modelling to globular proteins. Biophys. Chem. 93:159-170

Guinier A, Fournet G (1955) Small Angle Scattering of X-Rays. Wiley, New York

Janssen S, Mesot J, Holitzner L, Furrer A, Hempelmann R (1997) FOCUS: A hybrid TOF-spectrometer at SINQ. Physica B 234:1174-1176

Jasnin M, Moulin M, Haertlein M, Zaccai G, Tehei M (2008) Down to atomic-scale intracellular water dynamics. EMBO reports 9:543-547

Krueger S, Nossal R (1988) SANS studies of interacting hemoglobin in intact erythrocytes. Biophys. J. 53:97-105

Makarov VA, Andrews BK, Smith PE, Pettitt BM (2000) Residence Times of Water Molecules in the Hydration Sites of Myoglobin. Biophys. J. 79:2966-2974

Persson E, Halle B (2008) Cell water dynamics on multiple time scales. Proc. Natl. Acad. Scie. U.S.A. 105:6266-6271

Russo D, Murarka RK, Copley JRD, Head-Gordon T (2005) Molecular View of Water Dynamics near Model Peptides. J. Phys. Chem. B 109:12966-12975

Smith JC (1991) Protein Dynamics - Comparison of Simulations with Inelastic Neutron-Scattering Experiments. Q. Rev. Biophys. 24:227-291

Unruh T, Neuhaus J, Petry W (2007) The high-resolution time-of-flight spectrometer TOFTOF. Nuclear Instruments and Methods in Physics Research Section A: Accelerators, Spectrometers, Detectors and Associated Equipement 580:1414-1422

Wei YZ, A.C K, Sadeghi M, Sage JT, Tian WD, Champion PM, Sridhar S (1994) Protein Hydration Investigations with High-Frequency Dielectric Spectroscopy. J. Phys. Chem. 98:6644-6651

Wuttke J FRIDA: Fast Reliable Interactive Data Analysis

Zhang L, Wang L, Kao Y-T, Qiu W, Yang Y, Okobiah O, Zhong D (2007) Mapping hydration dynamics around a protein surface. Proc. Natl. Acad. Scie. U.S.A. 104:18461-18466

# 7. Conclusions Générales et Perspectives

La dynamique de l'hémoglobine dans les globules rouges en fonction de la température a été mesurée par diffusion quasiélastique de neutrons. La diffusion globale des macromolécules et la dynamique interne des protéines ont pu être séparées par les données et l'analyse. Les prédictions théoriques pour la diffusion des particules colloïdales à temps de courte durée ont été utilisées pour comparer les coefficients de diffusion de l'hémoglobine mesurés dans les globules rouges avec les coefficients de diffusion de l'hémoglobine à grande dilution mesurés par diffusion de lumière. Il a ainsi été montré que les molécules de l'hémoglobine se comportent comme si elles étaient confinées dans des cages formées par les protéines voisines sur les échelles de quelques picosecondes et de quelques Ångstroms. La dynamique interne de l'hémoglobine montre un changement de régime à 36.9°C. À des températures plus élevées que la température du corps humain, les chaînes latérales des amino acides occupent des volumes plus grands que prévu par la dépendance normale de la température. Ce phénomène a été interprété comme étant dû au dépliement partiel de la protéine à température physiologique, en accord avec des résultats d'expériences de dichroïsme circulaire (Digel et al. 2006 ; Zerlin et al. 2007). Il a été conclu que le changement de la dynamique à la température du corps pourrait refléter une augmentation de l'hydrophobicité de la surface, qui serait responsable pour l'agrégation des protéines, pour la baisse de la pression osmotique colloïdale et pour l'effet sur le passage vu dans les expériences de micropipette (Artmann et al. 1998 ; Artmann et al. 2008 ; Digel et al. 2006 ; Kelement et al. 2001). Cela indique que la transition macroscopique de « l'élasticité » des globules rouges à température physiologique a bien une base moléculaire au niveau de l'hémoglobine sur l'échelle ps-Å.

Pour but examiner si les observations du paragraphe précédent sont dues à des propriétés particulières du cytoplasme des globules rouges, la dynamique de l'hémoglobine pure en fonction de l'hydratation a été mesurée dans une série d'expériences neutroniques. Les techniques de diffusion élastique et quasiélastique de neutrons ont été utilisées pour mesurer la dynamique de la protéine en fonction de la température dans des échantillons de poudre

hydratée et en solution concentrée. Les temps de résidence entre les sauts locaux de l'ordre de quelques picosecondes, sont réduits en solution concentrée et augmentés en poudre hydratée d'hémoglobine. L'énergie d'activation entre les sauts locaux est également réduite en solution concentrée comparée à la poudre hydratée. La transition de géométrie des mouvements internes à température du corps a été vue dans la solution concentrée mais non dans la poudre hydratée. Ce résultat est en accord avec l'hypothèse que la dynamique de l'hémoglobine pure sur l'échelle ps-Å est responsable du changement de propriétés macroscopiques des globules rouges à température physiologique. Il a été conclu que les poudres hydratées ne représentent pas un bon modèle pour la dynamique de la protéine de l'ordre de quelques ps-Å, qui pourrait être corrélée à la fonction biologique.

Les résultats de ces deux études sur les globules rouges et l'hémoglobine inspirent les perspectives suivantes.

Il a été montré que la transition de l'hémoglobine est corrélée avec la température du corps d'une grande variété d'espèces (Zerlin et al. 2007). Les travaux de cette thèse ainsi que des travaux précédents sur des bactéries ont démontré l'efficacité de la diffusion de neutrons pour mesurer la dynamique moléculaire *in-vivo* dans les cellules (Jasnin et al. 2008 ; Tehei et al. 2004). En plus, une étude de diffusion de neutrons a montré que la dynamique des protéines dans des bactéries psychrophiles, mésophiles, thermophiles et hyperthermophiles s'adapte aux températures de vie respectives de ces bactéries (Tehei et al. 2004). Il serait intéressant d'étudier, par des expériences similaires, si la dynamique de l'hémoglobine dans des globules rouges des différentes espèces est également correlée avec la température physiologique de chacune de ces espèces.

Il a été postulé que l'hémoglobine en solution concentrée s'agrège à la température physiologique (Artmann et al. 1998 ; Digel et al. 2006 ; Kelemen et al. 2001). La diffusion de neutrons aux petits angles serait une méthode bien adaptée pour étudier l'agrégation de l'hémoglobine en solution, en fonction de la température. La diffusion de neutrons aux petits angles, en plus, ne cause pas de dommage de radiation, ce qui est le cas pour le rayonnement synchrotron.

La diffusion globale de l'hémoglobine a été mesurée à l'échelle de quelques picosecondes, ce qui a permis d'évaluer le coefficient de diffusion dans la limite des temps courts. Doster et

Longeville ont mesuré le coefficient de diffusion de l'hémoglobine dans les globules rouges dans la limite de temps courts et dans la limite de temps longs sur un spectromètre de spin écho à l'échelle des nanosecondes et nanomètres (Doster et Longeville 2007). Les auteurs ont trouvé que le coefficient de diffusion dans la limite de temps courts et longs est réduit comparé aux prédictions de la théorie hydrodynamique. Le coefficient de diffusion dans la limite de temps longs était faiblement réduit comparé à la valeur théorique, en revanche, le coefficient de diffusion dans la limite de temps courts a montré une déviation plus grande. La réduction de la dynamique dans la limite de temps longs a été interprétée par l'influence de la couche d'hydratation qui est lié à la surface de la protéine. Busch et co-auteurs ont mesuré la diffusion de la myoglobine en solutions concentrées sur un spectromètre à rétrodiffusion (Busch et al. 2007). Un coefficient de diffusion réduit a été trouvé, qui était en accord avec une étude de spin écho sur la diffusion de la myoglobine en solution concentrée (Longeville et al. 2003).

Le coefficient de diffusion de l'hémoglobine dans les globules rouges en fonction de la température et en fonction du temps d'observation pourrait être mesuré avec des spectromètres neutroniques à différentes résolutions en énergie. Il serait intéressant de mesurer le coefficient de diffusion dans la limite de temps longs en fonction de la température sur un spectromètre à rétrodiffusion (échelle ~ns) ou spin-écho (échelle ~100ns). Dans le cas de l'agrégation des protéines, le coefficient de diffusion dans la limite de temps longs sera réduit. Les propriétés de la réduction du coefficient de diffusion dans la limite de temps longs pendant l'agrégation des particules constituent un thème de recherche actuel dans la science de particules colloïdales. Il serait intéressant de comparer un système biologique aux résultats sur des systèmes colloïdaux physicochimiques.

La dynamique de l'eau cellulaire dans les globules rouges a été mesurée à l'échelle des quelques picosecondes et quelques Ångstroms avec la technique de la diffusion quasiélastique de neutrons, dans une grande gamme de température. Trois spectromètres de neutrons avec résolutions en temps de 40, 13 et 7 ps ont été combinés pour couvrir l'échelle de temps des mouvements de l'eau volumique à l'eau interfaciale. Une fraction de l'eau cellulaire d'environ 90% est caractérisée par un coefficient de diffusion translationnel similaire à celui de l'eau volumique. Les 10% restant présentent une dynamique ralentie de façon significative. La fraction ralentie a été attribuée à l'eau en interaction avec l'hémoglobine. Elle correspond à environ la moitié de l'eau dans la première couche d'hydratation de la protéine. Il a été

proposé précédemment que l'eau liée à la surface de l'hémoglobine pourrait être responsable pour l'effet de passage des globules rouges observé dans les expériences de micropipette (Kelemen et al. 2001). Les auteurs ont proposé qu'il y a de l'eau interfaciale ralentie qui 'dégèle' à la température du corps et qui est caractérisée par une dynamique similaire à l'eau volumique dans l'état 'dégelé'. La réduction de la viscosité des solutions de l'hémoglobine concentrée à la température du corps serait expliquée par la fraction de l'eau 'dégelée' qui diluerait la solution de la protéine. Les expériences de diffusion des neutrons ont montré qu'il existe en effet une fraction d'eau interfaciale avec une dynamique plus lente dans les cellules. Cette fraction baisse en augmentant la température. Par contre, on n'observe pas de changement brutal de la fraction de l'eau lente autour de la température physiologique. L'hypothèse que l'eau interfaciale est responsable pour la réduction de la viscosité des solutions de l'hémoglobine concentrée à la température du corps n'est pas confirmée par les expériences de neutrons. Une étude récente sur la dynamique de l'eau cellulaire dans *E. coli* a montré que l'eau majoritaire cellulaire présente une dynamique translationnelle et rotationnelle similaire à l'eau volumique (Jasnin et al. 2008). L'étude sur la dynamique de l'eau cellulaire dans les globules rouges a montré que ces résultats ne sont pas limités aux procaryotes mais sont aussi valables pour les eucaryotes.

Les propriétés spécifiques de l'eau d'hydratation et le couplage entre la dynamique de l'eau d'hydratation et de la protéine ont été montrées récemment. Paciaroni et al. ont utilisé la diffusion inélastique incohérente de neutrons pour mesurer la densité d'état des molécules d'eau dans la couche d'hydratation d'une protéine (Paciaroni et al. 2008). Les résultats ont montré que la densité d'état de l'eau dans la couche d'hydratation est significativement différente de la densité d'état des formes simples cristallines de la glace et ressemble à un mélange entre les formes amorphes de la glace de grande et faible densité. Le couplage entre la dynamique de la protéine et de l'eau a été étudié dans une expérience complémentaire par Wood et al. (Wood et al. 2008). L'étude a montré que les propriétés dynamiques de la protéine et de l'eau d'hydratation sont caractérisées par une transition dynamique à la même température d'environ 220 K. Des simulations de dynamique moléculaire de ce système ont montré que le début de la diffusion translationnelle des molécules d'eau dans la couche d'hydratation à 220 K est responsable pour la relaxation du réseau des liaisons d'hydrogène entre la protéine et les molécules d'eau, qui est à l'origine de la transition dynamique (Wood et al. 2007).

La dynamique de l'eau cellulaire a été mesurée dans une étude récente dans l'organisme halophile *Haloarcula marismortui* (Tehei et al. 2007). Cette étude a montré qu'environ 76% de l'eau cellulaire dans *H. marismortui* est caractérisée par une dynamique 250 fois plus lente que l'eau volumique. À 300 K l'eau cellulaire lente montrait des signes caractéristiques pour la dynamique en confinement. Cette étude a également montré qu'il n'y a pas de fraction majoritaire de l'eau cellulaire lente dans *E. coli* (Tehei et al. 2007). Une étude supplémentaire a montré que la fraction majoritaire de l'eau dans *E. coli* a des propriétés dynamiques similaires à l'eau volumique (Jasnin et al. 2008). La cellule halophile est un cas spécial. La cellule contient du KCl à concentration molaire dans le cytoplasme et les protéines halophiles sont seulement stables à cette haute concentration de sel. Les interactions des protéines halophiles avec le solvant sont particulièrement fortes et la couche d'hydratation des protéines halophiles contient des molécules d'eau et des ions (Madern et al. 2000). Tehei et al. ont suggéré qu'un effet de structuration entre les molécules d'eau, les ions du KCl en solution très concentré et les protéines halophiles est responsable pour la grande fraction d'eau lente dans le cytoplasme de *H. marismortui* (Tehei et al. 2007).

Les propriétés d'eau ralentie dans les globules rouges pourraient être examinées sur un spectromètre à rétrodiffusion à haute résolution en énergie (par exemple IN16 à l'ILL). IN16 a une résolution en énergie de 0.9 µeV qui correspond à une échelle de temps de l'ordre d'une nanoseconde. Il serait intéressant de mesurer le coefficient de diffusion et le temps de résidence de l'eau ralenti dans les globules rouges sur ce spectromètre sensible à l'échelle de la nanoseconde et d'étudier si cette fraction de l'eau lente montre des signes de la dynamique en confinement. De plus, des simulations de dynamique moléculaire de l'hémoglobine hydratée pourraient aider à identifier des molécules d'eau ralenties et à corréler leurs temps de résidence avec les données expérimentales.

# 7. General Conclusion and Perspectives

The technique of quasielastic neutron scattering was used to measure the dynamics of hemoglobin in whole human red blood cells as a function of temperature. Global macromolecular diffusion and internal protein dynamics could be separated from the measured data in the analysis. Theoretical predictions for the short-time self-diffusion of colloidal non-charged hard-sphere particles were used to compare the measured global diffusion coefficients of hemoglobin in red blood cells with diffusion coefficients of hemoglobin at infinite dilution, measured with dynamic light scattering. It was revealed that hemoglobin molecules in the picosecond and Ångstrom time and length scale behave as if they were trapped in cages formed by neighbouring proteins. The experiment showed that internal hemoglobin dynamics displays a sudden change at 36.9°C. Above body temperature amino acid side-chains occupy larger volumes than expected from normal temperature behaviour. The phenomenon was interpreted as partial unfolding of hemoglobin at body temperature, which is in agreement with results of circular dichroism experiments (Digel et al. 2006, Zerlin et al. 2007). It has been concluded that the change in protein dynamics at body temperature could reflect an increase in surface hydrophobicity of the surface of hemoglobin, responsible for pronounced protein aggregation, the drop in colloidal osmotic pressure and the passage effect seen in micropipette studies (Artmann et al. 1998; Kelemen et al. 2001; Digel et al. 2006; Artmann et al. 2008). It has been suggested further that protein dynamics and structural changes in the picosecond time range and Ångstrom length scale might be connected to a macroscopic effect on whole red blood cells.

With the aim to study if the observations of the previous paragraph are a particular property of the cytoplasmic environment of red blood cells, the dynamics of pure human hemoglobin as a function of hydration was studied in a series of neutron scattering experiments. Elastic and quasielastic incoherent neutron scattering were used to measure protein dynamics as a function of temperature. The residence times of localized jumps in the order of a few picoseconds were found to be significantly reduced in concentrated solution compared to fully

hydrated powder. Furthermore, the activation energy of the localised jump-diffusion process was found to be reduced for the solution sample as compared to the hemoglobin powder. Above human body temperature, and only in the solution sample, amino acid side-chain motions occupy larger volumes than expected from normal temperature dependence. The result is in agreement with the observed change in hemoglobin dynamics at body temperature in red blood cells. In that study it was suggested that hemoglobin dynamics in the order of a few picoseconds might be relevant for the properties of whole red blood cells. As the body temperature behaviour was found to be absent in the hydrated powder sample, it was concluded that hydrated powder samples do not describe all fast protein dynamics that are relevant for biological function.

The results on human hemoglobin dynamics stimulate the following perspectives.

Previous work of Zerlin et al. showed that the transition temperature of hemoglobin is directly correlated to the species' body temperature (Zerlin et al. 2007). The work of this thesis as well as previous work on bacteria showed the efficiency of neutron scattering to measure molecular dynamics in-vivo in cells (Tehei et al. 2004; Jasnin et al. 2008). It has already been shown with neutron scattering that average protein dynamics of psychrophile, mesophile, thermophile and hyperthermophile bacteria are adapted to the respective temperatures at which these bacteria live (Tehei et al. 2004). It would be now of scientific interest to study with neutron scattering if hemoglobin dynamics in red blood cells of different species is equally correlated to the body temperature of each of these species.

It has been postulated in recent work that hemoglobin shows pronounced aggregation at body temperature (Artmann et al. 1998; Digel et al. 2006; Kelemen et al. 2001). Small angle neutron scattering would be an excellent experimental method to investigate protein aggregation in concentrated solution as a function of temperature. Additionally, small angle scattering does not induce radiation damage, which is the case of synchrotron radiation.

In the thesis, global macromolecular diffusion of hemoglobin in red blood cells was measured in the picosecond and Ångstrom time and length scale, which allowed the determination of the short-time self-diffusion coefficient. Doster and Longeville measured the short-time and long-time self-diffusion coefficient of hemoglobin in red blood cells with neutron spin-echo spectroscopy in the nanosecond and nanometer time and length scale (Doster and Longeville

2007). The authors found that both the short-time and the long-time self-diffusion coefficients of hemoglobin were reduced as compared to predicted values of hydrodynamic theory. The long-time diffusion coefficient showed only a small deviation from the theoretical value, whereas the short-time diffusion coefficient exhibited a larger deviation. The reduction of the long-time diffusive dynamics was attributed to the influence from the protein hydration shell, which was supposed to stick to the surface of the protein and move in a joint way. Busch and co-authors studied the self-diffusion of myoglobin in concentrated solutions using neutron backscattering spectroscopy (Busch et al. 2007). A reduction of the diffusion coefficient was reported that was in good agreement with previous results of a neutron spin echo study on the diffusion of myoglobin in concentrated solutions (Longeville et al. 2003).

The diffusion coefficient of hemoglobin in red blood cells as a function of temperature and as a function of the observation time could be studied with neutron spectrometers of different energy resolution. It would be interesting to measure the behaviour of the long-time self-diffusion coefficient as a function of temperature on a backscattering spectrometer (time scale ~1ns) or on a spin echo instrument (time scale ~100ns). In the case of protein aggregation the long-time self-diffusion coefficient will be reduced. The reduction of the long-time diffusive dynamics during particle aggregation is a topic of scientific interest in the field of colloidal science. Colloidal particles are ideal model systems and it would be of interest to compare a biological system to the physicochemical results of colloidal research.

The dynamics of cytoplasmic water in the picosecond time and Ångstrom length scale was measured with quasielastic neutron scattering in a broad range of temperature. Three different neutron spectrometers with time resolutions of 40, 13, and 7 ps respectively were combined to cover time scales from that of bulk to that of interfacial water dynamics. The experiments revealed that around 90% of cellular water has got a translational diffusion coefficient similar to bulk water. A minor fraction of 10% cellular water was found with significantly slower dynamics that appeared immobile on the instrumental time scales. The correlation times of the slow water fraction need to be longer than 40 ps which was the highest time resolution in the study. The fraction of slowed down water was attributed to $H_2O$ molecules which are dynamically bound on the surface of hemoglobin. It was concluded that roughly 50% of the surface of hemoglobin is covered with dynamically bound water molecules. It has been suggested previously that bound water on the surface of hemoglobin could be responsible for the passage effect of red blood cells in micropipette experiments (Kelemen et al. 2001). The

authors proposed that there exists bound water on the surface of hemoglobin that would 'melt' at body temperature and would then exhibit faster dynamics similar to bulk water in the 'melted' state. The reduced viscosity of the hemoglobin solution above body temperature was then explained as a dilution effect of the protein solution by this additional bulk water. The neutron experiments on cellular water showed that a bound water fraction on the surface of hemoglobin exists in red blood cells. The immobile water fraction is reduced with increasing temperature but it does not exhibit any sudden changes at body temperature due to 'melting'. Therefore, the hypothesis that bound water causes the loss of viscosity in concentrated hemoglobin solutions above body temperature was not confirmed by the neutron scattering experiments. A previous study on cell water dynamics in *E. coli* has shown that the major fraction of cytoplasmic water has translational and rotational dynamics similar to bulk water (Janin et al. 2008). The study on cell water in red blood cells showed that not only cell water in prokaryote but also in eukaryotes has similar translational dynamics compared to bulk water in the picosecond and Ångstrom time-space window.

The specific dynamical properties of protein hydration water and the intimate coupling between hydration water and protein dynamics have been demonstrated recently. Paciaroni et al. used inelastic incoherent neutron scattering to measure the vibrational density of states of water molecules in the first hydration layer of maltose binding protein (Paciaroni et al. 2008). The results showed that the measured density of states of hydration water is significantly different from the density of states of simple crystalline ice and is similar to a mixture of both low- and high-density amorphous ice. The coupling between protein and hydration water dynamics was studied in a complementary experiment by Wood et al. (Wood et al. 2008). The study showed that both the protein and the hydration water exhibit a dynamical transition at the same temperature at around 220 K. Computer simulations on the same system were performed and revealed that the onset of translational diffusion of water molecules in the hydration layer at 220 K is responsible for the relaxation of the protein-water hydrogen-bonding network that leads to the measured dynamical transition (Wood et al. 2008).

The nature of the dynamical bound water fraction in red blood cells at physiological temperature could be further investigated with neutron experiments on a high resolution backscattering spectrometer (for example the instrument IN16 at ILL). IN16 has an energy resolution of 0.9 μeV which corresponds to a time scale in the order of one nanosecond.

A previous experiment on water dynamics in the halophilic organism *Haloarcula marismortui* revealed a major cellular water fraction of around 76% with 250 times slower dynamics than bulk water (Tehei et al. 2007). The slow water fraction at 300 K showed characteristic signs for confined motions in a restricted volume. That study also revealed that cell water dynamics in *E. coli* is not governed by such a slow water fraction (Tehei et al. 2007). As discussed above, a further study revealed that the major cell water fraction in *E. coli* has similar dynamical properties as bulk water (Jasnin et al. 2008). The halophilic cell is a special case. The cell accumulates large amounts of KCl in the molar level in its cytoplasm and halophilic proteins are only stable at such high salt concentrations. Solvent interactions of halophilic proteins are particularly strong and halophilic proteins bind both water and salt ions in their hydration shell (Madern et al. 2000). Tehei et al. therefore suggested that an ordering effect of water molecules, KCl and halophilic proteins is responsible for the large slow water fraction in *H. marismortui* (Tehei et al. 2007).

The work in this thesis showed that there exists a minor water fraction of ~10% in red blood cells with slow dynamics. The existence of such a small water fraction with reduced dynamics might also be possible in *E. coli* and other cells. In further work, it would be interesting to study if the slow water fraction in red blood cells, and possibly other types of cells, shows signs for confined dynamics and to quantify the residence times and diffusion coefficients of the slow water dynamics. Additionally, molecular dynamics simulations could be performed of one hemoglobin molecule surrounded with water. By performing sufficiently long simulations it might be possible to identify water molecules close to the surface of the protein with reduced dynamics and to correlate their residence times with the neutron measurements.

# 8. Abbreviations

| | |
|---|---|
| CD | circular dichroism |
| DLS | dynamic light scattering |
| DNA | deoxyribonucleic acid |
| E. coli | Escherichia coli |
| FRM-II | Forschungsreaktor München II |
| FWHM | full-widths at half-maximum |
| EINS | elastic incoherent neutron scattering |
| EISF | elastic incoherent structure factor |
| eV | electronvolt |
| Hb | hemoglobin |
| HWHM | half-widths at half-maximum |
| ILL | Institut Laue-Langevin |
| kDa | kilo Dalton |
| M | molar |
| MD | molecular dynamics |
| MSD | mean square displacements |
| MW | molecular weight |
| ns | nanosecond |
| NMR | nuclear magnetic resonance |
| ps picosecond | picosecond |
| PSI | Paul Scherrer Institut |

| | |
|---|---|
| q | magnitude of the scattering vector |
| QENS | quasielastic neutron scattering |
| RBC | red blood cells |
| rcf | relative centrifugal force |
| RNA | ribonucleic acid |
| SASA | surface accessible surface area |

# 9. References

Alberts B. AJ, J. Lewis, M. Raff, K. Roberts, P. Walter (2002) Molecular biology of the cell, 4th edn. Garland Science, New York

Artmann GM, Kelemen C, Porst D, Büldt G, Chien S (1998) Temperature transitions of protein properties in human red blood cells. Biophys. J. 75:3179-83

Artmann GM, Burns L, Canaves JM, Temiz-Artmann A, Schmid-Schonbein GW, Chien S, Maggakis-Kelemen C (2004) Circular dichroism spectra of human hemoglobin reveal a reversible structural transition at body temperature. Eur. Biophys. J. 33:490-6

Artmann GM, Zerlin KF, Digel I (2008) Hemoglobin Senses Body Temperature. In: Artmann GM, Chien S (eds) Bioengineering in Cell and Tissue Research, vol IV. Springer Verlag, Berlin, Heidelberg, pp 415-447

Austin RH, Beeson KW, Eisenstein L, Frauenfelder H, Gunsalus IC (1975) Dynamics of ligand binding to myoglobin. Biochemistry 14:5355-73

Ball P (2008) Water as an Active Constitutent in Cell Biology. Chem. Rev. 108:74-108

Bee M (1988) Quasielastic neutron scattering. Principles and Applications in Solid State Chemistry, Biology and Materials Science. Adam Hilger, Bristol and Philadelphia

Bellissent-Funel MC, Teixeira J, Bradley KF, Chen SH (1992) Dynamics of hydration water in protein. J. Phys. I France 2:995-1001

Bellissent-Funel MC, Chen SH, Zanotti JM (1995) Single-particle dynamics of water molecules in confined space. Phys. Rev. E 51:4558-4569

Bellissent-Funel MC, Zanotti JM, Chen SH (1996) Slow dynamics of water molecules on the surface of a globular protein. Faraday Discuss. 103:281-294

Bicout DJ, Zaccai G (2001) Protein Flexibilty from the Dynamical Transition: A Force Constant Analysis. Biophys. J. 80:1115-1123

Bu Z, Neumann DA, Lee SH, Brown CM, Engelmann DM, Han CC (2000) A view of dynamics changes in the molten globule-native folding step by quasielastic neutron scattering. J. Mol. Biol. 301:525-536

Busch, S., W. Doster, S. Longeville, V. Garcia Sakai, and T. Unruh (2007) Microscopic protein diffusion at high concentration. In QENS2006, P. E. Sokol, H. Kaiser, D. Baxter, R. Pynn, D. Bossev, M. Leuschner, editors. Materials Research Society, Bloomington, IN. 107–114.

Carlile CJ, Adams MA (1992) The Design of the IRIS Inelastic Neutron Spectrometer and Improvements to its Analysers. Physica B 182:431-440

Combet S, Pieper J, Coneggo F, Ambroise JP, Bellissent-Funel MC, Zanotti JM (2008) Coupling of laser excitation and inelastic neutron scattering: attempt to probe the dynamics of light-induced C-phycocyanin dynamics Eur. Biophys. J. 37:693-700

Cornicchi E, Marconi M, Onori G, Paciaroni A (2006) Controlling the Protein Dynamical Transition with Sugar-Based Bioprotectant Matrices: A Neutron Scattering Study. Biophys. J. 91: 289-297

Cusack S, Doster W (1990) Temperature dependence of the low frequency dynamics of myoglobin. Measurement of the vibrational frequency distribution by inelastic neutron scattering. Biophys. J. 58:243-251

Dellerue S, Bellissent-Funel MC (2000) Relaxational dynamics of water molecules at protein surface. Chem. Phys. 258:315-325

Dellerue S, Petrescu AJ, Smith JC, Bellissent-Funel MC (2001) Radially softening diffusive motions in a globular protein. Biophys. J. 81:1666-76

De Francesco A, Marconi M, Cinelli S, Onori G, Paciaroni A (2004) Picosecond Internal Dynamics of Lysozyme as Affected by Thermal Unfolding in Nonaqueous Environment. Biophys. J. 86:480-487

Demmel F, Doster W, Petry W, Schulte A (1997) Vibrational frequency shifts as a probe of hydrogen bonds: thermal expansion and glass transition of myoglobin in mixed solvents. Europ. Biophys. J. 26: 327-335

Diehl M, Doster W, Petry W, Schober H (1997) Water-coupled low-frequency modes of myoglobin and lysozyme observed by inelastic neutron scattering. Biophys. J. 73: 2726-2732

Digel I, Maggakis-Kelemen C, Zerlin KF, Linder P, Kasischke N, Kayser P, Porst D, Temiz Artmann A, Artmann GM (2006) Body temperature-related structural transitions of monotremal and human hemoglobin. Biophys. J. 91:3014-21

Doster, W, Bachleitner A, Dunau R, Hiebl M, Lüscher E (1986) Thermal properties of water in myoglobin crystals and solutions at subzero temperatures. Biophys. J. 50:213-219

Doster W, Cusack S, Petry W (1989) Dynamical transition of myoglobin revealed by inelastic neutron scattering. Nature 337:754-6

Doster W, Cusack S, Petry W (1990) Dynamic instability of liquidlike motions in a globular protein observed by inelastic neutron scattering. Phys. Rev. Let. 65:1080-1083

Doster W, Settles M (2005) Protein-water displacement distributions. Biochim. Biophys. Acta 1749: 173-186

Doster W, Longeville S (2007) Microscopic diffusion and hydrodynamic interactions of hemoglobin in red blood cells. Biophys. J. 93:1360-8

Elgsaeter A, Branton D (1974) Intramembrane particle aggregation in erythrocyte ghosts. I. The effects of protein removal. J. Cell. Biol. 63:1018-36

Ellis RJ, Minton AP (2003) Join the crowd. Nature 425:27-28

Engler N, Ostermann A, Niimura N, Parak F (2003) Hydrogen atoms in proteins: Positions and dynamics. Proc. Nat. Acad. Sci. U.S.A. 100:10243-10248

Ferrand M, Dianoux AJ, Petry W, Zaccai G (1993) Thermal Motions and Function of Bacteriorhodopsin in Purple Membranes - Effects of Temperature and Hydration Studied by Neutron-Scattering. Proc. Natl. Acad. Sci. U.S.A. 90:9668-9672

Fitter J, Lechner RE (1998) Incoherent neutron scattering (INS)

Fraczkiewicz R, Braun W (1998) Exact and Efficient Analytical Calculation of the Accessible Surface Areas and Their Gradients for Macromolecules. J. Comp. Chem. 19:319-333

Frauenfelder H, Petsko GA, Tsernoglou D (1979) Temperature-dependent X-ray diffraction as a probe of protein structural dynamics. Nature 280:558-63

Frauenfelder H, Parak F, Young RD (1988) Conformational substates in proteins. Annu Rev Biophys Biophys Chem 17:451-79

Fraunfelder H, Sligar SG, Wolynes PG (1991) The energy landscapes and motions of proteins. Science 254:1598-1603

Gabel F, Bicout D, Lehnert U, Tehei M, Weik M, Zaccai G (2002) Protein dynamics studied by neutron scattering. Q. Rev. Biophys. 35:327-67

Gabel F, Weik M, Doctor BP, Saxena A, Fournier D, Brochier L, Renault F, Masson P, Silman I, Zaccai G (2004) The influence of solvent composition on global dynamics of human butyrylcholinesterase powders: a neutron-scattering study. Biophys J 86:3152-65

Gabel F (2005) Protein dynamics in solution and powder measured by incoherent elastic neutron scattering: the influence of Q-range and energy resolution. Eur. Biophys. J. 34:1-12

Garcia de la Torre J (2001) Hydration from hydrodynamics. General considerations and applications of bead modelling to globular proteins. Biophys. Chem. 93:159-170

Gaspar AM, Appavou MS, Busch S, Unruh T, Doster W (2008) Dynamics of well-folded and natively disordered proteins in solution: a time-of-flight neutron scattering study. Eur. Biophys. J. 37:573-582

Goodsell DS (2000) http://mgl.scripps.edu/people/goodsell/illustration/public

Guinier A, Fournet G (1955) Small Angle Scattering of X-Rays. Wiley, New York

Hall D, Minton AP (2003) Macromolecular crowding: qualitative and semiquantitive successes, quantitative challenges. Biochim. Biophys. Acta 1649:127-139

Hall PL, Ross DK (1981) Incoherent neutron scattering functions for random jump diffusion in bounded and infinite media. Mol. Phys. 42:673-682

http://neutron.neutron-eu.net/n_nmi3 (2008) NMI3 - Integrated Infrastructure Initiative for Neutron Scattering and Muon Spectroscopy

http://www.ncnr.nist.gov/dave (2008) DAVE Data Analysis and Visualisation Environment

http://www.isis.rl.ac.uk/molecularSpectroscopy/osiris/Modes_manual.pdf (2008b) MODES a Graphic User Interface for Iris Data Analysis

Janssen S, Mesot J, Holitzner L, Furrer A, Hempelmann R (1997) FOCUS: A hybrid TOF-spectrometer at SINQ. Physica B 234:1174-1176

Jasnin M, Moulin M, Haertlein M, Zaccai G, Tehei M (2008) Down to atomic-scale intracellular water dynamics. EMBO reports 9:543-547

Jasnin M, Moulin M, Haertlein M, Zaccai G, Tehei M (2008) In vivo measurement of internal and global macromolecular motions in E. coli. Biophys. J. 95:857-864

Kelemen C, Chien S, Artmann GM (2001) Temperature transition of human hemoglobin at body temperature: effects of calcium. Biophys. J. 80:2622-30

Kendrew JC, Dickerson RE, Strandberg BE, Hart RG, Davies DR, Phillips DC, Shore VC (1960) Structure of myoglobin: A three-dimensional Fourier synthesis at 2 A. resolution. Nature 185:422-7

Knapp EW, Fischer SF, Parak F (1982) The influence of protein dynamics on Mössbauer spectra. J. Chem. Phys. 78:4701-4711

Krueger S, Nossal R (1988) SANS studies of interacting hemoglobin in intact erythrocytes. Biophys. J. 53:97-105

Lehnert U, Reat V, Weik M, Zaccai G, Pfister C (1998) Thermal motions in bacteriorhodopsin at different hydration levels studied by neutron scattering:

correlation with kinetics and light-induced conformational changes. Biophys. J. 75:1945-52

Lichtenegger H, Doster W, Kleinert T, Birk A, Sepiol B, Vogl G (1999) Heme-solvent coupling: a Mossbauer study of myoglobin in sucrose. Biophys. J. 76: 414-422

Longeville S, Doster W, Kali G (2003) Myoglobin in crowded solutions: structure and diffusion. Chem. Phys. 292:413–424

Madern D, Ebel C, Zaccai G (2000) Halophilic adaptation of enzymes. Extremophiles 4: 91-98

Makarov VA, Andrews BK, Smith PE, Pettitt BM (2000) Residence Times of Water Molecules in the Hydration Sites of Myoglobin. Biophys. J. 79:2966-2974

Mampe W, Ageron P, Bates C, Pendlebury JM, Steyerl A (1989) Neutron lifetime measured with stored ultracold neutrons. Phys. Rev. Lett. 63:593-596

Marconi M, Cornicchi E, Onori G, Paciaroni A (2008) Comparative study of protein dynamics in hydrated powders and in solution: A neutron scattering investigation. Chem. Phys. 345:224-229

McCammon JA, Harvey SC (1987) Dynamics of Proteins and Nuclear AcidsCambridge University Press, Cambridge, UK

Minton AP (2001) The Influence of Macromolecular Crowding and Macromolecular Confinement on Biochemical Reactions in Physiological Media. J. Biol. Chem. 276:10577-10580

Natali F, Peters J, Russo D, Barbieri S, Chiapponi C, Cupane A, Deriu A, Di Bari MT, Farhi E, Gerelli Y, Mariani P, Paciaroni A, Rivasseau C, Schirograve G, Sonvico F (2008) IN13 Backscattering Spectrometer at ILL: Looking for Motions in Biological Macromolecules and Organisms Neutron News 19:14-18

Paciaroni A, Cinelli S, Onori G (2002) Effect of the Environment on the Protein Dynamical Transition: A Neutron Scattering Study. Biophys. J. 83:1157-1164

Paciaroni A, Cornicchi E, De Francesco A, Marconi M, Onori G (2006) Conditioning action of the environment on the protein dynamics studied through elastic neutron scattering. Eur. Biophys. J. 35:591-599

Paciaroni A, Orecchini A, Cornicchi E, Marconi M, Petrillo C, Haertlein M, Moulin M, Schober H, Tarek M, Sacchetti F (2008) Fingerprints of Amorphous Icelike Behavior in the Vibrational Density of States of Protein Hydration Water. Phys. Rev. Let. 101:148104

Parak F, Knapp EW, Kucheida D (1982) Protein dynamics. Mossbauer spectroscopy on deoxymyoglobin crystals. J Mol Biol 161:177-94

Park SY, Yokoyama T, Shibayama N, Shiro Y, Tame JRH (2006) 1.25 angstrom resolution crystal structures of human haemoglobin in the oxy, deoxy and carbonmonoxy forms. J. Mol. Biol. 360:690-701

Perez J, Zanotti JM, Durand D (1999) Evolution of the internal dynamics of two globular proteins from dry powder to solution. Biophys. J. 77:454-69

Persson E, Halle B (2008) Cell water dynamics on multiple time scales. Proc. Natl. Acad. Scie. U.S.A. 105:6266-6271

Persson E, Halle B (2008) Cell water dynamics on multiple time scales. Proc. Natl. Acad. Scie. U.S.A. 105:6266-6271

Perutz MF, Rossmann MG, Cullis AF, Muirhead H, Will G, North ACT (1960) Structure of Haemoglobin: A Three-Dimensional Fourier Synthesis at 5.5-Å Resolution, Obtained by X-Ray Analysis. Nature 185:416-422

Perutz MF, G. Fermi, B. Luisi (1987) Stereochemistry of Cooperative Mechanisms in Hemoglobin. Accounts of Chemical Research 20:309-321

Pieper J, Buchsteiner A, Dencher NA, Lechner RE, Hauss T (2008) Transient Protein Softening during the Working Cycle of a Molecular Machine. Phys. Rev. Let. 100:228103

Réat V, Zaccai G, Ferrand M, Pfister C (1997) Functional dynamics in purple membranes Biological Macromolecular Dynamics. Adenine Press, New York, pp 117-122

Reat V, Patzelt H, Ferrand M, Pfister C, Oesterhelt D, Zaccai G (1998) Dynamics of different functional parts of bacteriorhodopsin: H-2H labeling and neutron scattering. Proc. Natl. Acad. Sci. U.S.A. 95:4970-5

Richter D (2003) Properties of the Neutron - Elementary Scattering Processes, vol Matter and Materials, Volume 15. Forschungszentrum Jülich

Roh JH, Curtis JE, Azzam S, Novikov VN, Peral I, Chowdhuri Z, Gregory RB, Sokolov AP (2006) Influence of hydration on the dynamics of lysozyme. Biophys J 91:2573-88

Roh JH, Novikov VN, Gregory RB, Curtis JE, Chowdhuri Z, Sokolov AP (2005) Onsets of anharmonicity in protein dynamics. Phys. Rev. Lett. 95:038101

Rupley JA, Careri G (1991) Protein hydration and function. Adv. Protein Chem. 41:37-172

Russo D, Perez J, Zanotti JM, Desmadril M, Durand D (2002) Dynamic transition associated with the thermal denaturation of a small beta protein. Biophys. J. 83:2792-2800

Russo D, Murarka RK, Copley JRD, Head-Gordon T (2005) Molecular View of Water Dynamics near Model Peptides. J. Phys. Chem. B 109:12966-12975

Sears VF (1966) THEORY OF COLD NEUTRON SCATTERING BY HOMONUCLEAR DIATOMIC LIQUIDS: II. HINDERED ROTATION. Can. J. Phys. 44:1299-1311

Sears VF (1992) Neutron scattering lengths and cross sections. Neutron News 3:26-37

Settles M (1996) Die Zeitabhängigkeit und die Geometry der intramolekularen Dynamik globulärer Proteine bis 100ps aus Neutronenstreudaten Physik Department E13, vol Dissertation. Technische Universität München, Garching

Singwi KS, Sjölander A (1960) Diffusive Motions in Water and Cold Neutron Scattering. Phys. Rev. 119:863-871

Smith JC (1991) Protein Dynamics - Comparison of Simulations with Inelastic Neutron-Scattering Experiments. Q. Rev. Biophys. 24:227-291

Stadler AM, Digel I, Artmann GM, Embs JP, Zaccai G, Büldt G (2008) Hemoglobin Dynamics in Red Blood Cells: Correlation to Body Temperature. Biophys. J. 95:5449-5461

Stradner A, Sedgwick H, Cardinaux F, Poon WC, Egelhaaf SU, Schurtenberger P (2004) Equilibrium cluster formation in concentrated protein solutions and colloids. Nature 432:492-5

Stradner A, Cardinaux F, Schurtenberger P (2006) A small-angle scattering study on equilibrium clusters in lysozyme solutions. J. Phys. Chem. B 110:21222-21231

Stradner A, Foffi G, Dorsaz N, Thurston G, Schurtenberger P (2007) New insight into cataract formation: Enhanced stability through mutual attraction. Phys. Rev. Let. 99:1-4

Tang KES, Dill K (1998) Native protein fluctuations: the conformational-motion temperature and the inverse correlation of protein flexibility with protein stability. J. Biomol. Struct. Dyn. 16:397-411

Tarek M, Tobias DJ (2002) Role of Protein-Water Hydrogen Bond Dynamics in the Protein Dynamical Transition. Phys. Rev. Lett. 88:138101

Tehei M, Madern D, Pfister C, Zaccai G (2001) Fast dynamics of halophilic malate dehydrogenase and BSA measured by neutron scattering under various solvent conditions influencing protein stability. Proc Natl Acad Sci U S A 98:14356-61

Tehei M, Franzetti B, Madern D, Ginzburg M, Ginzburg BZ, Giudici-Orticoni MT, Bruschi M, Zaccai G (2004) Adaptation to extreme environments: macromolecular dynamics in bacteria compared in vivo by neutron scattering. Embo Reports 5:66-70

Tehei M, Smith JC, Monk C, Ollivier J, Oettl M, Kurkal V, Finney JL, Daniel RM (2006) Dynamics of immobilized and native Escherichia coli dihydrofolate reductase by quasielastic neutron scattering. Biophys. J. 90:1090-7

Tehei M, Franzetti B, Wood K, Gabel F, Fabiani E, Jasnin M, Zamponi M, Oesterhelt D, Zaccai G, Ginzburg M, Ginzburg BZ (2007) Neutron scattering reveals extremely slow cell water in a Dead Sea organism. Proc. Natl. Acad. Sci. U.S.A. 104:766-71

Tehei M, Zaccai G (2007) Adaptation to high temperatures through macromolecular dynamics by neutron scattering. Febs J 274:4034-43

Teixeira J, Bellissentfunel MC, Chen SH, Dianoux AJ (1985) Experimental-Determination of the Nature of Diffusive Motions of Water-Molecules at Low-Temperatures. Phys. Rev. A 31:1913-1917

Tokuyama M, Oppenheim I (1994) Dynamics of Hard-Sphere Suspensions. Phys. Rev. E 50:R16-R19

Tournier AL, Xu J, Smith JC (2003) Translational Hydration Water Dynamics Drives the Protein Glass Transition. Biophys. J. 85:1871-1875

Tsai AM, Udovic TJ, Neumann DA (2001) The inverse relationship between protein dynamics and thermal stability. Biophys. J. 81:2339-2343

Unruh T, Neuhaus J, Petry W (2007) The high-resolution time-of-flight spectrometer TOFTOF. Nuclear Instruments and Methods in Physics Research Section A: Accelerators, Spectrometers, Detectors and Associated Equipement 580:1414-1422

Van Hove L (1954) Correlations in Space and Time and Born Approximation Scattering in Systems of Interacting Particles. Phys. Rev. 95:249-262

Volino F, Dianoux AJ (1980) Neutron Incoherent-Scattering Law for Diffusion in a Potential of Spherical-Symmetry - General Formalism and Application to Diffusion inside a Sphere. Mol. Phys. 41:271-279

Wei YZ, A.C K, Sadeghi M, Sage JT, Tian WD, Champion PM, Sridhar S (1994) Protein Hydration Investigations with High-Frequency Dielectric Spectroscopy. J. Phys. Chem. 98:6644-6651

Wood K, Plazanet M, Gabel F, Kessler B, Oesterhelt D, Tobias DJ, Zaccai G, Weik M (2007) Coupling of protein and hydration-water dynamics in biological membranes. Proc. Natl. Acad. Sci. U.S.A. 104:18049-54

Wood K, Grudinin S, Kessler B, Weik M, Johnson M, Kneller GR, Oesterhelt D, Zaccai G (2008a) Dynamical Heterogeneity of Specific Amino Acids in Bacteriorhodopsin. J. Mol. Biol. 380:581-591

Wood K, Lehnert U, Kessler B, Zaccai G, Oesterhelt D (2008b) Hydration dependence of active core fluctuations in bacteriorhodopsin. Biophys. J. 95:194-202

Wuttke J (2006) FRIDA (fast reliable inelastic data analysis) http://sourceforge.net/projects/frida

Yan YB, Wang Q, He HW, Zhou HM (2004) Protein thermal aggregation involves distinct regions: sequential events in the heat-induced unfolding and aggregation of hemoglobin. Biophys. J. 86:1682-90

Zaccai G (2000) How soft is a protein? A protein dynamics force constant measured by neutron scattering. Science. 288:1604-1607

Zanotti JM, Bellissent-Funel MC, Parello J (1999) Hydration-coupled dynamics in proteins studied by neutron scattering and NMR: The case of the typical EF-hand calcium-binding parvalbumin. Biophys. J. 76:2390-2411

Zerlin KF, Kasischke N, Digel I, Maggakis-Kelemen C, Temiz Artmann A, Porst D, Kayser P, Linder P, Artmann GM (2007) Structural transition temperature of hemoglobins correlates with species' body temperature. Eur. Biophys. J. 37:1-10

Zhang L, Wang L, Kao Y-T, Qiu W, Yang Y, Okobiah O, Zhong D (2007) Mapping hydration dynamics around a protein surface. Proc. Natl. Acad. Scie. U.S.A. 104:18461-18466

Zimmerman SB, Minton AP (1993) Macromolecular Crowding: Biochemical, Biophysical and Physiological Consequences. Ann. Rev. Biophys. Biomol. Struct. 22:27-65

# *10. Appendix*

## *10.1 From shell to cell: neutron scattering studies of biological water dynamics and coupling to activity*

The following article presents neutron scattering measurements of the dynamics of water in the hydration shell and the coupling between protein and water motion. Different biological systems were studied: a soluble protein, a membrane protein, Escherichia coli and red blood cells.

I contributed to the article with the measurement of water dynamics in red blood cells on the time-of-flight spectrometer TOFTOF at FRM-II, Munich.

Faraday Discussions Vol 141

# Water – From Interfaces to the Bulk

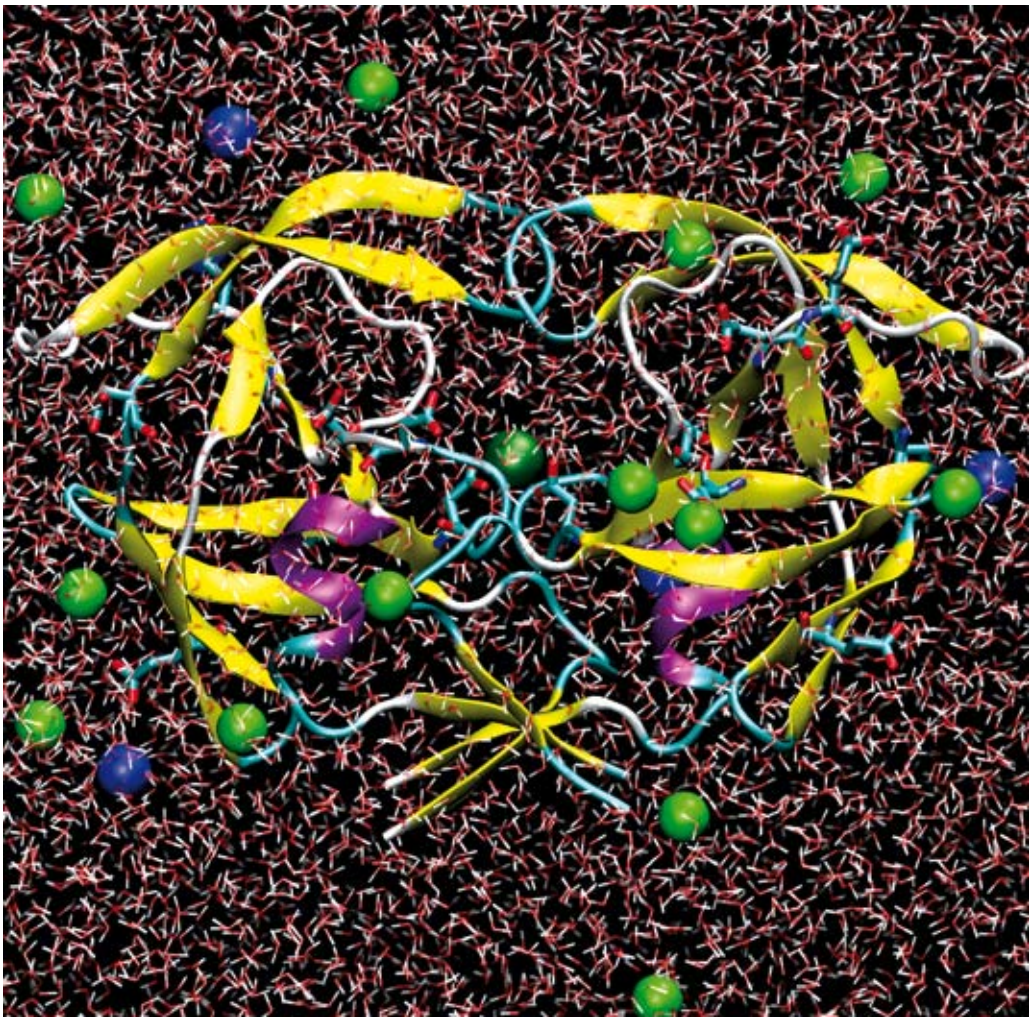

RSC Publishing

# From shell to cell: neutron scattering studies of biological water dynamics and coupling to activity†

A. Frölich,‡[a] F. Gabel,[a] M. Jasnin,[b] U. Lehnert,§[a] D. Oesterhelt,[c] A. M. Stadler,[b] M. Tehei,¶[b] M. Weik,[a] K. Wood‖[ab] and G. Zaccai*[ab]

*Received 1st April 2008, Accepted 19th June 2008*
*First published as an Advance Article on the web 31st October 2008*
**DOI: 10.1039/b805506h**

An integrated picture of hydration shell dynamics and of its coupling to functional macromolecular motions is proposed from studies on a soluble protein, on a membrane protein in its natural lipid environment, and on the intracellular environment in bacteria and red blood cells. Water dynamics in multimolar salt solutions was also examined, in the context of the very slow water component previously discovered in the cytoplasm of extreme halophilic archaea. The data were obtained from neutron scattering by using deuterium labelling to focus on the dynamics of different parts of the complex systems examined.

## Introduction

Understanding the dynamic state of water in biological systems and its influence on macromolecular activity is a major scientific challenge. The huge diversity displayed by living organisms is based on a few unifying principles. All known living organisms are constituted of cells or have been through a cellular stage. They require the full set of a variety of macromolecules of specific chemical type (DNA, RNA, proteins…), ions, specific small molecules and water, in order to thrive and reproduce. Life on Earth has colonized every possible niche in conditions that span extremes in solvent salinity and pH values, temperature and pressure. A scoop of soil, a sample of water, of ice, of air or even of rock from just about anywhere on Earth—including the poles, the tops of the highest mountain ranges, the deepest ocean trenches, neutral or alkaline salt lakes, or very hot acidic volcanic springs—are all likely to reveal biological activity. Ice usually has liquid inclusions, and organisms that live at temperatures well above 100 °C are under high pressure, in which the water is still liquid. As was debated at a Royal Society discussion published in 2004,[1] the availability of liquid water may well be the only environmental requirement for Life. The extreme halophilic archaea live in salt lakes and saline ponds in essentially saturated salt water; they counterbalance the osmotic pressure due to the external multimolar

[a]*Institut de Biologie Structurale, UMR 5075, CEA–CNRS–UJF, 41 rue Jules Horowitz, 38027 Grenoble, France*
[b]*Institut Laue Langevin, 6 rue Jules Horowitz, BP 156 Grenoble Cedex 9, France. E-mail: zaccai@ill.fr; Tel: +33 (0)4 76 20 76 79*
[c]*Max Planck Institut für Biochemie, Am Klopferspitz 18, D-82152 Martinsried, Germany*

† All the authors contributed equally to the work.
‡ Present address: Universität Karlsruhe, Germany
§ Present address: McKinsey & Co., London, UK
¶ Present address: AINSE, School of Chemistry, University of Wollongong, Australia
‖ Present address: University of Groningen, The Netherlands

NaCl concentration by accumulating multimolar KCl in their cytoplasm. Considering the inside of a cell is already very crowded with macromolecules, which occupy close to 30% of its volume, what is the state of the water compared to that in the bulk liquid? There are about 55 moles in a kilogramme of water. In a six molal solution of a fully ionised monovalent salt, therefore, there are 4.5 water molecules per ion. Ions may be coordinated by six water molecules, so that each and every water molecule has at least one ion as one of its nearest neighbours, leading to significantly reduced water activity. The existence of extreme halophiles proves that Life has adapted to reduced water activity, but there is no evidence that water can be done away with altogether in biological activity.

In this paper, we present and discuss results on water dynamics in different biological systems, and on the coupling between biological activity and the environment around macromolecules: water in the case of soluble proteins, water and lipids in the case of membrane proteins.

Neutron scattering is a particularly suited experimental technique to probe water dynamics under different conditions. Slow neutrons scatter off bound protons exchanging energy in the thermal range corresponding to the picosecond–nanosecond (ps–ns) time-scale, and momentum corresponding to the 0.1 nm length-scale. Energy-resolved incoherent neutron scattering, especially in the elastic (EINS) and quasielastic (QENS) scattering modes, have been informing us on water dynamics under different conditions for decades. Because the method relies on incoherent scattering, samples need not be crystalline or even monodisperse and measurements can be performed on highly complex systems such as living cells[2] or stacks of natural membranes.[3] The incoherent neutron scattering cross section of hydrogen is more than an order of magnitude larger than that of other atomic nuclei usually found in biological material and their isotopes, including deuterium, and the development of *in vivo* specific deuterium-labelling methods permitted the focus on water dynamics in complex biological samples, and its coupling with biological function and activity.

While a consensus has emerged that water molecules close to protein surfaces are dynamically slowed down with respect to bulk water molecules, quantitative aspects and the mechanisms involved remain the objectives of active research (reviewed by Ball[4]). Reports on the dynamics of water molecules close to protein surfaces measured by neutron spectroscopy were presented at a previous Faraday Discussion.[5,6] The factors found for the slowing down of the diffusion coefficient of hydration water compared to bulk water varied between 2 and 100, depending on the protein, temperature and hydration conditions. Bon *et al.*[7] studied hydration water in lysozyme crystals by QENS. They distinguished two water populations, denoted as "first" and "second" hydration shells, with diffusion coefficients slowed down by a factor of 10 and 50 compared to bulk water respectively. By combining EINS data from two spectrometers, Gabel and Bellissent-Funel[8] reported diffusion coefficients of deuterated C-phycocyanin hydration water, in the presence of trehalose molecules, which are slowed down by a factor of 10–15 with respect to bulk water. As has been pointed out, however, in Gabel *et al.*[9] and by Gabel and Bellissent-Funel,[8] results obtained at different energy resolutions, different wave-vector transfers and using different fit models are not directly comparable.

On the scale of the biological cell, water constitutes the malleable matrix that envelops and sustains intracellular components and biological activity. Considering that macromolecular concentration in the cytoplasm can reach 400 mg $ml^{-1}$, to what extent is water dynamics perturbed by steric confinement between macromolecular surfaces? Does the cell 'tame' water behaviour as some believe (reviewed by Ball[4])? While widely differing opinions concerning the dynamic state of water in the cell are represented in the biology community, there has been very little work on atomic-scale measurements of intracellular water dynamics in close to physiological conditions. Below, we present and discuss recent neutron scattering experiments performed on different cell systems, which shed light on *in vivo* intracellular water dynamics.

 

Hydration water is an integral and essential part of a protein structure. Without it the macromolecule would not be folded correctly. It is essential for the protein to fulfil its biological function. Devoid of hydration water, proteins are inactive[10] and lack essential motions, thus implicitly suggesting a close relationship between protein and hydration-water dynamics. The term 'slaving' has been used to express that water can impose its dynamical fingerprint on a protein.[11,12] Cryo-temperature-dependent neutron scattering experiments revealed the solvent dependence of dynamical transitions in soluble proteins[13–21] and in RNA[22] and provided insights into the coupling between them. Molecular dynamics simulations suggested the onset of water translational diffusion to be at the origin of the dynamical transition.[23,24] In contrast, however, the onset of hydration-water translational diffusion at 200 K, in a membrane, was not observed to trigger a dynamical transition in the membrane protein,[25,26] suggesting a more complex interaction between protein, water and the membrane lipid environment. Recent neutron scattering studies, using specific deuterium labelling, confirmed that a dynamical transition coincides with the onset of hydration water translational diffusion, in the case of a soluble protein,[27] but not in the case of a membrane protein.[3,28]

By using specific deuteration and samples with controlled hydration, water dynamics was measured directly by neutron scattering in the hydration shell around a soluble protein and a natural membrane and correlated with macromolecular dynamics, as well as *in situ* in prokaryotic and red blood cells.

Maltose binding protein (MBP) is a soluble monomeric protein of 41 kDa. It plays an essential role in the metabolism of *E. coli*.[29] *In vivo* deuteration of MBP allowed the direct extraction of hydration-water dynamics in neutron scattering experiments on the deuterated protein hydrated in $H_2O$. Water dynamics thus obtained were compared to protein dynamics obtained by measuring the natural abundance of MBP in $D_2O$.[27]

The purple membrane (PM) of *H. salinarum* is formed of a highly ordered two-dimensional lattice of archaeal specific lipids and the retinal binding protein, bacteriorhodopsin (BR).[30] BR functions as a light-driven proton pump. Its activity can be followed quite sensitively by spectroscopic methods because it is associated with a millisecond photocycle of protein conformational changes and retinal colour changes. Integral membrane proteins are active in a complex environment constituted of lipid hydrocarbon chains, lipid head groups and hydration water in contact with different parts of the protein. By using fully deuterated membranes hydrated in $H_2O$ and natural abundance membranes hydrated in $D_2O$, the coupling between hydration water and membrane dynamics has been explored.[3,28] In another set of experiments, the dynamic coupling between membrane protein and lipids was observed by applying *in vivo* deuterium labelling and *in vitro* reconstitution of PM. The samples allowed the observation of the lipid and protein dynamics, separately.

*In vivo* neutron scattering measurements in the cytoplasm of deuterated prokaryotic organisms revealed very different water-dynamic behaviour in bacteria and extreme halophilic archaea. In order to examine the effect of the high salt environment within halophilic archaea, water dynamics was measured in saturated KCl and NaCl solutions. The water dynamics inside red blood cells (RBC), which contain mainly the equivalent of a 300 mg $ml^{-1}$ solution of hemoglobin, was also measured.

The joint analysis of the results allowed us to propose a coherent view of water dynamics in the hydration shell, the lipid environment of a membrane protein and the intracellular milieu in various cell types, as well as of the dynamic coupling between biological activity and environment.

## Materials and methods

### Samples

The expression and purification of deuterated and natural abundance MBP has been described before.[27] For neutron scattering experiments, powders of deuterated and

natural abundance MBP were hydrated to a level of 0.4 g water per g MBP in $H_2O$ and $D_2O$ respectively (for details see Wood *et al.*[27]).

PM was extracted from natural abundance or fully deuterated cultures of *H. salinarum* as described before.[31,32] The experiments were performed on membrane-water stacks in $H_2O$ or $D_2O$ with lamellar spacings of 54 Å, corresponding to an inter-membrane water layer of 5 Å, and a hydration level of approximately 0.1 g water per g membrane.[28] The specifically labelled lipid and BR samples were prepared by delipidation and reconstitution as described in detail by Lehnert.[33] Three reconstitutions were prepared: (i) a control sample of hydrogenated BR and hydrogenated lipids (H-BR–H-lip or H–H); (ii) a sample with hydrogenated BR and deuterated lipids (H-BR–D-lip or H–D); (iii) a sample with deuterated BR and hydrogenated lipids (D-BR–H-lip or D–H). Several parameters were tested in order to find optimum reconstitution conditions. When the buoyant density (from a sucrose gradient) of the fully hydrogenated reconstitution (H–H) corresponded to native PM, the conditions were considered as correct and applied to the hybrid deuterated PM samples. The experimental values agreed well with the expected ones indicating that the lipid-to-BR ratio corresponded to that in natural PM. X-ray and neutron diffraction indicated poor lattice formation in the reconstituted samples. Light-induced cross-linking indicated that the probability of trimer formation in the reconstituted sample was smaller compared to dimer formation, in contrast to native PM. The UV absorption spectrum indicated a shift of the bound retinal peak to 567 nm, compared to 570 nm in native PM, as observed before in reconstituted samples. The lipid composition of the reconstituted samples was investigated in the negative-ion mode of electrospray ionisation (ESI) mass spectrometry. Traces of hydrogenated phospho- and glyco-lipids were observed indicating that they were not removed during the delipidation process. The hydrogenated contribution accounted for about 5% of the total. It arises from lipid strongly associated to the protein and that was not removed in the delipidation process. The special interaction between the glycolipids and the protein has been discussed by Weik *et al.*[34]

Deuterated *E. coli* (BLE21(DE3) strain) were cultivated as described previously.[35] Cell pellets containing $H_2O$ or $D_2O$ buffer were prepared in such a way as to reduce strongly the quantity of extracellular water in the sample, which was found to represent less than 7% of the total water (see Jasnin *et al.*[35] for details).

Deuterated *H. marismortui* cells were grown at 37°C to an optical density of 0.8–1 (late logarithmic phase) in the medium described before,[36] in which yeast extract was replaced by deuterated algal extract produced at the Max Planck Institut für Biochemie (Martinsried, Germany). For neutron scattering experiments, cells were pelleted in $D_2O$ or $H_2O$ buffer (see Tehei *et al.*[36] for details).

For the RBC experiments, samples of human venous blood were taken from healthy adults. The cells were washed with phosphate buffer solution (PBS) and were gassed with CO to increase the stability of hemoglobin. The glycocalyx matrix was removed as described elsewhere.[37] Half of the cells were then washed with $D_2O$ PBS buffer until the level of $H_2O$ was below 0.1%. No cell lysis was detected during the preparation and the shape of the cells was checked with optical microscopy.

## Neutron scattering

Elastic incoherent neutron scattering (EINS) experiments provide information on atomic mean-square displacements (MSD) in a sample as a function of temperature.[38] These are obtained from a Gaussian approximation plot of the scattered elastic intensity dependence on scattering vector amplitude,[39] $Q$: $\ln I(Q) = 1/6 \langle u^2 \rangle Q^2$. In an incoherent scattering situation, waves scattered by a single nucleus at different positions as it moves in time interfere to give a $Q$-dependent scattering pattern. The pattern then contains information on the shape of the volume traced by the moving particle in the same way as a small-angle scattering curve contains information on the shape of a particle in solution. The Gaussian approximation

 

given above is therefore a direct analogy to the Guinier approximation, with the radius of gyration squared defined as half the MSD value; the domain of validity of the approximation is for $\langle u^2 \rangle Q^2$ smaller than or about 2.[39] The time-scale examined of 1 ns on IN16 (http://www.ill.eu/in16/home/) at the Institut Laue Langevin (ILL) depends on the energy resolution of the spectrometer, while the range of the scattering vector, $Q$, in which the scattered intensity is measured, defines the length-scale which is of the order of 1 Å for IN16. Plots of MSD as a function of absolute temperature are called elastic scans. MSD are in absolute $Å^2$ units. An effective dynamic resilience expressed as an elastic force constant (in Newtons per metre) can be calculated from the inverse of the slope of $\langle u^2 \rangle$ *versus* $T$.[38,40] Elastic scans for proteins and membranes usually show a break in slope at about 200 K, which has been interpreted as a dynamical transition from a harmonic low-temperature regime to an anharmonic regime that has been modelled, for example, by a double-well free-energy potential.[15] In a quasi-harmonic approximation, the dynamical transition is associated with a significant decrease in resilience.

An exhaustive description of quasielastic incoherent neutron scattering (QENS) can be found in Bée.[41] QENS is measured as a function of both energy transfer and scattering vector, $Q$. On the energy scale, the elastic scattering appears as a peak centred on zero energy transfer whose width corresponds to the spectrometer resolution. The QENS appears as a significantly broader peak, also centred on zero energy transfer. The shape of the QENS peak and its $Q$ variation contain information on the time and geometry associated with the motion of the scattering particle. In the case of simple exponential diffusion processes, the QENS spectra can be fitted mathematically by Lorentzian functions. By applying various models, such as the jump diffusion, Singwi–Sjölander and Sears models (see Bée[41] for details), to fit the Lorentzian width as a function of $Q$, it is possible to calculate rotational relaxation and correlation times, translational residence time and translational and rotational diffusion coefficients for the scattering particle. Instruments used for QENS experiments were IN16 at ILL (energy resolution 0.9 μeV, corresponding to a time-scale of 1 ns, see above), BSS backscattering spectrometer (energy resolution also of 0.9 μeV, at the Jülich Neutron Centre, see http://www.jcns.info/), IN6 at ILL (energy resolution of 90 μeV, corresponding to a time scale of ~10 ps, see http://www.ill.eu/in6/home/), TOFTOF at the Munich FRM2 reactor (energy resolution of 100 μeV, similar to IN6; see ref. 42 for instrumental details), IRIS at the ISIS spallation neutron source at the Rutherford Laboratory (energy resolution of 17 μeV, corresponding to a time scale of ~50 ps, see http://www.isis.rl.ac.uk/molecularSpectroscopy/iris/), and IN5 at the ILL (http://www.ill.eu/in5/), which can be tuned for different energy resolution and $Q$-range values.

Data from the following neutron scattering experiments are discussed in the paper. In order to avoid laborious repetition and because different experimental conditions applied to the different studies, more detailed descriptions of experimental conditions are given in the relevant Figure caption or results section.

- Elastic scans on deuterated or natural abundance maltose binding protein in $H_2O$ or $D_2O$ collected on the IN16 spectrometer.
- Elastic scans on native and fully deuterated purple membrane in $H_2O$ or $D_2O$ collected on the IN16 spectrometer.
- Elastic scans on specifically deuterated (in the lipid or protein parts), reconstituted purple membrane collected on the IN16 spectrometer.
- QENS scans on IN6 and IRIS to measure water diffusion inside deuterated *E. coli*.
- QENS scans on TOFTOF to measure water diffusion inside red blood cells.
- QENS scans on IN16 and IN6 to measure water diffusion in deuterated *H. marismortui*, with a control experiment using BSS on deuterated *E. coli*.
- QENS scans on IN5 to measure water diffusion in concentrated solutions of NaCl and KCl.

## Results

### Hydration-water dynamics and coupling to the soluble maltose binding protein from *E. coli*

Water structure[43,44] and dynamics[5,8,9] at the vicinity of a soluble protein surface are different from in the bulk liquid state. MBP powders hydrated at 0.4 g water per g protein contain one hydration layer per protein molecule. The deuterated MBP in $H_2O$ gave access to the dynamics of hydration water, which contributes 73% to the total incoherent scattering cross section but only 2% in natural abundance MBP in $D_2O$. The MSD of water and protein motions, plotted in Fig. 1A, are similar up to 220 K, at which temperature they both exhibit a transition.[27] Above 220 K, the water MSD are above those of the protein.

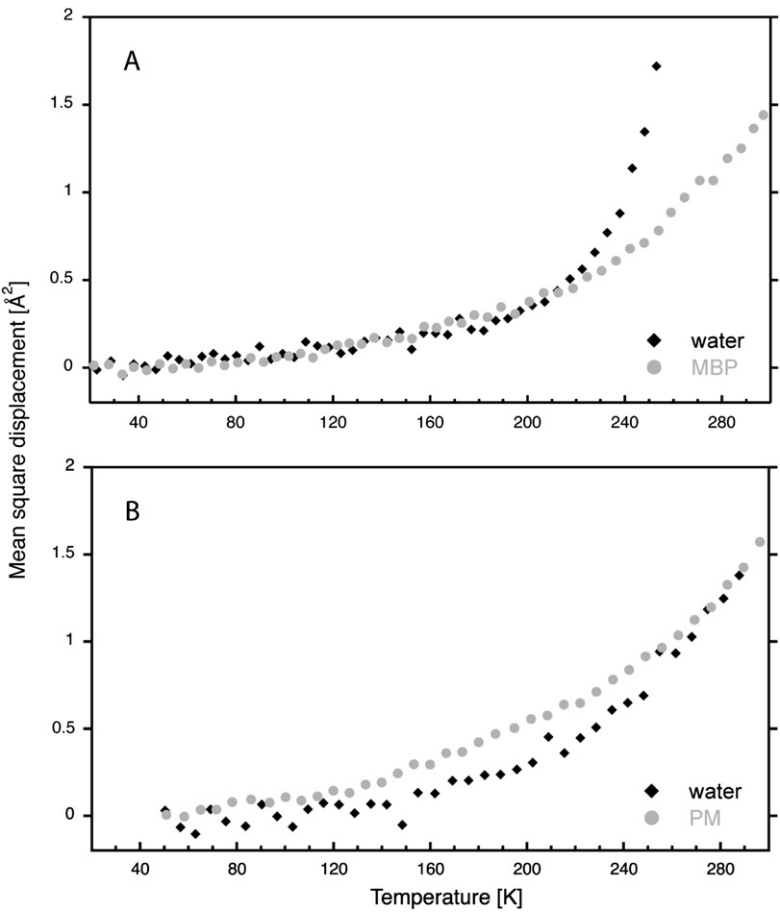


**Fig. 1** (A) Mean square displacements (MSD) of maltose binding protein (MBP) and its hydration water.[27] Dynamic transitions in the hydration water and in MBP take place at similar temperatures (~220 K). (B) MSD of purple membrane (PM) and its hydration water.[28] Dynamical transitions take place at 200 K in the hydration water and at 120 and 260 K in PM. The elastic scans were carried out on the IN16 spectrometer with an energy resolution of 0.9 μeV (full-width at half-maximum of the elastic peak and a wavelength of 6.275 Å[63]). MSD were extracted from data in the following $Q$ [$Q$ with units of $Å^{-1}$] ranges: $0.2 < Q^2 < 1.8$ for hydrogenated MBP in $D_2O$ (panel A, grey circles), $0.2 < Q^2 < 1.1$ for deuterated MBP in $H_2O$ (panel A, black diamonds), $0.2 < Q^2 < 1.5$ for hydrogenated PM in $D_2O$ (panel B, grey circles), $0.2 < Q^2 < 0.9$ for deuterated PM in $H_2O$ (panel B, black diamonds).

 

### Hydration water dynamics in purple membrane and coupling to bacteriorhodopsin and membrane lipids

PM stacks were hydrated to a level that corresponds to one hydration layer per membrane surface (*i.e.* 5 Å of inter-membrane water). EINS experiments on deuterated PM hydrated in $H_2O$ permitted us to access the dynamics of the first hydration layer directly. In the sample, 60% of the total incoherent scattering cross section was calculated to be due to the contribution of inter-membrane water. In contrast, as with the MBP samples discussed above, in natural abundance PM hydrated in $D_2O$ the contribution from hydration water is negligible and the total incoherent scattering cross section is strongly dominated by the PM (77% BR protein, 23% lipids), thus reflecting membrane dynamics. The elastic temperature scans are presented in Fig. 1B.[28] Hydration-water MSD increase linearly up to 200 K, at which temperature there is a break in slope suggesting a dynamical transition in water dynamics. The PM MSD show breaks in slope at 120 and 260 K, but not at 200 K.

The *in vitro* reconstituted PM samples were characterised by UV spectrophotometry, cross-linking experiments for BR trimer formation, mass spectrometry for lipid composition and deuterium labelling, and X-ray diffraction for lattice formation and order (see Materials and methods). Studying the reconstituted hydrogenated BR and hydrogenated lipids sample (H-BR–H-lip) probed the global dynamics of the whole membrane (68% of the incoherent scattering cross section is from BR, 31% from lipids), whilst in the hydrogenated BR, deuterated lipid sample (H-BR–D-lip) BR clearly dominated the signal (98%). Using deuterated BR with hydrogenated lipids (D-BR–H-lip) provided information on the lipid dynamics, which represent 92% of the incoherent scattering cross section. Fig. 2 presents the MSD measured for the H-BR–H-lip and D-BR–H-lip reconstituted samples at 93% relative humidity which represent, respectively, dynamics of global PM and of the native archaeal lipids in the membrane on the ns time-scale. The H-BR–D-lip sample MSD are not shown; they were very close and slightly below the H-BR–H-lip values, as expected from the BR-to-lipid ratio in the membrane composition. The MSD of the H-BR–H-lip sample are very similar to those of natural PM. The two-dimensional lattice in the reconstituted samples, however, was not as well ordered as in the natural membrane, indicating that membrane

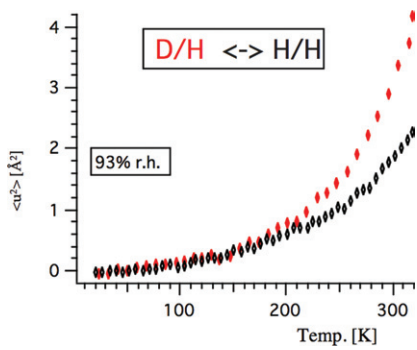


**Fig. 2** Mean-square displacements (MSD) extracted from the analysis of the elastically scattered neutron intensity, measured on the IN16 spectrometer at the ILL (energy resolution, full-width at half-maximum, of 0.9 μeV). The MSD, $\langle u^2 \rangle$, were calculated using the Gaussian approximation: $I_{el,T}(Q,\omega = 0) = A\exp\{-\langle u^2 \rangle Q^2/6\}$, in which $I_{el,T}(Q,\omega = 0)$ is the elastically scattered intensity at temperature $T$; $Q$ and $\omega$ are the momentum and energy transfer, respectively, and $A$ is a constant. Data are shown for the H-BR–H-lip (H–H) and D-BR–H-lip (D–H) reconstituted samples (see Materials and methods). Samples were hydrated to 93% relative humidity in $D_2O$.

internal dynamics in the ns time-scale is not influenced by lattice order. As seen in Fig. 2, between 20 and about 200 K, the MSD of both samples are the same, with a deviation from harmonic behaviour at about 150 K: PM and its lipid components have similar vibrational dynamics at very low temperatures and display the anharmonicity associated with methyl rotations from about 150 K.[14,45] We recall that PM lipids do not have fatty acid chains but phytol chains that are rich in methyl groups. Above 200 K, the MSD of the two samples become clearly different, with the archaeal phytol chains displaying greatly increased dynamics compared to the average membrane. In both samples shown in Fig. 2, further onsets of large-amplitude motions occur at 260 K, suggesting coupled increases in dynamics in the lipid and protein components of PM.

### Intracellular water dynamics in *E. coli* and red blood cells

*E. coli* water dynamics was studied in fully deuterated cell pellets resuspended in $H_2O$ and $D_2O$ buffers respectively. A subtraction of the cell spectra measured in $D_2O$ from the cell spectra measured in $H_2O$, scaled by the sample mass, provided a good approximation to the scattering signal from the water present in the samples. A sample of $H_2O$ buffer alone was measured as well, and used as a reference for interpreting the data. The measurements were carried out on two neutron spectrometers, IN6 and IRIS (see Materials and methods), to cover diffusive motions from those of bulk to interfacial water. IRIS and IN6 QENS spectra were well fitted using a single and two Lorentzian functions, respectively (see Jasnin *et al.*[35] for details). The Lorentzian extracted on IRIS was attributed to translational motions of cell water. Its half-width at half-maximum (HWHM), $\Gamma_T$, was extracted and best fitted using a jump diffusion model,[41] which describes diffusion between sites for the water protons with a mean residence time, $\tau_0$, at each site. We found the following values for the translational diffusion coefficients, $D_T$, and associated $\tau_0$: $D_T = 1.53 \times 10^{-5}$ cm$^2$ s$^{-1}$, $\tau_0 = 2.63$ ps at 281 K and $D_T = 2.39 \times 10^{-5}$ cm$^2$ s$^{-1}$, $\tau_0 = 2.16$ ps at 301 K. $D_T$ values are very close to those of bulk water at corresponding temperatures, with residence times about twice as long. The rotational water contribution emerged from the broad Lorentzian extracted from IN6 QENS spectra. We found the following rotational correlation times, $\tau_{cor,R}$: $\tau_{cor,R} = 1.96$ ps at 281 K, and 1.54 ps at 301 K. The values were close to the values extracted for the buffer under the same conditions and of the same order as the values measured for bulk water by QENS[46] and NMR.[47] From the two sets of data, we concluded that *E. coli* water dynamics is dominated by a bulk-like water component at physiological temperature. A similar conclusion was reached for water in RBC, indicating that the result was not restricted to bacteria (see below).

The diffusion of cytoplasmic water in whole human RBC was measured by QENS. RBC grow in the bone marrow of mammals, and deuterated material is not available so far. Natural abundance cells were measured in $H_2O$ and $D_2O$ buffers with high precision and the scattering data were subtracted from each other, to yield intensities representing the dynamics of water only. As a reference, $H_2O$ buffer solution was measured. The experiment was performed on the time-of-flight neutron spectrometer TOFTOF[42] at the Munich FRM2 reactor, with an energy resolution of 100 μeV, in the temperature range 290 to 320 K. The measured spectra in the $Q$-range from 0.5 to 1.5 Å$^{-1}$ were well fitted from −1.5 to +1.5 meV with a narrow and a broad Lorentzian function plus linear background, corresponding to translational and rotational motions of the water molecules respectively. The HWHM profile as a function of $Q^2$ of the narrow Lorentzian are in agreement with a jump diffusion model.[41] The translational diffusion coefficient, $D_T$, and the residence time, $\tau_0$, of water were obtained from the fits. The diffusion coefficients of cytoplasmic water are only slightly reduced compared to those obtained for the buffer solution, but interestingly the residence times of cytoplasmic water are on average five times higher than in buffer solution (details are given in Stadler *et al.*[48]).

 

### Extreme halophiles: a special case?

Intracellular water dynamics in *H. marismortui*, an extreme halophile originally isolated from the Dead Sea, was studied by QENS. Water motions in centrifuged cell pellets were measured by means of two spectrometers, IN6 and IN16, sensitive to motions with time-scales of 10 ps and 1 ns respectively (see Materials and methods). From IN6 time-of-flight data, using the model of Singwi and Sjölander,[49] a translational diffusion constant of $1.3 \times 10^{-5}$ cm$^2$ s$^{-1}$ was determined at 285 K for *H. marismortui* cells. The value is close to that found previously for other cells and close to that for bulk water, as well as that of the water in the 3.5 M NaCl solution bathing the cells.[50] A very slow water component was discovered from the IN16 data (energy resolution of 0.9 μeV). At 285 K, the values of HWHM are independent on $Q^2$. The water protons of this component displayed a residence time of 411 ps (compared with a few ps in bulk water). At 300 K, the residence time dropped to 243 ps and was associated with a translational diffusion of $9.3 \times 10^{-8}$ cm$^2$ s$^{-1}$, or 250 times lower than that of bulk water. The slow water accounts for about 76% of cell water in *H. marismortui*. No such slow water was found in *E. coli*, measured on the BSS backscattering spectrometer (energy resolution of 0.9 μeV, at the Jülich Neutron Centre (see http://www.jcns.info/)). It was hypothesized that the slow mobility of a large part of *H. marismortui* cell water indicates a specific water structure responsible for the large amount of $K^+$ bound within these extreme halophilic cells.

In order to estimate the influence of the solvent ions on the intracellular water dynamics in the extreme halophiles, we studied the diffusion coefficients of water in molar solutions of KCl and NaCl by QENS. To this end, a 3M KCl and a 4M NaCl (each at 50 mM Tris, pH = 7.6, $T = 298$ K) were measured on the instrument IN5 at the ILL (see Materials and methods for web details), at an energy resolution of 63 μeV ($\lambda = 6$ Å) in the wave-vector range $0.26 < Q < 1.87$. The quasielastic spectra were fitted in the energy transfer range −0.5 to +0.5 meV with a scattering law constituted of a linear background, an elastic intensity and a single quasielastic contribution, interpreted within the Singwi–Sjölander model.[49] The model assumes that individual water molecules diffuse during a time $\tau_1$ and vibrate during a time $\tau_0$ around an equilibrium position. In the approximation $\tau_1 \gg \tau_0$, we extracted the apparent diffusion coefficient, $D_{app}$, from the HWHM of the QENS spectra as a function of $Q$ (Fig. 3).

The following apparent diffusion coefficients (combining translational and rotational motions) were measured (the bulk water value is from the literature): $D_{app}$ (4M NaCl in $H_2O$, $T = 298$ K) $= 1.5 \times 10^{-5}$ cm$^2$ s$^{-1}$; $D_{app}$ (3M KCl in $H_2O$, $T = 298$ K) $= 2.0 \times 10^{-5}$ cm$^2$ s$^{-1}$ and $D_{app}$ (bulk water,[5] $T = 298$ K) $= 2.3 \times 10^{-5}$ cm$^2$ s$^{-1}$. The results showed clearly that the presence of molar salt concentration of NaCl or KCl hardly affects the diffusive properties of water. The findings supplement QENS data published earlier at different salt concentrations and temperatures.[51] Only a weak dependence of the water diffusion coefficient on NaCl concentration (up to 6 M NaCl) was found. In the case of KCl (up to 3.2 M), the diffusion coefficient was similar to that of bulk water. Furthermore, characteristic water frequencies (in the range from 100 to 1000 cm$^{-1}$) persisted up to 4.6 M KCl and 0.5 M NaCl respectively. It is only in the case of very small or highly charged ions ($Li^+$, $Mg^{2+}$, $La^{3+}$ *etc.*) that the authors could find a decrease of the water diffusion coefficient at higher concentrations (>1 M).

It can be concluded that the presence of high salt concentrations in the cytoplasm of extreme halophilic archaea, multimolar NaCl and KCl, is not responsible by itself for the very slow water component observed by Tehei *et al.*[36]

## Discussion

The hydration shell is vital to a macromolecule's biological activity. Without hydration water, proteins would lack not only their correctly folded structure but also the

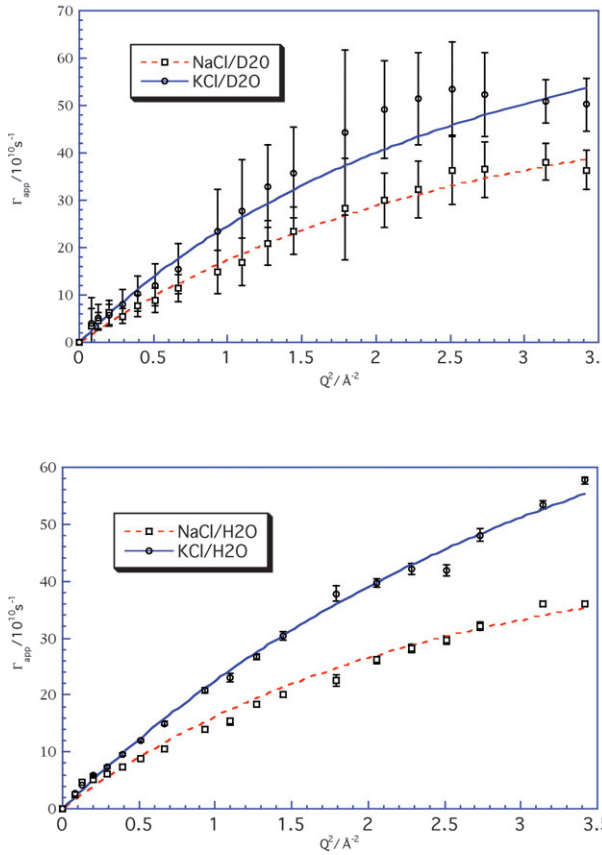


**Fig. 3** $Q^2$-Dependence of the Lorentzian half-widths at half-maximum (HWHM) extracted from the quasielastic spectra of the multimolar NaCl and KCl solutions measured on IN5 (see Materials and methods) with an energy resolution of 63 μeV. 4M NaCl and 3M KCl solutions were investigated both in $D_2O$ (top) and $H_2O$ (bottom). The continuous lines represent the fits obtained with the Singwi–Sjölander model,[49] which were used to extract the apparent diffusion coefficients.

conformational flexibility that *brings them to life* and allows their biological activity. Consequently, protein and hydration water dynamics are supposed to be intimately coupled. One way of exploring the coupling has exploited the so-called protein dynamical transitions, characteristic changes in MSD that appear in at temperatures between about 180 and 250 K. Do hydration-water MSD show similar behaviour, and if so, does the 'transition' temperature coincide with the protein dynamical transition temperature? The questions were addressed in the soluble MBP[27] and in PM,[3,28] by using neutron scattering combined with deuterium labelling to examine the dynamics of each component separately. The first layer of hydration water in both PM and MBP showed a characteristic change in MSD at temperatures between 200 and 220 K (Fig. 1) that was attributed to the onset of translational diffusion[3,27] as proposed earlier.[23] Water and protein transitions in MBP appeared at the same temperature (Fig. 1A), as expected from the intimate coupling between hydration water and soluble protein dynamics, which has been reported frequently in the literature (see *e.g.* Doster *et al.*;[15] Cordone *et al.*;[52] Fitter;[16] Réat *et al.*;[19] Tsai *et al.*;[21] Vitkup *et al.*;[53] Zaccai;[38] Paciaroni *et al.*;[18] Fenimore *et al.*;[11] Chen *et al.*;[13] Roh

 

*et al.*;[20] Swenson *et al.*;[54] Joti *et al.*;[17] and Doster[14]). In the case of PM, however, the hydration water and membrane transitions were found to be separated by as much as 60 K (Fig. 1B). The onset of water translational motion in the first[3,28] and second[25,26] hydration layers at 200 K did not trigger a dynamical transition in PM. The data from specifically labelled reconstituted PM permitted the separated observation of lipid and BR dynamics and showed that the membrane protein dynamics is coupled to the dynamics of its lipid environment, as has been suggested,[55,56] rather than to that of inter-membrane hydration water. The lipid component of PM constitutes only 25% of the membrane mass, and most of the lipid molecules are in contact with protein. The neutron data nevertheless established that the lipids in PM, above 200 K, display higher MSD and softer resilience than BR (Fig. 2). As discussed above, 200 K is the temperature of onset of hydration water translational diffusion. It appears, therefore, that lipid dynamics responds to the water. At 260 K there is another break in the MSD of the lipids towards a domain of even smaller resilience (larger slope with temperature), which coincides with a similar dynamic transition in BR. Early neutron diffraction experiments on PM, using $H_2O$–$D_2O$ exchange to highlight water location, and their comparison with data from lipid bilayer models, had shown the extent of hydration penetrating into the membrane around lipid head groups, and its dependence on the relative humidity of the sample environment.[57,58] Following these structural observations and the observation that PM activity was inhibited in the dry membrane, it has been speculated that a flexible lipid environment induced by high head-group hydration was essential for BR functional dynamics.[55] The parallel transitions in the lipid and BR MSD data at 260 K, observed in the reconstituted PM samples (Fig. 2), supports the hypothesis. At 200 K, the onset of translational diffusion in inter-membrane hydration water apparently induced some flexibility in the membrane lipids but not sufficiently to free high-amplitude protein motions. At 260 K, perhaps related to a 'melting' of head-group hydration water, both the lipid and BR components of the membrane display a dynamical transition to lower-resilience, high-amplitude MSD motions.

At the intracellular level, the studies on *E. coli* and RBC revealed that water dynamics is similar to the dynamics of water in the bulk state (Fig. 4D and zoomed in insets A, B, C). Our studies contributed to dismantle the concept that the cell somehow 'tames' water by modifying its dynamics compared to bulk water.[59] They confirmed the importance of hydration degree for water dynamics in confined geometries; in deuterated C-phycocyanin, for example, increasing water mobility had already been observed when hydration coverage reached one water layer.[60] The first macromolecular hydration layer accounts for about 0.4 to 0.5 g of water per g of macromolecule. Macromolecular concentrations in *E. coli* and RBC correspond to about 300 to 400 mg $ml^{-1}$, *i.e.* to four to six water layers around macromolecular surfaces. The analysis established that because of the relatively high hydration level and resulting low water confinement, intracellular water forms a network of communication that is as fluid as bulk water. In both *E. coli* and RBC, however, residence times were found to be increased by a factor of 2 and 5, respectively, suggesting that water molecules spend longer times in the first hydration shell of macromolecular structures than in the bulk phase.

The extreme halophilic archaea appeared to present an exceptional case with respect to cytoplasmic water mobility. The presence of multimolar NaCl and KCl salt concentrations in their cytoplasm is clearly not responsible by itself for the very slow water component observed by Tehei *et al.*[36] (Fig. 3). It was hypothesised that the slow mobility of a large part of *H. marismortui* cell water indicated a specific water structure, which would also be responsible for the large amount of $K^+$ bound within the extreme halophile cells. The absolute requirement of *H. marismortui* for a high salt environment and its ability to bind potassium ions specifically appear to be closely related to the low mobility of water in the cells. Halophilic proteins have been shown to have special hydration and ion-binding properties associated

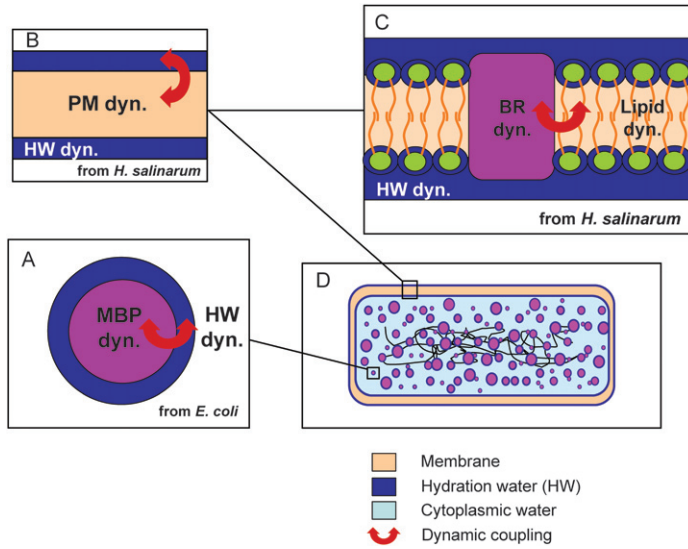


**Fig. 4** Summary Figure, which shows hydration and coupling 'from shell to cell'. The Figure illustrates the main points presented and discussed in the paper, drawn in a large schematic cell. (A) Hydration around a soluble protein and coupling with protein dynamics. (B) Hydration around a membrane not coupled to membrane protein dynamics. (C) Dynamic coupling between protein and lipid in the membrane. (D) Channels of free water flowing around the hydrated macromolecules in the cell and the special case of the extreme halophile.

with an excess of negative charge in carboxylic groups on their surface.[61] The interactions may be similar to those of structured water around potassium ions and protein carboxylic groups observed by MacKinnon[62] in the potassium channel protein. It would be of significant interest to measure water mobility in these systems, in order to assess if similar mechanisms are responsible for the slow water component in the extreme halophile.

## Acknowledgements

We thank Heloisa Nunes Bordallo, Bruno Demé, Bernhard Frick, Marek Koza, Mark F. Telling and Michaela Zamponi for their help during data collection at the Institut Laue-Langevin, at ISIS and at the Jülich Neutron Centre. This work was supported by the Commissariat à l'Energie Atomique, the Centre National de la Recherche Scientifique, the Université Joseph Fourier, an Agence Nationale de la Recherche Grant (project number JC05_45685), the European Union under the DLAB contracts HPRI-CT-2001-50035 and RII3-CT-2003-505925, and the Integrated Infrastructure Initiative for Neuron Scattering and Muon Spectroscopy (NMI3).

## References

1 *Philos. Trans. R. Soc. London, Ser. B*, 2004, **359**, 1–395.
2 M. Tehei, B. Franzetti, D. Madern, M. Ginzburg, B. Z. Ginzburg, M. T. Giudici-Orticoni, M. Bruschi and G. Zaccai, *EMBO Rep.*, 2004, **5**, 66–70.
3 K. Wood, M. Plazanet, F. Gabel, B. Kessler, D. Oesterhelt, D. J. Tobias, G. Zaccai and M. Weik, *Proc. Natl. Acad. Sci. U. S. A.*, 2007, **104**, 18049–18054.
4 P. Ball, *Chem. Rev.*, 2008, **108**, 74–108.
5 M. C. Bellissent-Funel, J. M. Zanotti and S. H. Chen, *Faraday Discuss.*, 1996, **103**, 281–294.
6 M. Settles and W. Doster, *Faraday Discuss.*, 1996, **103**, 269–280.
7 C. Bon, A. J. Dianoux, M. Ferrand and M. S. Lehmann, *Biophys. J.*, 2002, **83**, 1578–1588.

 

8 F. Gabel and M. C. Bellissent-Funel, *Biophys. J.*, 2007, **92**, 4054–4063.
9 F. Gabel, D. Bicout, U. Lehnert, M. Tehei, M. Weik and G. Zaccai, *Q. Rev. Biophys.*, 2002, **35**, 327–367.
10 J. A. Rupley and G. Careri, *Adv. Protein Chem.*, 1991, **41**, 37–172.
11 P. W. Fenimore, H. Frauenfelder, B. H. McMahon and R. D. Young, *Proc. Natl. Acad. Sci. U. S. A.*, 2004, **101**, 14408–14413.
12 I. E. Iben, D. Braunstein, W. Doster, H. Frauenfelder, M. K. Hong, J. B. Johnson, S. Luck, P. Ormos, A. Schulte, P. J. Steinbach, A. H. Xie and R. D. Young, *Phys. Rev. Lett.*, 1989, **62**, 1916–1919.
13 S. H. Chen, L. Liu, E. Fratini, P. Baglioni, A. Faraone and E. Mamontov, *Proc. Natl. Acad. Sci. U. S. A.*, 2006, **103**, 9012–9016.
14 W. Doster, *Eur. Biophys. J.*, 2008, **37**, 591–602.
15 W. Doster, S. Cusack and W. Petry, *Nature*, 1989, **337**, 754–756.
16 J. Fitter, *Biophys. J.*, 1999, **76**, 1034–1042.
17 Y. Joti, H. Nakagawa, M. Kataoka and A. Kitao, *Biophys. J.*, 2008.
18 A. Paciaroni, S. Cinelli and G. Onori, *Biophys. J.*, 2002, **83**, 1157–1164.
19 V. Réat, R. Dunn, M. Ferrand, J. L. Finney, R. M. Daniel and J. C. Smith, *Proc. Natl. Acad. Sci. U. S. A.*, 2000, **97**, 9961–9966.
20 J. H. Roh, J. E. Curtis, S. Azzam, V. N. Novikov, I. Peral, Z. Chowdhuri, R. B. Gregory and A. P. Sokolov, *Biophys. J.*, 2006, **91**, 2573–2588.
21 A. M. Tsai, D. A. Neumann and L. N. Bell, *Biophys. J.*, 2000, **79**, 2728–2732.
22 G. Caliskan, R. M. Briber, D. Thirumalai, V. Garcia-Sakai, S. A. Woodson and A. P. Sokolov, *J. Am. Chem. Soc.*, 2006, **128**, 32–33.
23 M. Tarek and D. J. Tobias, *Phys. Rev. Lett.*, 2002, **88**, 138101.
24 A. L. Tournier, J. Xu and J. C. Smith, *Biophys. J.*, 2003, **85**, 1871–1875.
25 M. Weik, *Eur. Phys. J. E: Soft Matter*, 2003, **12**, 153–158.
26 M. Weik, U. Lehnert and G. Zaccai, *Biophys. J.*, 2005, **89**, 3639–3646.
27 K. Wood, A. Frölich, A. Paciaroni, M. Moulin, M. Hartlein, G. Zaccai, D. J. Tobias and M. Weik, *J. Am. Chem. Soc.*, 2008, **130**, 4586–4587.
28 K. Wood, M. Plazanet, F. Gabel, B. Kessler, D. Oesterhelt, G. Zaccai and M. Weik, *Eur. Biophys. J.*, 2008, **37**, 619–626.
29 W. Boos and H. Shuman, *Microbiol. Mol. Biol. Rev.*, 1998, **62**, 204–229.
30 D. Oesterhelt, *Curr. Opin. Struct. Biol.*, 1998, **8**, 489–500.
31 D. Oesterhelt and W. Stoeckenius, *Methods Enzymol.*, 1974, **31**, 667–678.
32 H. Patzelt, A. S. Ulrich, H. Egbringhoff, P. Düx, J. Ashurst, B. Simon, H. Oschkinat and D. Oesterhelt, *J. Biomol. NMR*, 1997, **10**, 95–106.
33 U. Lehnert, Thesis in Biophysics, Université Joseph Fourier, Grenoble, 2002.
34 M. Weik, H. Patzelt, G. Zaccai and D. Oesterhelt, *Mol. Cell*, 1998, **1**, 411–419.
35 M. Jasnin, M. Moulin, M. Haertlein, G. Zaccai and M. Tehei, *EMBO Rep.*, 2008, **9**, 543–547.
36 M. Tehei, B. Franzetti, K. Wood, F. Gabel, E. Fabiani, M. Jasnin, M. Zamponi, D. Oesterhelt, G. Zaccai, M. Ginzburg and B. Z. Ginzburg, *Proc. Natl. Acad. Sci. U. S. A.*, 2007, **104**, 766–771.
37 A. Elgsaeter and D. Branton, *J. Cell Biol.*, 1974, **63**, 1018–1036.
38 G. Zaccai, *Science*, 2000, **288**, 1604–1607.
39 V. Réat, G. Zaccai, M. Ferrand and C. Pfister, in *Biological Macromolecular Dynamics: Workshop on Inelastic and Quasielatic Neutron Scattering in Biology*, ed. S. Cusack, H. Büttner, M. Ferrand, P. Langan and P. Timmins, Adenine Press, New York, 1996, pp. 117–122.
40 D. J. Bicout and G. Zaccai, *Biophys. J.*, 2001, **80**, 1115–1123.
41 M. Bée, *Quasielastic Neutron Scattering, Principles and Applications in Solid State Chemistry, Biology and Materials Science*, Adam Hilger, Bristol and Philadelphia, 1988.
42 T. Unruh, J. Neuhaus and W. Petry, *Nucl. Instrum. Methods Phys. Res., Sect. A*, 2007, **580**, 1414–1422, and erratum 585:1201.
43 F. Merzel and J. C. Smith, *Proc. Natl. Acad. Sci. U. S. A.*, 2002, **99**, 5378–5383.
44 D. I. Svergun, S. Richard, M. H. Koch, Z. Sayers, S. Kuprin and G. Zaccai, *Proc. Natl. Acad. Sci. U. S. A.*, 1998, **95**, 2267–2272.
45 J. H. Roh, V. N. Novikov, R. B. Gregory, J. E. Curtis, Z. Chowdhuri and A. P. Sokolov, *Phys. Rev. Lett.*, 2005, **95**, 038101.
46 J. Teixeira, M. C. Bellissent-Funel, S. H. Chen and A. J. Dianoux, *Phys. Rev. A*, 1985, **31**, 1913–1917.
47 G. Sposito, *J. Chem. Phys.*, 1981, **74**, 6943–6949.
48 A. M. Stadler, J. P. Embs, I. Digel, G. Artmann, G. Zaccai and G. Bueldt, *J. Am. Chem. Soc.*, 2008, submitted.
49 K. S. Singwi and A. Sjölander, *Phys. Rev.*, 1960, **119**, 863–871.

50 B. N. Brockhouse, *Nuovo Cimento, Suppl.*, 1958, **9**, 45.
51 P. Leung and G. Safford, *J. Phys. Chem.*, 1970, **74**, 3696–3709.
52 L. Cordone, M. Ferrand, E. Vitrano and G. Zaccai, *Biophys. J.*, 1999, **76**, 1043–1047.
53 D. Vitkup, D. Ringe, G. A. Petsko and M. Karplus, *Nat. Struct. Biol.*, 2000, **7**, 34–38.
54 J. Swenson, H. Jansson and R. Bergman, *Phys. Rev. Lett.*, 2006, **96**, 247802.
55 G. Zaccai, *J. Mol. Biol.*, 1987, **194**, 569–572.
56 M. Kamihira and A. Watts, *Biochemistry*, 2006, **45**, 4304–4313.
57 G. Zaccai and D. J. Gilmore, *J. Mol. Biol.*, 1979, **132**, 181–191.
58 P. K. Rogan and G. Zaccai, *J. Mol. Biol.*, 1981, **145**, 281–284.
59 P. Mentré, *Cell. Mol. Biol.*, 2001, **47**, 709–715.
60 M. C. Bellissent-Funel, J. M. Zanotti and S. H. Chen, *Faraday Discuss.*, 1996, **103**, 281–294.
61 D. Madern, C. Ebel and G. Zaccai, *Extremophiles*, 2000, **4**, 91–98.
62 R. MacKinnon, *FEBS Lett.*, 2003, **555**, 62–65.
63 B. Frick and M. Gonzalez, *Phys. B*, 2001, **301**, 8–19.

 

## *10.2 Dynamics of apomyoglobin in the α-to-β transition and of partially unfolded aggregated protein*

Protein dynamics during the α-to-β transition associated with amyloid formation was measured on the model system apo-myoglobin. Characteristic elements for the structural transition were found using wide angle X-ray solution scattering above around 55°C. Circular dichroism (CD) was measured as a function of temperature and solvent condition. The secondary structural content of apo-myoglobin during the structural transition was estimated from the CD data. Protein dynamics was measured with incoherent elastic neutron scattering. The data revealed a more resilient β-structure phase. A similar transition was found in holo-myoglobin that was attributed to protein unfolding and aggregation. Mean square displacements showed that the dynamical transition at around 200 K also occurs in a heat denatured aggregated protein.

I contributed to the article with the analysis and interpretation of the neutron scattering experiments, calculated the secondary structure content from the CD data and participated in the writing of the article.

Eur Biophys J
DOI 10.1007/s00249-008-0375-z

ORIGINAL PAPER

# Dynamics of apomyoglobin in the α-to-β transition and of partially unfolded aggregated protein

**E. Fabiani · A. M. Stadler · D. Madern · M. M. Koza · M. Tehei · M. Hirai · G. Zaccai**

Received: 5 June 2008 / Revised: 17 September 2008 / Accepted: 22 September 2008


**Abstract** Changes of molecular dynamics in the α-to-β transition associated with amyloid fibril formation were explored on apomyoglobin (ApoMb) as a model system. Circular dichroism, neutron and X-ray scattering experiments were performed as a function of temperature on the protein, at different solvent conditions. A significant change in molecular dynamics was observed at the α-to-β transition at about 55°C, indicating a more *resilient* high temperature β structure phase. A similar effect at approximately the same temperature was observed in holomyoglobin, associated with partial unfolding and protein aggregation. A study in a wide temperature range between 20 and 360 K revealed that a dynamical transition at about 200 K for motions in the 50 ps time scale exists also for a hydrated powder of heat-denatured aggregated ApoMb.

**Keywords** Amyloid former · Protein dynamics · Neutron · Circular dichroism

E. Fabiani · A. M. Stadler · M. M. Koza · M. Tehei · G. Zaccai (✉)
Institut Laue-Langevin, BP156, Grenoble, France
e-mail: zaccai@ill.fr

E. Fabiani · D. Madern
Institut de Biologie Structurale, Grenoble, France

E. Fabiani
Université Joseph Fourier, Grenoble, France

A. M. Stadler
Research Centre Juelich, Juelich, Germany

M. Hirai
Gunma University, Maebashi, Japan

*Present Address:*
E. Fabiani (✉)
CEA LETI Minatec Département des Technologies pour la Biologie et la Santé, Grenoble Cedex 9, France
e-mail: elisa.fabiani@cea.fr

*Present Address:*
M. Tehei
School of Chemistry, University of Wollongong, Wollongong, NSW 2522, Australia

M. Tehei
Australian Institute of Nuclear Science and Engineering (AINSE), Menai, NSW, Australia

## Introduction

Amyloidosis is an emerging category of diseases characterised by the extracellular accumulation of protein aggregates in body organs or tissues, including brain, liver, spinal cord and intestine. Even if the first cases of amyloidosis were described over 300 years ago, it is only within the past 20 years that the specific chemical composition and structure of amyloid protein formations have been understood. More than 20 different kinds of amyloidosis are known currently. They include Alzheimer's disease, Parkinson's disease, Huntington's disease and the "prion diseases" (Scrapie, Kuru, CJD, BSE, etc.). Therapeutic approaches have focussed on reducing the production of the protein, with different treatments for the different cases of amyloidosis.

Amyloid aggregation is closely related to protein folding issues. "Amyloid fibrils" consist of polymerised cross-β-sheet structures in which the beta-strands are arranged perpendicular to the long axis of the fibre. There are various causes for protein misfolding that could lead to amyloid formation. For example, in the absence of chaperones, certain proteins will fail to achieve their native state

and may associate with other unfolded polypeptide chains to form large amyloid fibrils. Misfolding can also occur when a protein is subjected to particular conditions, such as extremes of heat or pH. Understanding the physical bases of misfolding in these cases is of fundamental scientific and biotechnological importance. In the context it is important to characterise the forces that stabilise protein structure, and therefore its dynamics under relevant solvent conditions.

Apomyoglobin (ApoMb) was chosen for neutron, X-ray scattering and circular dichroism (CD) measurements because previous studies on the protein have shown that its fibril formation appears under particular conditions of temperature and pH (Fändrich et al. 2003). Before amyloid formation, ApoMb can adopt two well-defined structural conformations at pH 9: below 55°C, the *helix-rich native-like structure* α, and above 55°C, *the cross-β structure* characteristic of proteins that can generate amyloid deposits in humans. The transition arises because the helical structures in ApoMb are destabilised partially so that neighbouring strands will interact to form the cross-β structure between them. Amyloid structures differ from globular protein structures, which are always encoded in the amino acid sequence, because they do not depend on the presence of distinctive sequence patterns or specific intramolecular side-chain interactions. The structural aspects of the transition have been characterised by small and wide angle X-ray scattering (WAXS; Onai et al. 2007). The total structure factor observed showed two peaks at 0.58 and 1.34 $\text{Å}^{-1}$, which are strongly correlated with amyloid transformation (Onai et al. 2007). The peaks appear at pH 9 at 55°C, and become more pronounced as the temperature is raised. Further investigations of structure (Booth et al. 1997; Chamberlain et al. 2001) and folding dynamics (Takano et al. 2001; Canet et al. 1999, 2002) have led to a better understanding of the process involved in the conversion of globular proteins into amyloid fibrils.

The work reported concerns the measurement and comparison of the structure and dynamics, in a wide temperature range, of ApoMb under different solvent conditions (at pH 9 and pH 7, in $H_2O$ and $D_2O$), by using CD to characterise secondary structures, and energy resolved elastic neutron scattering. As it has been demonstrated for other biological systems, energy resolved neutron scattering provides quantitative information on the forces involved in the stabilisation of protein structures (Zaccai 2000). The scattering cross-section of $^1H$ dominates that of all other atoms in biological material, and of its isotope, deuterium $^2H$ (D). Thus, heavy water ($D_2O$) is often used to reduce the contribution of hydration water to the scattering signal. CD experiments were performed in $H_2O$ and $D_2O$, therefore, to characterise whether or not the α-to-β transition is affected by the solvent isotope.

A significant change in molecular dynamics towards a more resilient structure was observed for ApoMb at pH 9, at the α-to-β transition at about 55°C. A similar observation for holo-myoglobin (HoloMb) was attributed to partial unfolding and protein aggregation, indicating that denatured and aggregated protein display similar dynamics as β-amyloid. In a further examination of the dynamics of irreversibly heat-denatured and aggregated protein, a hydrated powder sample of ApoMb was shown to undergo a dynamical transition at about 200 K as has been observed for native HoloMb (Doster et al. 1989), purple membranes (Ferrand et al. 1993; Lehnert et al. 1998).

## Materials and methods

### ApoMb preparation

Apomyoglobin was obtained by removing the heme from HoloMb. Several protocols yield the apo-protein with similar properties. We successfully adapted the method of Rothgeb (Rothgeb and Gurd 1978) to obtain the apo-protein form in gram quantities for the neutron scattering experiments. The process was promoted by acid conditions in suitable solvent. An appropriate amount of lyophilised horse heart HoloMb purchased from SIGMA-ALDRICH was dissolved in water. The pH of the HoloMb solution was then lowered to 1.5 with concentrated HCl at 4°C. The acidified solution was extracted as quickly as possible with 4 volumes of 2-butanone. The upper organic layer was decanted, and the extraction was repeated at least twice more in order to obtain a hazy, colourless aqueous layer which was dialysed exhaustively against a dilute bicarbonate solution followed by pure water. After salt was completely removed by dialysis, the protein was lyophilised. For the neutron experiments, the powder was hydrated by pipetting uniformly buffer solutions to the sample to a level of 0.73 g $H_2O$/g protein or corresponding 0.8 g $D_2O$/g protein. This corresponds to approximately two hydration layers per protein and allows for pH effects. CD experiments were performed on the protein solution before lyophilisation.

### Solvent conditions

For neutron experiments, the lyophilised ApoMb was rehydrated under different solvent conditions in $H_2O$ and $D_2O$ potassium phosphate buffer (20 mM $KH_2PO_4$, pH/pD 7 and pH/pD 9). Potassium phosphate was purchased from SIGMA.

All solutions were obtained by dissolving the buffer in distilled water ($H_2O$) or heavy water ($D_2O$). The pH (pD) was adjusted to the desired value by adding acid or base.

The pD was calculated by adding 0.4 to the value measured on a normally calibrated pH metre (Lide 1999). The same buffer solution was used to adjust the pH (pD) of the protein solution for the CD experiments.

### Circular dichroism experiments

Circular dichroism measurements were used to check the $\alpha$-to-$\beta$ transition, the pH (pD) and temperature dependence of secondary structure. CD spectroscopy measures differences in the absorption of left-handed polarised light vs. right-handed polarised light, which arise due to structural asymmetry. The absence of regular structure results in 0 CD intensity, while an ordered structure results in a spectrum, which can contain both positive and negative signals. CD spectroscopy is particularly good for determining whether or not a protein is folded, and if so characterising its secondary structure. CD measurements were performed at the Institut de Biologie Structurale (IBS) and EMBL in Grenoble (France) by using a CD spectrometer equipped with a temperature-controlled cuvette holder. The far-UV CD spectral region (190–250 nm) was explored for different temperatures, pH and buffer conditions. The protein concentration was about 20 μM for all samples. The experiments were performed in the temperature range between 25 and 95°C. The data were analysed by subtracting the background CD spectrum and converting the spectra from millidegrees to molar ellipticity ($\theta$) in degrees·cm$^2$ per decimole residues using the measured protein concentration. Secondary structure analysis of the final CD data was carried out using the K2D web program (Andrade et al. 1993; Merelo et al. 1994).

### Neutron scattering experiments

Neutron scattering has proven to be a versatile tool for the study of the molecular dynamics of condensed matter in general (Bée 2000), and biological macromolecules and solvent interactions, in particular (Gabel et al. 2002; Paciaroni et al. 2002; Lehnert et al. 1998; Gabel and Bellissent-Funel 2007; Andreani et al. 1995; Pieper et al. 2004). The complexity of protein dynamics is reflected in a vast range of types of motion and corresponding associated time and length scales. Neutrons are sensitive in different ways to the motions of hydrogen (H) and its heavy isotope deuterium (D). Isotope labelling as well as the use of spectrometers with different energy resolution (corresponding to different time scales) considerably enriches the interpretation of scattering spectra. Elastic incoherent neutron scattering is a specific technique for the study of dynamical processes occurring on a time scale defined by the spectrometer resolution in energy. It provides atomic mean square displacement values (dominated by H atoms because of their large scattering cross-section compared to all the other atoms in biological samples) as a function of temperature, from which effective force constants can be obtained (Zaccai 2000).

The mean square displacement $<u^2>$ is derived from the analysis of the Elastic Area vs. $Q^2$ in a Gaussian approximation, where the Elastic Area is the area of the elastically scattered intensity and $Q$ is the modulus of the scattering vector, $(4\pi \sin \theta/2)/\lambda$ (Gabel et al. 2002) where $\theta$ is the scattering angle and $\lambda$ is the neutron wavelength.

$$<u^2> = -6\left(\frac{\mathrm{d}\ \ln(\text{Elastic Area})}{\mathrm{d}(Q^2)}\right) \quad (1)$$

The approximation is valid for values of $<u^2>\ Q^2$ smaller than or close to about 2, and the $Q$ ranges for the fit were chosen appropriately.

In cases for which the data quality is not sufficient to derive precise mean square displacement values, an analysis as a function of temperature of the total intensity sum in the same $Q$ range, can give a good indication of a transition in dynamical behaviour (Reat et al. 2000).

#### *At the Institut Laue-Langevin reactor neutron source*

Energy resolved elastic neutron scattering experiments on ApoMb and HoloMb were carried out at the Institut Laue-Langevin in Grenoble (France) on the spectrometer IN13 (http://www.ill.eu/YellowBook/IN13/). IN13 is a back-scattering spectrometer characterised by a high-energy resolution (of about 8 μeV, corresponding to 0.1 ns time scale) associated to a wide range of momentum transfer ($Q_{\max}$ ~4.7 Å$^{-1}$, corresponding to a length scale ~Ångstrom unit). Free and hydration water motions are too fast to be observed in this time-length window for $q > 1$ Å$^{-1}$ and contributes to the measured signal only as a negligibly low background. Measured data was analysed in the $q^2$-range from 1.5 to 5 Å$^{-2}$. In this high scattering vector range experiments in natural abundance water solvent are feasible with negligible $H_2O$ contribution (Tehei et al. 2004; Jasnin et al. 2008). An amount of 100 and 120 mg of re-hydrated ApoMb and HoloMb powder, respectively (0.73 g $H_2O$/g protein) at pH 9 was inserted in a flat aluminium cell with internal spacing of 0.3 mm, which was put in the IN13 sample environment at an angle of 135° with respect to the incident beam. The experiments were performed as a function of temperature (heating between 280 and 350 K). An displex device specific to IN13 was used for temperature control. The data were analysed as outlined above.

#### *At the ISIS spallation neutron source*

Neutron scattering experiments on a heat-denatured and aggregated ApoMb hydrated powder sample were carried out on the IRIS spectrometer at the ISIS spallation neutron

source, Chilton, UK. The denatured sample was obtained by heating the hydrated powder in a closed sample holder at 360 K and allowing incubation for 4 h. By exploiting the Pyrolitic Graphite PG(002) analyser configuration and the Beryllium filter, the covered momentum transfer range was between 0.3 and 1.8 $Å^{-1}$ with an energy resolution of 17 μeV (corresponding to a 50-ps time scale). The experiment was performed with $D_2O$ solvent, since diffusion of $H_2O$ would contribute strongly to the measured signal at the small scattering vector range covered by the instrument (Jasnin et al. 2008. An amount of 130 mg hydrated powder (0.8 g $D_2O$/g protein) at pH 9 in $D_2O$ was held in a flat aluminium cell with internal spacing of 0.3 mm, placed at an angle of 135° with respect to the incident beam. We estimated that $D_2O$ solvent contributes only with 2% to the total incoherent scattering cross-section. Therefore, it is justified to neglect the solvent contribution of $D_2O$. Each temperature point was collected for 4 h. The temperature scan was performed in a temperature range between 20 and 360 K in order to examine the mean square atomic displacements and effective force constants (Zaccai 2000). It was reported in literature that water in the secondary hydration shell of proteins can be vitrified during flash cooling to 100 K and crystallises during reheating at 200–210 K to cubic ice (Sartor et al. 1995). Even if there was a secondary hydration shell present in our sample, we did not observe ice formation during the experiment at low temperature as evidenced by the absence of ice Bragg peaks. We can only speculate about the reason, but the presence of buffer solution and not pure water might be an explanation. The temperature was controlled by heating the sample in a standard IRIS cryofurnace. First the sample was inserted at 280 K. Then it was heated up to 360 K to allow for heat denaturation. Afterwards the sample was cooled down to 20 K and the scattering at low temperatures was measured as a reference. In the following, the temperature scan was measured for different temperature points from 20 to 360 K. Heating and cooling rates were approximately in the order of 1–3 K $min^{-1}$. Mean square displacements were calculated from the analysis of the integrated intensity over a frequency window corresponding to instrumental resolution around the elastic peak, according to Eq. 1.

### Wide angle X-ray scattering experiments

To check an effect of change of solvent ($H_2O$ or $D_2O$) on α-to-β transition and amyloid transition of ApoMb, we have carried out WAXS measurement under the same solvent condition used before (Onai et al. 2007), where the $D_2O$ solvent was 50 mM Tris–DCl (2-amino-2-hydroxymethyl-1,3-propanediol hydrochloride) buffer at pD 9. The ApoMb concentration was 1% w/v. The WAXS measurement was performed by using the BL-40B2 spectrometer installed at the synchrotron radiation source (SPring-8) at the Japan Synchrotron Radiation Research Institute (JASRI), Japan. The X-ray wavelength, the sample-to-detector distance and the exposure time were 0.82 Å, 41 cm and 30 s, respectively. The details of the scattering data analysis were as reported previously (Hirai et al. 2004).

## Results and discussion

### Circular dichroism

The far-UV CD spectra of ApoMb are presented in Fig. 1 for all temperatures and solvent conditions explored. At room temperature, all spectra show two negative peaks at 207 and 222 nm and a positive one at 193 nm, characteristic of the alpha-helix structure (black curves). ApoMb shows the predominance of the alpha-helix structure until 55°C. Above 55°C and only at pH and pD 9, the beta-sheet contribution appears and replaces the alpha-helix secondary structure. This is evident in Fig. 1b, d by the shift of the minimum from 207 nm to at around 200 nm during heating (Fändrich et al. 2003) and by the behaviour of the beta-sheet content from the K2D analysis of the spectra shown in Fig. 2. Note that the K2D data show similar behaviour in $H_2O$ and $D_2O$ at corresponding pH or pD values, respectively. Synchrotron radiation experiments also showed similar behaviour at the large angle scattering features (indicative of secondary structure) irrespective of whether the sample was in $H_2O$ or $D_2O$ as shown below.

In Fig. 1a, b, at pD (pH) 7 in $D_2O$ and $H_2O$, the amplitudes of the two peaks are lowered with increasing temperature, consistent with the expected partial unfolding of the protein. Analysis of the spectra with the programme K2D (Fig. 2) yielded helix fractions of 70–80% and 40% at 20 and 70°C, respectively, while the beta fraction, which was negligible at room temperature increased to about 15% at high temperatures. A random fraction increased from 20–30% to 40–60% between 20 and 70°C. However, in Fig. 2 at pH (pD) 9 in $H_2O$ and $D_2O$, the helix fraction decreases rapidly to 15–25% between 20 and 70°C and the beta fraction increases up to 20–30% at 70°C, which is in agreement with an expected higher beta-sheet content at basic solvent conditions and high temperatures.

Previous CD experiments on HoloMb had shown partial unfolding of the protein at 65°C, total unfolding at 84.5 ± 1.0°C (Fändrich et al. 2003), with no indication of an α-to-β transition at 55°C at pH 9.

### X-ray scattering

Figure 3 shows the WAXS curve of ApoMb in $D_2O$ buffer at pH 9 depending on temperature from 25 to 65°C. As

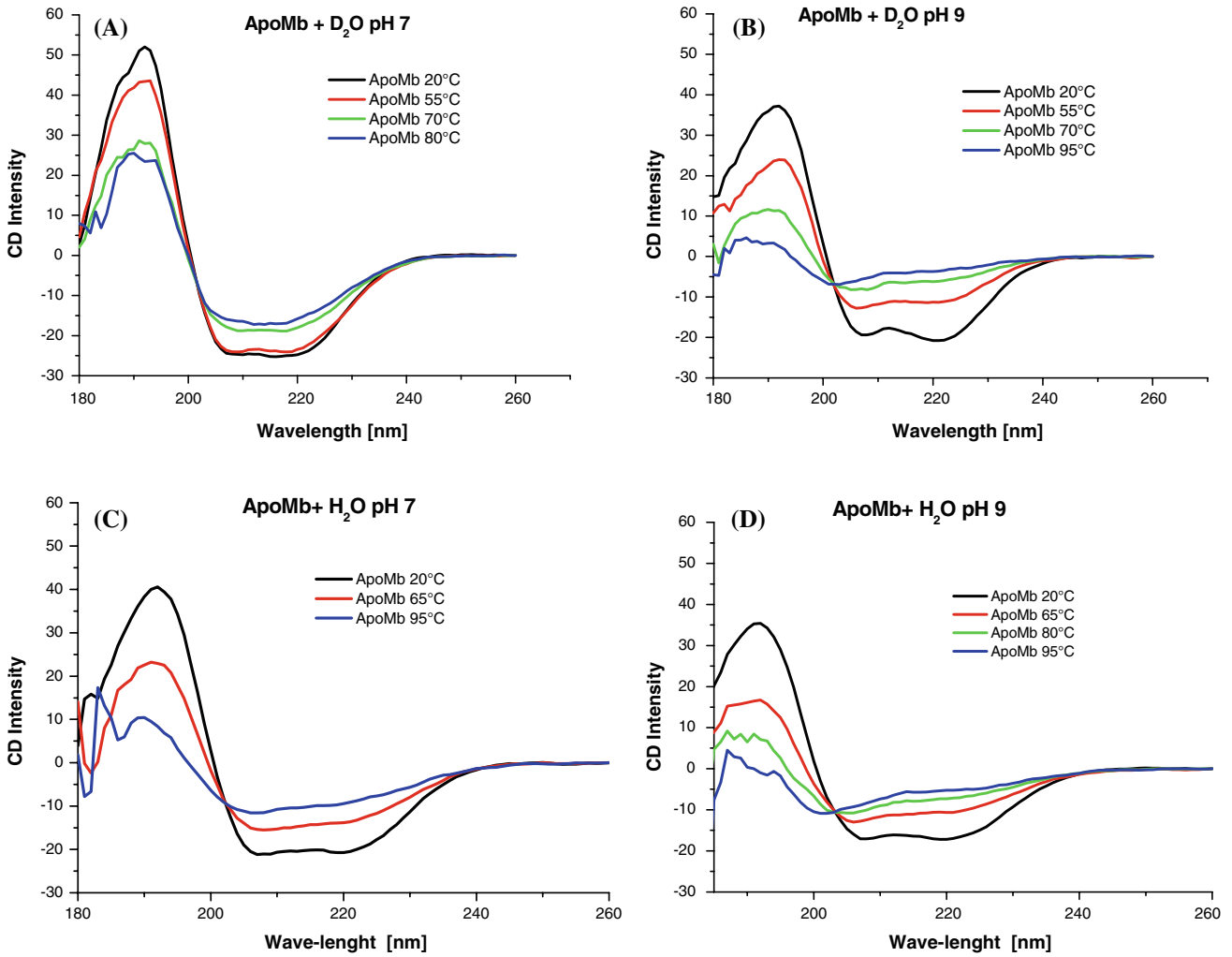


**Fig. 1** Circular dichroism data for apomyoglobin **a** in $D_2O$ at pH 7, **b** in $D_2O$ at pH 9, **c** in $H_2O$ at pH 7 and **d** in $H_2O$ at pH 9 in the temperature range between 20 and 95°C

reported previously (Hirai et al. 2004), we can discuss about the details of the structural transition of ApoMb in its different hierarchical levels that are the quaternary and tertiary structures ($q < \sim 0.2$ Å$^{-1}$), the inter-domain correlation and the intra-domain structure ($q = \sim 0.25$–$0.8$ Å$^{-1}$), and the secondary structure and the closely packed side chains in the hydrophobic cores ($q = \sim 1.1$–$1.9$ Å$^{-1}$), respectively. The arrows plotted in Fig. 3 indicate the typical features of the scattering curve of an amyloid formation. Namely, the peak at $q = \sim 1.35$ Å$^{-1}$, the broad peak at $q = \sim 0.60$ Å$^{-1}$ and the shoulder at $q = \sim 0.09$ Å$^{-1}$ correspond to the $\alpha$-to-$\beta$ transition (cross-$\beta$ structure), the pleated sheet stacking, and the oligomerisation of denatured ApoMb, respectively. These features appear simultaneously and are evidently seen above ~55°C. It should be mentioned that the positions of the peaks at $q = \sim 1.35$ and $\sim 0.60$ Å$^{-1}$ are slightly larger than those observed in $H_2O$ buffer (Onai et al. 2007). This suggests that in $D_2O$ solvent the formed stacking of the cross-$\beta$ is more compact as compared with that in $H_2O$ solvent.

## Neutron scattering

The total intensity analysis of the IN13 data at pH 9 is shown in Fig. 4. The curves for ApoMb and HoloMb both show a "transition" at about 55°C indicative of a more resilient (smaller rate of decrease with temperature) structure at the higher temperature. The CD data showed that in the case of ApoMb, the effect is correlated with the $\alpha$-to-$\beta$ transition. In HoloMb, the more resilient state seems to be associated with partial unfolding of the protein and aggregation in accordance with Fändrich et al. (2003). We present only summed elastic intensities as these are more precise to identify dynamical transitions (Reat et al. 2000). Calculation of mean square displacements gave errors bars that were to big to make any conclusion about a dynamical transition around 55°C.

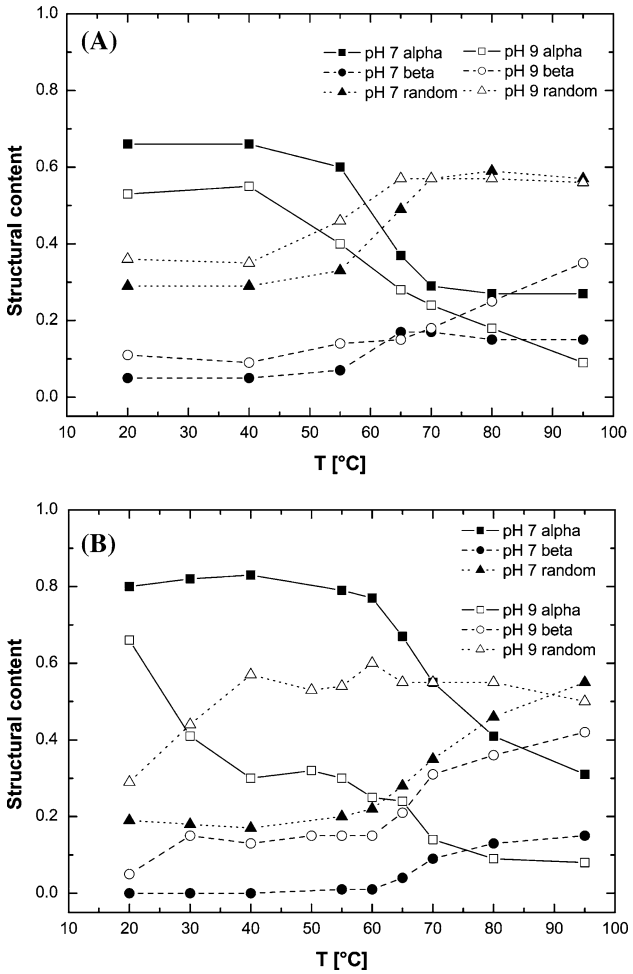


**Fig. 2** Analysis of the structural content of ApoMb at pH 7 and pH 9 in **a** $H_2O$ and **b** $D_2O$

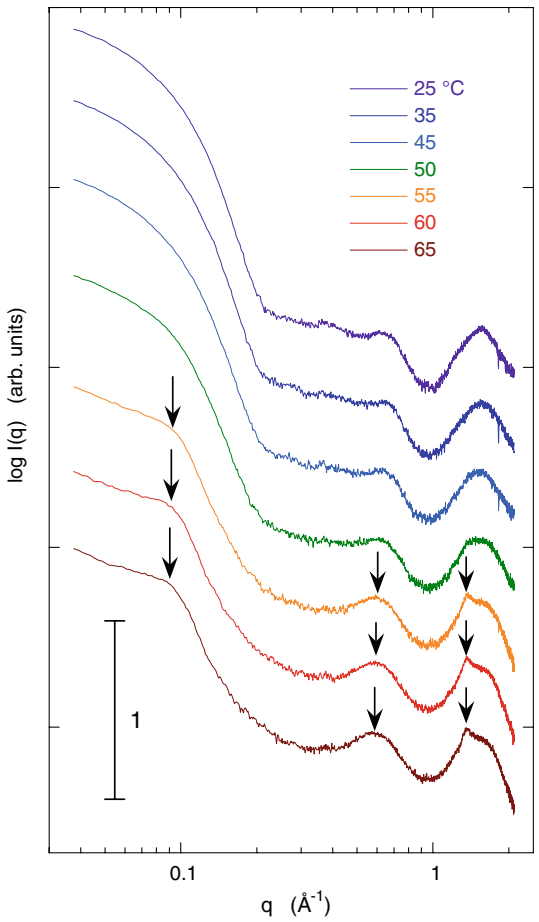


**Fig. 3** Wide angle X-ray scattering curve of apomyoglobin in $D_2O$ solvent at pH 9 in the temperature range from 25 to 65°C. The *arrows* (the peaks at $q = \sim 1.35$ and $\sim 0.60$ Å$^{-1}$, the shoulder at $q = \sim 0.09$ Å$^{-1}$) indicate typical features of amyloid transition. This transition occurred above ~55°C

As the temperature is increased and before total unfolding at higher temperatures, both ApoMb and HoloMb display a transition to a more resilient aggregated dynamic structure at about 55°C. In the case of ApoMb at pH 9, the structure is the $\beta$-structure associated with amyloid fibre formation. While in the case of HoloMb, the structure is likely due to partial unfolding and an undefined aggregate state (Fändrich et al. 2003). The transition to a more resilient high temperature dynamics structure at ~55°C was also observed in IN13 experiments on ApoMb at pH 7 (data not shown), suggesting that like for HoloMb, ApoMb at pH 7 partially unfolds and aggregates in this pre-transition to total unfolding. In order to explore further the dynamic behaviour of aggregated protein, a temperature scan of the elastic intensity was performed on heat-denatured ApoMb on the IRIS spectrometer at ISIS (Fig. 5). The 17 μeV energy resolution condition chosen on the instrument corresponds to a time scale of 50 ps. Interestingly, the data showed a dynamical transition for the sample at about 200 K, similar to that observed in hydrated

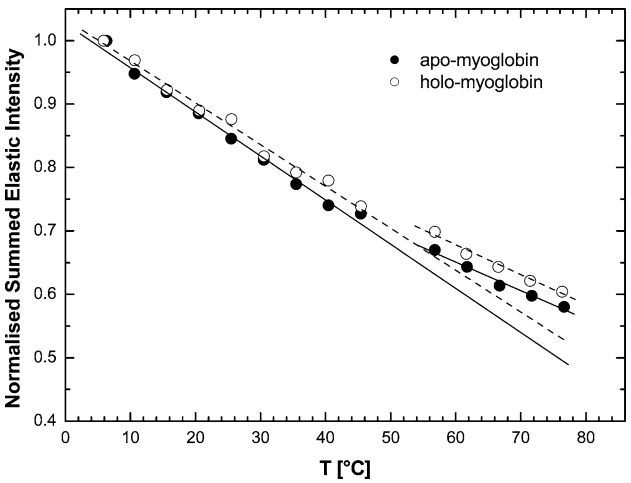


**Fig. 4** IN13 sum of intensities vs. temperature for apomyoglobin and holo-myoglobin. The *broken line* is a linear fit for holo-myoglobin and the straight line is a linear fit to apomyoglobin. Due to limitations of the temperature control, no experimental points could be measured between around 45 and 55°C

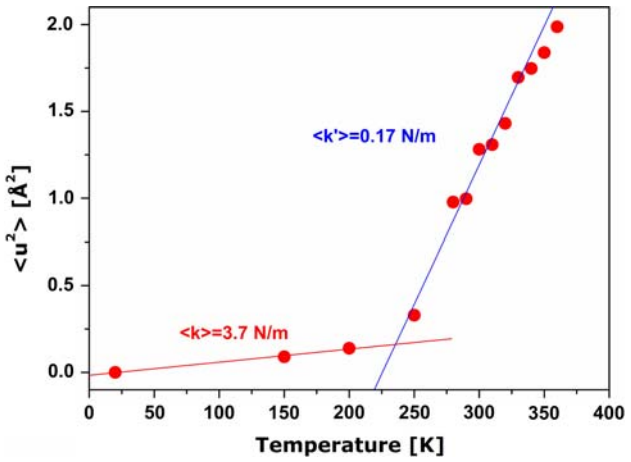


**Fig. 5** Mean square displacement $<u^2>$ vs. temperature from IRIS elastic scan measurements on heat-denatured and aggregated ApoMb. *Error bars* are within the *symbols*

native HoloMb (0.38 g $D_2O$/g protein) by Doster et al. (1989), indicating that the transition is also a property of heat-denatured and aggregated protein. The force constant $<k>$ and the effective force constant $<k'>$ were determined for the low temperature range below 200 K with $<k> = 3.7 \pm 0.3$ N m$^{-1}$ and above 200 K with $<k'> = 0.17 \pm 0.01$ N m$^{-1}$ (Zaccai 2000). In the 100 ps time range values of $<k> = 3$ N m$^{-1}$ and $<k'> = 0.3$ N m$^{-1}$ were obtained for hydrated HoloMb powder (Zaccai 2000). At low temperatures the force constants $<k>$ between ApoMb and HoloMb are similar. Above the dynamical transition temperature, the effective force constant $<k'>$ of ApoMb is significantly smaller than that of HoloMb. The higher degree of hydration of the ApoMb sample might facilitate protein motion and be the cause of this discrepancy.

## Conclusion

In this paper, ApoMb was used as a model biochemical system in order to explore the molecular changes of dynamics in the α-to-β transition associated with amyloid fibril formation. CD and neutron scattering experiments were performed on the protein, at pH 9 in $H_2O$ and $D_2O$, in a wide temperature range. Similar experiments were carried out on HoloMb, on the same solvent condition. WAXS was used to confirm the occurrence of the α-to-β transition of ApoMb in $D_2O$ solution at pD 9 by the appearance of characteristic Bragg peaks. CD experiments emphasised that the transition is present above 55°C and only at pH and pD 9 in dilute solution. ApoMb results show a significant change in molecular dynamics at the α-to-β transition at about 55°C, indicating a more *resilient* high temperature β structure phase. The behaviour of the holo-protein as function of temperature is associated with partial unfolding and protein aggregation.

**Acknowledgments** The authors acknowledge the IN13 and IRIS staffs for their support during the experiment at ILL and ISIS facilities. Thanks are due to Dr. Felix Fernandez-Alonso and Dr. Franz Demmel for helpful discussions. Technical and financial support from the ILL and ISIS facilities is gratefully acknowledged. The WAXS measurement was done under the approval of the JASRI Program Advisory Committee (Proposal #2006A1339). M. Tehei acknowledges the ILL, the AINSE, the CNRS and the Institut de Biologie Structurale (UMR 5075) for financial support of this work.

## References

Andrade MA, Chacón P, Merelo JJ, Morán F (1993) Evaluation of secondary structure of proteins from UV circular dichroism using an unsupervised learning neural network. Protein Eng 6:383–390

Andreani C, Filabozzi A, Menzinger F, Desideri A, Deriu A, Dicola D (1995) Dynamics of hydrogen atoms in superoxide dismutase by quasielastic neutron scattering. Biophys J 68:2519–2523

Bée M (2000) La diffusion quasiélastique des neutrons; introduction et principes généraux. Diffusion Quasiélastique des Neutrons. J Phys IV France 10:Pr1-1–Pr1-14

Booth DR, Sunde M, Bellotti V, Robinson CV, Hutchinson WL, Fraser PE, Hawkins PN, Dobson CM, Radford SE, Blake CCF, Pepys MB (1997) Instability, unfolding and aggregation of human lysozyme variants underlying amyloid fibrillogenesis. Nature 385:787–793

Canet D, Sunde M, Last AM, Miranker A, Spencer A, Robinson CV, Dobson CM (1999) Mechanistic studies of the folding of human lysozyme and the origin of amyloidogenic behaviour in its disease related variants. Biochemistry 38:6419–6427

Canet D, Last AM, Tito P, Sunde M, Spencer A, Archer DB, Redfield C, Robinson CV, Dobson CM (2002) Local cooperativity in the unfolding of an amyloidogenic variant of human lysozyme. Nat Struct Biol 9:308–315

Chamberlain AK, Receveur V, Spencer A, Redfield C, Dobson CM (2001) Characterization of the structure and dynamics of amyloidogenic variants of human lysozyme by NMR spectroscopy. Protein Sci 10:2525–2530

Doster W, Cusack S, Petry W (1989) Dynamical transition of myoglobin revealed by inelastic neutron scattering. Nature 337:754–756

Fändrich M, Forge V, Buder K, Kittler M, ChM Dobson, Diekmann S (2003) Myoglobin forms amyloid fibrils by association of unfolded polypeptide segments. Proc Natl Acad Sci USA 100:15463–15468

Ferrand M, Dianoux AJ, Petry W, Zaccai G (1993) Thermal motions and function of bacteriorhodopsin in purple membranes: effects of temperature and hydration studied by neutron scattering. Proc Natl Acad Sci USA 90(20):9668–9672

Gabel F, Bellissent-Funel MC (2007) C-phycocyanin hydration water dynamics in the presence of trehalose: an incoherent elastic neutron scattering study at different energy resolutions. Biophys J 92:4054–4063

Gabel F, Bicout D, Lehnert U, Tehei M, Weik M, Zaccai G (2002) Protein dynamics studied by neutron scattering. Q Rev Biophys 35:327–367

Hirai M, Koizumi M, Hayakawa T, Takahashi H, Abe S, Hirai H, Miura K, Inoue K (2004) Hierarchical map of protein unfolding

and refolding at thermal equilibrium revealed by wide-angle X-ray scattering. Biochemistry 43:9036–9049

Jasnin M, Moulin M, Haertlein M, Zaccai M, Tehei M (2008) Down to atomic-scale intracellular water dynamics. EMBO Rep 9:543–547

Lehnert U, Reat V, Weik M, Zaccai G, Pfister C (1998) Thermal motions in bacteriorhodopsin at different hydration levels studied by neutron scattering: correlation with kinetics and light-induced conformational changes. Biophys J 75:1945–1952

Lide DR (1999) CRC Handbook of chemistry and physics, 80th edn edn. CRC, Boca Raton

Merelo JJ, Andrade MA, Prieto A, Morán F (1994) Proteinotopic feature maps. Neurocomputing 6:443–454

Onai T, Koizumi M, Lu H, Inoue K, Hirai M (2007) Initial process of amyloid formation of apomyoglobin and effect of glycosphingolipid $G_{M1}$. J Appl Cryst 40:s184–s189

Paciaroni A, Cinelli S, Onori G (2002) Effect of the environment on the protein dynamical transition: a neutron scattering study. Biophys J 83:1157–1164

Pieper J, Irrgang KD, Renger G, Lechner RE (2004) Density of vibrational states of the light-harvesting complex II of green plants studied by inelastic neutron scattering. J Phys Chem B 108:10556–10565

Reat V, Dunn R, Ferrand M, Finney JL, Daniel RM, Smith JC (2000) Solvent dependence of dynamic transitions in protein solutions. Proc Natl Acad Sci USA 97:9961–9966

Rothgeb TM, Gurd FR (1978) Physical methods for the study of myoglobin. Methods Enzymol 52:73–86

Sartor G, Hallbrucker A, Mayer E (1995) Characterizing the secondary hydration shell on hydrated myoglobin, hemoglobin, and lysozyme powders by its vitrification behavior on cooling and its calorimetric glass → liquid transition and crystallization behavior on reheating. Biophys J 69:2679–2694

Takano K, Funahashi J, Yutani K (2001) The stability and folding process of amyloidogenic mutant human lysozymes. Eur J Biochem 268(1):155–159

Tehei M, Franzetti B, Madern D, Ginzburg M, Ginzburg BZ, Giudici-Orticoni MT, Bruschi M, Zaccai G (2004) Adaptation to extreme environments: macromolecular dynamics in bacteria compared *in vivo* by neutron scattering. EMBO Rep 5:66–70

Zaccai G (2000) How soft is a protein? A protein dynamics force constant measured by neutron scattering. Science 288:1604–1607

## *10.3* Hemoglobin senses body temperature

The following article presents a study on whole red blood cells using different experimental methods. The effect of heavy water on the passage transition of RBC was examined using the micropipette technique. RBC volume measurements were performed with very narrow micropipettes. The T1 relaxation time in RBC was measured with NMR. The colloid osmotic pressure of whole RBC in autologous plasma was determined as a function of temperature. The data revealed the onset of hemoglobin aggregation at body temperature. The use of heavy water results in a higher aggregation temperature. The mechanism was interpreted as being similar to a colloidal phase transition. It was concluded that hemoglobin senses body temperature.

I contributed to the article with the micropipette experiments on red blood cells in heavy water.

*European Biophysics Journal*, 2009, in revision

# Hemoglobin senses body temperature

Artmann G.M., Digel I., Zerlin K.F[1]., Maggakis-Kelemen Ch., Linder Pt., Porst D., Kayser P., **Stadler A.M.**[2], Dikta G., and A. Temiz Artmann

Aachen University of Applied Sciences and [1]Research Center Juelich,
Projektträger Juelich, 52428 Juelich, Germany
[2] Institute Laue Langevin, 38042, Grenoble, France

Contact address of corresponding author*:
Prof. Dr. rer.nat. habil. G. M. Artmann
University of Applied Sciences Aachen, Division Juelich
Ginsterweg 1
52428 Juelich
Phone: (0049) 241 6009 53073
E-mail: artmann@fh-aachen.de

**Abbreviations:** RBC – red blood cells, NMR – nuclear magnetic resonance, Hb hemoglobin, COP – colloid-osmotic pressure, temperature sensation

**Running Title:** Hemoglobin senses body temperature

**Keywords**: red blood cells, hemoglobin, temperature transition, body temperature, colloid osmotic pressure, confined water, glass transition, NMR $T_1$

* This article is dedicated to Ludwig Artmann who died on July 21, 2001 on a beautiful summer day during which we performed experiments far away. Ludwig Artmann was a man who encouraged us to be strong and to study hard no matter what were the costs.

**Abstract**

When aspirating human red blood cells (RBCs) into 1.3 µm pipettes (ΔP = -2.3kPa), a transition from blocking the pipette below a critical temperature Tc = 36.3 ± 0.3°C to passing it above the Tc occurred (micropipette passage transition). With a 1.1 µm pipette no passage was seen which enabled RBC volume measurements in particular above Tc. With increasing temperature RBCs lost volume significantly faster below than above a Tc = 36.4 ± 0.7 (volume transition). Colloid osmotic pressure (COP) measurements of RBCs in autologous plasma (25°C ≤ T ≤ 39.5°C) showed a Tc at 37.1 ± 0.2°C above which the COP rapidly decreased (COP transition). In NMR $T_1$-relaxation time measurements, the $T_1$ of RBCs in autologous plasma changed from a linear (r = 0.99) increment below Tc = 37 ± 1°C at a rate of 0.023 s/K into zero slope above Tc (RBC $T_1$ transition). In conclusion: An amorphous hemoglobin-water gel formed in the spherical trail, the residual partial sphere of the aspirated RBC. At Tc, a sudden fluidization of the gel occurs. All changes mentioned above happen at a distinct Tc close to body temperature. The Tc is moved + 0.8°C to higher temperatures when a $D_2O$ buffer is used. We suggest a mechanism similar to a “glass transition” or a “colloidal phase transition”. At Tc, the stabilizing Hb bound water molecules reach a threshold number enabling a partial Hb unfolding. Thus, Hb senses body temperature which must be inscribed in the primary structure of hemoglobin and possibly other proteins.

## Introduction

Nonlinearities in the physical, biological and chemical properties of cells (Hennig et al., 2002;Hennig et al., 2002), membranes (Gowrishankar et al., 1998) and biological molecules (Braxenthaler et al., 1997;Pascher, 2001) have developed into a growing field of interest. For some types of cells, intrinsic, pronounced nonlinearity is a well known feature, essential for normal cell function and successful signal transduction (Hennig et al., 2002). Some authors even prefer the term ´phase transition` instead of nonlinearities (Pollack, 2001a;Pollack, 2001b). The concept of nonlinearity and phase transitions in protein and cell function is on the brink of revolutionizing cell biology (Pollack, 2001b).

Nonlinear features of hemoglobin (Hb) function have been repeatedly reported (Lukin et al., 2003;Bettati et al., 1998). Allosteric properties regarding its R-T transition and oxygen binding (Bettati et al., 1998) suggest increased dynamics of "ligation intermediate" species and the distinctive role of the hydration shell in Hb function (Knapp et al., 1999;Levantino et al., 2003). For many years it was assumed that the hemoglobin solution viscosity monotonically depended on temperature and concentration (Danish and Harris, 1983;Chien et al., 1982;Muller et al., 1992). However, none of these studies used highly elevated, non-physiological Hb concentrations (i.e. significantly higher than 33 g $dL^{-1}$). In fact, investigators ended their studies at concentrations too low to observe an accelerated viscosity drop around body temperature (Kelemen et al., 2001). In our previous studies on human red blood cells (RBCs) that began a decade ago, sudden temperature-induced changes in passage behavior through narrow micropipettes were found (micropipette passage transition) (Artmann et al., 1998). Hemoglobin was identified as the molecule causing the transition. Further studies on these discontinuities using RBCs and/or standardized Hb solutions showed nonlinear changes at temperatures all close to the human body temperature (Kelemen et al., 2001;Zerlin et al., 2007e;Artmann et al., 2004;Hennig et al., 2002). Lately we showed that Hb obtained from monotreme animals such as the echidna and the platypus, having body temperatures of 33°C, underwent a temperature transition around their respective body temperatures (Digel et al., 2006). All these and further studies (Zerlin et al., 2007d) suggested that the structural transition in hemoglobin involving an unknown mechanism is linked to the species` body temperature. However, for methodological reasons, many of these studies did not reflect the natural environment which Hb molecules reside in.

This paper aims to show that the sudden structural transition of hemoglobin at body temperature (Artmann et al., 1998) can be shown in a series of other experiments: 1) RBC volume changes as measured with micropipettes, 2) by colloid osmometry, and 3) by NMR $T_1$

relaxation time measurements (Zefirova et al., 1991) using individual RBCs or whole blood, respectively. The results gave hints on the molecular mechanism of the structural transition. They supported the idea put forward earlier (Kelemen et al., 2001) that a Hb structural rearrangement was initiated by a steady thinning of the Hb bound water shell with rising temperature. Below Tc, the bound water shell stabilized the molecule. At Tc this had reached a threshold. It enabled a molecular rearrangement initiating the transitions observed. It occurs in the spherical trail of an aspirated RBC where a Hb-water gel forms below Tc. At Tc this gel suddenly turns fluid caused by a break down of intermolecular Van der Waals forces. The fact that Tc depends on the species` body temperature implies that this temperature is somehow inscribed in the primary Hb structure. Thus, the Tc observed may generally reflect body temperature and the Hb molecule “senses” this particular temperature by undergoing certain structural transitions.

## Materials and Methods

**Blood sample preparation:** Blood samples were obtained from healthy donors in EDTA-filled syringes, centrifuged at 500×g for 10 min and with the buffy coat removed from the pellet. Samples were obtained and processed just before the beginning of an experiment. This paper presents data obtained with intact RBCs.

Micropipette measurements: In micropipette experiments used for single cell volume determinations washed RBCs were used. After centrifugation, the RBC pellet was re-suspended in HEPES buffer (pH = 7.4, 300mOsm) at a hematocrit of 0.1%. In a separate set of experiments, $D_2O$ was used instead of $H_2O$ for HEPES buffer preparation.

NMR measurements: In the the NMR as well as in the COP experiments, RBCs were resuspended in autologous blood plasma. The major differences to real blood in the NMR and COP experiments were 1) the absence of shear stress, 2) the absence of leucocytes and thrombocytes, and 3) an elevated hematocrit. The preparation protocols were essential for the results presented below. Plasma and RBC pellets were separated and degassed for 5min. For samples containing RBC, 0.5 mL plasma and 0.225 mL $D_2O$ were added to 3.5 mL RBC pellet.

Colloid osmotic pressure (COP) measurements: The RBC pellet was re-suspended with autologous plasma. The average hematocrit was 77.6 ± 5.3 % (N = 16 blood samples).

**Micropipette System Set-up:** Aspiration experiments for individual RBC volume determination were carried out with an inverted microscope and bright field light (1000 x ) microscopy (CLSM, AxioverT 100, Carl Zeiss, Göttingen, Germany). A micromanipulator system (Luigs and Neumann, Ratingen, Germany), a hydrostatic pressure system and a temperature chamber (Cell and Tissue Technology, Aachen, Germany) at an accuracy of ± 0.2°C were used for micropipette experiments. Cylindrical micropipettes with an inner diameter of 1.1 μm were pulled (Mecanex SA, Nyon, Switzerland; BB-CH-PC) from borosilicate glass tubes (World Precision Instruments, Berlin, Germany). The inner diameter was measured microscopically using image analysis. The aspiration pressure was adjusted at -2.3kPa.

**Single RBC volume measurements:** For individual RBC volume determinations of N = 12 RBCs one and the same micropipette was used. Procedure of volume determination: An RBC was aspirated at T = 34.5 °C and geometrical data (Figure 1) were obtained. The cell was then blown out. The temperature was raised by about 0.3 to 0.4 °C and equilibrated. The same cell was re-aspirated and the new geometrical data were measured. The cell was blown out and the

temperature was raised again and so on. This way the relative volume change of the particular cell could be measured highly accurate. Cell data could easily be compared with each other since the same pipette was used for all twelve cells. The temperature was adjusted between 34.5 and 39.5 °C. In order to avoid irreversible hemoglobin denaturing, 39.5 °C was not exceeded (Williamson, 1993). For the passage transition experiments in D2O buffer N=40 RBC were aspirated at each temperature. The same micropipette was used in the measurement series.

RBC volume determinations (Figure 1, A and B) were carried out with established methods (Engstrom et al., 1992). An individual RBC was pulled into the pipette at 34.5°C. The final aspiration pressure ΔP = -2.3 kPa was build up slowly until a steady state was reached i.e. when the RBC tongue length no longer showed any visible changes (Figure 1 A). Thus, microscopic images of aspirated RBCs were acquired at steady state conditions. From these images, geometrical parameters (Figure 1 B) were determined. The RBC volume was calculated as follows (equations 1a-1c):

$V_1 = \pi / 12 \cdot p^3$ (spherical tongue cap) (Eq.1a)

$V_2 = 1/4 p^2 \pi \cdot (l - 1/2 p)$ (cylindrical tongue volume) (Eq.1b)

$V_3 = \pi h^2 / 3 \cdot ((3d/2) - h))$, where $h = 1/2d + (1/2d^2 - 1/2p^2)^{1/2}$ (Eq.1c)

(trail outside the pipette).

The equations describe volumes measured with a circular pipette and cylindrical tip (for abbreviations see Figure 1 B). The total RBC volume was $V = V_1+V_2+V_3$.

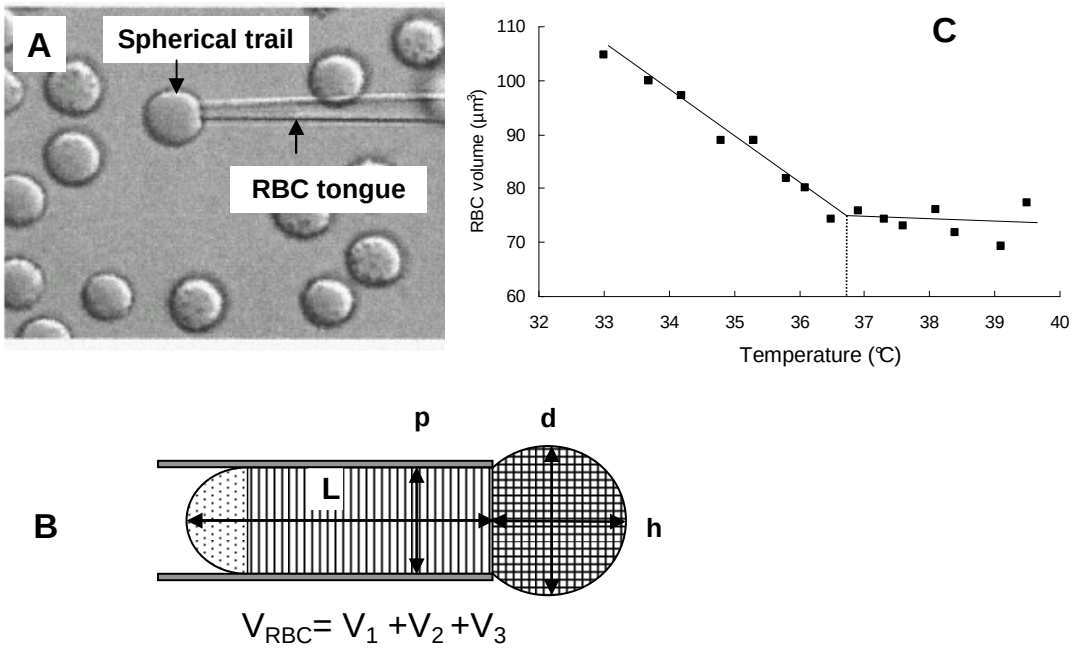


**Figure 1**: **A**: Typical micropipette aspiration experiment. The spherical trail outside the pipette is clearly visible. The arrow indicates the end of the aspirated RBC's tongue. **B**: Individual volume compartments of an aspirated RBC used for single cell volume calculation. **C:** Volume change over temperature of an individual RBC. There was a clear turning point indicating a critical temperature at Tc. The slopes of the linear curve below and above Tc differed significantly according to the statistical analysis applied.

**Hemoglobin molecular radius estimations from micropipette experiments:** At an aspiration pressure of -2.3 kPa, the pulling force vector acting on an aspirated RBC tongue and pointing into the micropipette had a higher norm than the colloid osmotic force vector caused by the very high Hb concentration inside the spherical RBC trail (Kelemen et al., 2001) pointing outwards. At this pressure, it was reasonable to assume that most of the cytosolic bulk water had been squeezed out and cytosolic Hb molecules together with their bound water shell were closely packed, leaving only traces of unbound water within the intermolecular gaps. We have developed a simple geometrical model to estimate the Hb molecular radius, $r_{Hb}$, under the boundary condition of a circumferential isotropic membrane tension compressing the Hb molecules inside RBCs during aspiration. We considered physiological data as the intracellular Hb concentration in RBCs, $C_{Hb,}$ = 330 g/L, molecular weight of tetrameric human Hb, $MW_{Hb}$ = 64.000 g/Mol, and an average RBC volume of $V_{RBC}$ = 88 fL. The molecular Hb radius was calculated using following equations (2a-2c):

$$Hb_{RBC} = c_{Hb} \cdot V_{RBC} \quad \text{(Eq.2a)}$$

$$N_{Hb} = N_a \cdot Hb_{RBC} / MW_{Hb} \quad \text{(Eq.2b)}$$

$$r_{Hb} = (3V_{RBC} / 4\pi \cdot N_{Hb})^{1/3} \quad \text{(Eq.2c)}$$

where $N_A$ is Avogadro's number, $Hb_{RBC}$ is the total intracellular Hb content of a single RBC, and where $N_{Hb}$ is the number of Hb molecules per RBC. For the calculation of the number of hydration layers per hemoglobin molecule, it was assumed that the amount of 0.35g H2O/ g protein corresponds to one hydration layer. A physiological concentration of hemoglobin at 330 g/L in red blood cells at conditions was assumed. The concentration of hemoglobin in the aspirated cells was calculated using the measured cell volume. The amount of cell water was then estimated by assuming a constant density of the hemoglobin solution. The number of hydration layers was finally obtained by dividing the amount of cellular water per hemoglobin molecule by the assumed value for one hydration layer.

**NMR measurements:** NMR $T_1$ relaxation time measurements were carried out with samples inserted into NMR tubes at temperatures of 15, 25, 30, 35, 37, 39 and 42°C, respectively. The samples were allowed to equilibrate for 10 min at each temperature step. A DRX 600 (Bruker Co., Germany) NMR device was used for $T_1$ measurements carried out at a static magnetic field strength of 14.7 T corresponding to a Larmor frequency of 600 MHz (Finnie et al., 1986;Zefirova et al., 1991). An inversion recovery pulse sequence was used and data were analyzed with the XMGR software (http://math.nyu.edu/aml/software/xmgrace.html).

**Colloid osmotic pressure (COP) measurements:** The colloid osmometer (Wescor Co., USA) was placed into a heating chamber at 39 °C and the temperature was equilibrated for 30 min. Then the blood plasma sample was injected into the measurement chamber and the colloid osmotic pressure (COP) was observed. When steady state was reached, this value was taken as the COP of the plasma sample at this temperature. Afterwards, the sample was exchanged with the RBC-in plasma sample and the procedure was repeated. Subsequently, the blood plasma and the RBC-in plasma COP were obtained at steps of about 1°C going stepwise down to 29°C.

**Statistical data analysis (Dikta et al., 2006):** The volumes of 12 RBCs were measured at temperatures of 34.5, 36.4 ( = Tc), and 39.5 (°C). For each cell, three dependent observations were available, while the 12 measurements at each temperature step were independent of each other, since they originated from different cells.

To check whether the expected volume at the temperature Tc = 36.4°C was less than the one at 34.5°C, a t-test was applied, where the differences (D1) between individual RBC volumes at 34.5°C and Tc = 36.4°C were taken as

$$D1 = \text{RBC volume } (T_c = 36.4°C) - \text{RBC volume } (34.5°C). \qquad \text{(Eq. 3a)}$$

These differences were checked for normality by the Shapiro-Wilks test. If this test showed no significant departure from normality, the one-sided t-test was applicable. The t-test was used to check the null-hypothesis that the expected value of the difference was zero against the alternative that the expected value of the difference was less than zero. A significant departure from the null hypothesis must therefore be interpreted as a significant negative slope of the first straight line in Figure 2. The same approach was used to check the second straight line between Tc = 36.4 and 39.5°C, i.e. to analyze

$$D2 = \text{RBC volume } (39.5° C) - \text{RBC volume } (Tc = 36.4 °C) \qquad \text{(Eq.3b)}$$

Since D1 and D2 can be associated with one of the two slopes, they can be used to check for differences (D) between the two slopes. For each cell, the D = *D2-D1* calculation was performed and analyzed statistically as described above.

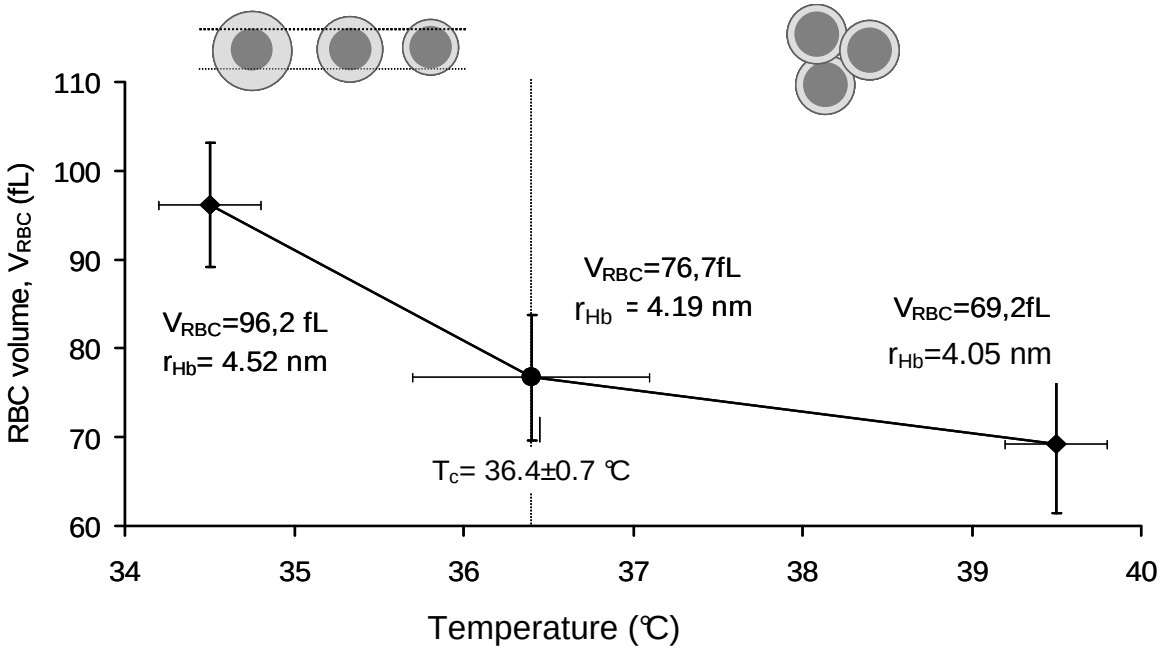


**Figure 2:** RBC volume vs. temperature during micropipette aspiration (mean ± SD, N = 12 cells). The volume of individual RBCs was taken at 15 different temperature steps between 34.5 and 39.5 °C at steps of about 0.3 to 0.4 degree (compare Figure 1). For the sake of clarity in this Figure 2 there are only three data points shown. The RBC volume decreased with increasing temperature but at two significantly different slopes below and above Tc = 36.4 ± 0.7 °C, respectively. Below Tc, RBCs lost volume at a rate of 7.8 fL/K, and above at 3 fL/K. The inserts represent Hb molecule schemes; dark: hemoglobin, light: remaining cytosolic water per molecule. On the left: the remaining cytosolic water decreased continuously. Right: The water decreased further, however at a significantly lower rate. The error bars in vertical direction include systematic and random errors. However, these error bars are dominated by the varying individual RBC volumes.

**Results**

This paper presents data obtained with intact RBCs from healthy donors. Except for the micropipette experiments in single cell volume determinations, RBCs remained in their natural chemical environment - in blood plasma. There was no shear force acting on the cells during measurements, no leucocytes and thrombocytes were present, and the hematocrit was elevated. These preparation protocols were essential for the results presented below.

**Micropipette experiments:** During RBC aspiration (Figure 1), tongue formation was observed to occur in two time-phases, 1) a fast initial entrance phase which typically lasted less then a second and 2) a subsequent slow creeping phase for a couple of seconds where the tongue length usually changed less then 10%. A steady state of tongue length was considered to be reached, when an aspiration pressure of -12 kPa was applied for a short time and no further tongue length increment was observed. Figure 1 C shows a typical volume (Formula 1) vs. temperature curve of one individual. The average volume over temperature data of twelve individual RBCs showed a distinct and significant change in slope with a significant kink at Tc = 36.4 ± 0.7 (N = 12) (Figure 2). The RBC volume below Tc decreased at a rate of 7.8 fL/K with increasing temperature. Setting on $T_c$, the rate was decreased to only 3 fL/K. The calculated average RBC volume data at various t

emperatures are shown in Table 1.

| Temperature (°C) | Mean RBC volume (fL) | Hemoglobin molecule volume ($nm^3$) | Hemoglobin molecule radius (nm) | Number of hydration layers per Hemoglobin molecule |
|---|---|---|---|---|
| 25°C | MCV = 88±6 | 321,6* | 4.25* | 6 |
| 34.5 ± 1°C | 96.2 ± 7 | 352,0 | 4.38 | 7 |
| $T_c$ = 36.4 °C | 76.7±7.1 | 280,3 | 4.06 | 5 |
| 39.5°C | 69.2 ± 7.8 | 252,3 | 3.92 | 4 |

**Table 1:** Estimated RBC and hemoglobin molecule data resulting from micropipette experiments (Legend: MCV, mean cellular RBC volume, * calculated for freely suspended RBCs at an average volume of 88 fL). Please note that Hb molecules were mechanically confined and under elevated pressure due to pipetting.

Statistical analysis revealed that the data were normally distributed since the Shapiro test resulted in 0.5029 for D1, in 0.6798 for D2, and in 0.7433 for D (see methods). The p-values of the t-test were p (D1) = 0.0000, p (D2) = 0.0021, and p (D) = 0.0016 and confirmed that all three differences deviated significantly from the null hypothesis. Thus, the slopes between 34.5°C and Tc and between Tc and 39.5°C, respectively were both significantly negative. In addition, the slope in the lower temperature range was significantly more negative than the one above Tc. With formulae 2a-2d Hb molecular volumes, surfaces and radii were estimated from the micropipette data (Table 1). The Hb radii correspond to a water layer thinning rate per one individual Hb molecule of 0.084 nm/K below Tc and of 0,052 nm/K above, respectively.

**NMR $T_1$ measurements:** Two NMR $T_1$ relaxation time measurements were carried out in parallel 1) with blood plasma containing 83% RBCs (RBC-in-plasma sample, Figure 3A) and 2) with blood plasma alone (plasma-only-sample, Figure 3B). With both samples, a two-phasic behavior of $T_1$ vs. temperature was observed, showing a transition temperature at Tc = 37 ± 1°C. The RBC-in-plasma-sample showed a change from a steady, linear (r = 0.99) increment of $T_1$ below Tc at a rate of 0.023 s/K. Setting on at Tc, T1 did not show any visible dependency of temperature.

The plasma-only-sample showed converse characteristics: No temperature dependency below 37°, a transition temperature at 37°C and a decrease with temperature at the modest rate of $3.8 \cdot 10^{-3}$ above Tc (Figure 3B). The $T_1$ of the plasma-only-sample was about three to five times higher as compared to the RBC-in-plasma-sample.

**Colloid osmotic pressure experiments:** As shown in Figure 4, the COP of the plasma-only-sample increased linearly up to 39.5°C. The COP of the RBC-in-plasma-sample was in general 2 mmHg lower than the one of pure plasma samples at the same temperature. Setting on at Tc = 37.1 ± 0.2°C, the COP of the RBC containing sample decreased rapidly and significantly.

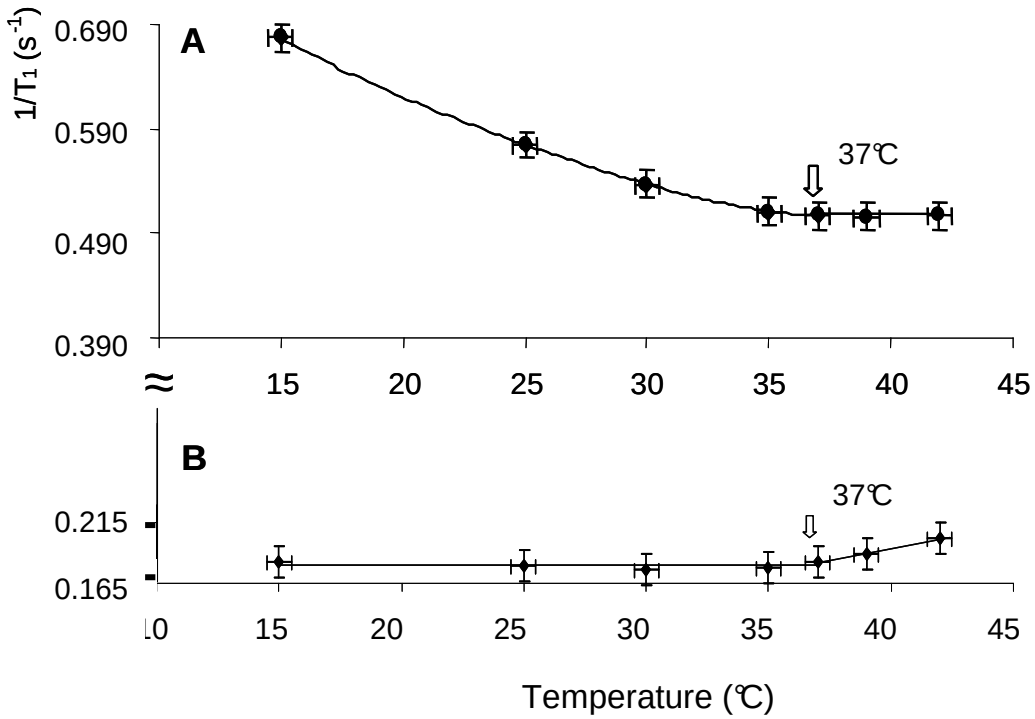


**Figure 3:** NMR $T_1$ relaxation time data. A) blood plasma containing 83 volume-% RBCs (RBC-in-plasma-sample). The $T_1$ relaxation time increased with temperature at a rate of about 0.023 s/K below 37°C (310 K). Above 37°C, it remained almost constant. B) blood plasma alone (plasma-only-sample). The $T_1$ change over temperature in the plasma sample (B) showed converse characteristics, i.e. no change below 37° and an increase above 37° (note the different scales $1/T_1$ used in the two graphs).

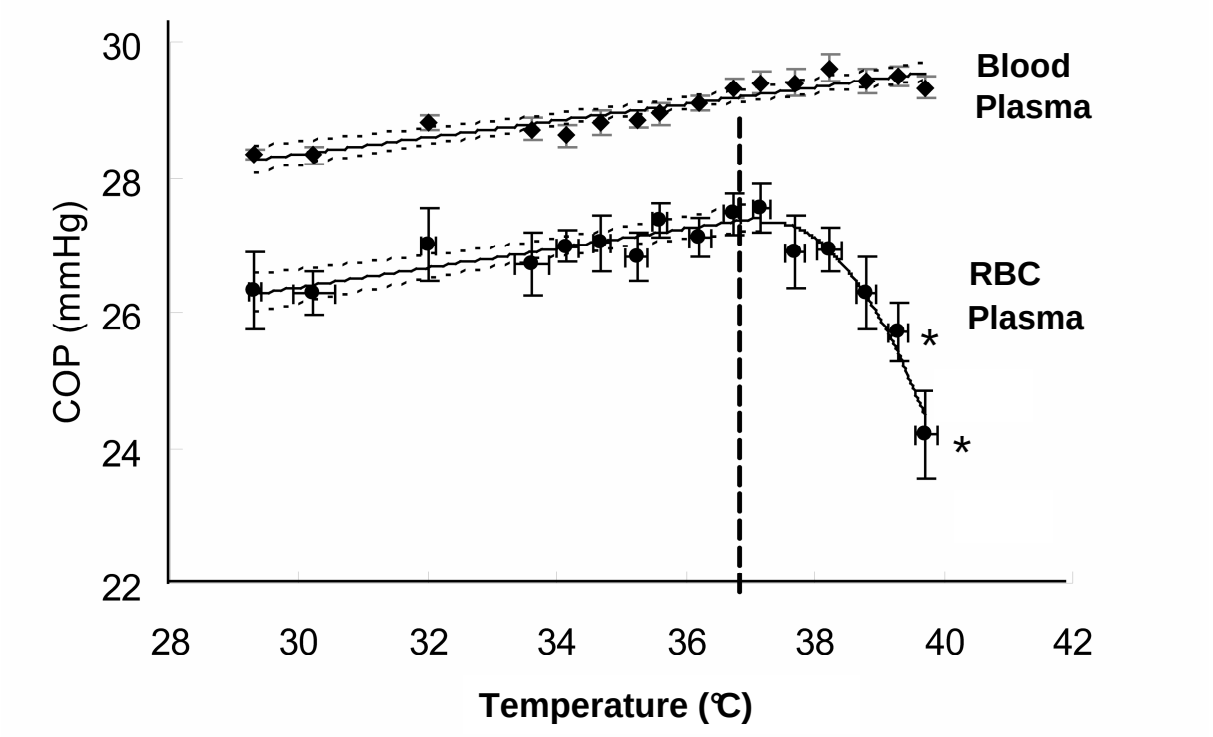


**Figure 4:** Temperature course of the colloid osmotic pressure (COP) over temperature. Upper curve: Blood plasma without RBC (plasma-only sample), below: RBCs re-suspended in autologous plasma at an average of 77,6 ± 5.3 volume-% RBC (RBC-in-plasma-sample). At each temperature step, N = 16 individual samples of healthy donors were measured (average ± 1 SEM). The 95% confidence interval is indicated with dotted lines. The RBC-in-plasma-sample showed a 2mmHg lower COP below Tc and a linear increment with temperature and was in parallel with the plasma-only-sample. Beginning at Tc = 37°C, its COP dropped significantly. Instead, the plasma-only sample showed a regular temperature course with no turning point at 37 °C.

**Discussion**

There is growing evidence that the cell cytosol has the properties of a hydrogel consisting of proteins, protein-bound and bulk water. The current opinion is controversial. Some studies showed that the cell cytosol of cells mainly consists of bulk water (Stadler et al., 2008b;Zaccai, 2004), some that the cell content predominantly is gel-like (Pollack, 2001a;Pollack, 2001b). However, the methods probe either microscopic or macroscopic properties and the results might not be directly comparable. Sudden phase transition like changes of protein function or cell behavior, respectively, could also be related to protein-bound and bulk water effects. In our earlier studies (Figure 5) a sharp temperature transition of RBC passage behavior through narrow pipettes occurred within less than a degree Celsius at Tc = 36.3 ± 0.3°C (Artmann et al., 1998;Artmann et al., 2004;Kelemen et al., 2001). Moreover, studies with hemoglobins from various species with body temperatures different from those of humans revealed that temperature transitions occurred as well. Those critical temperatures were close to the specific species` body temperature (Digel et al., 2006;Zerlin et al., 2007c). We concluded that the hemoglobin molecule senses the species' body temperature by undergoing a partial unfolding at Tc (Stadler et al., 2007;Stadler et al., 2008a). Thus, the critical transition temperature separates two distinctly different physical molecular stages and, consequently, cellular behaviors.

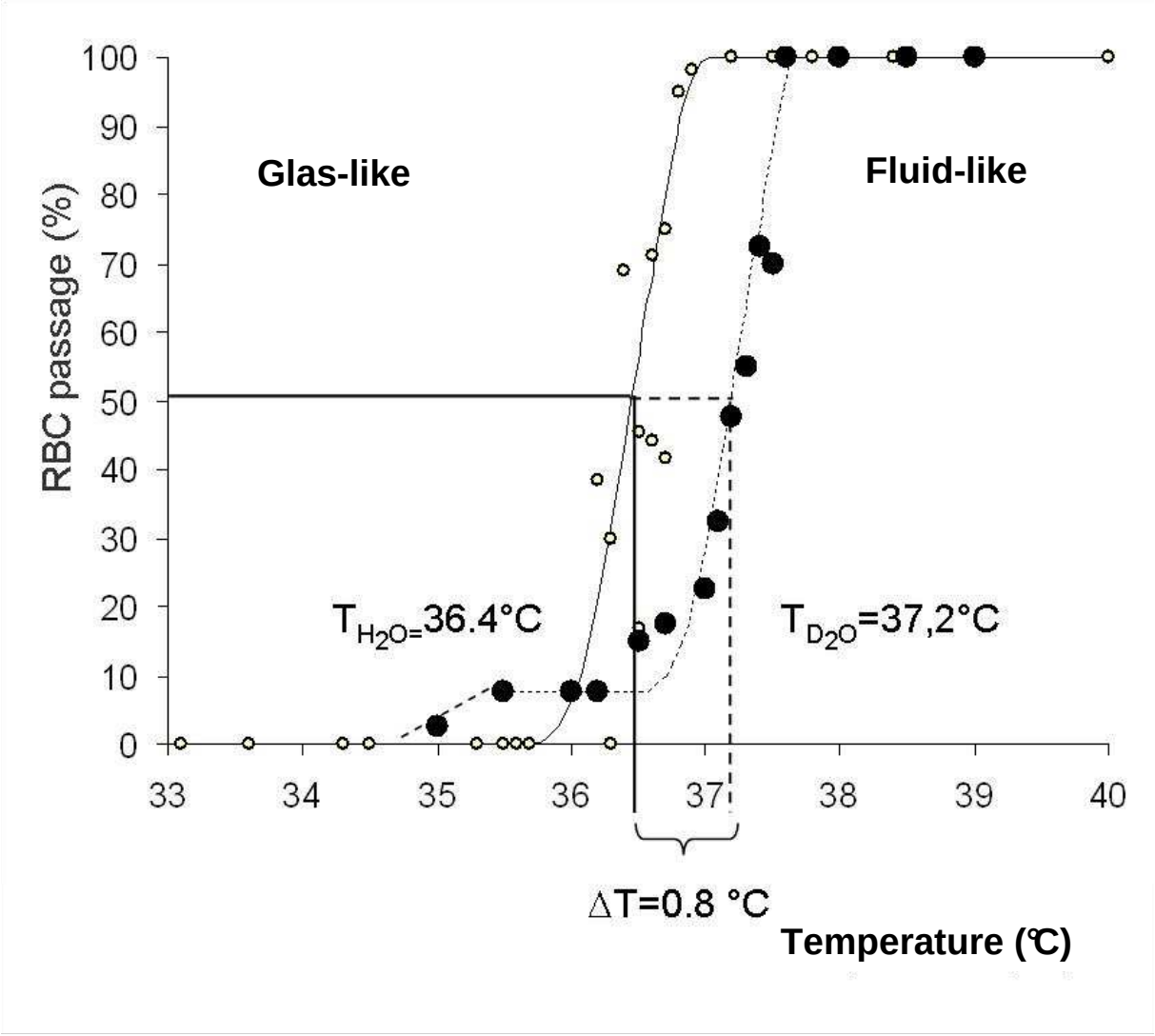


**Figure 5:** Micropipette passage experiment. The red blood cell passage curves were obtained with human RBCs. **Left curve:** RBCs were suspended in a $H_2O$ based buffer (Artmann et al., 1998), **Right curve:** RBCs were suspended in a $D_2O$ based buffer (Buldt et al., 2007;Stadler et al., 2007;Artmann et al., 1998). The Tc measured with $H_2O$ based buffer was by 0.7 - 0.8°C smaller then the one with $D_2O$ buffer. This indicated that stronger water bonds exerted by deuterium replacing hydrogen caused a shift in the critical temperature by 0.7 - 0.8 °C.

**Micropipette RBC volume measurements:** When an RBC enters a narrow micropipette, an isotropic RBC membrane tension builds up until balance of forces was established (Evans, 1983;Hochmuth et al., 1979;Chien et al., 1978). During the aspiration process, cellular bulk water was squeezed out across the membrane and the RBC lost volume (Fairbanks et al., 1971;Farinas et al., 1993;Jay, 1996;Poschl et al., 2003;Walz et al., 1997;Yokoyama et al., 1978). In our experiments a short term increase of the aspiration pressure up to -12 kPa did not show any further RBC volume decrement. Thus, the Hb molecules inside RBCs were assumed to be in closest possible contact to each other leaving only traces of bulk water inside the RBC, if at all. The remaining cell water must therefore be trapped between (mostly) hemoglobin molecules and must be constrained in its transversal diffusion (Dencher et al., 2000). This conclusion seems to contradict recent neutron scatter experiments which showed that only 10% of the RBC´s cytosolic water exhibit reduced dynamics (Stadler et al., 2007). However, in the spherical trail of an aspirated RBC the cytosol is compressed due to the aspiration pressure. The remaining distance between adjacent Hb molecules was estimated to be about ten water molecule diameters only (Kelemen et al., 2001). Such protein water arrangement should reduce the translational diffusion of water molecules. A hemoglobin-water-gel had formed in the RBC`s spherical trail (Figure 1) which did not allow RBC passage through the pipette below Tc (Artmann et al., 1998).

However, why do at Tc the RBCs set on passing the pipette in an almost step-function like manner (Figure 5)? From figure 5 must be concluded, that the transition is related to hemoglobin-water interaction. It is known, that hydrogen bonds formed by heavy water are a little more stable than those in normal water. The average protein dynamics was measured with neutron scattering in Escherichia coli (Jasnin et al., 2008). Mean protein flexibility and macromolecular resilience (protein 'stiffness') were found to be reduced in D2O compared to H2O buffer. It was concluded that D2O favors the packing of non-polar residues in the core of the protein and at the same time enhances the sampling of conformational substates. The reduced protein flexibility and enhanced sampling rate of conformational substates in D2O would therefore contribute to thermal stabilization of protein structure. Micropipette passage experiments carried out with a heavy water buffer ($D_2O$ buffer) showed a temperature transition at only 0.7 – 0.8 degrees higher temperature (Figure 5). Interestingly, in a completely different biological system (*Tetrahymena* cells) the optimum temperature for cell division shifted upward as the heavy water concentration was increased. A maximum shift of 1 °C was observed in 40% heavy water (Moner, 1972). It is well known from neutron small angle experiments that D2O causes protein aggregation in certain systems. If only simple

protein aggregation would be the cause for the passage phenomenon observed in micropipette experiments, then the usage of heavy water would cause a reduced passage temperature as compared to normal water. However, the micropipette experiments revealed that the passage temperature in D2O buffer is increased compared to H2O buffer. Recent neutron scattering experiments with RBCs and hemoglobin solutions, respectively, revealed that at Tc a small partial unfolding of Hb molecules occurred (Stadler et al., 2007;Stadler et al., 2008a;Stadler et al., 2008b). We concluded that this effect initiated the fluidization of aspirated RBCs and their passage through the pipette. Probably the hemoglobin´s surface hydrophobicity pattern changed as well which was followed by cytsosolic Hb aggregation. Therefore, the stabilizing effect of heavy water on protein flexibility and on thermal unfolding might be the cause for the increase of the passage temperature observed in micropipette experiments (Buldt et al., 2007;Stadler et al., 2007;Goldenfeld and N., 1992).

RBC volume vs. temperature experiments were carried out with micropipettes (Linderkamp and Meiselman, 1982). The inner pipette diameter of 1.1µm was small enough to prevent any RBC passages. Measurements performed between 34.5°C and 39.5°C showed that the RBC volume decreased in general with increasing temperature. However, this happened at two significantly different slopes. There was a critical temperature of Tc = 36.4 ± 0.7°C observed where the volume vs. temperature curves showed a kink.

The RBC volume of 96.2 fL ± 7.0 at 34.5°C and -2.3 kPa (Table 1) fit to 94.3 fL at -1.96 kPa and to 91.2 fL at 2.45 kPa aspiration pressure at room temperature, respectively, as observed in an earlier publication. With the set of formulae developed for estimating the Hb molecular volume inside an RBC during aspiration (formulae 2a-d), we determined Hb molecule radii, $r_{Hb}$, (Table 1). Results on $r_{Hb}$ were surprisingly consistent with those derived in previous light scattering data (Zerlin et al., 2007b;Digel et al., 2006). This method, thus, may be a step forward in terms of estimating the Hb molecule radius (Engstrom and Sandstrom, 1989;Engstrom and Meiselman, 1996).

The major findings of these RBC volume experiments were that RBCs lost volume with increasing temperature significantly more readily below than above Tc. Obviously, the Hb molecules handle water in two distinctly different ways below and above Tc, respectively.

Discussing a decreasing molecular radius for Hb with increasing temperature (Figure 2, Table 1) seemed to contradict two earlier findings: Light scattering data (Zerlin et al., 2007a;Digel et al., 2006) as well as preliminary X-ray diffraction studies (Buldt et al., 2007) showed increasing hydrodynamic radii and lattice constants with increasing temperatures until Tc was

reached. The preliminary X-ray studies with Hb-crystals showed in addition, that the Hb crystal disintegrated at Tc (Figure 6 A).

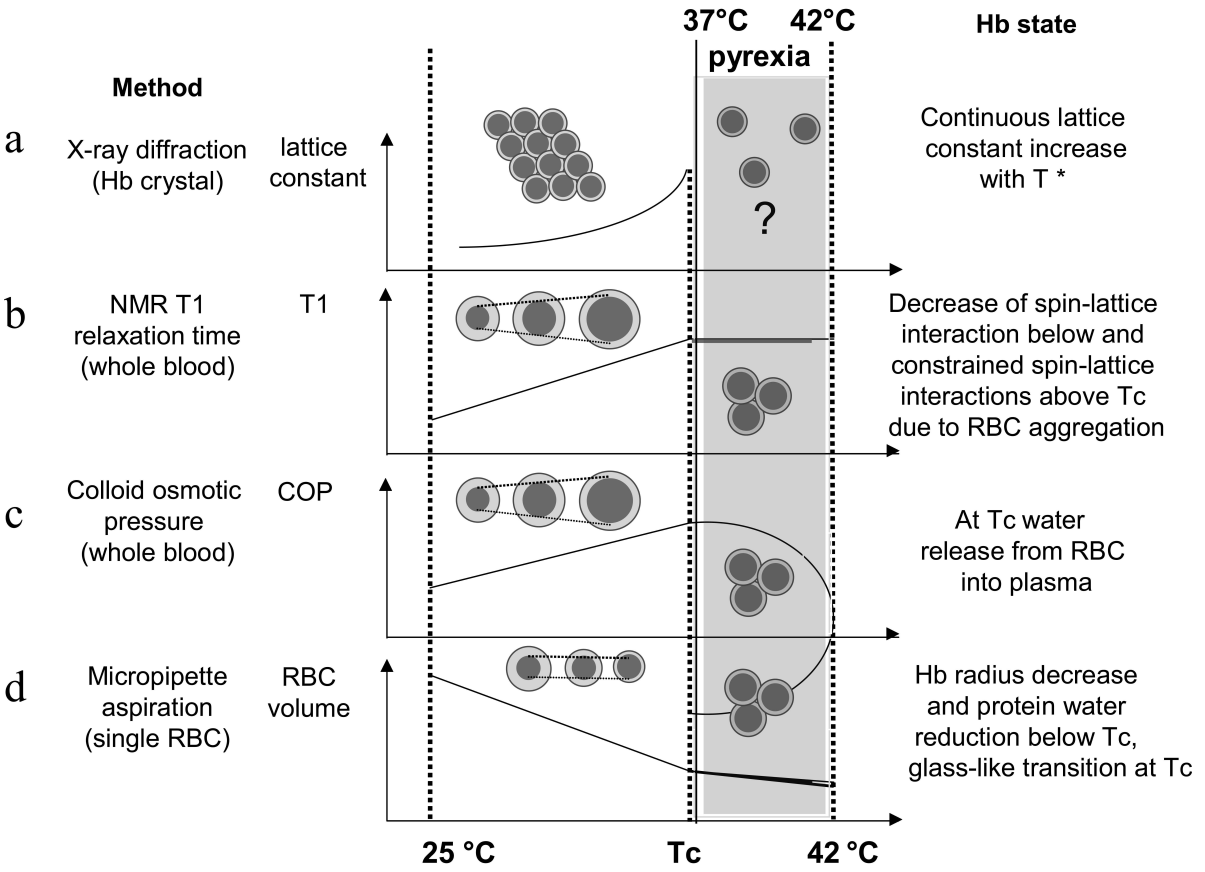


**Figure 6:** Summary slide: **A)** X-ray diffraction: Below Tc, the Hb crystal lattice constant increases disproportionate with increasing temperature. At Tc, the Hb crystal disintegrates (Buldt et al., 2007), **B)** NMR $T_1$ relaxation time (RBC in plasma-sample): Below Tc, $T_1$ increment, at Tc, structural Hb transition, above Tc, no net $T_1$ change with temperature, **C)** Colloid osmotic pressure (RBC-in-plasma sample): Below Tc, the COP increases, at Tc = 37.1 ± 0.2°C on-set of Hb aggregation causing RBCs to release cell water - COP decreases, **D)** Micropipette aspiration (single RBCs): Hb molecule volume remains unchanged with temperature due to hydrostatic pressure inside the spherical trail of the aspirated RBC and bound water turns into bulk water. This was squeezed out due to aspiration pressure. At Tc, glass-like-transition and further RBC volume loss occur because of hemoglobin aggregation.

In postulating two assumptions, a clearer understanding of the volume loss of RBCs with rising temperature was achieved. First, during aspiration the fluctuations of the cytosolic Hb molecules as well as the cell water diffusion are mechanically constrained. The Hb molecule could not expand with temperature as it does in free solution and crystals. Water diffusion was as well constricted. Second, the number of water molecules associated with hemoglobin continuously decreased ("melted off") and this water was squeezed out from the cell. This effect caused the RBC volume loss below Tc where the hemoglobin water complex had the consistency of an amorphous gel. The term "melting" used here is just a more descriptive word for a shift of the equilibrium between Hb-bound water and bulk water toward bulk water (Cameron et al., 1988).

At Tc the amount of Hb bound water molecules had reached a threshold value at which the Hb-water complex was destabilized. This enabled the partial unfolding and the assumed Hb surface hydrophobicity changes. The latter initiated Hb molecular aggregation which we also found in neutron scattering experiments (Stadler et al., 2007;Digel et al., 2006;Zerlin et al., 2007i).

Above Tc, with increasing temperature ongoing cytosolic Hb aggregation determined the RBC volume loss (Figure 6) due to colloid osmotic effects. We concluded that Hb aggregation lead to an imbalance of the osmotic pressures inside vs. outside the cell constituting of native blood plasma. As consequence RBCs release water to the blood plasma to re-balance osmotic pressures. Thus, the colloid osmotic pressure decreased above Tc with increasing temperature (Figure 4, see discussion below).

**NMR $T_1$ measurements:** NMR $T_1$ relaxation time data reflect magnetic interactions of hydrogen nuclei with their environment (lattice). However, interpreting them when the sample consisted of complex protein water solutions is not simple (Victor et al., 2005;Kiihne and Bryant, 2000). Although these measurements were not in the focus of this study, they revealed important information. The RBC-in plasma sample consisted of 83 % RBCs and 17 % blood plasma, thus the protons participating in the NMR experiment originated in its majority from water, both protein-bound and free, of hemoglobin, and to a smaller percentage of human albumin. At 83% hematocrit the NMR sample contained 26.4 g $dL^{-1}$ Hb. Thus, the $T_1$ signal can be attributed to an high extend to Hb-internal proton interactions and Hb-proton interactions with their water-proton environment. We observed a critical temperature at Tc = 37 ± 1°C (Figure 3). Below Tc, $T_1$ rose linearly with increasing temperature. We concluded that these interactions became less and less strong. Since we observed at the same time a "melting-off" of water from hemoglobin (Figure 1 and Figure 2 and table I) much of this

signal increment may have derived from increasing bulk water. At Tc, the $T_1$ (T)-curve turned into zero slope. Thus, Tc represents the onset of a temperature interval where the $T_1$ relaxation time became independent of temperature. Interestingly, in the plasma-only sample the T1 (T)-curve showed exactly a vice versa behavior: Zero slope below Tc and a small negative slope above. In summary, above Tc temperature did not affect any longer the spin lattice interactions in the RBC-in-plasma sample but began increasing the spin lattice interactions in the plasma-only sample. In other words, in the RBC-in plasma sample the intramolecular proton-proton interactions as well as the hemoglobin-proton to water interactions have overruled the interaction of plasma proteins with water. This might arise from the partial unfolding of hemoglobin at Tc and its consequences for hemoglobin aggregation and changes of the hemoglobin bound and free water balance (Artmann et al., 2004;Kiihne and Bryant, 2000;Stadler et al., 2007;Stadler et al., 2008a).

**Colloid osmotic pressure (COP) of RBC suspensions in blood plasma:** Some effects in cells can only be seen when cells and proteins are kept in their natural environment (Eisenberg, 2003;Zheng and Pollack, 2003;Lucas et al., 1991;Todd, III and Mollitt, 1994;Artmann et al., 1998). In our studies, COP data were obtained from both plasma-only-samples and RBC-in-plasma-samples at a hematocrit of 77.6 as function of temperature (Figure 4). In contrast to micropipette experiments, COP data were gathered both at shear stress-free conditions within the RBC cytosol and at a cell internal hydrostatic pressure unmodified by external mechanical forces acting on RBC membranes (Figure 6C, D). It was found that 1) the COP of the plasma-only-sample at 29°C fits to the physiological COP found in text books, 2) it increased linearly with temperature, and 3) it did not show any kink (change in slope) at any temperature. However, the RBC-in-plasma-sample as compared to the plasma-only-sample below 1) exhibited a visible but not significant 2mmHg lower COP, and 2) showed a turning point at Tc = 37°C where the COP began decreasing with temperature (Figure 4). Thus, a temperature transition was observed in COP measurements at mechanically unaffected conditions.

How can the COP drop above Tc be explained? For low protein concentrations the COP follows van´t Hoff`s law. In the plasma-only-sample therefore the COP increased linearly with temperature. As for the RBC-in-plasma-sample (Figure 4), however, things are more complex. Two sample volume compartments must be considered, 1) the volume occupied by RBCs, on average 77.6 ± 5.3 %, and 2) the remaining plasma volume at 22.4%. The COP of this sample should be identical to the plasma-only-sample since RBCs are too big to contribute significantly to the COP. In order to understand why the COP of the RBC-in-

plasma-samples dropped above Tc, we need to remember that the COP depends upon the particle number in the RBC cytosol and not on its total protein content. When Hb molecules inside RBCs aggregate as suggested and confirmed earlier (Digel et al., 2006;Zerlin et al., 2007h;Stadler et al., 2008a;Stadler et al., 2008b) then the particle number and at the same time the intracellular COP decrease. Consequently, cell water moves outwards, diluting the outside plasma until equilibrium is reached. Due to this extra water derived form the RBCs cytosol above Tc the COP of whole RBC-in-plasma-sample decreased.

**The global picture:** In many experiments on the temperature dependency of Hb properties using light scattering, CD spectroscopy (Artmann et al., 2004;Digel et al., 2006;Zerlin et al., 2007g), micropipette volume (Figure 2) or Hb viscosity measurements (Kelemen et al., 2001) a transition temperature, Tc, was found. However, the transition gradient was never as sharp as in the micropipette passage change (Figure 5) and in the viscosity experiments of highly concentrated Hb solutions (Kelemen et al., 2001). This implies an unknown mechanism making these two particular transitions significantly sharper. We suggest that $T_C$ marks the temperature at which a colloidal phase transition of second order occurred (Goldenfeld and N., 1992;Heller and Hofer, 1975;Landau, 2007). In the micropipette passage experiments, the transition would take place inside the spherical trail of the aspirated RBC where the Hb concentration was between 45 g $dL^{-1}$ and 50 g $dL^{-1}$ (Kelemen et al., 2001). Below Tc, a "disordered Hb-water gel" was formed consisting of hemoglobin plus bound water and cellular water with dynamics similar to bulk water (i.e. in physical terms "amorphous glass" or "colloidal system with gel like properties"). Below Tc, sample enthalpy, entropy and volume are continuous functions of temperature. Near the "glass like transition" temperature, Tc, the hemoglobin `glass` or 'colloidal gel' would suddenly "soften" and set on flowing under mechanical cytosolic shear forces exerted when an RBC enters the micropipette (Figure 5). Above Tc the spherical trail's cytosol (Figure 2) would exhibit properties approaching those of an ordinary fluid (Artmann et al., 1998;Kelemen et al., 2001), although still more viscous than low-molecular weight liquids. We suggest that the very sharp micropipette passage transition represents a phenomenon similar to a "glass transition" or "colloidal phase transition" common to many polymers and proteins (Craig and Terentjev, 2005;Hill et al., 2005;Smith et al., 2004). In strict classical sense the term "glass transition" or "dynamic transition" is used for a change in protein dynamics at 200K (-73°C). However, some "glass transition" features fit surprisingly well to the properties of the temperature transition observed in the micropipette experiments.

What would now be the links of physics to physiology? Our answer is that Tc 1) marks the set-point of a species body temperature originating from a partial unfolding of hemoglobin at Tc (Digel et al., 2006;Zerlin et al., 2007f;Stadler et al., 2008a;Stadler et al., 2008b), 2) Tc represents the set point of a reversible Hb denaturation (Artmann et al., 2004), finally, Tc marks the beginning of the pyrexia zone on the temperature scale. In this pyrexia zone, depending on the actual stage of cell internal Hb aggregation followed by COP changes cell water moves in and out of the cell depending on the direction of temperature change (Figure 4). The latter might contribute to blood homeostasis during fever. The pyrexia zone in humans ends physiologically at a temperature, $T_{ID}$ = 42,6 °C, where proteins thermally denature irreversibly. The pyrexia zone might now be defined by two distinct temperatures, the lower one marked by Tc and the upper one marked by $T_{ID}$. Evidently, new perspectives on cell biophysics using completely different approaches from those used by molecular and cell biologists will become more and more important in our attempt to understand cells as gels, and muscles as engines based on principles of polymer science.

**Acknowledgements**

This work was supported by the Ministry of Innovation, Science, Research and Technology of the State of North Rhine-Westphalia to G. M. Artmann and by the Centre of Competence in Bioengineering Juelich, Germany. Dipl.-Ing. Carsten Meixner acquired most of the COP data. NMR data were acquired together with the Giuseppe Melachini, Ph.D., University of California, San Diego, USA. The work was supported by great discussions with Prof. Y.C. Fung and Prof. Shu Chien, University of California, San Diego. We thank Prof. Georg Büldt, Research Center Jülich, Germany, who supported us with DSC and X-ray structural studies on Hb crystals. Additionally, we thank J. Zaccai, Institute Laue-Langevin (ILL) in Grenoble for good discussions.

**Reference List**


1. Artmann,G.M., L.Burns, J.M.Canaves, A.Temiz-Artmann, G.W.Schmid-Schonbein, S.Chien, and C.Maggakis-Kelemen. 2004. Circular dichroism spectra of human hemoglobin reveal a reversible structural transition at body temperature. *Eur. Biophys. J.* 33:490-496.

2. Artmann,G.M., C.Kelemen, D.Porst, G.Buldt, and S.Chien. 1998. Temperature transitions of protein properties in human red blood cells. *Biophys. J.* 75:3179-3183.

3. Bettati,S., A.Mozzarelli, and M.F.Perutz. 1998. Allosteric mechanism of haemoglobin: rupture of salt-bridges raises the oxygen affinity of the T-structure. *J. Mol. Biol.* 281:581-585.

4. Braxenthaler,M., R.Unger, D.Auerbach, J.A.Given, and J.Moult. 1997. Chaos in protein dynamics. *Proteins* 29:417-425.

5. Buldt, G., Artmann, G. M., Zaccai, G., Digel, I., and Stadler, A. M. Differences of water and D2O binding to proteins; temperature dependent DSC measurements and lattice constants of hemoglobin crystals. 7-5-2007. Personal Communication

6. Cameron,I.L., V.A.Ord, and G.D.Fullerton. 1988. Water of hydration in the intra- and extra-cellular environment of human erythrocytes. *Biochem. Cell Biol.* 66:1186-1199.

7. Chien,S., R.G.King, A.A.Kaperonis, and S.Usami. 1982. Viscoelastic properties of sickle cells and hemoglobin. *Blood Cells* 8:53-64.

8. Chien,S., K.L.Sung, R.Skalak, S.Usami, and A.Tozeren. 1978. Theoretical and experimental studies on viscoelastic properties of erythrocyte membrane. *Biophys. J.* 24:463-487.

9. Craig,A. and E.M.Terentjev. 2005. Stretching globular polymers. I. Single chains. *J. Chem. Phys.* 122:194901.

10. Danish,E.H. and J.W.Harris. 1983. Viscosity studies of deoxyhemoglobin S: evidence for formation of microaggregates during the lag phase. *J. Lab Clin. Med.* 101:515-526.

11. Dencher,N.A., H.J.Sass, and G.Buldt. 2000. Water and bacteriorhodopsin: structure, dynamics, and function. *Biochim. Biophys. Acta* 1460:192-203.

12. Digel,I., C.Maggakis-Kelemen, K.F.Zerlin, P.Linder, N.Kasischke, P.Kayser, D.Porst, A.A.Temiz, and G.M.Artmann. 2006. Body temperature-related structural transitions of monotremal and human hemoglobin. *Biophys. J.* 91:3014-3021.

13. Dikta,G., M.Kvesic, and C.Schmidt. 2006. Bootstrap Approximations in Model Checks for Binary Data. *Journal of the American Statistical Association* 101:521-530.

14. Eisenberg,H. 2003. Adair was right in his time. *Eur. Biophys. J.* 32:406-411.

15. Engstrom,K.G. and H.J.Meiselman. 1996. Effects of pressure on red blood cell geometry during micropipette aspiration. *Cytometry* 23:22-27.

16. Engstrom,K.G., B.Moller, and H.J.Meiselman. 1992. Optical evaluation of red blood cell geometry using micropipette aspiration. *Blood Cells* 18:241-257.

17. Engstrom,K.G. and P.E.Sandstrom. 1989. Volume regulation in mouse pancreatic islet cells as studied by a new technique of microperifusion. *Acta Physiol Scand.* 137:393-397.

18. Evans,E.A. 1983. Bending elastic modulus of red blood cell membrane derived from buckling instability in micropipet aspiration tests. *Biophys. J.* 43:27-30.

19. Fairbanks,G., T.L.Steck, and D.F.Wallach. 1971. Electrophoretic analysis of the major polypeptides of the human erythrocyte membrane. *Biochemistry* 10:2606-2617.

20. Farinas,J., A.N.Van Hoek, L.B.Shi, C.Erickson, and A.S.Verkman. 1993. Nonpolar environment of tryptophans in erythrocyte water channel CHIP28 determined by fluorescence quenching. *Biochemistry* 32:11857-11864.

21. Finnie,M., G.D.Fullerton, and I.L.Cameron. 1986. Molecular masking and unmasking of the paramagnetic effect of iron on the proton spin-lattice (T1) relaxation time in blood and blood clots. *Magn Reson. Imaging* 4:305-310.

22. Goldenfeld and N. 1992. Lectures on Phase Transitions and the Renormalization Group.

23. Gowrishankar,T.R., W.E.I.CHEN, and R.C.Lee. 1998. Non-Linear Microscale Alterations in Membrane Transport by Electropermeabilization. *Ann NY Acad Sci* 858:205-216.

24. Heller,K.B. and M.Hofer. 1975. Temperature dependence of the energy-linked monosaccharide transport across the cell membrane of Rhodotorula gracilis. *J. Membr. Biol.* 21:261-271.

25. Hennig,M.H., K.Funke, and F.Worgotter. 2002. The Influence of Different Retinal Subcircuits on the Nonlinearity of Ganglion Cell Behavior. *J. Neurosci.* 22:8726-8738.

26. Hill,J.J., E.Y.Shalaev, and G.Zografi. 2005. Thermodynamic and dynamic factors involved in the stability of native protein structure in amorphous solids in relation to levels of hydration. *J. Pharm. Sci.* 94:1636-1667.

27. Hochmuth,R.M., P.R.Worthy, and E.A.Evans. 1979. Red cell extensional recovery and the determination of membrane viscosity. *Biophys. J.* 26:101-114.

28. Jasnin,M., M.Tehei, M.Moulin, M.Haertlein, and G.Zaccai. 2008. Solvent isotope effect on macromolecular dynamics in E. coli. *Eur Biophys J* 37:613-617.

29. Jay,D.G. 1996. Role of band 3 in homeostasis and cell shape. *Cell* 86:853-854.

30. Kelemen,C., S.Chien, and G.M.Artmann. 2001. Temperature transition of human hemoglobin at body temperature: effects of calcium. *Biophys. J.* 80:2622-2630.

31. Kiihne,S. and R.G.Bryant. 2000. Protein-bound water molecule counting by resolution of (1)H spin-lattice relaxation mechanisms. *Biophys J* 78:2163-2169.

32. Knapp,J.E., M.A.Oliveira, Q.Xie, S.R.Ernst, A.F.Riggs, and M.L.Hackert. 1999. The structural and functional analysis of the hemoglobin D component from chicken. *J. Biol. Chem.* 274:6411-6420.

33. Landau,L.D.a.L.E.M. 2007. *Statistical Physics Part 1 (*of *Course of Theoretical Physics).* Pergamon.

34. Levantino,M., A.Cupane, and L.Zimanyi. 2003. Quaternary structure dependence of kinetic hole burning and conformational substates interconversion in hemoglobin. *Biochemistry* 42:4499-4505.

35. Linderkamp,O. and H.J.Meiselman. 1982. Geometric, osmotic, and membrane mechanical properties of density-separated human red cells. *Blood* 59:1121-1127.

36. Lucas,C.E., A.M.Ledgerwood, W.J.Rachwal, D.Grabow, and J.M.Saxe. 1991. Colloid oncotic pressure and body water dynamics in septic and injured patients. *J. Trauma* 31:927-931.

37. Lukin,J.A., G.Kontaxis, V.Simplaceanu, Y.Yuan, A.Bax, and C.Ho. 2003. Quaternary structure of hemoglobin in solution. *Proc. Natl. Acad. Sci. U. S. A* 100:517-520.

38. Moner,J.G. 1972. The effects of temperature and heavy water on cell division in heat-synchronized cells of tetrahymena. *J Protozool.* 19:382-385.

39. Muller,G.H., H.Schmid-Schonbein, and H.J.Meiselman. 1992. Development of viscoelasticity in heated hemoglobin solutions. *Biorheology* 29:203-216.

40. Pascher,T. 2001. Temperature and driving force dependence of the folding rate of reduced horse heart cytochrome c. *Biochemistry* 40:5812-5820.

41. Pollack,G.H. 2001a. Cells, Gels and the Engines of life. Ebner and Sons, Seattle.

42. Pollack,G.H. 2001b. Is the cell a gel--and why does it matter? *Jpn. J. Physiol* 51:649-660.

43. Poschl,J.M., C.Leray, P.Ruef, J.P.Cazenave, and O.Linderkamp. 2003. Endotoxin binding to erythrocyte membrane and erythrocyte deformability in human sepsis and in vitro. *Crit Care Med.* 31:924-928.

44. Smith,J.C., F.Merzel, A.N.Bondar, A.Tournier, and S.Fischer. 2004. Structure, dynamics and reactions of protein hydration water. *Philos. Trans. R. Soc. Lond B Biol. Sci.* 359:1181-1189.

45. Stadler,A.M., I.Digel, G.M.Artmann, J.P.Embs, G.Zaccai, and G.Buldt. 2008a. Hemoglobin dynamics in red blood cells: correlation to body temperature. *Biophys J* 95:5449-5461.

46. Stadler,A.M., J.P.Embs, I.Digel, G.M.Artmann, T.Unruh, G.Buldt, and G.Zaccai. 2008b. Cytoplasmic water and hydration layer dynamics in human red blood cells. *J Am. Chem. Soc.* 130:16852-16853.

47. Stadler, A. M., Zerlin, K. F., Digel, I., Artmann, G. M., Embs, J. P., Buldt, G., and Zaccai, G. Dynamics of hemoglobin and water in human red blood cells and concentrated hemoglobin solutions. Abstract 128. 14-7-2007. London, European Biophysics Congress. 14-7-2007. Conference Proceeding

48. Todd,J.C., III and D.L.Mollitt. 1994. Sepsis-induced alterations in the erythrocyte membrane. *Am. Surg.* 60:954-957.

49. Victor,K., A.Van Quynh, and R.G.Bryant. 2005. High frequency dynamics in hemoglobin measured by magnetic relaxation dispersion. *Biophys J* 88:443-454.

50. Walz,T., T.Hirai, K.Murata, J.B.Heymann, K.Mitsuoka, Y.Fujiyoshi, B.L.Smith, P.Agre, and A.Engel. 1997. The three-dimensional structure of aquaporin-1. *Nature* 387:624-627.

51. Williamson,D. 1993. The unstable haemoglobins. *Blood Rev.* 7:146-163.

52. Yokoyama,K., T.Terao, and T.Osawa. 1978. Membrane receptors of human erythrocytes for bacterial lipopolysaccharide (LPS). *Jpn. J. Exp. Med.* 48:511-517.

53. Zaccai,G. 2004. The effect of water on protein dynamics. *Philos. Trans. R. Soc. Lond B Biol. Sci.* 359:1269-1275.

54. Zefirova,T.P., A.N.Glebov, E.N.Gur'ev, R.S.Mavliautdinov, and O.I.Tarasov. 1991. [Nuclear magnetic relaxation of aqueous solutions of proteins, plasma, erythrocytes, and blood]. *Biull. Eksp. Biol. Med.* 112:378-381.

55. Zerlin,K.F., N.Kasischke, I.Digel, C.Maggakis-Kelemen, A.A.Temiz, D.Porst, P.Kayser, P.Linder, and G.M.Artmann. 2007i. Structural transition temperature of hemoglobins correlates with species' body temperature. *Eur. Biophys. J.*

56. Zerlin,K.F., N.Kasischke, I.Digel, C.Maggakis-Kelemen, A.A.Temiz, D.Porst, P.Kayser, P.Linder, and G.M.Artmann. 2007a. Structural transition temperature of hemoglobins correlates with species' body temperature. *Eur. Biophys. J.*

57. Zerlin,K.F., N.Kasischke, I.Digel, C.Maggakis-Kelemen, A.A.Temiz, D.Porst, P.Kayser, P.Linder, and G.M.Artmann. 2007b. Structural transition temperature of hemoglobins correlates with species' body temperature. *Eur. Biophys. J.*

58. Zerlin,K.F., N.Kasischke, I.Digel, C.Maggakis-Kelemen, A.A.Temiz, D.Porst, P.Kayser, P.Linder, and G.M.Artmann. 2007c. Structural transition temperature of hemoglobins correlates with species' body temperature. *Eur. Biophys. J.*

59. Zerlin,K.F., N.Kasischke, I.Digel, C.Maggakis-Kelemen, A.A.Temiz, D.Porst, P.Kayser, P.Linder, and G.M.Artmann. 2007e. Structural transition temperature of hemoglobins correlates with species' body temperature. *Eur. Biophys. J.*

60. Zerlin,K.F., N.Kasischke, I.Digel, C.Maggakis-Kelemen, A.A.Temiz, D.Porst, P.Kayser, P.Linder, and G.M.Artmann. 2007g. Structural transition temperature of hemoglobins correlates with species' body temperature. *Eur. Biophys. J.*

61. Zerlin,K.F., N.Kasischke, I.Digel, C.Maggakis-Kelemen, A.A.Temiz, D.Porst, P.Kayser, P.Linder, and G.M.Artmann. 2007h. Structural transition temperature of hemoglobins correlates with species' body temperature. *Eur. Biophys. J.*

62. Zerlin,K.F., N.Kasischke, I.Digel, C.Maggakis-Kelemen, A.A.Temiz, D.Porst, P.Kayser, P.Linder, and G.M.Artmann. 2007d. Structural transition temperature of hemoglobins correlates with species' body temperature. *Eur. Biophys. J.*

63. Zerlin,K.F., N.Kasischke, I.Digel, C.Maggakis-Kelemen, A.A.Temiz, D.Porst, P.Kayser, P.Linder, and G.M.Artmann. 2007f. Structural transition temperature of hemoglobins correlates with species' body temperature. *Eur. Biophys. J.*

64. Zheng,J.M. and G.H.Pollack. 2003. Long-range forces extending from polymer-gel surfaces. *Phys. Rev. E. Stat. Nonlin. Soft. Matter Phys.* 68:031408.

**Summary**

Incoherent quasielastic and elastic neutron scattering were used to measure protein and cell water dynamics in the picosecond time and Ångstrom length scale.

Hemoglobin dynamics was measured in human red blood cells, *in vivo*. The experiments revealed a change in the geometry of internal protein dynamics at 36.9°C, human body temperature. Above this temperature amino acid side-chain dynamics occupy larger volumes than expected from normal temperature dependence. Global macromolecular diffusion was interpreted according to theoretical concepts for short-time self-diffusion of non-charged hard sphere colloids.

The influence of hydration on hemoglobin dynamics was studied with neutron scattering. The residence times of localized jumps in the order of a few picoseconds were found to be significantly reduced in concentrated solution compared to fully hydrated powder. The change in the geometry of amino acid side-chain dynamics at body temperature was found in concentrated hemoglobin solution, but the body temperature transition in protein dynamics was absent in fully hydrated powder. This indicated that picosecond protein motions responsible for the body temperature transition are activated only at a sufficient level of hydration, and that hydrated powders may not reflect fully all functional protein dynamics.

The dynamics of cell water in human red blood cells was measured with quasielastic incoherent neutron scattering. A major fraction of around 90% of cell water is characterized by a translational diffusion coefficient similar to bulk water. A minor fraction of around 10% of cellular water exhibits reduced dynamics. The slow water fraction was attributed to dynamically bound water on the surface of hemoglobin, which accounts for approximately half of the hydration layer.

**Keywords:** incoherent neutron scattering, hemoglobin, red blood cells, cell water dynamics, protein dynamics, body temperature,

**Résumé**

Les techniques de diffusion incohérente élastique et quasiélastique de neutrons ont été utilisées pour mesurer la dynamique de la protéine et de l'eau cellulaire sur les échelles de quelques picosecondes et de quelques Ångstroms.

La dynamique de l'hémoglobine a été mesurée dans les globules rouges, *in vivo*. La dynamique interne de la protéine montre un changement de régime à 36.9°C, la température physiologique. À des températures plus élevées que la température physiologique, les chaînes latérales des amino acides occupent des volumes plus grands que prévu par la dépendance normale sur la température. La diffusion globale de l'hémoglobine a été interprétée avec la théorie pour la diffusion des particules colloïdales à temps de courte durée.

L'influence de l'hydratation sur la dynamique de l'hémoglobine a été étudiée avec la diffusion de neutrons. Les temps de résidence entre les sauts locaux dans l'ordre de quelques picosecondes sont réduits en solution concentrée et augmentés en poudre d'hémoglobine hydratée. La transition dans la géométrie des mouvements internes à la température du corps a été trouvée dans la solution concentrée, mais pas dans la poudre hydratée. Il a été conclu que les poudres hydratées ne représentent pas un bon modèle pour la dynamique de la protéine dans l'ordre de quelques picosecondes, qui est corrélée à la fonction biologique.

La dynamique de l'eau cellulaire dans les globules rouges a été mesurée avec la technique de diffusion incohérente quasiélastique de neutrons. Une fraction de l'eau cellulaire d'environ 90% est caractérisée par un coefficient de diffusion translationnel similaire à celui de l'eau volumique. Les 10% restant présentent une dynamique ralentie de façon significative. La fraction ralentie a été attribuée à l'eau en interaction avec l'hémoglobine. Elle correspond à environ la moitié de l'eau dans la première couche d'hydratation de la protéine.

**Mots clefs:** diffusion incohérente de neutrons, hémoglobine, globules rouges, dynamique de l'eau cellulaire, dynamique de la protéine, température physiologique